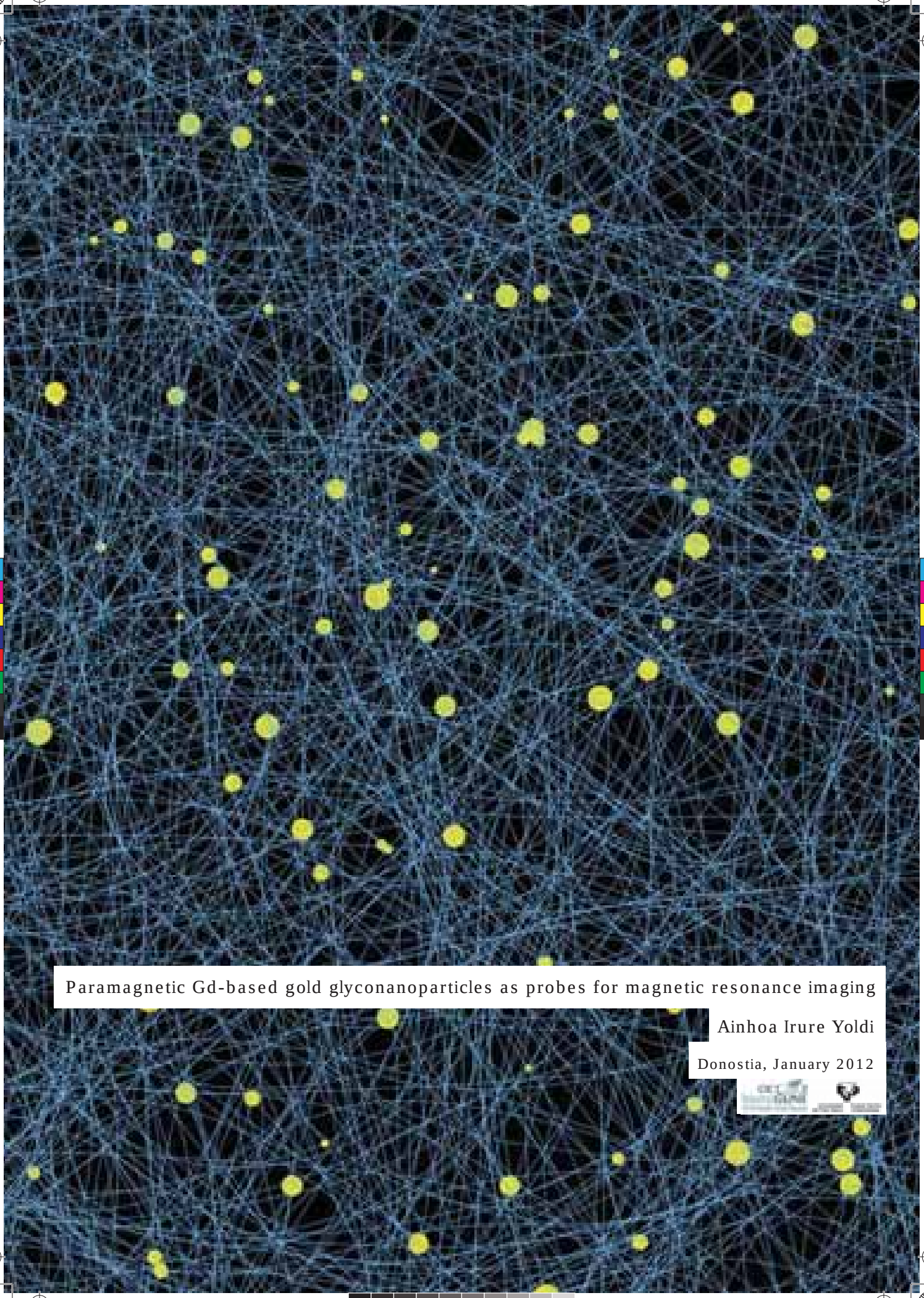

Paramagnetic Gd-based gold glyconanoparticles as probes for magnetic resonance imaging

Ainhoa Irure Yoldi

Donostia, January 2012

Paramagnetic Gd-based gold glyconanoparticles as probes for magnetic resonance imaging

Ainhoa Irure Yoldi

Donostia, 2012

Universidad del País Vasco Euskal Herriko Unibertsitatea

AUTORIZACION DE LOS DIRECTORES DE TESIS

PARA SU PRESENTACION

Prof. Soledad Pénades Ullate con N.I.F. 02683273R y Dr. Marco Marradi con N.I.E. X-7352065-T como Directores de la Tesis Doctoral: Paramagnetic Gd-based gold glyconanoparticles as probes for magnetic resonance imaging, realizada en el Laboratorio de Gliconanotecnología en el Centro de Investigación Cooperativa en Biomateriales (CIC biomaGUNE) y presentada en el departamento de Ciencia y Tecnología de Polímeros, por la Doctoranda Doña Ainhoa Irure Yoldi, autorizamos la presentación de la citada Tesis Doctoral, dado que reúne las condiciones necesarias para su defensa.

En San Sebastian, a 1 de febrero de 2012

LOS DIRECTORES DE LA TESIS

Fdo.: Soledad Penadés Ullate

Fdo.: Marco Marradi

Universidad del País Vasco Euskal Herriko Unibertsitatea

AUTORIZACION DEL PONENTE DE TESIS

PARA SU PRESENTACION

Dr. Juan José Iruin como Ponente de la Tesis Doctoral:

Paramagnetic Gd-based gold glyconanoparticles as probes for magnetic resonance imaging,

realizada en el Laboratorio de Gliconanotecnología en el Centro de Investigación Cooperativa en Biomateriales (CIC biomaGUNE) y presentada en el departamento de Ciencia y Tecnología de Polímeros por la Doctoranda Doña Ainhoa Irure Yoldi, y dirigida por Prof. Soledad Penadés Ullate y Dr. Marco Marradi, autorizo la presentación de la citada Tesis Doctoral en el Departamento de Ciencia y Tecnología de Polímeros dado que reúne las condiciones necesarias para su defensa.

En San Sebastian, a de de 2012

EL PONENTE DE LA TESIS

Fdo.: Juan José Iruin

Universidad del País Vasco Euskal Herriko Unibertsitatea

CONFORMIDAD DEL DEPARTAMENTO

El Consejo del Departamento de Ciencia y Tecnología de Polímeros,

en reunión celebrada el día de de 2012 ha acordado dar la conformidad a la admisión a trámite de presentación de la Tesis Doctoral titulada: Paramagnetic Gd-based gold glyconanoparticles as probes for magnetic resonance imaging, dirigida por la Prof. Soledad Penadés Ullate y el Dr. Marco Marradi, y presentada por Doña Ainhoa Irure Yoldi ante este Departamento.

En San Sebastian, a de de 2012

Vº Bº DIRECTOR/A DEL DEPARTAMENTO SECRETARIO/A DEL DEPARTAMENTO

Fdo.: José Ignacio Eguiazabal Ortiz de Elguea Fdo.: Agustín Etxeberria Lizarraga

Universidad del País Vasco Euskal Herriko Unibertsitatea

ACTA DE GRADO DE DOCTOR

ACTA DE DEFENSA DE TESIS DOCTORAL

DOCTORANDA: Doña Ainhoa Irure Yoldi
TITULO DE LA TESIS: Paramagnetic Gd-based gold glyconanoparticles as probes for magnetic resonance imaging

El Tribunal designado por la Subcomisión de Doctorado de la UPV/EHU para calificar la Tesis Doctoral arriba indicada y reunido en el día de la fecha, una vez efectuada la defensa por el doctorando y contestadas las objeciones y/o sugerencias que se le han formulado, ha otorgado por_____la calificación de:
unanimidad ó mayoría

En San Sebastian, a de de 2012

EL/LA PRESIDENTE/A, EL/LA SECRETARIO/A,

Fdo.: Fdo.:

Dr/a: Dr/a:

VOCAL 1º, VOCAL 2º, VOCAL 3º,

Fdo.: Fdo.: Fdo.:

Dr/a: Dr/a: Dr/a:

EL/LA DOCTORANDO/A,

Fdo.:

This thesis has been carried out in the Laboratory of Glyconanotechnology, Biofunctional Nanomaterials Unit of the Centro de Investigación Cooperativa en Biomateriales (CIC biomaGUNE). The research was financially supported by a fellowship from Departamento de Educación del Gobierno Vasco (Programa de ayudas para formación y perfeccionamiento de personal investigador, del departamento de educación, universidades e investigación), and the Spanish Ministry of Science and Innovation (grant CTQ2008-04638).

TABLE OF CONTENTS

<u>Chapter 3.</u> Application of paramagnetic Gd-based gold glyconanoparticles for *in vivo* Magnetic Resonance Imaging of glioma in mice

1. Results
   - 1.1 *In vivo* imaging of glioma and whole-body biodistribution after injection of $GlcC_5S$-Au-SC_{11}DO3A-Gd GNP prepared by "direct" method
     - MR Imaging of glioma in mice
     - Biodistribution and toxicity of $GlcC_5S$-Au-SC_{11}DO3A-Gd in tumour injected mice
     - Excretion, biodistribution, and toxicity assay of $GlcC_5S$-Au-SC_{11}DO3A-Gd injected in healthy mice
   - 1.2 Imaging of glioma in mice and biodistribution after injection of $GlcC_5S$-Au-SC_{11}DO3A-Gd GNPs prepared by Ligand Place Exchange (LPE)
     - MR Imaging of glioma in mice
     - Biodistribution and toxicity of $GlcC_5S$-Au-SC_{11}DO3A-Gd in tumour injected mice
2. Discussion
3. Experimental part

ACKNOWLEDGEMENTS

I want to thank first of all my boss during the last four years, Prof. Soledad Penadés, for the opportunity to develop this research project and for giving me freedom to work on it in the borderline between organic chemistry, materials science and biochemistry. I have to thank here also Dr. Marco Marradi, my thesis supervisor, who taught me all what I know now about organic chemistry and who supported and helped me during these for years.

I also want to remember all present and past members of the laboratory of glyconanotechnology in which I have been working for their support during these years, not only in matters related to research.

I want to thank also, all other contributors to this Thesis: The group of Dr. Carles Arús, especially Dr. Ana Paula Candiota, from the Grup d'Aplicacions Biomèdiques de la RMN (GABRMN) in Universitat Autónoma de Barcelona, and the group of Dr. Simó Schwartz, especially Ibane Abasolo from CIBBIM-Nanomedicine, Hospital Universitari Vall d'Hebron, also in Barcelona, for *in vivo* experiments and biodistribution assays. I have to thank also Daniel Padró, from CICbiomaGUNE, who helps me with all the images taken from cellular experiments.

Finally I have to mention in these acknowledgments my parents, Carmelo and Malen, and Lander who have been there every day during this Thesis.

ABBREVIATION LIST

AFM = atomic force microscopy

AIBN = azobisisobutyronitrile

ALB = albumin

ALP = alkaline phosphatase

ALT = alanine transaminase

AST = aspartate transaminase

BAIB = bisacetoxyiodobenzene

BIL = bilirubin

BBB = blood brain barrier

BUN = blood urea nitrogen

BzCl = benzoyl chloride

CLIO = cross-linked iron oxide nanoparticles

CREA = creatinine

CT = computed tomography

DBU = 1,8-diazabicyclo[5.4.0]undec-7-ene

DCE = dynamic contrast enhanced

DC-SIGN = dendritic cell-specific intercellular adhesion molecule-3-grabbing non-integrin

DIPEA = *N,N*-diisopropylethylamine

DMAP = 4-dimethylaminopyridine

DMF = dimethylformamide

DNA = deoxyribonucleic acid

DO3A = 1, 4, 7, 10-tetraazacyclododecane-1, 4, 7-triacetic acid

DOTA = 1, 4, 7, 10-tetraazacyclododecane-1, 4, 7, 10-tetraacetic acid

DOTA-amine = 1, 4, 7, 10-tetraazacyclododecane-1, 4, 7-triacetic acid-*N*-(2-aminoethyl)ethanamide

DTPA = diethylenetriaminepentaacetic acid

DTTA = diethylenetriaminetetraacetic acid

EdA=ethylene diamide

EDTA = ethylenediamine tetraacetic acid

ESI = electrospray ionization

FCC = flash column chromatography

FBS = fetal bovin serum

FFC = fast field cycling

FOV = field of view

Gal = galactose

Glc = glucose

GLU = serum glucose

GNP = glyconanoparticles

HBTU = *O*-(benzotriazol-1-yl)-*N,N,N′,N′*-tetramethyluronium hexafluorophosphate

HE = haemotoxylin-eosin

HEPES = 4-(2-hydroxyethyl)-1-piperazineethanesulfonic acid

HOBt = hydroxybenzotriazole

HR-MS = high resolution mass spectrometry

ICP = inductively coupled plasma

ID = injected dose

IR = infrared

IST = interslice-thickness

ITC = isothermal titration calorimetry

Lac = lactose

sLe^X = sialyl Lewis X

LPE = ligand place exchange

MALDI-TOF = matrix-assisted laser desorption/ionization–time-of-flight

Man = mannose

MPIO = micrometer-sized particles of iron oxide

MRI = magnetic resonance imaging

MS = mass spectrometry

MSME = multi slice – multi echo

MTS = 3-(4.5-dimethylthiazol-2-yl)-5-(3-carboxymethoxyphenyl)-2-(4-sulfophenyl)-2H-tetrazolium

MTT 3-(4,5-dimethylthiazol-2-yl)-2,5-diphenyltetrazolium bromide

MTX = matrix

MW = molecular weight

MWCO = molecular weight cut-off

NA = number of averages

NMR = nuclear magnetic resonance

NS = number of slices

PBS = phosphate buffered saline

PEG = polyethylen glycol

PET = positron emission tomography

QD = quantum dot

RARE = rapid acquisition by relaxation enhancement

RCE = relative contrast enhancement

ROI = region of interest

RPMI = Roswell Park Memorial Institute

r.t. = room temperature

SD = standard deviation

SPR = surface plasmon resonance

TAT = total acquisition time

TFA = trifluotoacetic acid

THF = tetrahydrofuran

TE = echo time

TEM = transmission electron microscopy

TEMPO = 2,2,6,6-tetramethylpiperidine-*N*-oxide

TIPS = triisopropyl silane

TMSOTf = trimethylsilyl triflate

TP = total proteins

TR = repetition time

TrtCl = trityl chloride

USPIO = ultrasmall superparamagnetic iron oxide

UV = ultraviolet

ABSTRACT

The construction of novel multifunctional bionanomaterials to better reveal life processes at the nanoscale and with potential applications in medicine is a key challenge of nanotechnology. Our group has experience in preparing gold and magnetic nanoclusters, as well as semiconductor nanocrystals functionalized with different types of carbohydrates (glyconanoparticles). They were designed to better understand the mechanism of carbohydrate-mediated interaction and to apply as anti-adhesion agents or as molecular probes for magnetic resonance imaging (MRI)

Magnetic Resonance Imaging (MRI) is one of the most used diagnostic techniques to obtain anatomical images, information on the physical-chemical state of tissues. No use of harmful high-energy radiation, clinic resolution close to 1 mm^2, and exceptional soft tissue contrast, are some of the characteristics which make MRI an ideal technique for medicinal diagnostics. Nowadays, most of the MRI contrast agents in clinical use are paramagnetic complexes, usually gadolinium [Gd(III)] chelates that enhance the brightness of T_1-weighted images (positive signal). However, an important limitation of these small molecular contrast agents is their low sensitivity (low relaxivity, low contrast), due to non-specific biodistribution in the body. The development of high sensitive contrast agents with targeted properties for observing concrete biological events, both at cellular and molecular level, is strongly needed.

Our laboratory recently developed an approach to obtain Gd-based glyconanoparticles as MRI paramagnetic probes (T_1-contrast agents) modifying the organic shell through insertion of Gd(III) complexes on the gold nanoclusters. Therefore, it was possible to obtain biocompatible paramagnetic glyconanoparticles which present similar or higher longitudinal relaxivities (r_1) to contrast agents in clinical use as Dotarem® and Magnevist®.

The main goal of this Thesis is to improve the preparation of this kind of nanoparticles by means of a novel synthetic methodology, which allows the construction of high relaxivity paramagnetic probes in a well-reproducible way (Chapter 1). The targeting properties of the Gd-based glyconanoparticles (Gd-GNPs) were first studied *in vitro*. The nanoparticles are not toxic to cells at concentrations as high up to 0.1 mg/mL and show excellent biocompatibility conferred by the sugar's presence. Thanks to the information encoded in sugars, we demonstrate that these Gd-GNPs can work as T_1 specific reporters of cellular surface carbohydrate receptors of Burkitt lymphoma Raji, hepatocytes HepG2 and murine glioma GL261 cell lines (Chapter 2). Finally, with these novel MRI probes we performed *in vivo* detection of gliomas in mice and the probes biodistribution (Chapter 3). These studies confirm that the Gd-based glyconanoparticles can be used as paramagnetic contrast agents for brain tumour detection in mice.

The evaluation of the biodistribution and toxicological profile show that the glyconanoparticles are mainly excreted by kidneys, although some accumulation in liver occurs. However, no significant impairment of the renal or hepatic function is induced.

To sum up, the preparation, characterization and application of a small library of paramagnetic Gd-based glyconanoparticles as biocompatible, biofunctional and water-soluble probes for Magnetic Resonance Imaging (MRI) has been achieved in this PhD Thesis.

RESUMEN

La construcción de nuevos bionanomateriales multifuncionales con aplicaciones potenciales en medicina es un reto para la nanotecnología. Nuestro grupo tiene experiencia en la preparación de nanoclusters de oro, magneticos y semiconductores funcionalizados con diferentes tipos de carbohidratos (gliconanopartículas). Estas gliconanopartículas se diseñaron para comprender mejor el mecanismo de las interacciones biológicas controladas por carbohidratos y para su aplicación como agentes anti-adhesión o como agentes de contraste para resonancia magnética de imagen (MRI).

La Resonancia Magnética de Imagen (MRI) es una de las técnicas más empleadas para obtener imágenes anatómicas e información sobre el estado físico-químico de un tejido. Las características de la MRI como son una resolución próxima a 1 mm^2, no emplear radiación de alta energía y el buen contraste obtenido en los tejidos blandos, hacen de esta una técnica ideal para el diagnóstico clínico. Actualmente, la mayoría de los agentes de contraste en uso clínico son complejos paramagnéticos, generalmente quelatos de gadolinio [Gd(III)], que aumentan la señal en las imágenes pesadas en T_1 (obtención de imágenes más brillantes). No obstante, una de las limitaciones de estos agentes de contraste (pequeñas moléculas) es su baja sensibilidad (baja relajatividad, bajo contraste) debido a una biodistribución no específica en el cuerpo. Por ello, es necesario desarrollar una investigación básica orientada a la creación de agentes de contraste muy sensibles y que puedan dirigirse a una diana biológica concreta para observar procesos patológicos a nivel celular y molecular.

Nuestro laboratorio ha desarrollado recientemente un método para obtener gliconanopartículas basadas en gadolinio (Gd-GNPs) como agentes de contraste paramagnéticas para MRI (T_1). El método se basa en la inserción controlada mediante un enlace oro-azufre en un cluster de oro de complejos de Gd(III) y azúcares. De este modo, fue posible obtener gliconanopartículas paramagnéticas biocompatibles con una relajatividades longitudinales (r_1) parecidas o superiores a la de los agentes de contraste empleados en clínica, tales como Dotarem® y Magnevist®.

El principal objetivo de esta Tesis es mejorar la preparación de este tipo de nanopartículas mediante el desarrollo de una nueva metodología sintética (en sus siglas en inglés LPE) que permite preparar las gliconanopartículas paramagnéticas con relajatividad alta de un modo reproducible (Capítulo 1). El uso de estas gliconanopartículas basadas en Gd como vectores se estudio primero *in vitro*. Las nanopartículas no son tóxicas para las células a concentraciones tan altas como 0.1 mg/mL y son biocompatibles gracias a la presencia de los azúcares. Gracias a la

información codificada por los azúcares, estas Gd-GNPs actúan como agentes T_1 específicos de receptores de carbohidratos presentes en la superficie de las líneas células Burkitt linfoma Raji, hepatocitos HepG2 y glioma murino GL261 (Capítulo 2). Finalmente, la detección, *in vivo*, de gliomas en ratones mediante MRI, la biodistribución y el perfil toxicológico fueron llevados a cabo con estos nuevos agentes de contraste (Capítulo 3). Estos estudios confirmaron que las Gd-GNPs pueden ser empleadas como agentes de contraste paramagnéticos para la detección de tumores en ratones. La evaluación de la biodistribución y el perfil toxicológico mostró que las gliconanopartículas son excretadas principalmente por los riñones aunque hay algo de acumulación en el hígado. No obstante, las funciones renal y hepática no se ven afectadas significativamente.

En resumen, hemos sido capaces en esta Tesis de preparar, caracterizar y aplicar una pequeña librería de gliconanopartículas paramagnéticas basadas en gadolinio. Estas Gd-GNPs son biocompatibles, biofuncionales y solubles en agua y puede usarse como agentes de contraste para Resonancia Magnética de Imagen

INTRODUCTION AND OBJECTIVES

INTRODUCTION AND OBJECTIVES

This Thesis is focussed on the preparation of high sensitive paramagnetic contrast agents based on gold glyconanoparticles as diagnostic tools for magnetic resonance imaging (MRI). This goal is part of a more broad research program of our laboratory aiming at the development of targeted magnetic probes based on glyconanoparticles for their application in the early diagnostic of biomedical problems by MRI. Although since the eighties an extensive and excellent research is being developed to obtain smart probes for more sensitive MRI, only a few of these probes are presently in clinical use. MRI is one of the most potent diagnostic methods and there is a strong interest in developing tools to improve its potency. To achieve this aim, different strategies are being developed which include the application of nanotechnologies.

Nanotechnology offers tremendous potential for future biomedical technology. Nanostructured materials have emerged as novel diagnostic and therapeutic agents for the future medical field due to their unique characteristics such as superparamagnetic or fluorescent properties, and size comparable to biomolecules. Especially, nano-materials with different properties can offer multifunctional medical platforms, which make possible to accomplish multimodal imaging, and simultaneous diagnosis and therapy. [1], [2] For example, after their discovery, quantum dots (QDs) - semiconductor nanocrystals - were soon recognized to be uniquely suited for bioimaging, including *in vivo* fluorescence imaging and *ex vivo* immunofluorescence. [3] Polymeric nanoparticles, including dendrimers, have also been explored extensively for diagnosis and therapeutics. [4] Natural nanoparticles, such as viruses or lipoproteins, have also been broadly employed for a variety of applications, such as gene delivery and imaging. [5], [6] They can be combined with inorganic nanoparticles to create so-called hybrid nanostructures that can be tailored for specific applications. [7] Nanoparticulate aggregates of lipids have also been

[1] J. Cheon, J.H. Lee, *Acc. Chem. Res.* **2008**, 41, 1630–1640 (Synergistically Integrated Nanoparticles as Multimodal Probes for Nanobiotechnology)
[2] J. Xie, G. Liu, H. S. Eden, H. Ai, and X. Chen, *Acc. Chem. Res.* **2011**, 44, 883-892 (Surface-Engineered Magnetic Nanoparticle Platforms for Cancer Imaging and Therapy).
[3] I. L Medintz,. H. T Uyeda,. E. R Goldman and H. Mattoussi, *Nat. Mater.* **2005**, 4, 435–446 (Quantum Dot Bioconjugates for Imaging, Labelling and Sensing).
[4] C. C. Lee, J. A MacKay, J. M Frechet and. F. C Szoka, *Nat. Biotechnol.* **2005**, 23, 1517–1526 (Designing Dendrimers for Biological Applications)
[5] M. A. Kay, J. C Glorioso and L.Naldini, *Nat. Med.* **2001**, 7, 33–40 (Viral Vectors for Gene Therapy: The Art of Turning Infectious Agents into Vehicles of Therapeutics)
[6] J. C. Frias, K. J.Williams, E. A. Fisher and Z. A. Fayad, *J. Am. Chem. Soc.* **2004**, 126, 16316–16317 (Recombinant HDL-Like Nanoparticles: A Specific Contrast Agent for MRI of Atherosclerotic Plaques).
[7] X. Huang, L. M. Bronstein, J. Retrum, C. Dufort, I. Tsvetkova, S. Aniagyei, B. Stein, G. Stucky, B. McKenna, N. Remmes, D. Baxter, C. C. Kao and B. Dragnea, *Nano. Lett.* **2007**, 7, 2407–2416 (Self- Assembled Virus-Like Particles with Magnetic Cores)

investigated for biomedical purposes. [8] Iron oxide and gold nanoparticles were recognized to have extraordinary features for diagnostics as well as therapeutics. [9] For example, iron oxide nanoparticles have been employed extensively as contrast for magnetic resonance imaging (MRI) [10] but can also be used for thermal ablation, [11] while gold is suitable for optical detection [12] as well as for laser-activated thermal ablation. [13]

As mentioned above, there is a special interest in developing tools to improve diagnostics by MRI. This Thesis is focussed on the preparation of paramagnetic Gd-based gold glyconanoparticles as novel probes mainly for the diagnostic of glioma by MRI.

Over the last years, magnetic resonance imaging (MRI) has evolved into one of the most powerful diagnostic techniques in clinical medicine and biomedical research. [14] MRI is primarily used to produce anatomical images, but it also gives information on the physical-chemical state of tissues, flow diffusion and motion. No use of harmful high energy radiation, clinic resolution close to 1 mm^2, and exceptional soft tissue contrast are some of the characteristics which make MRI an ideal technique for medicinal diagnostics. The basic principle of MRI is based on the application of a magnetic field to induce alignment of the nuclear magnetization of hydrogen atoms by nuclear magnetic resonance (NMR). The hydrogen atoms from water that are present in the body are primarily observed. Pulse sequences can be varied to highlight differences among tissues that have different proton density, longitudinal (T_1) or transverse (T_2) relaxation times, different rates of water diffusion, or different chemical shifts. In spite of this, the use of chemical systems which can increase the signal differences between adjacent regions is strongly required to gain sensitivity. [15] Such substances are named “contrast agents” and their function is to shorten the relaxation times of bulk water protons.

[8] D. Peer, J. M. Karp, S. Hong, O. C. Farokhzad, R. Margalit and R. Langer, *Nat. Nanotechnol.* **2007**, 2, 751–760 (Nanocarriers as an Emerging Platform for Cancer Therapy).
[9] H. Liao, C. L. Nehl and J. H. Hafner, *Nanomedicine* **2006**, 1, 201–208 (Biomedical Applications of Plasmon Resonant Metal Nanoparticles).
[10] J. W. M. Bulte, D. L. Kraitchman *NMR Biomed*. **2004**, 17, 484–499 (Iron Oxide MR Contrast Agents for Molecular and Cellular Imaging).
[11] I. Hilger, R. Hiergeist, R. Hergt, K. Winnefeld, H. Schubert and W. A. Kaiser, *Invest. Radiol.* **2002**, 37, 580–586 (Thermal Ablation of Tumors Using Magnetic Nanoparticles: an in Vivo Feasibility Study).
[12] X. Qian, X. H. Peng, D. O. Ansari, Q. Yin-Goen, G. Z. Chen, D. M. Shin, L. Yang, A. N. Young, M. D. Wang and S. Nie, *Nat. Biotechnol.* **2008**, 26, 83–90 (In Vivo Tumor Targeting and Spectroscopic Detection with Surface-Enhanced Raman Nanoparticle Tags).
[13] D. P. O’Neal, L. R. Hirsch, N. J. Halas, J. D. Payne and J. L. West, *Cancer Lett.* **2004**, 209, 171–176 (Photo-thermal Tumor Ablation in Mice Using Near Infrared-Absorbing Nanoparticles).
[14] Magnetic Resonance Imaging: Methods and Biologic Applications, ed. Pottumarthi V. Prasad, Humana Press Inc. Totana, New Jersey, **2006.**
[15] P. Caravan, *Chem. Soc. Rev.* **2006**, 35, 512–523

In 1948, Bloch *et al.* published the use of the paramagnetic ferric nitrate salt to enhance the relaxation rates of the water protons. [16] Thirty years later, Lauterbur *et al.* produced the first MR image by using a Mn(II) salt in order to distinguish between different tissues on the basis of the differential relaxation times. [17] The strong expansion of medical imaging has prompted the development of a new class of MRI contrast agents based on paramagnetic and superparamagnetic probes which are designed for administration to patients in order either to enhance the contrast between normal and diseased tissue or to indicate organ function or blood flow. [18]

All magnetic resonance contrast agents work by reducing the longitudinal (T_1) or transverse (T_2) relaxation times of the target tissue, and are thus commonly describe as either "T_1-agents" or "T_2-agents" depending on whether the relative reduction in relaxation times caused by the contrast agent is greater for the longitudinal (T_1) or transversal (T_2) relaxation times. The ability of the agent to reduce the T_1 and T_2 relaxation times are respectively describes by the r_1 and r_2 relaxivity values of the agent.

Paramagnetic probes ("T_1-agents") have a permanent magnetic moment. In aqueous solution, a dipolar magnetic interaction between the electronic magnetic moment of the paramagnetic atom and the much smaller magnetic moments of the protons of the nearby water molecules is established (Figure 1). Random fluctuations in this dipolar magnetic interaction, mainly as result of molecular motions, reduce both longitudinal (T_1) and transverse (T_2) relaxation times of the water protons, although the reduction in T_2 is smaller than in T_1.

On the other hand, "T_2-agents" are superparamagnetic in nature. These contrast agents are, usually, iron oxide particles made up of several thousand magnetic ions. The superparamagnetic properties appear when the magnetic ions are mutually aligned in the presence of an external magnetic filed, resulting in particles with a very large permanent magnetic moment (Figure 1).

[16] F. Bloch, W.W. Hansen and M. Packard, *M. Phys. Rev*. **1946**, 70, 474 (The nuclear induction experiment).
[17] P.C. Lauterbur, M.H. Mendoca-Dias and A.M. Rudin, Frontiers of Biological Energetics, ed. P.L. Dutton, L.S. Leigh and A. Scarpa, Academic Press, New York, **1978**, p. 752.
[18] E. Toth, L. Helm and A. E. Merbach, in The Chemistry of Contrast Agents in Medical Magnetic Resonance Imaging, ed. A. E. Merbachand E. Tóth, Wiley, Chichester, **2001**, pp. 45–119.

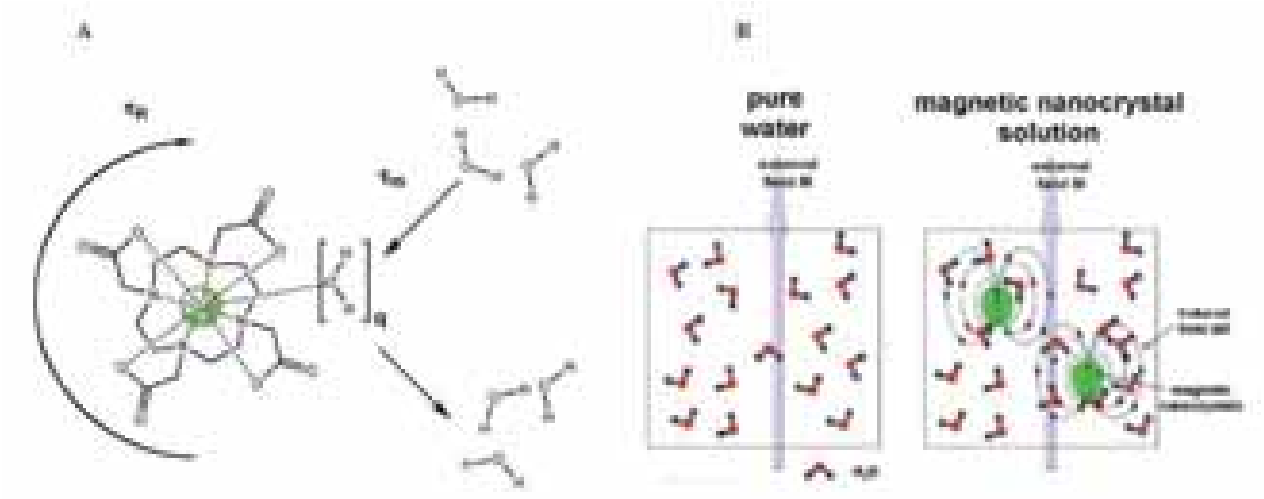

Figure 1. A) *Three important factors that determine the relaxivity of Gd(III)-based MR contrast agents: hydration number (q), the mean residence lifetime of bound water molecules (τ_m), and the rotational correlation time (τ_R). (Figure taken from reference 19).* ***B) Left:*** *Pure water under an external magnetic field.* ***Right:*** *The influence of superparamagnetic iron oxide nanoparticles in water molecules under an external magnetic field. (Figure taken from reference 20)*

Nowadays, most of the MRI contrast agents in clinical use are paramagnetic complexes, usually gadolinium (Gd^{3+}) chelates, since Gd(III) has seven unpaired electrons which make it the most paramagnetic stable metal ion. [18], [21], [22] On the contrary, the use of the iron oxide-based T_2 contrast agents is quite limited due to a series of drawbacks such as "negative" contrast and relatively large size of the particles. [10], [21] In Figure 2, some of the contrast agents in clinical use are represented.

[19] J. L. Major and T. J. Meade, *Acc. Chem. Res.* **2009**, 42, 893-903 (Bioresponsive, Cell-Penetrating, and Multimeric MR Contrast Agents)
[20] http://bme240.eng.uci.edu/students/08s/ykim30/03.htm
[21] P. Caravan, J. J. Ellison, T. J. McMurry, and R. B. Lauffer *Chem. Rev.* **1999**, 99, 2293-2352 (Gadolinium(III) Chelates as MRI Contrast Agents: Structure, Dynamics, and Applications)
[22] P. Hermann, J. Kotek, V. Kubicek, I. Lukes, *Dalton Trans*. **2008**, 3027-3047 (Gadolinium(III) Complexes as MRI Contrast Agents: Ligand Design and Properties of the Complexes)

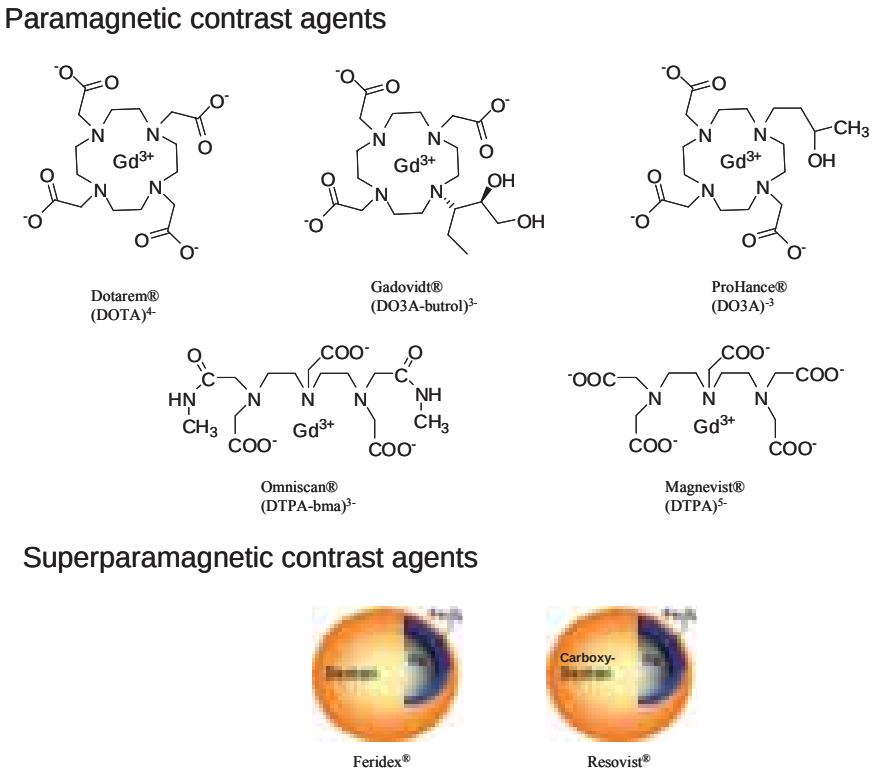

Figure 2: *Some of the contrast agents in clinical use. Gadovist®, Dotarem®, ProHance®, Omniscan® and Magnevist® are paramagnetic contrast agents. Feridex IV® and Resovist® are superparamagnetic contrast agents.*

Paramagnetic Gd(III) complexes enhance the signal in T_1-weighted images (signal-increasing effect) and, therefore, the obtained images are brighter than the once without contrast agent. Gd-based contrast agents present limitations. As Gd(III) is toxic, small chelating agents are used to form complexes which are thermodynamically stable and kinetically inert. In clinical use Gd(III) complexes such as Magnevist® $[Gd(DTPA)(H_2O)]^{2-}$ and Dotarem® $[Gd(DOTA)(H_2O)]^{-}$ are usually injected *in vivo* at millimolar concentrations because they are not specific and their relaxivity is rather low (~3 $mM^{-1}s^{-1}$). According to the Solomon-Bloembergen-Morgan theory of paramagnetic relaxation, [23] the relaxivity of a Gd-based contrast agent can be enhanced in three ways: By increasing the number of water molecules (represented by q) coordinated to the Gd center; by reducing the tumbling rate ($1/\tau_R$) of the contrast agent; and by keeping the exchange rate of the inner sphere water molecules on Gd ($1/\tau_M$) at an optimum value (e.g., $\tau_M \approx 10$ ns) (Figure 1A). [24], [25], [26] One of the widely used strategies to potentially increase the relaxivity

[23] N. Bloembergen, L. O. Morgan, *J. Chem. Phys*. **1961**, 34, 842–850 (Proton relaxation times in paramagnetic solutions. Effects of electron spin relaxation)
[24] P. Caravan, *Chem. Soc. Rev.* **2006**, 35, 512–523 (Strategies for increasing the sensitivity of gadolinium based MRI contrast agents)

of such agents is to slow the tumbling of the complex by using macromolecular conjugates of Gd(III) chelates. [15] These macro-conjugates have another advantage over the Gd(III) chelates: An extended lifetime in the blood pool which is necessary for magnetic resonance applications. However, none of these Gd-based macromolecular products have still been approved for humans.

The recent advances in nanotechnology have allowed the development of new types of magnetic probes based on nanoparticles which can be applied not only in MRI, [27], [28], [29] but also in tandem with other imaging techniques for targeted multimodal imaging and simultaneous diagnosis and therapy. [1], [30], [31], [32] As an example, Gd-loaded liposomes and/or micelles, [33], [34], [35], polymers and dendrimers [36] [37], dextran-coated $GdPO_4$ [38], or Gd_2O_3 [39] nanoparticles are worth to be mentioned. The main advantage of this kind of nanoparticles is the high Gd-loading. However, uniform sizes of the cores have still not been demonstrated and concerns about the release of Gd(III) species *in vivo* have been not fully addressed.

One of the limitations of Gd-based contrast agents in clinical use/trials is that they are non-targeted molecules and thus much attention is being devoted to design of agents which recognize molecular markers at cell surface and thus accumulate the Gd-chelates at specific sites (targeted).

---

[25] S. Aime, M. Botta, M. Fasano, S. Geninatti Crich, E. Terreno, *Coord. Chem. Rev.* **1999**, 185–186, 321–333 (^{1}H and ^{17}O-NMR relaxometric investigations of paramagnetic contrast agents for MRI. Clues for higher relaxivities)

[26] M. Botta, *Eur. J. Inorg. Chem.* **2000**, 399–407 (Second Coordination Sphere Water Molecules and Relaxivity of Gadolinium(III) Complexes: Implications for MRI Contrast Agents)

[27] P. J. Endres, T. Paunesku, S. Vogt, T. J. Meade, and G. E. Woloschak *J. Am. Chem. Soc.* **2007**, 129, 15760-15761 (DNA−TiO_2 Nanoconjugates Labeled with Magnetic Resonance Contrast Agents).

[28] D. E. Sosnovik, R. Weissleder, *Curr. Opin. Biotechnol.* **2007**, 18, 4–10 (Emerging concepts in molecular MRI)

[29] E. Terreno, D. Delli Castelli, A. Viale, S. Aime *Chem. Rev.* **2010**, 110, 3019–3042 (Challenges for Molecular Magnetic Resonance Imaging)

[30] L. Frullano, T. J. Meade *J. Biol. Inorg. Chem.* **2007**, 12, 939–949 (Multimodal MRI contrast agents)

[31] J. Kim, Y. Piao, T. Hyeon, *Chem. Soc. Rev.* **2009**, 38, 372–390 (Multifunctional nanostructured materials for multimodal imaging, and simultaneous imaging and therapy)

[32] J. Gao, H. Gu, B, Xu, *Acc. Chem. Res.* **2009**, 42, 1097–1107 (Multifunctional Magnetic Nanoparticles: Design, Synthesis, and Biomedical Applications)

[33] R. W. Storrs, F. D. Tropper, H. Y. Li, C. K. Song, J. K. Kuniyoshi, D. A. Sipkins, K. C. P. Li, M. D. Bednarski, *J. Am. Chem. Rev.* **1995**, 117, 7301–7306 (Paramagnetic Polymerized Liposomes: Synthesis, Characterization, and Applications for Magnetic Resonance Imaging)

[34] N. Kamaly, A. D. Miller *Int. J. Mol. Sci.* **2010**, 11, 1759–1776 (Paramagnetic Liposome Nanoparticles for Cellular and Tumour Imaging)

[35] P. M. Winter, K. Cai, S. D. Caruthers, S. A. Wickline, G. M. Lanza, *Exp. Rev. Med. Dev.* **2007**, 4, 137–145 (Emerging nanomedicine opportunities with perfluorocarbon nanoparticles)

[36] C. H. Reynolds, N. Annan, K. Beshah, J. H. Huber, S. H. Shaber, R. E. Lenkinski, and J. A. Wortman, *J. Am. Chem. Soc.* **2000**, 122, 8940-8945 (Gadolinium-loaded nanoparticles: new contrast agents for magnetic resonance imaging).

[37] A. J. L. Villaraza, A. Bumb, M. W. Brechbiel, *Chem. Rev.* **2010**, 110, 2921–2959 (Macromolecules, Dendrimers, and Nanomaterials in Magnetic Resonance Imaging: The Interplay between Size, Function, and Pharmacokinetics)

[38] H. Hifumi, S. Yamaoka, A. Tanimoto, D. Citterio and K. Suzuki, *J. Am. Chem. Soc.* **2006**, 128, 15090-15091 (Gadolinium-based hybrid nanoparticles as a positive MR contrast agent).

[39] M.A. McDonald and K.L. Watkin, *Acad. Radiol.* **2006**, 13, 421-427 (Investigations into the Physicochemical Properties of Dextran Small Particulate Gadolinium Oxide Nanoparticles).

[40] Most examples of targeted and/or stimuli responsive magnetic probes consist in small molecules. Examples include systems which enable protein targeting [41] and responsive agents to enzymes, [42] pH, [43] and red-ox potential. [44] Nanoparticles offer also advantage to develop targeted contrast agents. [45] The advances in nanotechnology have allowed the design of complex nanoparticles which can be targeted after suitable biofunctionalization. In this way, the benefit of having nanoparticles as macromolecular probes can also take advantage of the possibility of attaching to their surface targeting molecules which can selectively direct the nanoparticles to a specific organ or tissue in the body. Furthermore, the opportunity to insert different types of ligands gives rise to multifunctional agents for multimodal applications. This is a quite general strategy which is not limited to T_1-contrast agents. Modification of the surface of superparamagnetic fluorescent cross-linked iron oxide nanoparticles (CLIO-Cy5.5) (T_2 contrast agents) by multivalent attachment of different small molecules with chemical functional groups such as primary amines, alcohols, carboxylic acids, sulfidryls and anhydrides allowed the modulation of the affinities for resting and activated macrophages for macrophage imaging. [46] RGD peptides [47] and twin arginine translocase (TAT) peptides [48] have been also used as targeting agents in paramagnetic (Gd-based liposomes) and superparamagnetic (dextran coated superparamagnetic iron oxide nanoparticles) probes, respectively. Usually, antibodies are the preferential vectors to make the contrast agents accumulate in cells that express the targeted biomarkers. Regard to this, much work has been devoted to the development of immunoliposomes for MRI. [49] For example, Gd-loaded liposomes displaying good T_1-relaxivity (r_1 ~18 $mM^{-1}s^{-1}$) were employed to image angiogenesis in tumours by incorporation of specific antibodies for $\alpha_v\beta_3$

[40] Dmitri Artemov *J. Cell. Biochem*. **2003**, 90, 518–524 (Molecular Magnetic Resonance Imaging With Targeted Contrast Agents)
[41] P. Caravan *Acc. Chem. Res.* **2009**, 42, 851-862 (Protein-Targeted Gadolinium-Based Magnetic Resonance Imaging (MRI) Contrast Agents: Design and Mechanism of Action)
[42] A.Y. Louie, M.M. Hüber, E.T. Ahrens, U. Rothbächer, R. Moats,R.E. Jacobs, S.E. Fraser and T.J. Meade, *Nat. Biotechnol.* **2000**, 18, 321-25 (*In vivo* visualization of gene expression using magnetic resonance imaging)
[43] Zhou J. Y. Payen J. F., Wilson D. A., Traystman R. J., van Zijl P. C. M., *Nat. Med.* **2003**, 9, 1085-1090
[44] S. Aime, Z. Baranyai, E. Gianolio, and E. Terreno. Paramagnetic Contrast Agents in "Molecular and Cellular MR Imaging" Edited by M. M. J. Modo and J. W. M. Bulte CRC Press Taylor & Francis Group, Boca Raton London and New York, **2007,** Chapter 3, pp 48-49.
[45] S. Aime, Z. Baranyai, E. Gianolio, and E. Terreno. Paramagnetic Contrast Agents in "Molecular and Cellular MR Imaging" Edited by M. M. J. Modo and J. W. M. Bulte CRC Press Taylor & Francis Group, Boca Raton London and New York, **2007**, Chapter 3, pp 37-58.
[46] R. Weissleder, K. Kelly, E.Y. Sun, T. Shtatlan and L. Josephson, *Nat. Biotechnol.* **2005**, 23, 1418-1423 (Cell specific targeting of nanoparticles by multivalent attachment of small molecules).
[47] P. M. Winter, A. M. Morawski, S. D. Caruthers, R. W. Fuhrhop, H. Zhang, T. A. Williams, J. S. Allen, E. K. Lacy, J. D. Robertson, G. M. Lanza and S. A. Wickline, *Circulation* **2003**, 108, 2270-2274 (Molecular Imaging of Angiogenesis in Early-Stage Atherosclerosis With $\alpha_v\beta_3$-Integrin–Targeted Nanoparticles).
[48] L. Josephson, C.H. Tung,. A. Moore and R. Weissleder, *Bioconjugate Chem.* **1999**, 10, 186–191, (High-efficiency intracellular magnetic labeling with novel superparamagnetic-Tat peptide conjugates).
[49] D. Kozlowska, P. Foran, P. MacMahon, M.J. Shelly, S. Eustace, and R.O'Kennedy, *Adv. Drug Deliv. Rev*. **2009**, 61, 1402-1411 (Molecular and magnetic resonance imaging: The value of immunoliposome)

integrins. [50] Antibody-functionalized superparamagnetic nanoparticles have also been proposed: Weissleder established the feasibility of using T_2-MRI to detect endothelial pro-inflammatory states by conjugation of CLIO nanoparticles to anti-human E-selectin (CD62E) $F(ab')_2$ antibody fragments for E-selectin targeting. [51] Our group has recently demonstrated that superparamagnetic glyconanoparticles, where the carbohydrate lactose ensures water-solubility, stability and biocompatibility, can specifically label leukocytes or erythrocytes in human blood *in vitro* depending on the antibody attached to the nanoparticles surface. [52]

During the last years, **gold nanoparticles** have attracted much attention as nanotechnology tools due to their easy way of preparation, functionalization and shape control. [53], [54] The thiol chemistry at gold surface has been widely exploited for the preparation of monolayer-protected clusters due to the possibility of changing structure, composition, and properties of the resulting nanotools. [55] In addition, gold nanoparticles can be potentially used in different biomedical fields such as therapy (hyperthermia, drug vectorization, gene delivery, etc.), imaging, and plasmon resonance-based biosensing. [56]

Gold nanoclusters represent also a good platform for introducing Gd-complexes to convert the nanoparticles into paramagnetic tools. In 2003, our laboratory addressed the conversion of sugar-protected gold nanoclusters into paramagnetic ones by introducing Gd chelates onto the cluster surface with the idea of detecting glioma by MRI in the early stage of formation. [57] In 2006, Roux and Tillement reported the encapsulation of small gold nanoparticles (~2.5 nm mean gold diameter) within a multilayered gadolinium chelates bound to each other through disulfide bonds. [58] These nanoparticles showed a moderate increase in relaxivity (r_1= 3.9 $mM^{-1}s^{-1}$) respect to Gd–DTPA (diethylenetriaminepentaacetic acid) (r_1= 3.0 $mM^{-1}s^{-1}$) at 7 T, but could be also used as

[50] D. A Sipkins. D. A. Cheresh, M. R. Kazemi, L. M. Nevin, M. D. Bednarski and K. C. Li, *Nat. Med*. **1998**, 4, 623-626 (Detection of tumor angiogenesis *in vivo* alphaVbeta3-targeted magnetic resonance imaging)

[51] H.W. Kang, L. Josephson, A. Petrovsky, R. Weissleder and A. J.Bogdanov, *Bioconjugate Chem.* **2002**, 13, 122-27 (Magnetic resonance imaging of inducible E-selectin expression in human endothelial cell culture).

[52] J. Gallo, I. García, N. Genicio, D. Padro, S. Penadés, *Biomaterials* **2011**, 32, 9818-9825 (Specific labelling of cell populations in blood with targeted immuno-fluorescent/magnetic glyconanoparticles)

[53] A. Guerrero-Martínez, J. L. Alonso-Gómez, B. Auguié, M. M. Cid and L. M. Liz-Marzan, *Nanotoday* **2011**, 6, 381-400 (From individual to collective chirality in metal nanoparticles).

[54] A. S. Thakor, J. Jokerst, C. Zavaleta, T. F. Massoud, and S. S. Gambhir, *Nano Lett.* **2011**, 11, 4029-4036 (Gold nanoparticle: A revival in precious metal administration to patients).

[55] A.C. Templeton, M.P. Wuelfing and R.W. Murray, *Acc. Chem. Res.*, **2000**, 33, 27-36 (Monolayer protected cluster molecules)

[56] E. Boisselier and D. Astruc, *Chem. Soc. Rev*. **2009**, 38, 1759 (Gold nanoparticles in nanomedicine: preparations, imaging, diagnostics, therapies and toxicity).

[57] D. Álcantara Parra, PhD Thesis, Sevilla, **2008**. (Diseño y síntesis de gliconanopartículas magnéticas. Aplicaciones como agentes de contraste en resonancia magnética de imagen)

[58] P.J. Debouttière, S. Roux, F. Vocanson, C. Billotey, O. Beuf, A. Favre-Réguillon, Y. Lin, S. Pellet-Rostaing, R. Lamartine, P. Perriat and O. Tillement, *Adv. Funct. Mater*. **2006**, 16, 2330–2339 (Design of gold nanoparticles for magnetic resonance imaging.)

X-ray Computed Tomography (CT) probes. [59], [60] Inspired by these works, Kim and collaborators used gold nanoparticles of 12 nm (gold diameter) as bimodal contrast agents after functionalization with a conjugate of DTPA and cysteine [61] or DTPA and penicillamine. [62] They achieve quite high relaxivity (~20 $mM^{-1}s^{-1}$) at low magnetic fields (1.5 T). Moriggi *et al.* demonstrated that gold nanoparticles functionalized with a rigid DTTA (diethylenetriaminetetraacetic acid) thiol-ended derivative can reach r_1 = 50 $mM^{-1}s^{-1}$ at 60 MHz (1.41 T), but these values suffer a dramatic decrease at higher fields. [63]

Very recently, paramagnetic gold nanoparticles coated with targeting ligands have also been proposed for both *in vitro* and *in vivo* use. Chung *et al.* reported that gold nanoparticles functionalized with anti-HER2 antibodies chemically conjugated to DTPA-Gd (23.7 $mM^{-1}s^{-1}$ at 1.5 T) can be used to target breast cancer cells for combined MRI and phototherapy. [64] Chechik *et al*. exploited Gd-loaded and biotin-derivatized gold nanoparticles as avidin-targeted MRI contrast agents. [65] While peptides, proteins, oligonucleotides and antibodies have been extensively used to construct hybrid biomaterials, carbohydrate-based materials are still in their infancy. Most of the examples of biomedical applications with glyconanomaterials consist of metallic nanoparticles coated with structural polysaccharides as biocompatible protection (e.g. dextran and carboxy-dextran coated magnetic nanoparticles; Figure 2) or as carriers in drug-delivery systems (e.g. alginate [66] and chitosan [67] nanoparticles). Recently, Gd(III)-labeled nanoparticles with covalently attached oligonucleotides have been used by Mirkin and Meade for cell targeting resulting in very good contrast *in vitro*. [68] Although non specific, these Gd-

[59] C. Alric, J. Taleb, G. L. Duc, C. Mandon, C. Billotey, A. L. Meur-Herland, T. Brochard, F. Vocanson, M. Janier, P. Perriat, S. Roux and O. Tillement, *J. Am. Chem. Soc*. **2008**, 130, 5908–5915 (Gadolinium chelate coated gold nanoparticles as contrast agents for both X-ray computed tomography and magnetic resonance imaging)

[60] C. Alric, R. Serduc, C. Mandon, J. Taleb, G. Le Duc, A. Le Meur-Herland, C. Billotey, P. Perriat, S. Roux and O. Tillement *Gold Bulletin* **2008** 41, 90-97 (Gold nanoparticles designed for combining dual modality imaging and radiotherapy).

[61] J.A. Park, H.K. Kim, J.H. Kim, S.W. Jeong, J.C. Jung, G.H. Lee, J. Lee, Y. Chang and T.-J. Kim, *Bioorg. Med. Chem. Lett.* **2010**, 20, 2287–2291 (Gold nanoparticles functionalized by gadolinium–DTPA conjugate of cysteine as a multimodal ioimaging agent).

[62] H.K. Kim, H.-Y. Jung, J.A. Park, M.I. Huh, J.C. Jung, Y. Chang and T.J. Kim, *J. Mater. Chem*. **2010**, 20, 5411–5417 (Gold nanoparticles coated with gadolinium-DTPA-bisamide conjugate of penicillamine (Au@GdL) as a T_1-weighted blood pool contrast agent)

[63] L. Moriggi, C. Cannizzo, E. Dumas, C. R. Mayer, A. Ulianov and L. Helm, *J. Am. Chem. Soc*. **2009**, 131, 10828–10829 (Gold Nanoparticles Functionalized with Gadolinium Chelates as High-Relaxivity MRI Contrast Agents)

[64] Y. T. Lim, M. Y. Cho, B. S. Choi, J. M. Lee and B. H. Chung, *Chem. Commun*. **2008**, 4930–4932 (Paramagnetic Au-NPs for dual modal bioimaging and phototherapy of cancer cells)

[65] M. F. Warsi, R. W. Adams, S. B. Duckett and V. Chechik, *Chem. Commun*. **2010**, 46, 451–453 (Gd-functionalised Au nanoparticles as targeted contrast agents in MRI: relaxivity enhancement by polyelectrolyte coating).

[66] M.D Chavanpatil,.; A Khdair,.; J. Panyam, *Pharm. Res*. **2007**, 24, 803-810. (Surfactant–polymer nanoparticles: a novel platform for sustained and enhanced cellular delivery of water-soluble molecules)

[67] J. H. Park, S. Kwon, M. Lee, H. Chung, J. H. Kim, Y. S. Kim, R. W. Park, I. S. Kim, S. B. Seo, I. C. Kwon and S. Y. Jeong, *Biomaterials* **2006**, 27, 119-126 (Self-assembled nanoparticles based on glycol chitosan bearing hydrophobic moieties as carriers for doxorubicin: In vivo biodistribution and anti-tumor activity)

[68] Y. Song, X. Xu, K.W. MacRenaris, X.Q. Zhang, C.A. Mirkin and T.J. Meade, *Angew. Chem. Int. Ed*. **2009**, 48, 1–6

containing DNA–gold nanoparticles could efficiently penetrate cells and accumulate in such a way to successfully perform cellular MR imaging.

On the other hand, carbohydrate-based MRI probes have been less often used to specifically target cells receptors in spite of the enormous information that carbohydrates encode (the so-called "glyco-code"). [69] Apart of being good candidates for targeting, carbohydrates have been used to confer hydrophilicity to small molecules contrast agents slowing their molecular motion and increasing the water density surrounding the paramagnetic metal ion. [70] [71] The introduction of sugar molecules also enhances water solubility of the contrast agent, considered to be highly beneficial by enhancing renal excretion and so, increasing clearance from the vasculature. [70] Fulton *et al.* synthesized symmetric and medium molecular weight (MW) conjugates incorporating glucose or galactose groups linked via four dendritic wedges to a central Gd complex. These compounds present high relaxivities (r_1 = 23.5 $mM^{-1}s^{-1}$ and r_1 = 19.6 $mM^{-1}s^{-1}$ respectively). The presence of a well-defined network of second-sphere water molecules localized between the glucose (or galactose) groups and the Gd(III) ion could significantly contribute to increase relaxivity. [72] The group of Meade proposed the covalent attachment of Gd(III) complexes to β-cyclodextrins to generate novel contrast agents (r_1 = 12.2 $mM^{-1}s^{-1}$). [73] These compounds possesses from three to seven Gd(III) chelates per molecule, and exhibit excellent biocompatibility.

The couple sugar-metallic nanoparticle (glyconanoparticles) has also attracted much attention in order to address biological problems (not exclusively related to MRI) by means of carbohydrate-mediate recognition in tandem with detection properties of nanoparticles. [74], [75] For example, Huang *et al.* reported that superparamagnetic glyconanoparticles (T_2 agents) can work as MRI sensors to detect and differentiate cancer cells based on the different expression of carbohydrate receptors at cell surface. [76] Davis and collaborators demonstrated that cross-linked iron oxide

---

[69] H.J. Gabius, H.C. Siebert, S. Andry, J. Jiménez-Barbero, and H. Rüdiger, *ChemBiChem* **2004,** 5, 740-764 (Chemical Biology of the Sugar Code)

[70] L. Cipolla, M. Gregori and P.-W. So, *Curr. Med. Chem.* **2011,** 18, 1002-1018 **(**Glycans in Magnetic Resonance Imaging: Determinants of Relaxivity to Smart Agents, and Potential Applications in Biomedicine**)**

[71] A. Barge, G. Cravotto, B. Robaldo, E. Gianolio and S. Aime, *J. Inclusion Phenom. Macrocycl. Chem.* **2007**, 57, 489-495 (New CD derivatives as self-assembling contrast agents for magnetic resonance imaging).

[72] D. Fulton, E.M. Elemento, S. Aime, L. Chaabane, M. Botta and D. Parker, *Chem. Commun.* **2006**, 1064-1066 (Glycoconjugates of gadolinium complexes for MRI applications).

[73] Y. Song, E.K. Kohlmeir and T.J. Meade, *J. Am. Chem. Soc.* **2008**, 130, 6662-6663 (Systems of multimeric MR contrast agents for cellular imaging).

[74] M. Marradi, M. Martín-Lomas and S. Penadés, *Adv. Carbohydr. Chem. Biochem.* **2010**, 64, 211–290 (Glyconanoparticles: Polyvalent tools to study carbohydrate-based interactions)

[75] El-Boubbou K. and Huang X. *Curr. Med. Chem.* **2011**, 18, 2060-2078 (Glyco-Nanomaterials: Translating Insights from the "Sugar-Code" to Biomedical Applications)

[76] K. El-Boubbou, D. C. Zhu, C. Vasileiou, B. Borhan, D. Prosperi, W. Li and X. Huang, *J. Am. Chem. Soc.* **2010**, 132, 4490-4499 (Magnetic Glyco-Nanoparticles: A Tool To Detect, Differentiate and Unlock the Glyco-Codes of Cancer via Magnetic Resonance Imaging).

(CLIO) amine-functionalized dextran-coated nanoparticles are an efficient platform for the incorporation of multiple copies of sialyl Lewis X (sLe^X) tetrasaccharide and that these superparamagnetic glyconanoparticles can visualise *in vivo* by MRI the expression of P-selectins after brain injury on activated endothelial cells outside the blood brain barrier. [77] As far as we know, these two works are the only ones that make use of the glyco-code for MRI application of nanoparticles. Both works use superparamagnetic iron oxide glyconanoparticles (T_2-imaging probes) and do not include gold in their core.

Our laboratory has been pioneer in the conjugation of thiol-ending glycoconjugates to gold-based nanoclusters for the preparation of water-soluble gold glyconanoparticles (GNPs). [78], [79] The carbohydrate ligands are "covalently" linked to the metallic (gold) nucleus (Figure 3) and this coating confers to the nanomaterials stability and solubility, biocompatibility and non toxicity in biological media. At the same time, because carbohydrates are implicated in many cell recognition mechanisms and cell-signalling phenomena, they can be used to target specifically defined cells *in vivo*, as already mentioned. Multivalent presentation of carbohydrates on the nanoparticles allows an efficient targeting by enhancing the affinity of binding to the corresponding receptor, a phenomena which is known as the glycocluster effect. [80] The glyconanoparticle technology [79] allows the preparation of a variety of water-soluble glycoclusters with different ligand density and variable linkers to modulate rigidity and flexibility and to confer accessibility to the ligands. The nature (hydrophilic or hydrophobic), the length and the flexibility of the spacer can be selected to control the presentation of the carbohydrates on the cluster surface, which influences their accessibility to the ligands and behaviour during the molecular recognition events.

[77] S. I. van Kasteren, S. J. Campbell, S. Serres, D. C. Anthony, N. R. Sibson and B. G. Davis, *Proc. Natl. Acad. Sci. USA,* **2009**, 106, 18-23 (Glyconanoparticles allow pre-symptomatic in vivo imaging of brain disease).
[78] J.M. de la Fuente, A.G. Barrientos, T.C. Rojas, J. Rojo, J. Canada, A. Fernandez and S. Penades, *Angew. Chem. Int. Ed.* **2001**, 40, 2257-2261 (Gold Glyconanoparticles as Water-Soluble Polyvalent Models To Study Carbohydrate Interactions)
[79] J. M. de la Fuente, S. Penadés, *BBA,* **2006**, 1760, 636–651 (Glyconanoparticles: Types, synthesis and applications in glycoscience, biomedicine and material science).
[80] Y.C. Lee and R.T. Lee, *Acc. Chem. Res*. **1995**, 28, 321-327. (Carbohydrate-Protein interactions: Basis of Glycobiology)

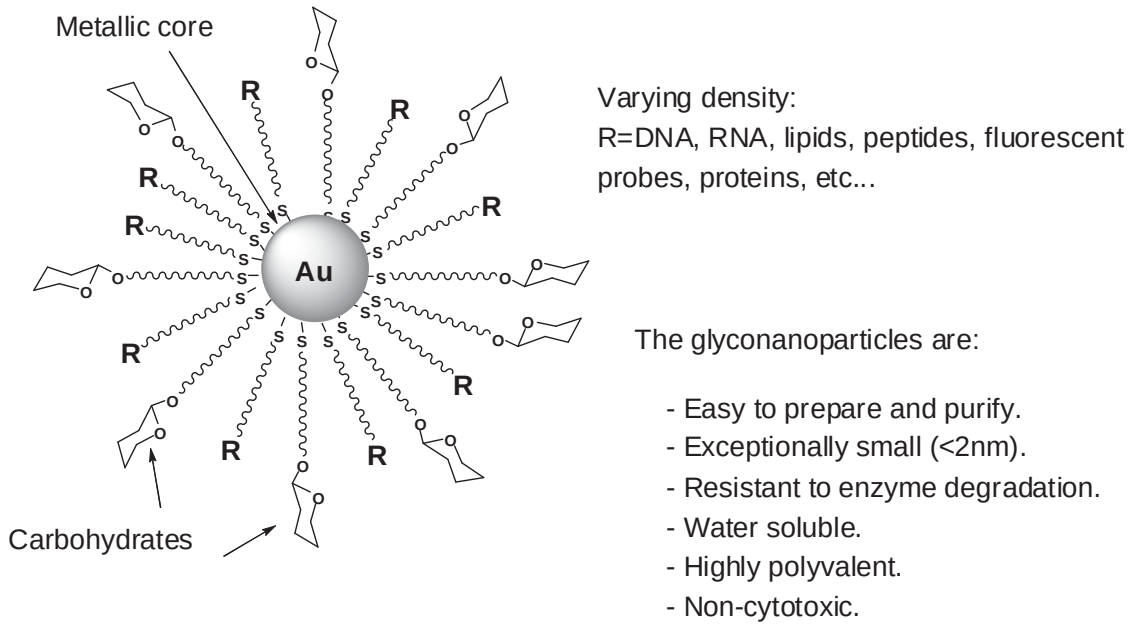

Figure 3: *Glyconanoparticles (GNPs) as multivalent and multifunctional carbohydrate-based nanomaterials.*

The preparation of the glyconanoparticles was performed by a one-step method ("direct" method) through addition of a methanolic or aqueous solution of thiol-ending glycoconjugates of the dissacharide lactose (Galβ1-4Glcβ1) or the trisaccharide Lewis X (Galβ1-4[Fucα 1-2]GlcNAcβ1, Le^X) to an aqueous solution of tetrachloroauric acid ($HAuCl_4$) and subsequent reduction with $NaBH_4$. [78] These GNPs were originally prepared to investigate the selective self-recognition of the Le^X antigen via carbohydrate-carbohydrate interaction by different techniques: isothermal titration calorimetry (ITC), transmission electron microscopy (TEM), atomic force microscopy (AFM), and surface plasmon resonance (SPR). [81] This methodology provides a versatile way to prepare in one-step a great variety of polyvalent carbohydrate arrays on three-dimensional scaffolds with globular shape. The GNPs prepared in this way are water soluble, stable in solution, non-cytotoxic and the metallic core diameter is between 1 to 2 nanometers (Figure 3). Following this method, a variety of hybrid glyconanoparticles with different carbohydrate densities (high and low) have been prepared by our laboratory in a controlled way. The design and preparation of a small library of multivalent gold glyconanoparticles presenting truncated (oligo)mannosides of the high-mannose undecasaccharide $Man_9GlcNAc_2$ (*manno*-GNPs) is an

[81] J. M. de la Fuente and S. Penadés, *Glycoconj. J.* **2004**, 21, 149–163 (Understanding carbohydrate-carbohydrate Interactions by means of glyconanotechnology)

example. [82] These GNPs were tested as inhibitors of lectin DC-SIGN binding to gp120 of human immunodeficiency virus (HIV) [82] and as inhibitors of DC-SIGN-mediated HIV *trans*-infection of human T cells. [83] In addition, the glyconanoparticle platform provides the possibility to attach other molecules on the surface of the same nanoparticles (fluorescent probes [84], peptides [84], sulfate-ended ligands [85]), to get multifunctional nanoplatforms. In general, many groups took profit of this technology to prepare GNPs and a number of reviews account for that. [74], [79], [86], [87], [88]

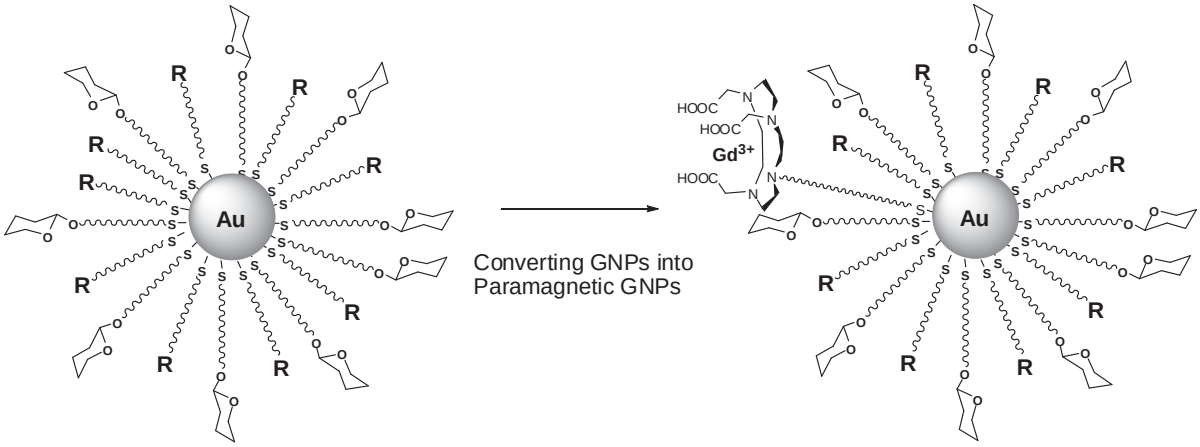

Figure 4: *From gold glyconanoparticles to paramagnetic Gd-based gold glyconanoparticles.*

Gold GNPs can be converted directly into paramagnetic probes by modifying the organic shell through the introduction of a gadolinium complex as an additional ligand (Figure 4). Hybrid glyconanoparticles having on the same gold nanoplatform sugar conjugates and Gd(III) chelates

[82] O. Martínez-Ávila, K. Hijazi, M. Marradi, C. Clavel, C. Campion, C. Kelly, and S. Penadés *Chem. Eur. J.* **2009**, 15, 9874-9888 (Gold Manno-Glyconanoparticles: Multivalent Systems to Block HIV-1 gp120 Binding to the Lectin DC-SIGN).

[83] O. Martínez-Ávila, L. M. Bedoya, M. Marradi, C. Clavel, J. Alcamí, and S. Penadés, *ChemBioChem* **2009**, 10, 1806–1809 (Multivalent Manno-Glyconanoparticles Inhibit DC-SIGN-Mediated HIV-1 Trans-Infection of Human T Cells)

[84] R. Ojeda, J. L. de Paz, A. G. Barrientos, M. Martín-Lomas and S. Penadés, *Carbohydr. Res*. **2007**, 342, 448–459. (Preparation of multifunctional glyconanoparticles as a platform for potential carbohydrate-based anticancer vaccines)

[85] P. Di Gianvincenzo, M. Marradi, O. M. Martínez-Ávila, L. Miguel Bedoya, J. Alcamí and Soledad Penadés, *Bioorg. Med. Chem. Lett.* **2010**, 20, 2718–2721 (Gold nanoparticles capped with sulfate-ended ligands as anti-HIV agents)

[86] I. Garcia, J. Gallo, M. Marradi and S. Penadés in Engineered Carbohydrate-Based Materials for Biomedical Applications, ed. R. Narain, Wiley, New Jersey, **2011**, pp. 213-259.

[87] Synthesis and Biological Applications of Glycoconjugates, Bentham E-book, ed: O. Renaudet, co-ed: N. Spinelli, **2011**, Chapter 10, pp 164-202 (Glycoliposomes and Metallic Glyconanoparticles in Glycoscience)

[88] *Prog. Mol. Biol. Transl. Sci*., Elsevier **2011**, 104, Chapter 4, 141-173 (Carbohydrate-Based Nanoparticles for Potential Applications in Medicine)

have been prepared in our laboratory using the one-step ("direct") method. [89] The combination of sugars and a Gd-complex can provide a contrast agent with targeting properties, high biocompatibility and high loading of Gd. [57] Glucose was selected with the idea of crossing the blood brain barrier and reaches easier the tumor.

Thiol-ending neoglycoconjugates of glucose, galactose or lactose were used in tandem with *N*-alkyl (pentyl or undecanyl) tetraazacyclododecane triacetic acid (DO3A) derivative to coat the gold nanoclusters. It was found that both sugar stereochemistry and the relative position of the sugar with respect to the Gd (III) ion seem to control the relaxivity values of these GNPs. The best Gd-based GNPs yielded T_1-relaxivity above 20 $mM^{-1}s^{-1}$, which is over six times the value of in clinical use Dotarem®. These GNPs were used for *in vivo* imaging of glioma in mice. The results showed that at the same Gd(III) concentration glucose-bearing Gd-based GNPs are able to enhance the contrast in the tumoral zones better than in clinical use contrast agents Dotarem®, while lactose-bearing Gd-based GNPs do not seem to reach the tumor, although they highly enhance the contrast outside the brain. It seems that the nature of the sugar also influences the behaviour of GNPs as *in vivo* contrast agents. Probably, liver uptake is responsible for the less effective *in vivo* contrast enhancement of $LacC_5S$-Au-SC_{11}DO3A:Gd GNPs (e.g. nanoparticles coated with ~90% of lactose conjugate and ~10% of Gd complex) in the brain tumor. It is known that the asialoglycoprotein receptor which is expressed exclusively in hepatic parenchymal cells binds specifically to galactosyl-terminal glycoproteins [90] and thus it could be responsible of this uptake. To the best of our knowledge, there are no other examples of GNPs that incorporate Gd (III) in the organic shell.

The main aim of the work presented in this PhD Thesis was to improve the first results obtained in our laboratory in the synthesis of glyconanoparticles as MRI contrast agents by the "direct" method, [89] to study the targeting properties of the Gd-based glyconanoparticles for *in vitro* labelling specifically cells, and to apply them to the *in vivo* detection of gliomas by MRI. One of the limitations of the Gd-based paramagnetic gold GNPs prepared by the "direct" method is related to the control of the Gd(III) amount in each GNP. Gd-loading was low and changes from one GNP to another, probably due to additional chelation of Gd cations by the hydroxy groups of the sugars. We considered, thus, necessary to develop a reproducible method of preparation of Gd-based GNPs in which we control the amount of Gd(III) without loosing the high relaxivity

[89] M. Marradi, D. Alcántara, J. Martínez de la Fuente,M. L. García-Martín, S.Cerdán and S. Penadés, *Chem. Commun.* **2009**, 26, 3922–3924 (Paramagnetic Gd-based gold glyconanoparticles as probes for MRI: tuning relaxivities with sugars).

[90] J. Lunney and G. Ashwell, *Proc. Natl. Acad. Sci. U. S. A.* **1976**, 73, 341-343 (A hepatic receptor of avian origin capable of binding specifically modified glycoproteins)

values obtained by the "direct" method. For this reason, we set up a new protocol based on the Murray's "thiol for thiol" ligand place exchange (LPE) method [91] in which 100% sugar-coated GNPs were incubated with thiol-ended Gd-complexes conjugates.

Once we had in hands the tool, the next step would have been to test its effectiveness as T_1 receptor reporter in cellular models taking advantage of the targeting properties of the "glyco-code" of the carbohydrates. Following the cellular experiments, the GNPs would have been be tested as paramagnetic contrast agents for *in vivo* brain tumor detection in mice and the results compared with those obtained with the GNPs prepared by "direct" synthesis. The *in vivo* experiments have been carried out in collaboration with the Grup d'Aplicacions Biomèdiques de la RMN (GABRMN) at the Universitat Autónoma de Barcelona headed by Carles Arús. Finally, biodistribution and toxicological profile experiments have been performed in collaboration with the group of Simó Schwartz (CIBBIM-Nanomedicine, Hospital Universitai Vall d'Hebron) associated to the Universitat Autónoma de Barcelona, in order to check the behaviour of the GNPs inside the body.

The concrete aims which were proposed in this Thesis can be divided as follows (Scheme 1):

1. Preparation of a small library of Gd-based paramagnetic gold glyconanoparticles by setting up a "thiol for thiol" ligand place exchange (LPE) method. Different spacers, neoglycoconjugates and DO3A derivatives were used to obtain the best relaxivity values. Characterization of the GNPs was performed by physico-chemical techniques (NMR, IR, UV, elemental analysis, TEM, ICP, etc.), and measurement of their longitudinal (T_1) and transversal (T_2) relaxation times allowed the calculation of the corresponding relaxivities (r_1 and r_2).
2. Application of three of the GNPs prepared to the labelling of cells in order to check whether they could work as T_1 specific reporters of cellular surface receptors.
3. *In vivo* studies of the GNPs synthesized to confirm that they can be used as paramagnetic contrast agents for brain tumor detection in mice and evaluation of the biodistribution and toxicological profile.

[91] M. J. Hostetler, A. C. Templeton, and R. W. Murray, *Langmuir,* **1999**, 15, 3782-3789 (Dynamics of place-exhange reactions on monolayer-protected gold cluster molecules)

Scheme 1: *Objectives proposed in this Thesis.*

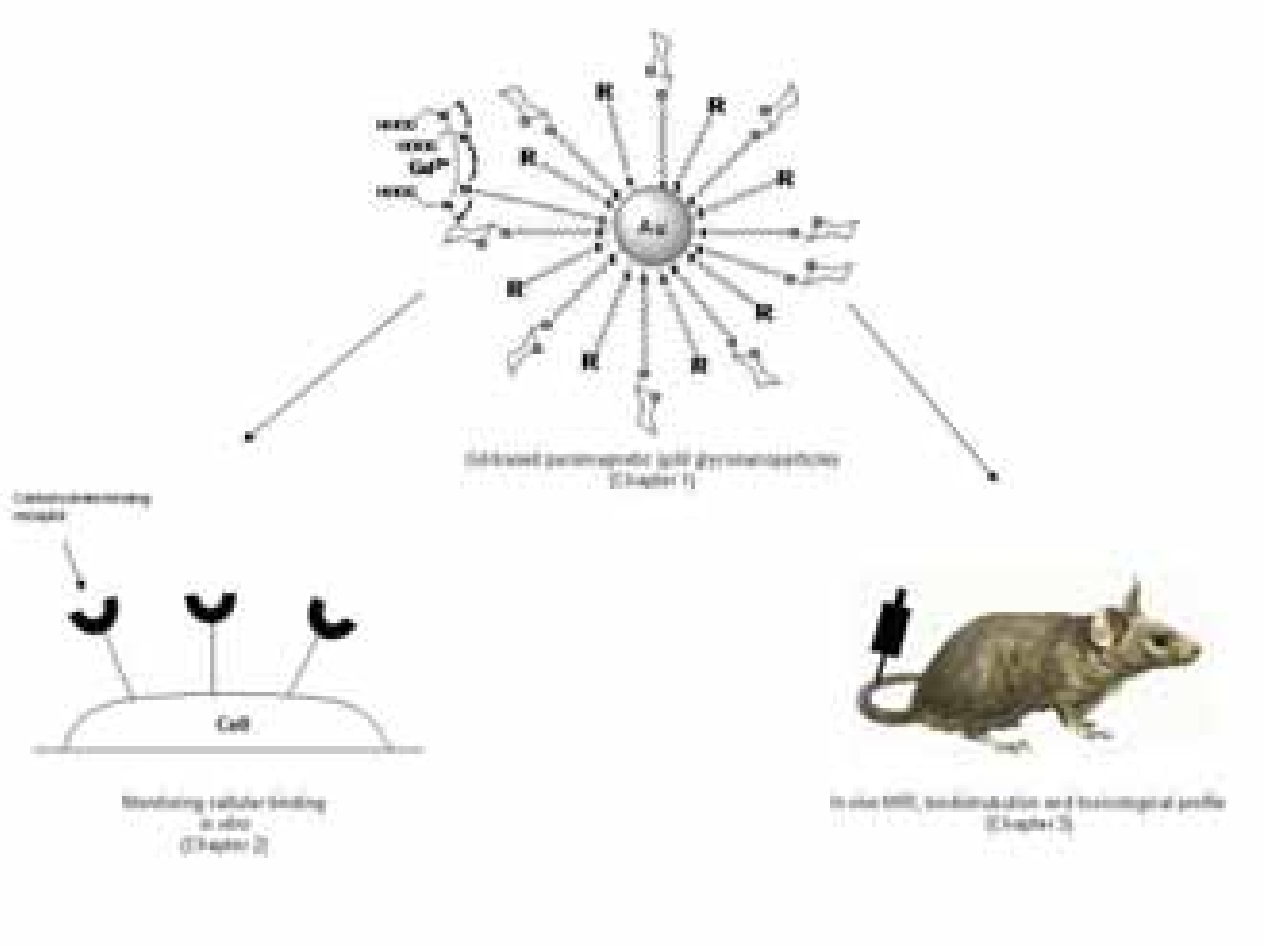

CHAPTER 1

PREPARATION AND CHARACTERIZATION OF Gd-BASED PARAMAGNETIC GOLD GLYCONANOPARTICLES

PREPARATION AND CHARACTERIZATION OF Gd-BASED PARAMAGNETIC GOLD GLYCONANOPARTICLES

The preparation of water soluble and biofunctional gold glyconanoparticles (GNPs) in which the ligands (glycoconjugates and DO3A derivatives) are covalently linked to the gold surface needs the conjugation of carbohydrates and chelating agents to a spacer ending in a thiol group, as the "soft" character of both gold and sulfur allows the formation of stable bonds. [1] A comprehensive review on the preparation of gold glyconanoparticles (GNPs) has been recently published. [2] There are mainly two protocols for the preparation of GNPs: (i) A "direct" method that consists in controlling the growth of nascent metal by *in situ* reduction of a gold salt in the presence of ligands bearing a thiol-ending group [3]; (ii) A "stepwise" method that makes use of ligand place exchange (LPE) reactions between the attached thiol ligands on preformed gold nanoparticles and thiol-derivatized ligands to be inserted onto the gold surface. Figure 1.1 shows the main methods for the preparation of gold glyconanoparticles.

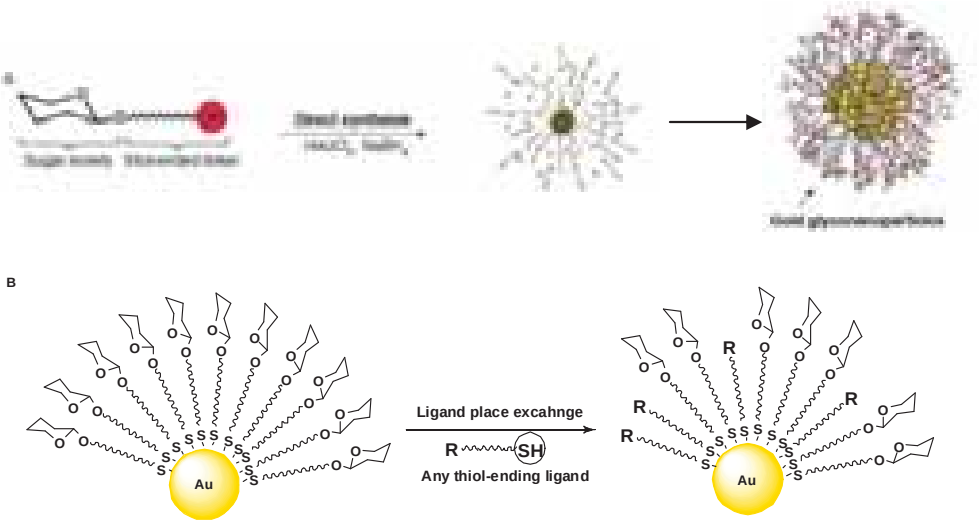

Figure 1.1: *Main methods for the preparation of gold glyconanoparticles (GNPs). (A) "Direct" synthesis based on the reduction of a Au(III) salt and in situ protection of the gold nanocluster with thiol-armed glycoconjugates. (B) Ligand place exchange (LPE) reactions based on the treatment of preformed gold nanoparticles with thiol-derivatized glycoconjugates. [2]*

[1] C.S. Weisbecker, M.V. Merrit and G.M. Whiteside, *Lagmuir,* **1996**, 12, 3763-3772 (Molecular Self-Assembly of Aliphatic Thiols on Gold Colloids).
[2] M. Marradi, M. Martín-Lomas and S. Penadés, *Adv. Carbohydr. Chem. Biochem*., **2010**, 64, 211-290 (GNPs Polyvalent Tools to Study Carbohydrate-Based Interactions)
[3] M. Brust, M. Walker, D. Bethell, D. J. Schiffrin, and R. Whyman, *J. Chem. Soc. Chem. Commun*, **1994**, 801–802 (Synthesis of thiol-derivatized gold nanoparticles in a 2-phase liquid–liquid system)

In this Thesis, hybrid gold glyconanoparticles coated with different sugar conjugates and DOTA derivatives were prepared mainly by LPE protocol. The GNPs coated only with sugars were first prepared by the "direct" method and then submitted to ligand exchange with the Gd-complex derivatives previously prepared.

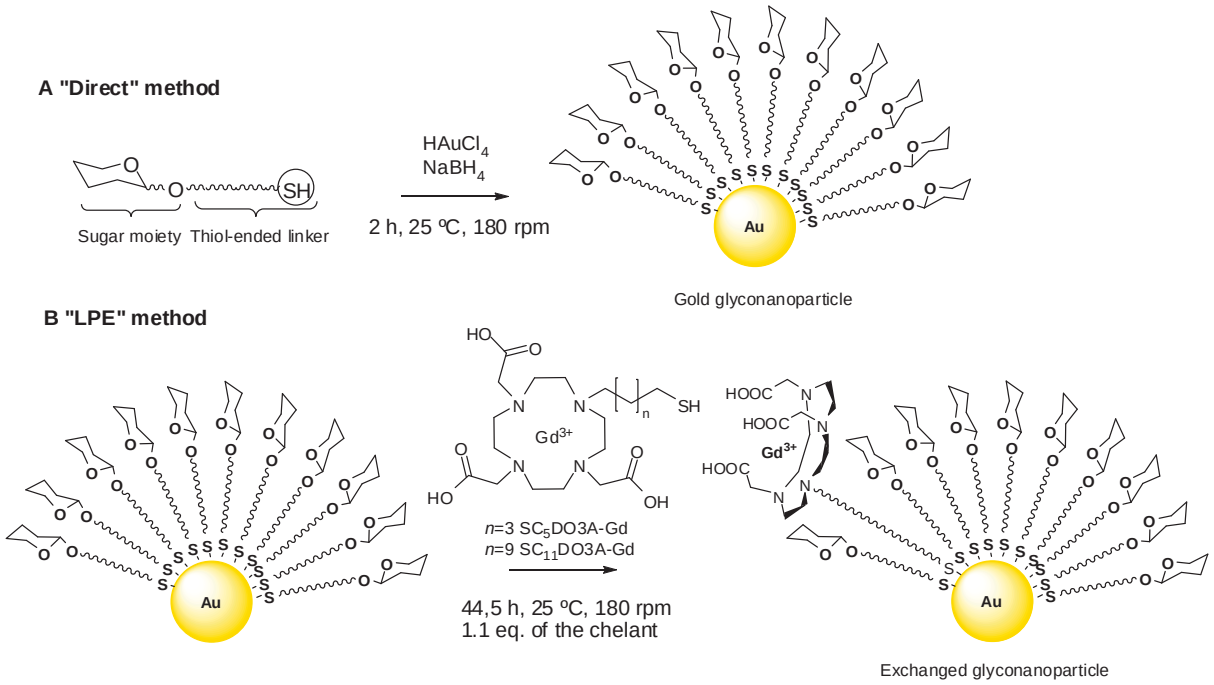

Figure 1.2: *Synthetic strategies for the preparation of Gd-based paramagnetic gold glyconanoparticles. (A) "Direct" method to obtain 100% sugar-coated GNPs and (B) subsequent incubation of these GNPs with Gd-containing thiol-ending ligands to convert them into paramagnetic probes by ligand place exchange (LPE) reactions.*

The "direct" method, based on the modification of the two-phase Brust-Schiffrin's synthesis [3], has been set up in our laboratories for the preparation of broad variety of water-soluble sugar-functionalized gold nanoparticles (Figure 1.1A). [4] Gd-based gold GNPs were first prepared by adding an aqueous solution of tetrachloroauric acid to a methanolic solution of a mixture of variable proportions of glycoconjugates and DOTA derivatives in reducing conditions. [5] In this way, stable dispersion of < 5 nm sized thiol-coated gold nanoparticles were obtained, which could be isolated and re-dissolved without aggregation or decomposition. After that, the conversion of these hybrid gold GNPs into paramagnetic probes was achieved by incubation with Gd(III) salts

[4] J. M. de la Fuente, S. Penadés, *BBA,* **2006**, 1760, 636–651 (Glyconanoparticles: Types, synthesis and applications in glycoscience, biomedicine and material science).
[5] M. Marradi, D. Alcántara, J. Martínez de la Fuente, M. L. García-Martín, S.Cerdán and S. Penadés, *Chem. Commun.,* **2009**, 26, 3922–3924 (Paramagnetic Gd-based gold glyconanoparticles as probes for MRI: tuning relaxivities with sugars)

(Figure 1.2A). [5] We observed that the incubation with Gd(III) of the GNPs obtained in by "direct" method lacks of reproducibility because some of the Gd(III) is chelated by the hydroxy groups of the sugars. Thus, we decided in this Thesis to address the preparation of the paramagnetic GNPs by the "stepwise" method in order to improve the reproducibility and obtain a better control over the Gd(III) content in the GNPs. In this approach, gold glyconanoparticles having 100% of the selected sugar were first prepared and then submitted to ligand place exchange with a Gd-complex conjugate (Figure 1.2B).

The advantage of this LPE methodology consists in the introduction onto the gold surface of the previously prepared Gd-chelates, resulting in a better control of the amount of Gd(III) in the GNPs. Following this approach, a small library of paramagnetic Gd-based gold glyconanoparticles has been prepared and characterized and their relaxation times T_1 and T_2 have been determined at 1.41 (60 MHz) and 11.7 (500 MHz) Teslas (T). The diameter of the gold core can be correlated to the number of ligands present on the GNP [6]. For example, the size of the gold cores of the GNPs here prepared range from 1.5 to 2.5 nm which can content between 116 and 586 gold atoms and 40 to 135 ligand chains on the surface. Depending on the LPE reaction, the number of Gd-complex ligand can vary. Figure 1.3 is a schematic representation of the structure of the paramagnetic glyconanoparticles prepared. Three monosaccharides, glucose (Glc), galactose (Gal), and mannose (Man) and three disaccharides, maltose (*maltose*), cellobiose (*cellobiose*), and lactose (Lac) were selected for the preparation.

[6] M. J. Hostetler *et al.*, *Langmuir,* **1998**, 14, 17-30. (Alkanethiolate gold cluster molecules with core diameters from 1.5 to 5.2 nm: Core and monolayer properties as a function of core size).

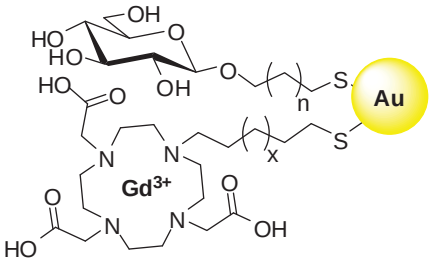

n=0, x=7 $GlcC_2S$-Au-SC_{11}DO3A-Gd
n=1, x=7 $GlcC_3S$-Au-SC_{11}DO3A-Gd
n=3, x=7 $GlcC_5S$-Au-SC_{11}DO3A-Gd
n=3, x=1 $GlcC_5S$-Au-SC_5DO3A-Gd
n=5, x=7 $GlcC_7S$-Au-SC_{11}DO3A-Gd
n=7, x=7 $GlcC_9S$-Au-SC_{11}DO3A-Gd

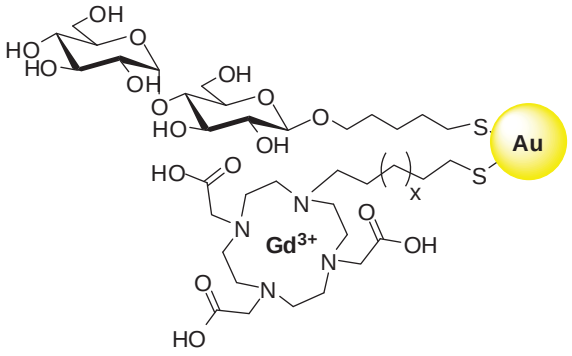

x=7 *Maltose*C_5S-Au-SC_{11}DO3A-Gd
x=1 *Maltose*C_5S-Au-SC_5DO3A-Gd

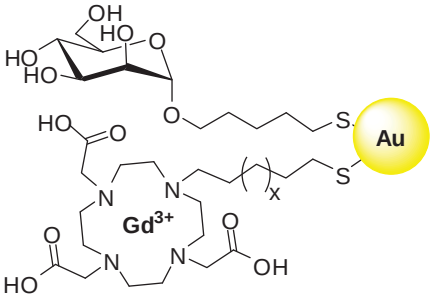

x=7 $ManC_5S$-Au-SC_{11}DO3A-Gd
x=1 $ManC_5S$-Au-SC_5DO3A-Gd

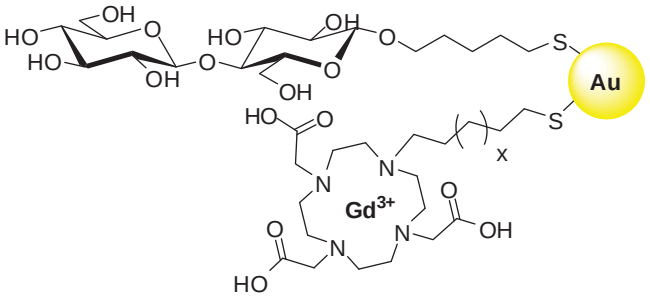

x=7 *Cellobiose*C_5S-Au-SC_{11}DO3A-Gd
x=1 *Cellobiose*C_5S-Au-SC_5DO3A-Gd

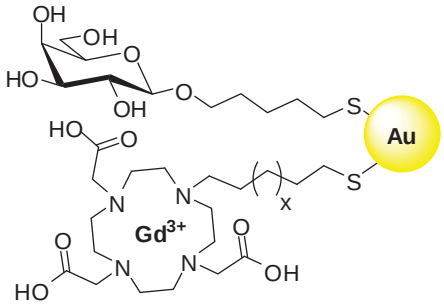

x=7 $GalC_5S$-Au-SC_{11}DO3A-Gd
x=1 $GalC_5S$-Au-SC_5DO3A-Gd

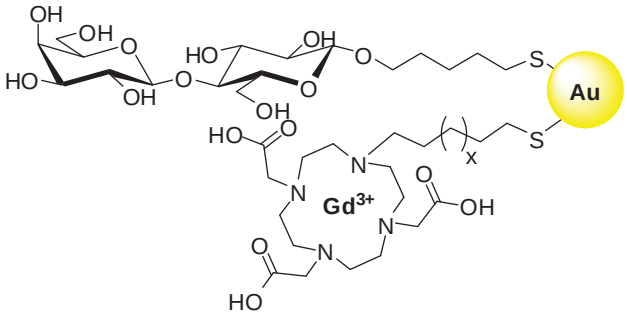

x=7 $LacC_5S$-Au-SC_{11}DO3A-Gd
x=1 $LacC_5S$-Au-SC_5DO3A-Gd

Figure 1.3: *Schematic representation of the paramagnetic Gd-based gold glyconanoparticles prepared in this Thesis by ligand place exchange (LPE) reactions.*

1. Spacers, neoglycoconjugates and DO3A derivatives

The first step for the preparation of GNPs is the synthesis of the molecules implicated in their formation: Neoglycoconjugates and DO3A or DOTA-derivatives bearing a thiol-ending linker. Different carbohydrate conjugates of the monosaccharides β-glucose, β-galactose and α-mannose and the disaccharides β-maltose, β-lactose and β-cellobiose were selected to check their influences both in magnetic properties [longitudinal (T_1) and transversal (T_2) relaxation times and the corresponding relaxivities (r_1 and r_2)] and behaviour in cells. Glucose, galactose, mannose and lactose are involved in the metabolism of cells, while maltose and cellobiose are no implicated in the biochemistry of cells, although they can be recognized by membrane receptors of the cells. Different types of linear and alifatic primary alcohols having at the other *C*-terminus a thiol-protected functionality [11-(*S*-acetyl)mercaptoundecan-1-ol and 5-(*S*-acetyl)mercaptopentan-1-ol] or a functional group which could be interconverted into a thiol functionality at a later stage of the synthetic process (4-penten-1-ol, allyl alcohol, 2-bromoethanol, 7-bromoheptan-1-ol and 9-bromononan-1-ol), were conjugated to the protected sugars in order to have in hand suitable thiol-ending glycoconjugates for attaching them to the gold nanoclusters by thiol chemistry.

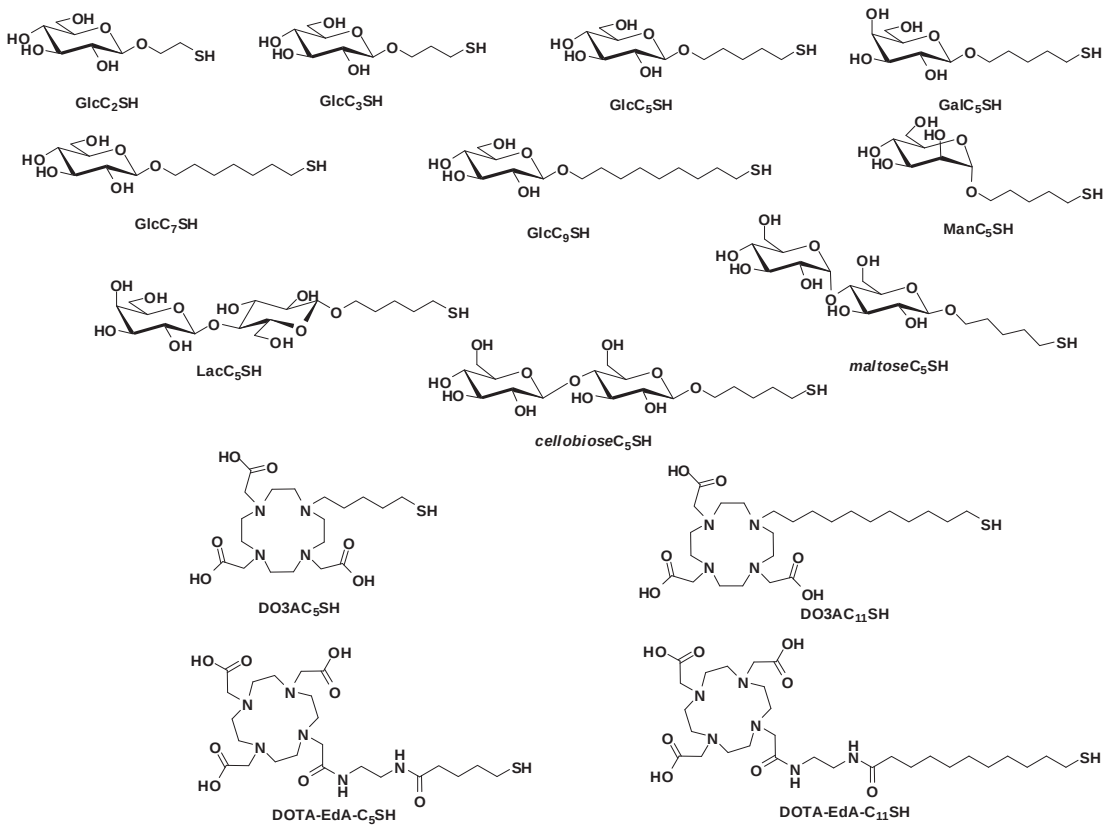

Figure 1.4: *Neoglycoconjugates, DO3A derivatives and DOTA-EdA derivatives synthesized in this Thesis to prepare the paramagnetic Gd-based gold glyconanoparticles.*

On the other hand, 1, 4, 7, 10-tetraazacyclododecane-1, 4, 7-triacetic acid (DO3A) derivatives and 1, 4, 7, 10-tetraazacyclododecane-1, 4, 7-triacetic acid-*N*-(2-aminoethyl)ethanamide (DOTA-amine) derivatives were selected to chelate the Gd(III) cation. In order to attach these chelating agents to the gold surface, the DO3A and the DOTA-amine were functionalized with a five or an eleven carbon atoms thiol-ending linker (1-bromo-5-triphenilmethylmercaptopentane or 1-bromo-11-triphenilmethylmercaptoundecane for DO3A; 5-(*S*-acetyl)mercaptopentanoic acid or 11-(*S*-acetyl)mercaptoundecanoic acid for DOTA-amine) to obtain the derivatives $DO3AC_5SH$, $DO3AC_{11}SH$, DOTA-EdA-C_5SH and DOTA-EdA-$C_{11}SH$ (EdA=ethylene diamide) depicted in Figure 1.4.

The preparation of glycoconjugates, DO3A derivatives and DOTA-EdA derivatives required the previous synthesis of bifunctional spacers having a thiol-protecting group at one terminus and a reacting group at the other terminus as explained in the next paragraph.

1.1 *Synthesis of spacers*

Five different bifunctional linkers were synthesised: 11-(*S*-acetyl)mercaptoundecan-1-ol (**1**) [7], 1-bromo-11-triphenilmethylmercaptoundecane (**2**), 11-(*S*-acetyl)mercaptoundecanoic acid (**3**), 5-(*S*-acetyl)mercaptopentanoic acid (**4**) and 1-bromo-5-triphenilmethylmercaptopentane (**6**) (Schemes 1.1 and 1.2). 5-(*S*-acetyl)mercaptopentan-1-ol was synthesized following the method published by us. [8]

11-(*S*-acetyl)mercaptoundecan-1-ol (**1**) was obtained by the reaction of the commercial 11-bromoundecanol with potassium thioacetate (KSAc) in dimethylformamide (DMF) with 70% yield after purification by flash column chromatography (FCC) (Scheme 1.1). Similarly, commercial 4-bromopentanoic acid was reacted with KSAc in DMF to afford 5-(*S*-acetyl)mercaptopentanoic acid (**4**). After purification by FCC, 65% yield was obtained (Scheme 1.1). The ^{1}H-NMR spectra of the thioacetyl derivatives showed a singlet at 2.32 ppm (**1**) and 2.25 ppm (**4**) corresponding to the methyl of the thioacetate group. The triplet which corresponds to the methylene group in α-position respect to the sulphur atom shifted at lower ppm (2.86 ppm) comparing to the methylene next to the bromo functional group (3.42 ppm).

[7] A. G. Barrientos, J. M. de la fuente, T. C. Rojas, A. Fernández and S. Penadés, *Chem. Eur. J.*, **2003**, 9, 1909-1921 (Gold Glyconanoparticles: Synthetic Polyvalent Ligands Mimicking Glycocalyx-Like Surfaces as Tools for Glycobiological Studies)

[8] O. Martínez-Ávila, K. Hijazi, M. Marradi, C. Clavel, C. Campion, C. Kelly, and S. Penadés *Chem. Eur. J.* **2009**, 15, 9874-9888 (Gold Manno-Glyconanoparticles: Multivalent Systems to Block HIV-1 gp120 Binding to the Lectin DC-SIGN).

In order to get compound **2**, **1** was first treated with sodium methoxide (MeONa) in methanol followed by the addition of trityl chloride (TrtCl) in dry tetrahydrofuran (THF) to obtain, after purification by FCC, 11-triphenylmethylmercaptoundecan-1-ol (**5**) with 52% yield (Scheme 1.1). [9] In the ^{1}H-NMR spectrum, the singlet at 2.32 ppm disappeared and aromatic signals corresponding to the trityl group (7.42-7.20 ppm) appeared. Also, the triplet which correspond to the methylene group in α position respect to the sulphur atom shifted form 2.86 ppm in **1** (SAc) to 2.13 ppm in **5** (STrt). Afterwards, **5** was dissolved in dry dichloromethane and then triphenylphosphine and tetrabromomethane were added to afford 1-bromo-11-triphenilmethylmercaptoundecane (**2**) with 63% yield after purification by FCC (Scheme 1.1). In the ^{1}H-NMR spectrum, the triplet at 3.63 ppm characteristic of the methylene bonded to the alcohol disappeared and a triplet at 3.42 ppm characteristic of the methylene bonded to the bromine atom appeared, confirming that the functional group interconversion was successful.

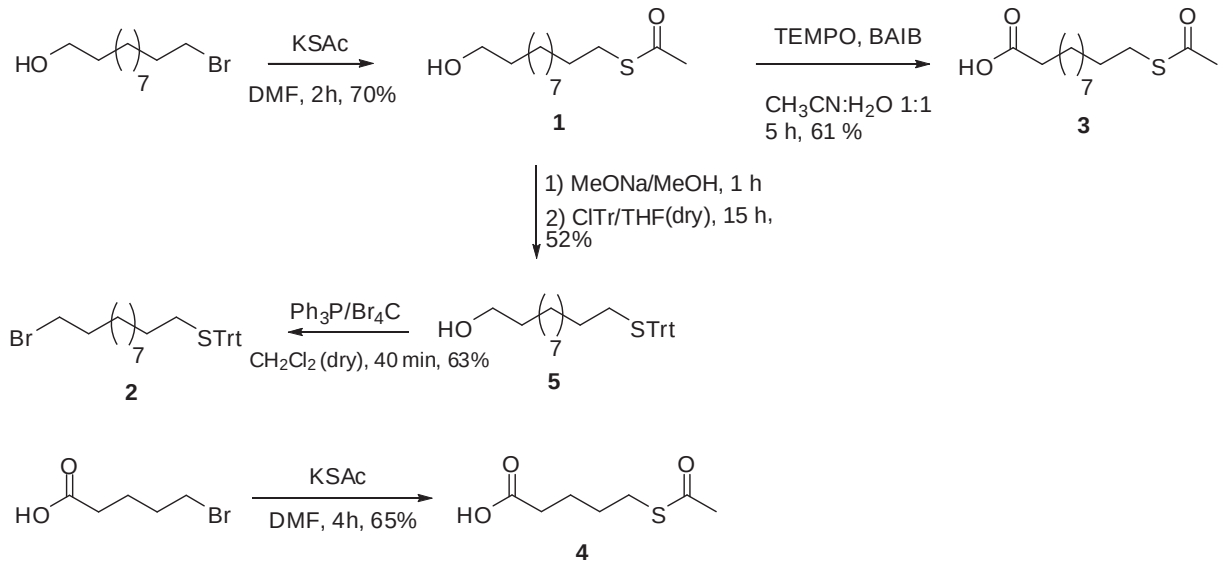

Scheme 1.1: *Synthesis of 11-(S-acetyl)mercaptoundecan-1-ol (**1**), 1-bromo-11-triphenilmethylmercaptoundecane (**2**), 11-(S-acetyl)mercaptoundecanoic acid (**3**) and 5-(S-acetyl)mercaptopentanoic acid (**4**).*

11-(*S*-acetyl)mercaptoundecanoic acid (**3**) was obtained by the reaction of 11-(*S*-acetyl)mercaptoundecan-1-ol (**1**) with bisacetoxyiodobenzene (BAIB) and 2,2,6,6-tetramethylpiperidine-*N*-oxide (TEMPO) in acetonitrile (CH_3CN):water (H_2O) (1:1). After purification by FCC 61% yield was obtained (Scheme 1.1). In the ^{1}H-NMR spectrum, the triplet at

[9] P.S.Ghosh, G. Han, B. Erdogan, O. Rosado, S.A. Krovi and V.M. Rotello, *Chem Biol. Drug Des*. **2007**, 70, 13-18 (Nanoparticles Featuring Amino Acid-functionalized Side Chains as DNA Receptors - HO-C11-STrt).

3.64 ppm characteristic of the methylene bonded to the alcohol disappeared and a triplet at 2.34 ppm corresponding to the methylene bonded to the acid functional group appeared.

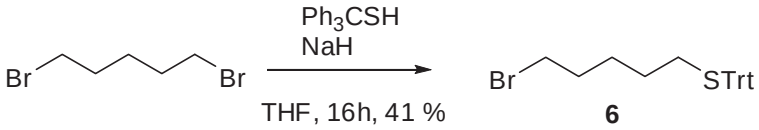

Scheme 1.2: *Synthesis of 1-bromo-5-triphenilmethylmercaptopentane (**6**).*

1-Bromo-5-triphenilmethylmercaptopentane (**6**) was obtained in a single step by simultaneous addition of a THF solution of and 1,5-dibromopenthane to a suspension of sodium hydride. ^{1}H-NMR spectrum showed signals in the aromatic range 7.4-7.2 ppm corresponding to trityl group. ^{13}C-NMR showed a new peak at 33.5 ppm corresponding to the methylene group bonded to the bromide atom in addition to the signal at 31.6 ppm which corresponds to methylene group in α-position respect to the sulphur atom. Although the yield was low after purification by FCC (41%), this reaction is straightforward (Scheme 1.2).

1.2 *Synthesis of neoglycoconjugates*

The neoglycoconjugates of β-glucose ([GlcC_2S-]$_2$ [10],[GlcC_3S-]$_2$ [11],[GlcC_5S-]$_2$ [8], [GlcC_7S-]$_2$, [GlcC_9S-]$_2$), β-galactose ([GalC_5S-]$_2$), α-mannose ([ManC_5S-]$_2$) [8], β-maltose (5, 5'-Dithiobis[pentyl(α-D-glucopyranosyl) (1→4)-β-D-glucopyranoside], [*maltose*C_5S-]$_2$), β-cellobiose (5, 5'-Dithiobis[pentyl(β-D-glucopyranosyl) (1→4)-β-D-glucopyranoside], [*cellobiose*C_5S-]$_2$) and β-lactose (5,5'-dithiobis[pentyl-α-D-galactopyranosyl](1→4)-β-D-glucopyranoside, [LacC_5S-]$_2$) [7] having thiol-ending aliphatic linker were synthesized following established procedures based on the chemistry of carbohydrate protecting groups/glycosidation/deprotection of the glycoconjugates. The monosaccharides conjugated to a protected thiol-ending linker (GlcC_3SAc, GlcC_5SAc [8], ManC_5SAc [8], GalC_5SAc) were obtained after radical addition of thioacetic acid to the double bond of the corresponding peracetylated *n*-alkenyl glycosides, in turn obtained by Fisher glycosylation using alken-1-ols as

[10]R. Ojeda, J. L. de Paz, A. G. Barrientos, M. Martín-Lomas and S. Penadés, *Carbohydr. Res*. **2007**, 342, 448–459 (Preparation of multifunctional glyconanoparticles as a platform for potential carbohydrate-based anticancer vaccines).
[11] B. T. Houseman, E. S. Gawalt, and M. Mrksich, *Langmuir,* **2003**, 19, 1522-1531 (Maleimide-Functionalized Self-Assembled Monolayers for the Preparation of Peptide and Carbohydrate Biochips).

glycosyl acceptors. A similar strategy was used to obtain *cellobiose*C_5SAc, but in this case a classic Köenigs-Knorr reaction was performed on peracetylated cellobiosyl bromide using penten-1-ol as acceptor before the radicalic addition of thioacetic acid. Longer thiol-ending aliphatic linkers were inserted into peracetylated glucose in order to obtain GlcC_7SAc and GlcC_9SAc after Fisher glycosylation using the corresponding bromo-alcohols as acceptors and further displacement of the bromine by nucleophilic substitution. This latter approach was also used to obtain *maltose*C_5SAc. On the other hand, anomeric trichloroacetimidates were used as glycosyl donors to obtain lactose- and glucose-conjugates with five and two carbon-atoms linkers respectively by using pent-4-en-1-ol and 2-bromoethanol as acceptors (LacC_5SAc, GlcC_2SAc). [7] Methanolysis [12] was used as final step to deprotect the *S*-acetyl and *O*-acetyl protecting groups (*O*-benzoyl in the case of [LacC_5S-]$_2$). Unless otherwise stated, the glycosylation reactions were highly diastereoselective (> 95%) and the major anomer (β for glucose, galactose, maltose and lactose, and α for mannose conjugates).

The synthesis of thiol-ending **β-glucose** derivatives ([GlcC_xS-]$_2$, x=2, 3, 5, 7, 9) was achieved starting from the pentaacetylated glucose. In order to synthesise [**GlcC_3S-]$_2$** and [**GlcC_5S-]$_2$**, glycosidation of pentaacetylated glucose with 2-propen-1-ol or 4-penten-1-ol in the presence of trifluoroboroetherate ($BF_3{\cdot}Et_2O$) in dry CH_2Cl_2 afforded the corresponding peracetylated glycosides after purification by FCC (56% yield and 66% yield, respectively). The latter compounds were then treated with thioacetic acid (AcSH), in the presence of azobisisobutyronitrile (AIBN), in THF to afford *S*-acetyl derivatives (84% yield and 66% yield, respectively). [**GlcC_3S-]$_2$** and [**GlcC_5S-]$_2$** [8] neoglycoconjugates were obtained as a mixture of thiols and disulfides after a methanolysis reaction (Scheme 1.3) in 98% and 84% yield, respectively.

[12] G. Zemplén, *Ber. Dtsch. Chem. Ges.* **1927**, 60, 1555-1564 (Decomposition of reducing disaccharides, VII Determination of the constitution of maltose).

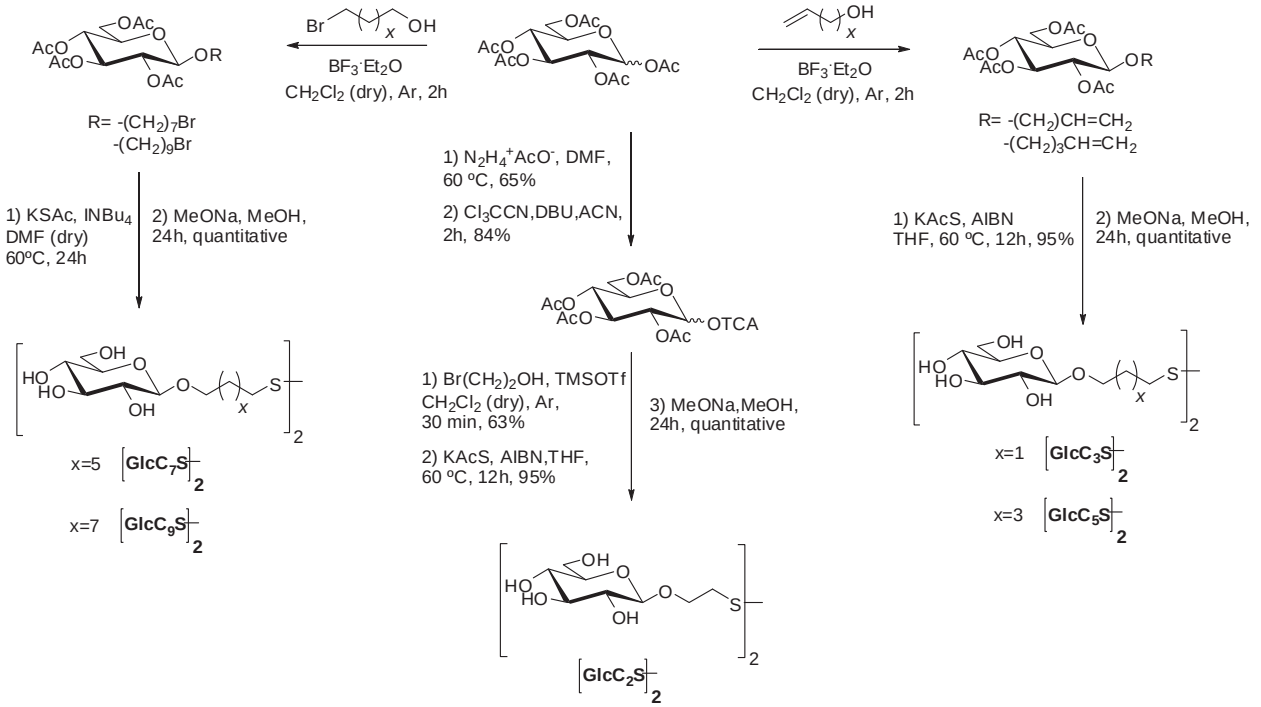

Scheme 1.3: *Synthesis of β-glucose derivatives [$GlcC_2S$-]$_2$ [10], [$GlcC_3S$-]$_2$ [11], [$GlcC_5S$-]$_2$ [8], [$GlcC_7S$-]$_2$ and [$GlcC_9S$-]$_2$ obtained as a mixture of thiol and disulfide.*

Similarly, 7-bromoheptan-1-ol and 9-bromononan-1-ol were reacted with pentaacetylated glucose and $BF_3{\cdot}Et_2O$ in dry CH_2Cl_2 obtaining 31% and 34% of the corresponding glycosylation products after purification by FCC. These bromo-derivatives were then treated with potassium thioacetate (KSAc) in dry DMF to provide $GlcC_7SAc$ (89% yield) and $GlcC_9SAc$ (34% yield) which, after a methanolysis reaction, gave the corresponding [**$GlcC_7S$-]$_2$** (83%) and [**$GlcC_9S$-]$_2$** (57%) as a mixture of thiols and disulfides (Scheme 1.3).

Glucose trichloroacetimidate was used as glycosyl donor to obtain $[GlcC_2S]_2$ neoglycoconjugate. Pentaacetylated glucose was treated with hydrazine acetate ($N_2H_4{}^+AcO^-$) in DMF to deprotect the anomeric position (65% yield). After purification by FCC, the product was reacted with trichloroacetonitrile (Cl_3CCN) under basic conditions in acetonitrile (CH_3CN) to afford the trichloroacetimidate in 84% yield. The glycosidation of commercial acceptor 2-bromoethanol with the glucose trichloroacetimidate gave the corresponding glycoside in 63% yield. The nucleophylic substitution of the bromide group by a thioacetate group was carried out in THF in the presence of KSAc in a good yield (95%). A methanolysis reaction of the derivative provided [**$GlcC_2S$-]$_2$** neoglycoconjugate as a mixture of thiol and disulfide in quantitative yield [7] (Scheme 1.3).

The **β-galactose** derivative ([$GalC_5S$-]$_2$) was synthesised using the same protocol described above to obtain [$GlcC_5S$-]$_2$. Pentaacetylated galactose was reacted with 4-penten-1-ol in dry CH_2Cl_2 in the presence of $BF_3{\cdot}Et_2O$. After purification by FCC, 55% of the *S*-acetyl derivative was obtained. AcSH was radically added to the double bond and the *S*-acetyl derivative (85% yield) was then deprotected by methanolysis to afford [**$GalC_5S$-]$_2$** as a mixture of thiol and disulfide in 87% yield (Scheme 1.4).

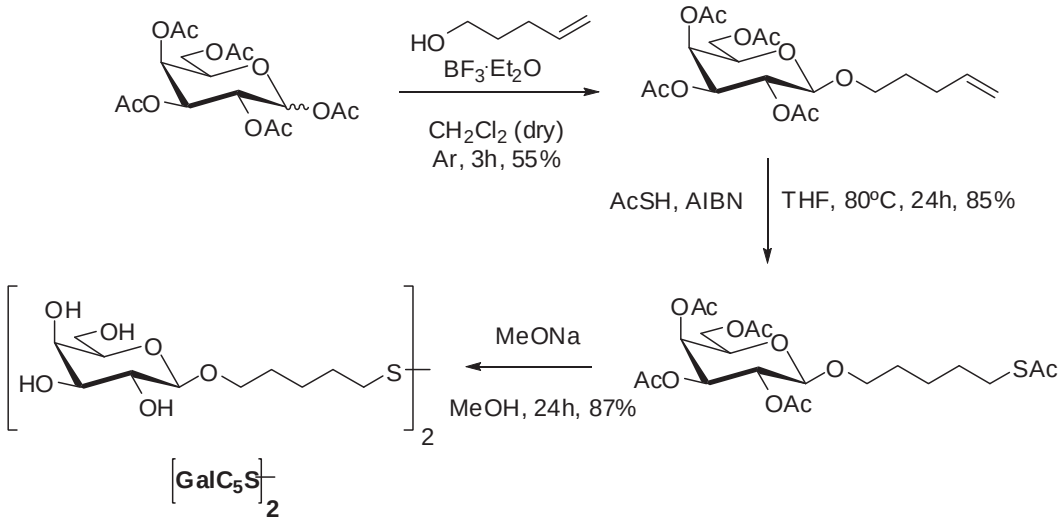

Scheme 1.4: *Synthesis of β-galactose derivative [$GalC_5S$-]$_2$ obtained as a mixture of thiol and disulfide.*

The **β-mannose** neoglycoconjugate was synthesized following a published procedure. [8] Briefly, starting from 4-pentenyl-α-D-mannopyranoside obtained by the Fraser-Reid method (69% yield) [13], peracetylation was carried out using Ac_2O in pyridine (97% yield). The radical addition of AcSH to the double bond gave the corresponding thiol-derivative in 74% yield after purification by FCC. This compound was treated with MeONa in methanol to afford the deprotected product as a mixture of thiol and disulfide (**[$ManC_5S$-]$_2$**) in quantitative yield (Scheme 1.5).

[13] B. Fraser-Reid, U. E. Udodong, Z. Wu, H. Ottosson, J. R. Merritt, C. S. Rao, C. Roberts and R. Madsen, *Synlett*, **1992**, 927-942 (*n*-Pentenyl Glycosides in Organic Chemistry: A Contemporary Example of Serendipity).

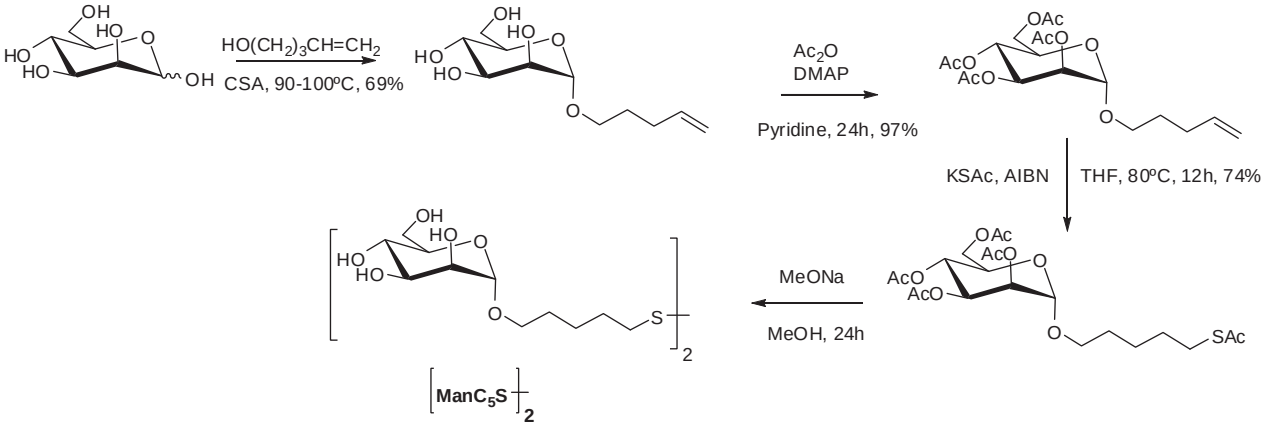

Scheme 1.5: *Synthesis of β-mannose derivative [ManC$_5$S-]$_2$ [8] obtained as a mixture of thiol and disulfide.*

The **β-maltose** derivative was prepared as follows. Octaacetylated maltose was glycosylated with 5-(*S*-acetyl)mercaptopentan-1-ol in dry CH_2Cl_2 using $BF_3{\cdot}Et_2O$ (55% yield, after purification by FCC). [14] The methanolysis reaction was used to fully deprotect the maltose derivative and obtain the corresponding mixture of thiol and disulfide (**[*maltose*C$_5$S-]$_2$**) in quatitative yield (Scheme 1.6).

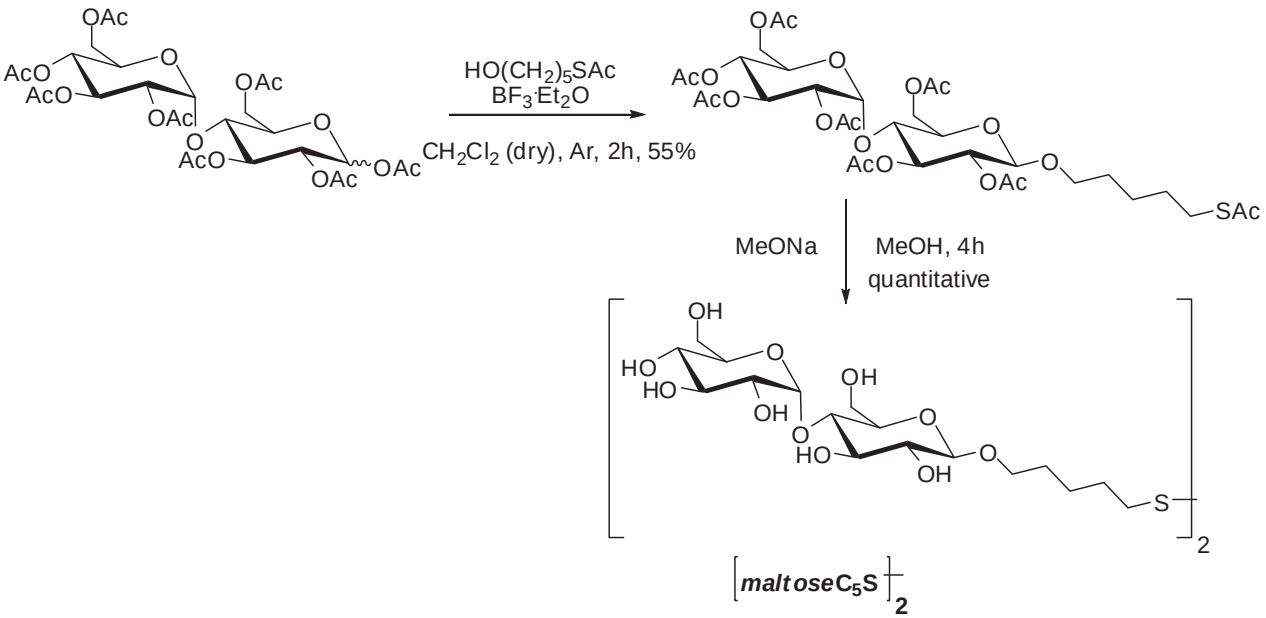

Scheme 1.6: *Synthesis of β-maltose derivative [maltoseC$_5$S-]$_2$ obtained as a mixture of thiol and disulfide.*

[14] A. Yamada, K. Hatano, K. Matsuoka, T. Koyama, Y. Esumi, H. Koshino, K. Hino, K. Nishikawa, Y Natoric and D. Terunuma, *Tetrahedron,* 62, **2006**, 5074–5083 (Syntheses and Vero toxin-binding activities of carbosilane dendrimers periphery-functionalized with galabiose).

The **β-cellobiose** neoglycoconjugate ([***cellobiose*C$_5$S-]$_2$**) was synthesized starting from peracetylated cellobiose which was activated with bromidic acid in dry CH_2Cl_2 (96% yield). The resulting bromo-derivative was used as glycosyl donor in a classical Köenigs-Knorr reaction with 4-penten-1-ol. This reaction afforded a mixture of the α and the β anomers which could be separated by column chromatography. In the ^{1}H-NMR spectrum the anomeric proton of the β anomer (*J*= 8.0 Hz) appears at 4.44 ppm while the α anomer (*J*= 5.2 Hz) at 5.65 ppm after separation by FCC. AcSH was added to the double bond of the β derivative by a radical addition (97% yield) and, afterwards the deprotection of the compound was carried out using MeONa in methanol. The final compound was obtained as a mixture of thiol and disulfide [**cellobioseC$_5$S-]$_2$** in quantitative yield (Scheme 1.7).

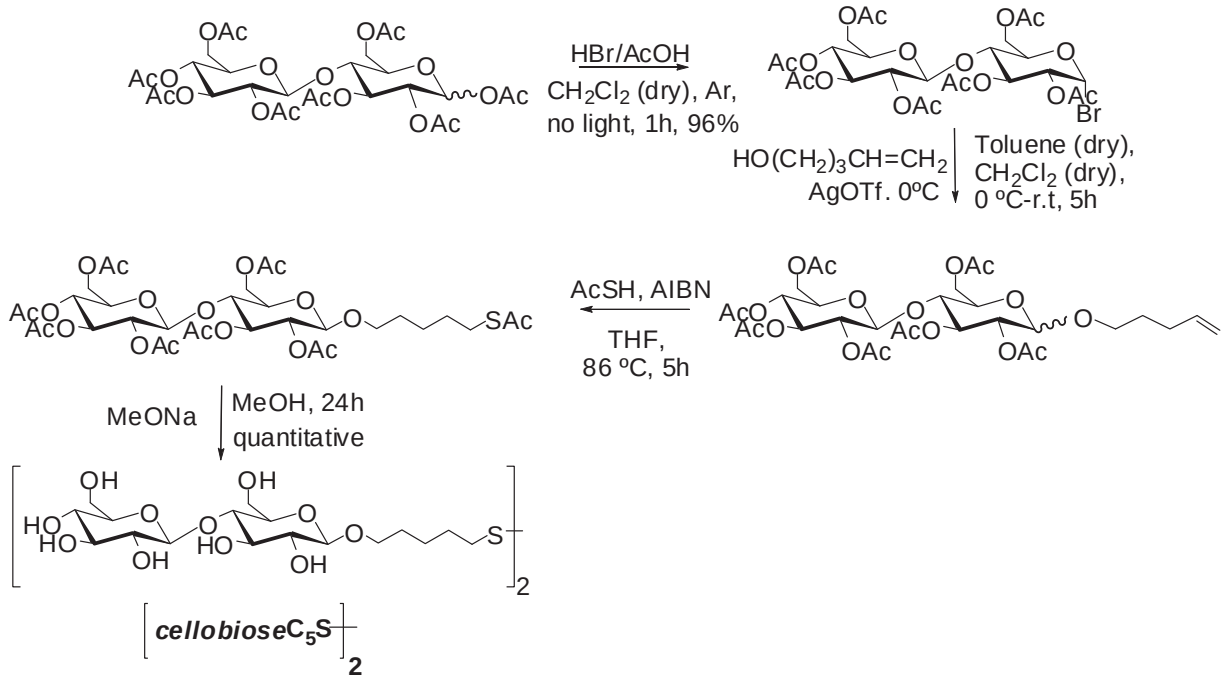

Scheme 1.7: *Synthesis of β-cellobiose derivative [cellobioseC$_5$S-]$_2$ as a mixture of thiol and disulfide.*

Perbenzoylated **β-lactose** was quantitatively obtained by reacting lactose with benzoyl chloride (BzCl) in pyridine using 4-dimethylaminopyridine (DMAP) as catalyst. The trichloroacetimidate used as a glycosyl donor was obtained by selective de-*O*-benzoylation at the anomeric centre (74% yield, after purification by FCC) and subsequent treatment with Cl_3CCN and 1,8-diazabicyclo[5.4.0]undec-7-ene (DBU) in CH_2Cl_2 (81% yield, after purification by FCC). Glycosidation of 4-penten-1-ol, with the benzoylated lactose derivative in the presence of trimethylsilyl triflate (TMSOTf) as the promoter, gave the corresponding *n*-pentenyl glycoside derivative in 70% yield after purification by FCC. The treatment with AcSH using AIBN as

catalyst (95%) and later deprotection by methanolisis afforded a mixture of thiol and disulfide **[LacC$_5$S-]$_2$** in 52% yield (Scheme 1.8). [7]

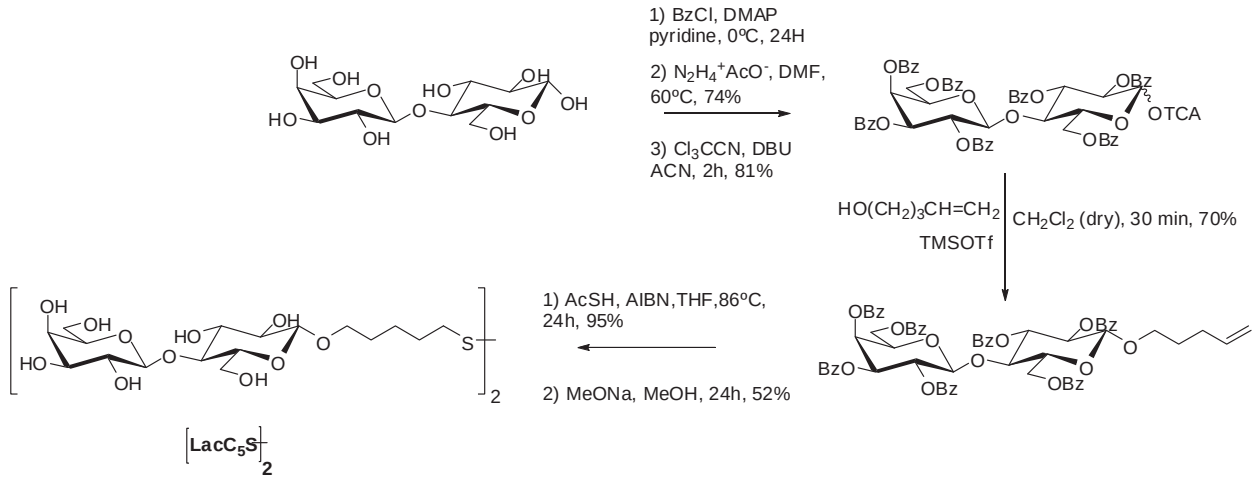

Scheme 1.8: *Synthesis of β-lactose derivative [LacC$_5$S-]$_2$ [7] as a mixture of thiol and disulfide.*

1.3 *Synthesis of DO3AC$_5$SH, DO3AC$_{11}$SH, DOTA-EdA-C$_5$SH and DOTA-EdA-C$_{11}$SH derivatives*

Gd(III) cation used in paramagnetic contrast agents is a heavy metal ion with high toxicity as a free ion. In order to avoid this toxicity and to improve the biodistribution in the body, the Gd-based contrast agents are in the form of ionic complexes with strong chelating ligands. Derivatives of poliaminocarboxylic acids as diethylen-triamine-pentaacetic acid (DTPA) or 1, 4, 7, 10-tetraazacyclododecane-1, 4, 7, 10-tetraacetic acid (DOTA), which form thermodynamically stable and kinetically inert complexes with Gd(III), are suitable chelating agents and their Gd(III) complexes are already in clinical use. [15] In this Thesis, two different chelating ligands were selected: A derivative of DO3A which has three carboxylic groups instead of four as DOTA and a derivative of DOTA-amine which presents an ethylene diamide linked to a carboxylic group of the macrocycle by a peptide bond. DO3A is an heptadentate ligand while Gd(III) is nine-coordinated. This means that DO3A chelats Gd(III) less strongly than DOTA-amine, which is an octadentate ligand. The toxicity of the DO3A-Gd is higher because the probability of releasing

[15] P. Hermann, J. Kotek, V. Kubicek and I. Lukes, *Dalton Trans.* **2008**, 23, 3027-3047. (Gadolinium(III) complexes as MRI contrast agents: ligand design and properties of the complexes)

free Gd(III) in the body after injection. [15] We have used both DO3A and DOTA-EdA derivatives for the preparation of the Gd-based paramagnetic gold glyconanoparticles.

Four derivatives were synthesised, two of them by *N*-alkylation of DO3A with 1-bromo-11-triphenilmethylmercaptoundecane (**2**) or 1-bromo-5-triphenilmethylmercaptopentane (**6**) and the other two by peptidic coupling between DOTA-EdA and 11-(*S*-acetyl)mercaptoundecanoic acid (**3**) or 5-(*S*-acetyl)mercaptopentanoic acid (**4**).

The **DO3A** derivatives 1, 4, 7,-tris(carboxymehyl)-10-(11-mercaptoundecyl)-1, 4, 7, 10-tetraazacyclododecane ($DO3AC_{11}SH$) and 1, 4, 7,-tris(carboxymethyl)-10-(5-mercaptopentyl)-1, 4, 7, 10-tetraazacyclododecane ($DO3AC_5SH$) were obtained treating *tert*-butyl-1, 4, 7,10-tetraazacyclododecane-1, 4, 7-triyl)triacetate ($DO3A^tBu$) in dry DMF with spacer **2** or **6** in the presence of potassium carbonate (K_2CO_3) (Scheme 1.9). After purification by FCC, the ^{1}H-NMR spectra of $DO3A^tBuC_{11}STrt$ and $DO3A^tBuC_5STrt$ showed signals at 7.50-7.20 ppm, which correspond to the aromatic protons of the trityl group. A triplet at 2.13 ppm indicated the methylene in α-position to the sulphur atom. Between 2.70 and 2.20 ppm, broad signals corresponding to the cyclen moiety were observed. The aliphatic protons of the spacers appeared around 1.40-1.20 ppm and the *tert*-butyl groups presented a signal at 1.60-1.30 ppm.

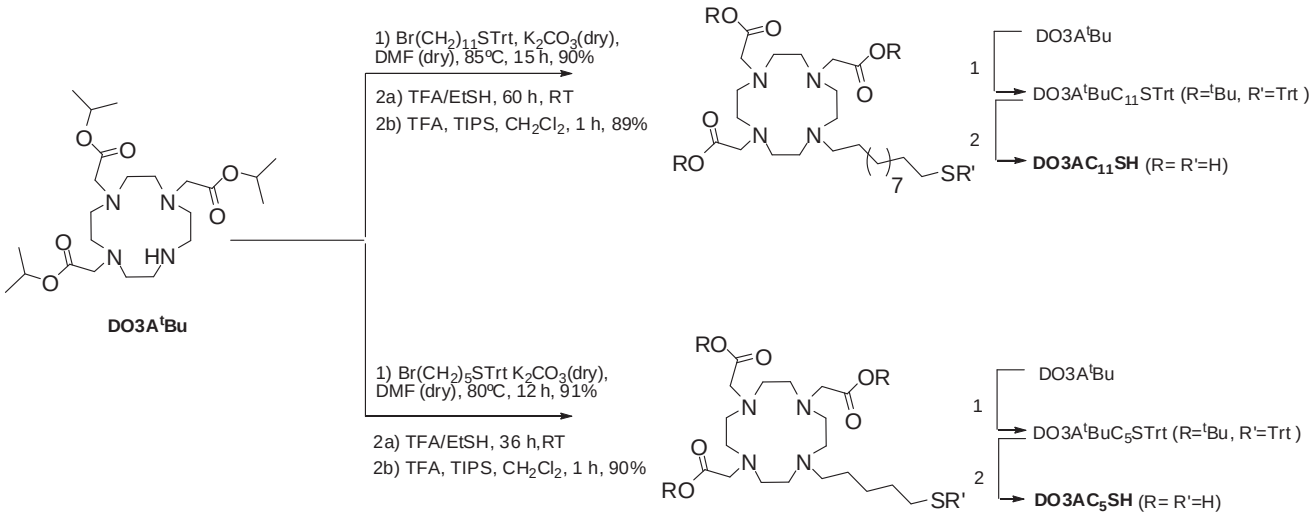

Scheme 1.9: *Synthesis of $DO3AC_{11}SH$ and $DO3AC_5SH$ derivatives. The final compounds were obtained as a mixture of thiol and disulfide.*

The obtained $DO3A^tBuC_{11}STrt$ (90% yield) or $DO3A^tBuC_5STrt$ (91% yield) was deprotected with trifluotoacetic acid (TFA) in an excess of ethanothiol (EtSH) which caught the isopropyl carbocation produced. After 60 or 36 hours, respectively, triisopropyl silane (TIPS) was added in order to trap the aromatic carbocations formed. Finally, after 1 hour, the TFA was eliminated by

evaporation and the product was purified by recristalization with diethyl ether to obtain DO3AC_{11}SH (89% yield) or DO3AC_5SH (90% yield) as a mixture of thiol and disulfide (yellow solids). In the ^{1}H-NMR spectra of DO3AC_{11}SH and DO3AC_5SH the signals of aromatic protons of the trityl group (around 7.40 ppm) disappeared as well as the signals of the *tert*-butyl groups (around 1.40 ppm), indicating the total deprotection of the compounds.

As stated before, the DO3A derivatives are heptadentate chelating agents, so that an octadentate ligand derivatives (**DOTA-EdA)** were also synthesized to have more stable Gd-complexes and to reduce the toxicity of the Gd-complex. 1, 4, 7,-tris(carboxymethyl)-10-ethylene diamide(10-mercaptoundecyl)-1, 4, 7, 10-tetraazacyclododecane (DOTA-EdA-C_{11}SH) and 1, 4, 7,-tris(carboxymethyl)-10-ethylene diamide(10-mercaptopentyl)-1, 4, 7, 10-tetraazacyclododecane (DOTA-EdA-C_5SH) were prepared by reacting DO3A^{t}Bu-*N*-(2-aminoethyl)ethane amide with **3** or **4** linkers in DMF in the presence of *O*-(benzotriazol-1-yl)-*N,N,N′,N′*-tetramethyluronium hexafluorophosphate (HBTU) and hydroxybenzotriazole (HOBt) and using *N,N*-diisopropylethylamine (DIPEA) as a base (Scheme 1.10).

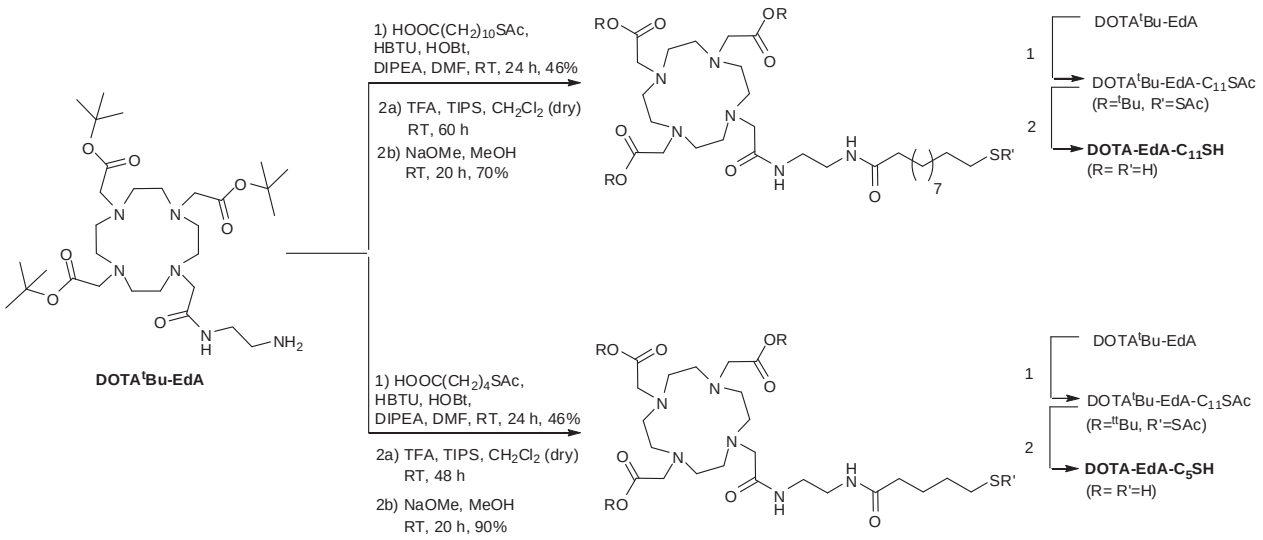

Scheme 1.10: *Synthesis of DOTA-EdA-C_{11}S and DOTA-EdA-C_5S derivatives. The final compounds were obtained as a mixture of thiol and disulfide.*

After the peptide coupling, the obtained compound (DOTA^{t}Bu-EdA-C_{11}SAc in 46% yield or DOTA^{t}Bu-EdA-C_5SAc in 46% yield) was purified by FCC. The ^{1}H-NMR spectrum of DOTA^{t}Bu-EdA-C_{11}SAc showed two singlets at 6.74 and 6.48 ppm which correspond to the protons of the two amides. The methylene groups of the ethylene diamine showed a singlet at 3.31 ppm. The methylene in α-position to the sulphur atom showed a triplet at 2.84 ppm. A singlet at 2.30 ppm corresponding to the methyl of the thioacetate group was also detected. Between 3.41 and 2.00

ppm, broad signals were observed, corresponding to the cyclen moiety. *Tert*-butyl groups gave two singlets at 1.44 and 1.43 ppm and the aliphatic protons of the spacers appeared around 1.32-1.23 ppm. The mass spectrum of the compound DOTA^{t}Bu-EdA-C_{11}SAc showed a peak at 858.5 m/z which corresponds to $[M+H]^+$. Similarly, the ^{1}H-NMR spectrum of DOTA^{t}Bu-EdA-C_5SAc showed two singlets at 7.07 and 6.80 ppm which correspond to the 2 amides protons. A multiplet between 2.91-2.89 ppm showed the methylene in α-position to the sulphur atom. A singlet at 2.30 ppm corresponding to the methyl of the thioacetate group was also detected. *Tert*-butyl groups gave a doblet at 1.47 ppm. The mass spectrum of the compound DOTA^{t}Bu-EdA-C_5SAc showed a peak at 795.5 m/z which corresponds to $[M+Na]^+$. Two sequential deprotection reactions were then performed to obtain the complete deprotection of DOTA^{t}Bu-EdA-C_{11}SAc and DOTA^{t}Bu-EdA-C_5SAc without isolation of the intermediates. First, TFA and TIPS were added to a solution of the compound in dry CH_2Cl_2 in order to remove the *tert*-butyl groups; second, the acetyl group bonded to the sulphur was removed by using sodium methoxide (NaOMe) in methanol (MeOH). After 20 hours, the MeOH was eliminated by evaporation and the product was redissolved in water and freeze-dried to obtain DOTA-EdA-C_{11}SH (70% yield) or DOTA-EdA-C_5SH (90% yield) as a mixture of thiol and disulfide. In the ^{1}H-NMR spectra of DOTA-EdA-C_{11}SH and DOTA-EdA-C_5SH, the signals of the methyl group of the thioacetate at 2.30 ppm and the signals of the *tert*-butyl groups at 1.44, 1.43 and 1.47 ppm disappeared, indicating the total deprotection of the chelants. This fact was confirmed by mass spectrometry of DOTA-EdA-C_{11}SH which gave a peak at 648.1 m/z corresponding to $[M+H]^+$ and of DOTA-EdA-C_5SH which showed a peak at 585.3 m/z corresponding to $[M+Na]^+$.

All the details of the synthesis of spacers, glycoconjugates and DO3A and DOTA derivatives are reported in the experimental part.

2. Direct synthesis of Gd-based paramagnetic gold glyconanoparticles

The preparation of hybrid gold nanoparticles functionalized with different glycoconjugates and a derivative of DO3A (HSC_{11}DO3A or HSC_5DO3A) capable to chelate paramagnetic ions was previously achieved in our laboratory by a "direct" method. [5] Two GNPs were prepared during this PhD by the "direct" method ($LacC_5S$-Au-SC_{11}DO3A-Gd and $GlcC_5S$-Au-SC_{11}DO3A-Gd) in order to compare them with the GNPs previously prepared in the laboratory using the same methodology.

Briefly, a gold salt was reduced in the presence of a mixture of thiol-ending glycoconjugate and 10% of tetraazacyclododecane triacetic acid (DO3A) thiol-ending derivatives ($HSC_{11}DO3A$ or HSC_5DO3A). This suspension was vigorously shaken for 2 h at 25 ºC. The supernatant was removed and the residue was dissolved in milliQ water and purified by dialysis. In order to convert the resulting gold nanoparticles into paramagnetic one, the GNPs were incubated in 4-(2-hydroxyethyl)-1-piperazineethanesulfonic acid (HEPES) buffer (pH=7.4) with gadolinium chloride ($GdCl_3$) and then washed with ethylenediaminetetraacetic acid (EDTA) in order to remove the Gd (III) in excess. GNPs were washed several times with water until the washings were negative for the Orange Xylenol test (Scheme 1.11). [16] The amount of Gd (III) present in the GNPs was then measured by inductively coupled plasma atomic emission spectroscopy (ICP-AES) and the properties as contrast agents *in vitro* (relaxivity) were also measured.

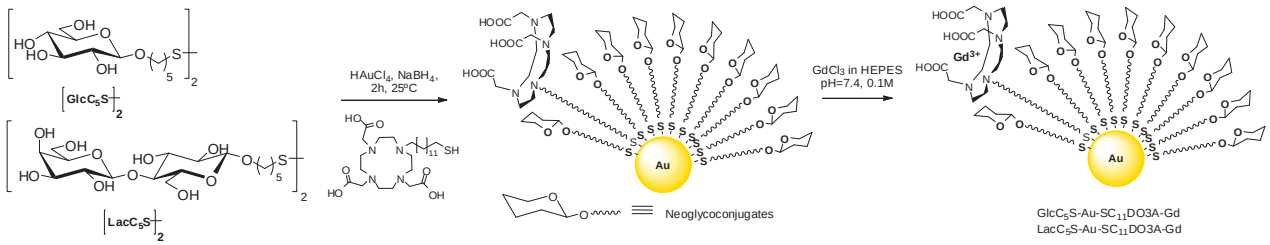

Scheme 1.11: *Synthesis of paramagnetic Gd-based gold glyconanoparticles (GNPs) by "direct" method.*

In the case of the previous work the amount of Gd(III) [5] in the $LacC_5S$-Au-$SC_{11}DO3A$-Gd was 0.5% the same that in the GNP synthesized in this Thesis (Table 1.1). However, the relaxivity values of both $LacC_5S$-Au-$SC_{11}DO3A$-Gd were different, obtaining r_1= 25.2 $s^{-1}mM^{-1}$ in the previous work *versus* r_1= 13.5 $s^{-1}mM^{-1}$ in this Thesis. In the case of $GlcC_5S$-Au-$SC_{11}DO3A$-Gd, both the Gd(III) content and the relaxivity significantly differ: r_1 of GNP synthesized in the previous work was 3.1 $s^{-1}mM^{-1}$, while the GNP synthesized for this Thesis was 6.2 $s^{-1}mM^{-1}$; the percentage of Gd(III) was more than double amount of Gd(III) in $GlcC_5S$-Au-$SC_{11}DO3A$-Gd prepared in this Thesis (6.1% *vs* 2.5%). The high amount of Gd(III) obtained could be explained by coordination of Gd(III) to the hydroxy groups of the sugars. This chelation is weaker than the one obtained with DO3A compound and the Gd(III) could be lost through the body after injection of the GNPs in living animals.

[16] P.-J. Debouttière, S. Roux, F. Vocanson, C. Billotey, O. Beuf, A. Favre-Réguillon, Y. Lin, S. Pellet-Rostaing, R. Lamartine, P. Perriat, and O. Tillement, *Adv. Funct. Mater.*, **2006**, 16, 2330-2339 (Design of Gold Nanoparticles for Magnetic Resonance Imaging)

Table 1.1: *Relaxivities and amount of Gd(III) of the GNPs synthesized in this Thesis and in reference [5] by the "direct" method.*

GNPs	r_1 (s^{-1} mM^{-1})		% Gd (in mass)	
	Thesis	**Values from ref. 5**	**Thesis**	**Values from ref. 5**
$LacC_5S$-Au-SC_{11}DO3A-Gd	13.5±0.8	25.2±0.2	0.55±0.2	0.5±0.1
$GlcC_5S$-Au-SC_{11}DO3A-Gd	6.2±0.8	3.1±0.4	6.1±0.4	2.5±0.1

The "direct" method employed to prepare these GNPs is **not well reproducible** and presents difficulties in the purification step as no exhaustive dialysis of GNPs could be performed because of the risk of losing the chelated Gd. In search for loading higher amounts of Gd(III) into GNPs, to improve, reproduce and aavoid chelation by the sugars, we applied the LPE method for the preparation of Gd-based paramagnetic gold glyconanoparticles.

3. Preparation of Gd-based paramagnetic gold glyconanoparticles by ligand place exchange method

In order to improve the properties as MRI probes of the Gd-based paramagnetic gold GNPs obtained with the "direct" method [5], the GNPs were prepared in two steps as shown in Scheme 12: (i) Preparation of glyconanoparticles 100%-coated with thiol-ending glycoconjugates; [7] (ii) Incubation of the so-obtained GNPs with DO3A-Gd complexes functionalized with thiol-ending linkers and subsequent functionalization by "thiol-for-thiol" ligand place exchange (LPE) reactions between the glycoconjugates at gold surface and incoming DO3A-Gd complexes. [17]

[17] M. J. Hostetler, A. C. Templeton, and R. W. Murray, *Langmuir,* **1999**, 15, 3781-3789 (Dynamics of Place-Exchange Reactions on MP Au Cluster Molecules).

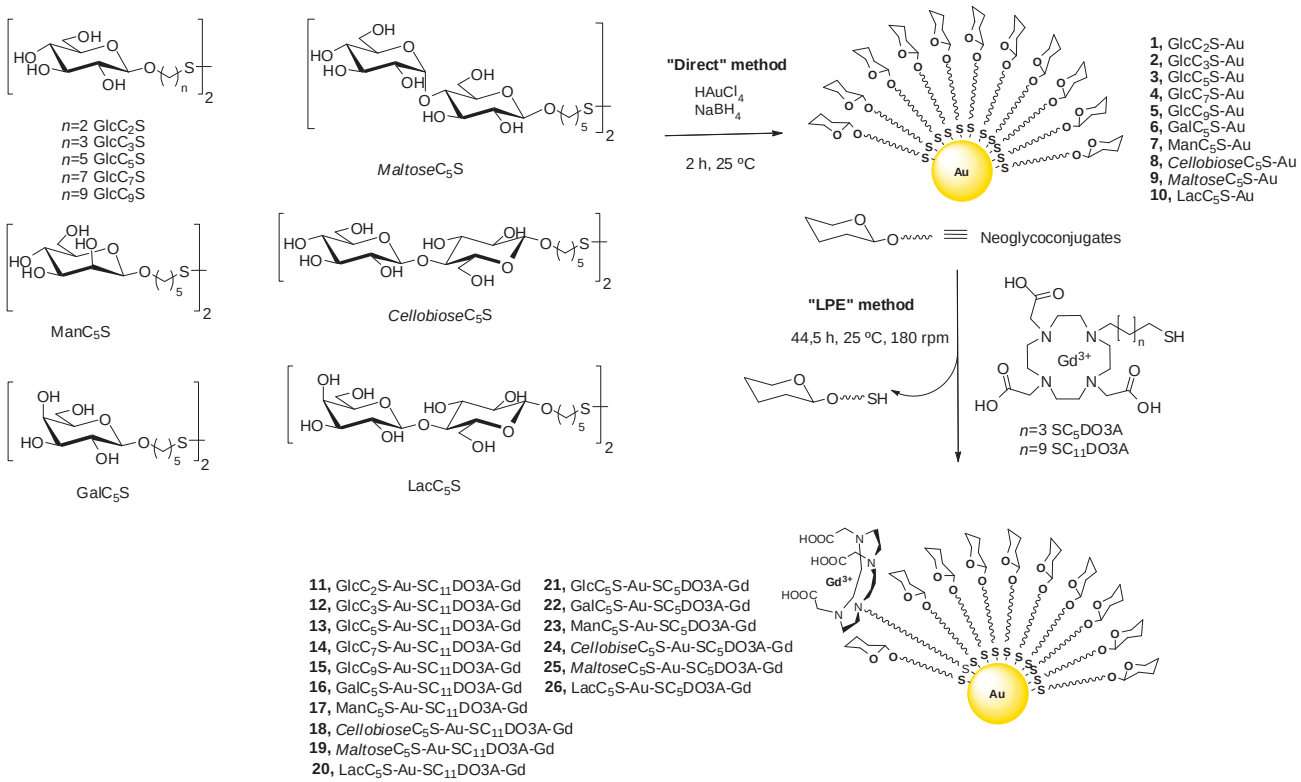

Scheme 1.12: *Synthesis of paramagnetic Gd-based gold glyconanoparticles (GNPs) by Ligand Place Exchange (LPE) of 100% sugar-coated gold GNPs and Gd-chelates.*

(i) The gold GNPs 100%-coated with the glycoconjugates were prepared following the *in situ* procedure reported by us [7] through reduction of a gold salt ($HAuCl_4$) with $NaBH_4$ in the presence of the glycoconjugates. (ii) After purification by dialysis, lyophilisation and characterization, the prepared GNPs were re-dissolved in water and incubated with a solution of HSC_5DO3A-Gd or $HSC_{11}DO3A$-Gd in HEPES buffer (Scheme 1.12).

For the complexation of Gd(III) cations, the DO3A derivatives were incubated with 0.9 equivalents $GdCl_3$ in HEPES buffer (0.1 M pH=7.4). The choice of using 0.9 equivalents of the Gd(III) salt for the incubation was taken in order to avoid free Gd(III) in solution.

The resulting complexes were characterized by IR, ^{1}H-NMR and ^{17}O-NMR, and the relaxivity values were calculated after measurements of the relaxation times T_1 and T_2 at different Gd(III) concentrations. The IR spectra of $HSC_{11}DO3A$-Gd and HSC_5DO3A-Gd showed the band corresponding to the stretching of carboxylic groups (COOH and COO^-) at 1592, 1397 cm^{-1} for $HSC_{11}DO3A$-Gd and 1588, 1397 cm^{-1} for HSC_5DO3A-Gd. The starting chelating agents $DO3AC_{11}SH$ and DO3AC5SH showed signals at 1637 and 1682 cm^{-1} for C=O stretching, respectively. The shift to lower wavelengths indicated that the complexation of Gd(III) is in

agreement with the literature. [18] Due to the presence of the paramagnetic cation Gd(III), the ^{1}H-NMR spectra in D_2O at 500 MHz of the complexes showed an increased broadening of the signals respect to the starting chelating agents that impeded the proton assignment. ^{17}O-NMR measurements were performed to determine the number of the water molecules directly coordinated to the Gd(III) ion (q). [19] The obtained values confirmed the presence of two water molecules in the inner-sphere of the chelating agent, as expected for DO3A derivative. The value found for HSC_{11}DO3A-Gd was $q = 2.0 \pm 0.2$ and for HSC_5DO3A-Gd was $q = 2.1 \pm 0.2$.

The HSC_{11}DO3A-Gd and HSC_5DO3A-Gd solutions in HEPES buffer (pH=7.4, 0.1M) were used, directly, for the LPE reactions in such a way that Gd(III) was introduced by "thiol for thiol" exchange in an extremely controlled manner onto the 100% glyco-functionalised GNPs. [17]
After incubation of the gold GNPs with 1.1 equivalents of the Gd(III) complexes for 44 hours at 180 rpm in an orbicalical shaker and several washings with water until the ^{1}H-NMR spectrum of the washings did not show HSC_5DO3A-Gd or HSC_{11}DO3A-Gd, the resulting Gd-based paramagnetic gold GNPs were freeze-dried. The amount of Gd(III) introduced was around 3-5% (Table 1.3) as determined by ICP-AES. These conditions (1.1 equivalents of the Gd(III) complexes, 44 hours and 25ºC) for the LPE reaction were selected after a series of experiments which were performed by changing different parameters of incubation (DO3A-Gd complex concentration, temperature, time) and using the $GlcC_5S$-Au as testing GNP.
One of the strategies used to have a better contrast agent is to increase the amount of Gd(III) present in the paramagnetic contrast agent [16]. For this reason, the first parameter to be changed was the equivalents of the Gd(III) complexes keeping time (44 h) and temperature (25 ºC) constant (Table 1.2).

[18] G.M. Nicolle, È. Tòth, K.P. Eisenwiener, H. R. Mäcke and A.M. Merbach, *J. Biol. Inorg. Chem.,* **2002**, 7, 757-769 (From monomers to micelles: investigation of the parameters influencing proton relaxivity.)
[19] K. Djanashvili and J.A. Peters, *Contrast Media Mol. Imaging*, **2007**, 2, 67-71 (How to determine the number of inner-sphere water molecules in Lanthanide(III) complexes by ^{17}O-NMR spectroscopy. A technical note).

Table 1.2: *Longitudinal and transversal relaxivities of Gd-based GNPs varying equivalents of incoming ligand or the temperature.*

GNPs	Conditions			r_1 ($sm^{-1}M^{-1}$)	r_2 ($sm^{-1}M^{-1}$)	% Gd
	Eq.	Time	T (ºC)			
$GlcC_5S$-Au-**SC_5DO3A-Gd**	1.1	44 h	25	16.9	27.9	3.1 ± 0.6
	7	44 h	25	Precipitates		
	1.1	44 h	45	11.4	18.8	3.8 ± 0.6
$GlcC_5S$-Au-**SC_{11}DO3A-Gd**	1.1	44 h	25	7.4	11.9	4.7 ± 0.1
	1.1	1 week	25	15.1	28.8	3.7 ± 0.2
	3	44 h	25	10.0	17.2	4.7 ± 0.2

At 44 h, 25 ºC and 1.1 equivalents of **HSC_5DO3A-Gd**, the amount of Gd(III) was 3.1% and the relaxivity value r_1=16.9 $s^{-1}mM^{-1}$. When 7 equivalents of the starting linker Gd-complex, **HSC_5DO3A-Gd**, were used (44 h, 180 rpm, 25 ºC) the GNP precipitates. Using 1.1 equivalents of the complex and 45ºC, the amount of Gd(III) in the GNP is practically the same that the one obtained at 25 ºC. For **HSC_{11}DO3A-Gd** under the same conditions (44h, 25ºC and 1.1 eq.) the amount of Gd(III) was 4.7% and the relaxivity value r_1=7.4 $sm^{-1}M^{-1}$. In addition, two different conditions were then tried: one week of incubation and 3 equivalents of the complex (Table 1.2). After a week of incubation with 1.1 equivalents of the complex, the amount of Gd (III) in the GNP is similar to the one obtained incubating 44 hours. It seems that the LPE reach equilibrium at 44h and increasing the time of incubation does not lead to further entry of HSC_{11}DO3A-Gd. When 3 equivalents of the complex were used, the Gd (III) introduced in the GNP was 4.7%, the same than that obtained with 1.1 eq at the same experimental conditions.

By comparing the relaxativity values of $GlcC_5S$-Au-SC_5DO3A-Gd incubated at 25ºC or 45ºC a strange behaviour is observed. Having same amount of Gd(III), the relaxivity value is lower at 45ºC (r_1= 11.4 $sm^{-1}M^{-1}$ *vs* r_1= 16.9 $sm^{-1}M^{-1}$). A similar phenomenon happens with $GlcC_5S$-Au-SC_{11}DO3A-Gd when incubated with different number of equivalents (Table 1.2). Having higher amount of Gd(III), the relaxivity is lower (4.7%, r_1= 10.0 $sm^{-1}M^{-1}$ *vs* 3.7%, r_1= 15.1 $sm^{-1}M^{-1}$). These particular results could be explained by the position of the Gd-ligands onto the gold surface. It may be that when the exchange is forced (45 ºC in the case of $GlcC_5S$-Au-SC_5DO3A-Gd or 3 equivalents in the case of $GlcC_5S$-Au-SC_{11}DO3A-Gd), the amount of DO3A-Gd derivative on the gold surface increases, increasing the amount of Gd(III) in the GNPs. However, some of these Gd-complexes are less available and the water molecules are not able to interact with Gd(III). More studies are needed in order to confirm this supposition.

3.1 ***Characterization of the GNPs***.

The paramagnetic Gd-based gold GNPs were characterized by TEM, UV-Vis, IR, ^{1}H-NMR and inductively coupled plasma atomic emission spectroscopy (ICP-AES) before measuring the relaxation times T_1 and T_2 *in vitro* by using a 60 MHz Minispec in order to calculate the relaxivity values (r_1 and r_2) on the basis of the Gd(III) content of each paramagnetic GNP. The relaxation times of water solutions of Gd-based GNPs, were also measured in "phantoms" at 11.7 T. In addition, $GlcC_5S$-Au-SC_{11}DO3A-Gd GNP was characterized by Z-potential, ^{17}O-NMR and Proton Nuclear Magnetic Relaxation Dispersion (^{1}H-NMRD) spectroscopy.

^{1}H-NMR spectra. The ^{1}H-NMR spectra of Gd-based paramagnetic GNPs showed broad signals due to the presence of Gd(III) and they can not be assigned. However, these broad signals fit with the signals obtained for the free ligands.

UV-Vis spectra. The UV-visible absorption spectrum of gold GNPs $GlcC_3S$-Au-SC_{11}DO3A-Gd, $GlcC_7S$-Au-SC_{11}DO3A-Gd, $GlcC_9S$-Au-SC_{11}DO3A-Gd, $ManC_5S$-Au-SC_{11}DO3A-Gd, $ManC_5S$-Au-SC_5DO3A-Gd, *cellobiose*C_5S-Au-SC_{11}DO3A-Gd, *cellobiose*C_5S-Au-SC_5DO3A-Gd, *maltose*C_5S-Au-SC_{11}DO3A-Gd and *maltose*C_5S-Au-SC_5DO3A-Gd showed a band around 520 nm corresponding to the surface plasmon band of the gold. (See experimental part for further details) The gold GNPs having a diameter of the gold nanocluster below 2 nm ($GlcC_2S$-Au-SC_{11}DO3A-Gd glyconanoparticles, $GalC_5S$-Au-SC_{11}DO3A-Gd glyconanoparticles, $GalC_5S$-Au-SC_5DO3A-Gd glyconanoparticles, $LacC_5S$-Au-SC_{11}DO3A-Gd glyconanoparticles and $LacC_5S$-Au-SC_5DO3A-Gd glyconanoparticles) did not show this band. Due to the double distribution of $GlcC_5S$-Au-SC_{11}DO3A-Gd and $GlcC_5S$-Au-SC_5DO3A-Gd the plasmon band is observed in these GNPs too.

Infrared(IR) spectra. IR spectra of the Gd-loaded gold GNPs showed peaks around 3400, 2900, 2800 and 1600 cm^{-1}. The bands at 2900-2800 cm^{-1} correspond to the aliphatic groups and the peak at 1600 cm^{-1} correspond to the C=O stretching of COO^- coordinated to Gd^{3+}. This band at 1600 cm^{-1} was absent in the starting 100%-sugar coated gold GNPs and appeared after the LPE.

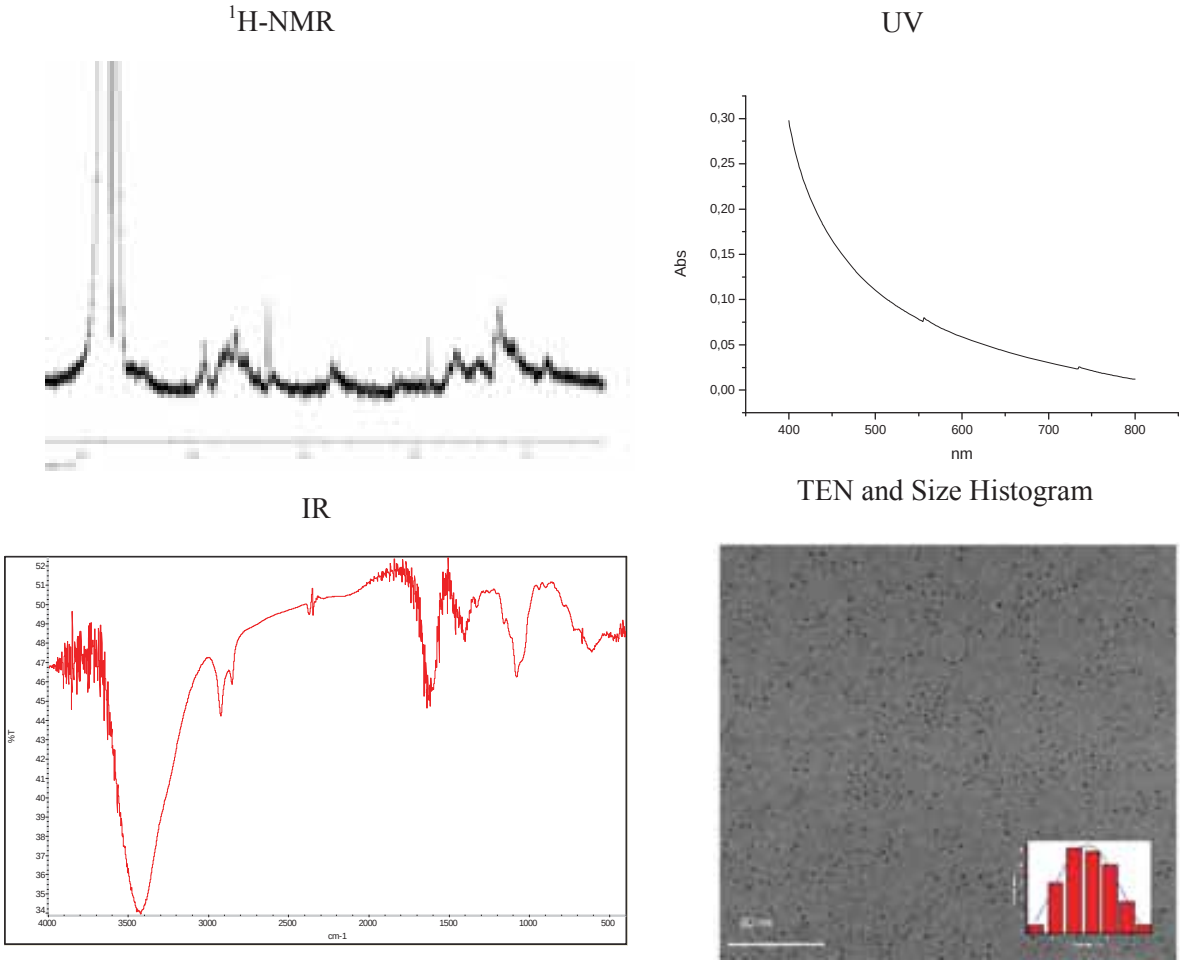

Figure 1.5: *Characterization of LacC$_5$S-Au-SC$_{11}$DO3A-Gd GNPs. ^{1}H-NMR spectra, UV spectra, IR spectra, TEM and size histogram (as an input).*

Transmission Electron Microscopy (TEM). TEM micrographs allowed the determination of the gold nanoclusters size (average diameter with the approximation of spherical shape). To obtain the size distribution at least 300 particles were count and no less than 3 different TEM photographs per GNP. Table 3 shows the diameter of the different GNPs. All the GNPs show an exceptionally small average core size (1.8 – 2.4 nm), with a uniform monomodal dispersion except of GlcC$_5$S-Au-SC$_{11}$DO3A-Gd and GlcC$_5$S-Au-SC$_5$DO3A-Gd which show a double distribution with the mean size of 1.5 ± 0.3 nm (75%) and 4.3 ± 0.6 nm (25%) and 2.0 ± 0.3 nm (75%) and 4.8 ± 0.5 nm (25%), respectively. No significant change in size was noticed after LPE reactions on 100% GNPs.

^{1}H-NMR spectra, UV-Vis spectra, Infrared (IR) spectra and Transmission Electron Microscopy (TEM) micrographs of all the GNPs can be found in the Appendix.

Based on the data of TEM (average diameters), ICP-AES and elemental analysis an average molecular formula for the Gd-based paramagnetic GNPs was assigned (Table 1.3).

Table 1.3: *Chemical properties of the prepared paramagnetic glyconanoparticles.*[a]

GNPs	% Gd	TEM (nm)	M_w (KDa)	Molecular formula
$GlcC_2S$-Au-$SC_{11}DO3A$-Gd	3.4±0.2	1.8±0.2	76	$Au_{201}(C_8H_{15}O_6S)_{107}(C_{25}H_{47}N_4O_6S)_{16}Gd_{16}$
$GlcC_3S$-Au-$SC_{11}DO3A$-Gd	3.3±0.2	1.9±0.3	165	$Au_{314}(C_9H_{17}O_6S)_{20}(C_{25}H_{47}N_4O_6S)_{33}Gd_{33}$
$GlcC_5S$-Au-$SC_{11}DO3A$-Gd	4.7±0.1	1.5±0.3 4.3±0.6	59	$Au_{140}(C_{11}H_{21}O_6S)_{70}(C_{25}H_{47}N_4O_6S)_{17}Gd_{17}$
$GlcC_5S$-Au-SC_5DO3A-Gd	3.1±0.2	2.0±0.3 4.8±0.5	56	$Au_{140}(C_{11}H_{21}O_6S)_{76}(C_{19}H_{36}N_4O_6S)_{11}Gd_{11}$
$GlcC_7S$-Au-$SC_{11}DO3A$-Gd	4.1±0.2	1.8±0.3	97	$Au_{225}(C_{13}H_{25}O_6S)_{115}(C_{25}H_{47}N_4O_6S)_{25}Gd_{25}$
$GlcC_9S$-Au-$SC_{11}DO3A$-Gd	3.2±0.2	1.8±0.2	121	$Au_{314}(C_{15}H_{29}O_6S)_{125}(C_{25}H_{47}N_4O_6S)_{25}Gd_{25}$
$GalC_5S$-Au-$SC_{11}DO3A$-Gd	4.2±0.2	1.7±0.1	75	$Au_{201}(C_{11}H_{21}O_6S)_{77}(C_{25}H_{47}N_4O_6S)_{20}Gd_{20}$
$GalC_5S$-Au-SC_5DO3A-Gd	3.6±0.2	1.7±0.2	72	$Au_{201}(C_{11}H2_1O_6S)_{80}(C_{19}H_{35}N_4O_6S)_{17}Gd_{17}$
$ManC_5S$-Au-$SC_{11}DO3A$-Gd	3.0±0.2	2.4±0.4	112	$Au_{314}(C_{11}H_{21}O_6S)_{127}(C_{25}H_{47}N_4O_6S)_{21}Gd_{21}$
$ManC_5S$-Au-SC_5DO3A-Gd	4.1±0.2	1.8±0.2	113	$Au_{314}(C_{11}H_{21}O_6S)_{119}(C_{19}H_{35}N_4O_6S)_{29}Gd_{29}$
cellobioseC_5S-Au-$SC_{11}DO3A$-Gd	2.1±0.2	1.8±0.2	92	$Au_{314}(C_{17}H_{32}O_6S)_{61}(C_{25}H_{47}N_4O_6S)_{12}Gd_{12}$
cellobioseC_5S-Au-SC_5DO3A-Gd	2.1±0.2	2.0±0.1	91	$Au_{314}(C_{17}H_{31}O_6S)_{61}(C_{19}H_{35}N_4O_{60}S)_{12}Gd_{12}$
maltoseC_5S-Au-$SC_{11}DO3A$-Gd	3.1±0.2	1.8±0.2	139	$Au_{314}(C_{17}H_{31}O_{11}S)_{131}(C_{25}H_{47}N_4O_6S)_{28}Gd_{28}$
maltoseC_5S-Au-SC_5DO3A-Gd	3.6±0.2	1.8±0.2	137	$Au_{314}(C_{17}H_{31}O_{11}S)_{127}(C_{19}H_{35}N_4O_6S)_{32}Gd_{32}$
$LacC_5S$-Au-$SC_{11}DO3A$-Gd	2.7±0.2	1.7±0.3	129	$Au_{314}(C_{17}H_{31}O_{11}S)_{116}(C_{25}H_{47}N_4O_6S)_{22}Gd_{22}$
$LacC_5S$-Au-SC_5DO3A-Gd	3.7±0.2	1.6±0.2	128	$Au_{314}(C_{17}H_{31}O_{11}S)_{108}(C_{19}H_{35}N_4O_6S)_{30}Gd_{30}$

[a] Gd content calculated from ICP-AES analysis**,** size of gold cores from TEM, and molecular formula of the GNPs by combining elemental analysis and TEM.

Z-potential. Figure 1.6 shows the zeta potential of $GlcC_5S$-Au-$SC_{11}DO3A$-Gd as a function of pH value. The data obtained at 0.150 mg/mL of GNP in HEPES, reveals that the particles have a significant negative charge on the surface between pH 4.4 and 8.4. The surface charge decreases drastically between 7.4 and 8.4 pH as a result of the deprotonation of the carboxyl group.

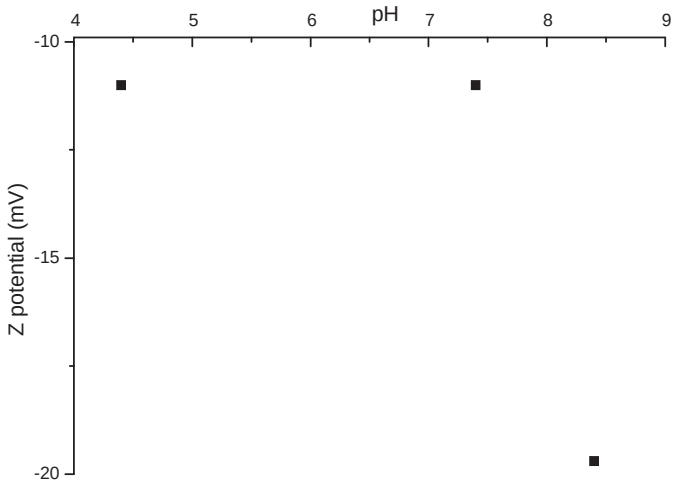

Figure 1.6: *Zeta potential of $GlcC_5S$-Au-SC_{11}DO3A-Gd glyconanoparticle (GNP) as a function of pH value. The data was obtained at 0.150 mg/mL of GNP in HEPES.*

^{17}O-NMR. The presence of water molecules in the inner-sphere of a paramagnetic lanthanide complex is reflected in the ^{17}O-NMR data of water. [19] The number of the water molecules directly coordinated to the Gd(III) ion (q) is calculated from Equation 1, where Δ is the lanthanide-inducted shift (calculated from Equation 2), <S> is a constant characteristic for each lanthanide compound and F is a constant which depends on the temperature (Equation 3). Number q was determined for an aqueous (D_2O) solution of $GlcC_5S$-Au-SC_{11}DO3A-Gd $ManC_5S$-Au-SC_{11}DO3A-Gd and $GalC_5S$-Au-SC_{11}DO3A-Gd containing 6 mM, 5.6 mM and 6.2 mM of Gd(III) respectively. As expected for a heptadentate chelating agent (DO3A), the GNP showed q~2 (Table 1.4).

Equation 1: $\boldsymbol{q = \Delta / \langle S \rangle \times F}$

Equation 2: $\Delta = -(\delta_{obserb} - \delta_{D2O}) / P_{m,}$ where $P_m = [Gd^{3+}] / [H_2O]$

Equation 3: $F = -2.407 \times 10^4 / T\ (K)$

Table 1.4: *Paramagnetic ion concentration, temperature and measured ppm in ^{17}O-NMR experiments for the calculation of the number of the water molecules directly coordinated to the Gd(III) ion (q).*

Compound	[Gd] or [Dy] (mM)	T (ºC)	δ_{obserb} (ppm)	δ_{D2O} (ppm)	*q*
$HSC_{11}DO3A$-Dy	6.4	70	-1.884	-1.409	~2.0
HSC_5DO3A-Dy	6.1	70	-1.901	-1.451	~2.1
$GlcC_5S$-Au-$SC_{11}DO3A$-Gd	6	60	-1.515	-1.063	~1.8
$GalC_5S$-Au-$SC_{11}DO3A$-Gd	6.2	60	-1.914	-1.462	~1.8
$ManC_5S$-Au-$SC_{11}DO3A$-Gd	5.6	60	-1.894	-1.462	~1.9

Proton Nuclear Magnetic Relaxation Dispersion (^{1}H-NMRD) spectroscopy. Longitudinal proton relaxation rates were measured for $GlcC_5S$-Au-$SC_{11}DO3A$-Gd and Dotarem® (DOTA-Gd) at 0.7 mM and 37 ºC (Figure 1.7). ^{1}H-NMRD studies performed with low molecular weight Gd(III)-based contrast agents [20] showed how r_1 decreases when the magnetic field increases. The measurements done with Dotarem® at 37 ºC indicate that it reaches a plateau at ~60 MHz (~3 $sm^{-1}M^{-1}$). GNPs are macromolecules and r_1 reaches a maximum at 20 MHz and then decrease, as it is expected for these types of compounds. [21]

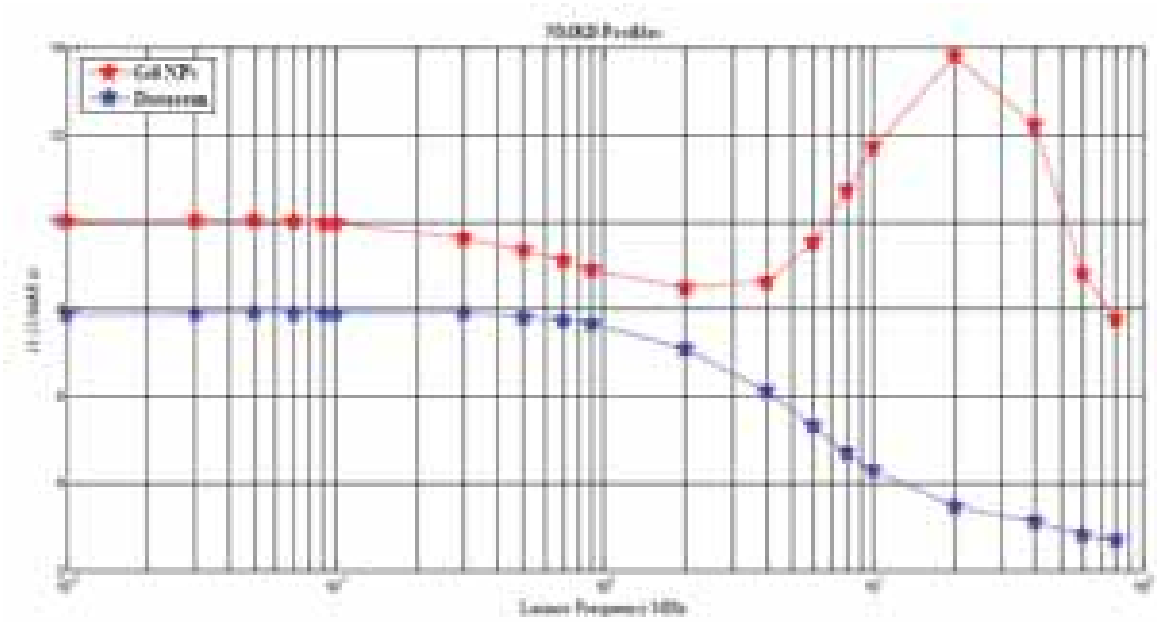

Figure 1.7: *^{1}H NMRD spectroscopy of $GlcC_5S$-Au-$SC_{11}DO3A$-Gd (red) and Dotarem® (DOTA-Gd) (blue) at 0.7 mM and 37 ºC, as measured between 10^{-2} MHz and 10^2 MHz (2.2 T)*

[20] S. Laurent, L. Vander Elst and . N. Muller., *Contrast Media Mol. Imaging*, **2006**, 1, 128-137
[21] S. Aime, M. Botta, S. Geninatti Crich, G. Giovenzana, G. Palmisano and M. Sistie *Chem. Commun.*, **1999**, 1577–1578 (A macromolecular Gd(III) complex as pH-responsive relaxometric probe for MRI applications).

Relaxivities r_1 and r_2. The ability of a paramagnetic contrast agent to reduce the longitudinal relaxation time T_1 is described by the relaxivity (r_1), which is the slope of the curve obtained by plotting the concentration of the contrast agent in terms of Gd(III) millimolarity *vs* the corresponding $1/T_1$ (T_1 in seconds). The amount of Gd(III) present in the GNPs was measured by (ICP-AES). The longitudinal (T_1) and transversal (T_2) relaxation times were measured at five different concentrations of GNPs (10, 5, 2.5, 1.25, 0.625 mg/mL) in MilliQ water, at 1.41 T. The relaxivity values r_1 and r_2 were obtained from the slopes of the curves $1/T_{1(2)}$ *vs* the concentration of Gd(III) expressed in mM and are reported in Tables 1.5-1.7. The ratio between the transverse and longitudinal relaxivities (r_2/r_1) in the paramagnetic GNPs is in the range 1.5-1.8, i.e. these nanoparticles have a large paramagnetic property (high r_1) with tiny magnetic anisotropy (low r_2) in agreement with the typical relaxation properties of T_1-agents.

The relaxivity values of the free Gd-complexes were also measured. The relaxativity values below the critical micellar concentration (c.m.c) of the HSC_{11}DO3A-Gd ligand is r_1=6.6 $s^{-1}mM^{-1}$. The HSC_{11}DO3A-Gd complex can form micelles at 3 mM concentration; the r_1 value above the c.m.c is 16.3 $s^{-1}mM^{-1}$. On the contrary, HSC_5DO3A-Gd ligand can not form micelles and only showed one relaxivity value, r_1=6.4 $s^{-1}mM^{-1}$.

GNPs coated with 100% sugar (the starting material before incubation with the Gd-complexes) are not paramagnetic and did not show any appreciable difference with respect to water in terms of T_1.

Table 1.5: *Longitudinal and transversal relaxivities of $GlcC_xS$-Au-SC_{11}DO3A-Gd GNPs measured in water at 1.41 T and 37 ºC.*

GNPs	r_1 ($s^{-1}mM^{-1}$)	r_2 ($s^{-1}mM^{-1}$)	% Gd
$GlcC_2S$-Au-SC_{11}DO3A-Gd	7.1±0.9	11.0±0.6	3.4±0.2
$GlcC_3S$-Au-SC_{11}DO3A-Gd	6.3±0.7	10.5±0.6	3.3±0.2
$GlcC_5S$-Au-SC_{11}DO3A-Gd	7.4±0.7	11.9±0.4	4.7±0.1
$GlcC_7S$-Au-SC_{11}DO3A-Gd	7.1±0.9	11.8±0.1	4.1±0.2
$GlcC_9S$-Au-SC_{11}DO3A-Gd	7.5±0.6	13.0±0.4	3.2±0.2
HSC_{11}DO3A-Gd	6.6±0.2	10.2±0.1	ND
Dotarem®	3.0±0.1	3.6±0.1	ND

ND: Not determined.

Table 1.6: *Longitudinal and transversal relaxivities of glycoC_5S-Au-SC_{11}DO3A-Gd NPs measured in water at 1.41 T and 37 ºC.*

GNPs	r_1 ($s^{-1}mM^{-1}$)	r_2 ($s^{-1}mM^{-1}$)	% Gd
GlcC_5S-Au-SC_{11}DO3A-Gd	7.4±0.7	11.9±0.4	4.7±0.1
GalC_5S-Au-SC_{11}DO3A-Gd	8.0±0.9	12.9±0.8	4.2±0.2
ManC_5S-Au-SC_{11}DO3A-Gd	9.7±0.6	16.5±0.1	3.0±0.2
cellobioseC_5S-Au-SC_{11}DO3A-Gd	11.2±0.9	21.3±0.7	2.1±0.2
maltoseC_5S-Au-SC_{11}DO3A-Gd	12.8±0.8	21.4±0.8	3.1±0.2
LacC_5S-Au-SC_{11}DO3A-Gd	12.9±0.9	21.5±0.9	2.0±0.2
HSC_{11}DO3A-Gd	6.6±0.2	10.2±0.1	ND
Dotarem®	3.0±0.1	3.6±0.1	ND

ND: Not determined.

Table 1.7: *Longitudinal and transversal relaxivities of glycoC_5S-Au-SC_5DO3A-Gd NPs measured in water at 1.41 T and 37 ºC.*

GNPs	r_1 ($s^{-1}mM^{-1}$)	r_2 ($s^{-1}mM^{-1}$)[1]	% Gd
GlcC_5S-Au-SC_5DO3A-Gd	16.9±0.4	27.9±0.8	3.1±0.2
GalC_5S-Au-SC_5DO3A-Gd	18.0±0.3	30.6±0.9	3.6±0.2
ManC_5S-Au-SC_5DO3A-Gd	15.5±0.9	25.9±0.4	4.1±0.2
cellobioseC_5S-Au-SC_5DO3A-Gd	16.6±0.9	30.7±0.9	2.1±0.2
maltoseC_5S-Au-SC_5DO3A-Gd	14.7±0.6	25.7±0.5	3.6±0.2
LacC_5S-Au-SC_5DO3A-Gd	17.0±0.8	29.5±0.1	3.7±0.2
HSC_5DO3A-Gd	9.4±0.2	10.6±0.2	ND
Dotarem®	3.0±0.1	3.6±0.1	ND

ND: Not determined.

In vitro MRI at 11.7 T (phantoms). MR images of "phantoms" of GNPs were carried out at 11.7 T using a Gradient Echo Sequence with TR (Repetition time) = 400 ms and TE (Echo time)= 4.7 ms. T_1-weighted images of phantoms containing aqueous solution of GNPs (with Gd (III) varying from 5 to 200 μM) confirmed that these GNPs behave as positive contrast agents: the phantoms appear brighter than the negative control (water). The phantom containing the highest amount of Gd(III) (200 μM) appears the brightest (Figure 1.8A).

In order to obtain T_1 values from the images, a region of interest (ROI) was drawn on each of the phantoms in the image at a given slice. The mean signal intensity of the ROI was computed at all

the repetition times. These data were then fitted to a saturation recovery exponential function. The calculated lowest T_1 values (highest r_1) correspond to the brightest images.

A

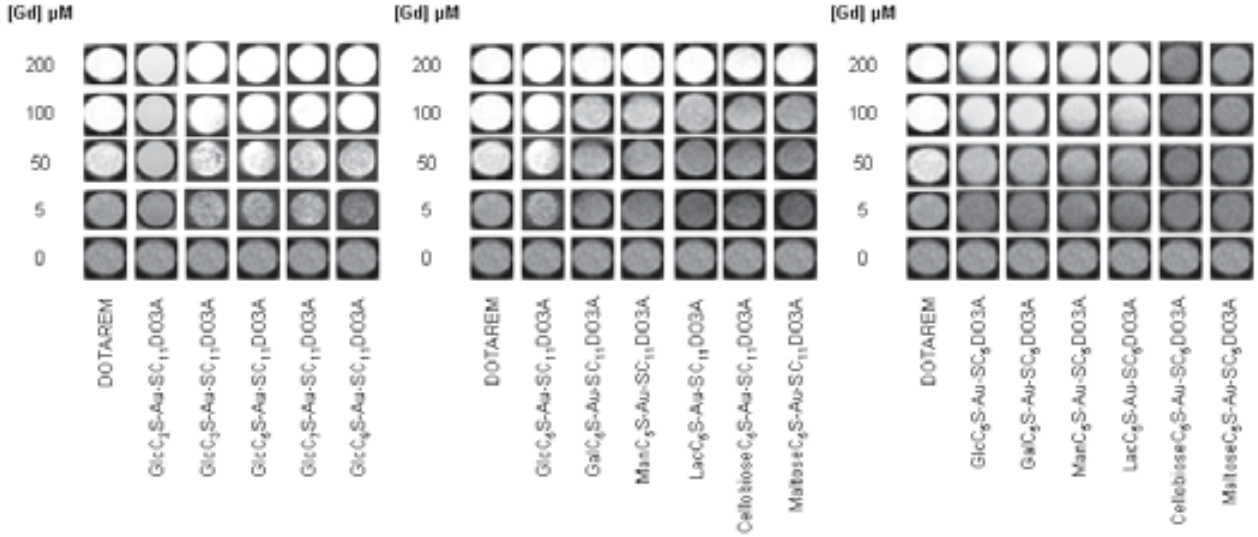

B

GNPs	r_1 ($s^{-1}mM^{-1}$) 1.41 T	r_1 ($s^{-1}mM^{-1}$) 11.7 T
$GlcC_2S$-Au-SC_{11}DO3A-Gd	7.1±0.9	1.8±0.8
$GlcC_3S$-Au-SC_{11}DO3A-Gd	6.3±0.7	2.1±0.9
$GlcC_5S$-Au-SC_{11}DO3A-Gd	7.4±0.7	2.5±0.9
$GlcC_7S$-Au-SC_{11}DO3A-Gd	7.1±0.9	2.0±0.7
$GlcC_9S$-Au-SC_{11}DO3A-Gd	7.5±0.6	2.7±0.9
$GalC_5S$-Au-SC_{11}DO3A-Gd	8.0±0.9	2.1±0.9
$ManC_5S$-Au-SC_{11}DO3A-Gd	9.7±0.6	2.3±0.6
cellobioseC_5S-Au-SC_{11}DO3A-Gd	11.2±0.9	2.8±0.7
maltoseC_5S-Au-SC_{11}DO3A-Gd	12.8±0.8	3.5±0.9
$LacC_5S$-Au-SC_{11}DO3A-Gd	12.9±0.9	4.4±0.9
$GlcC_5S$-Au-SC_5DO3A-Gd	16.9±0.4	4.0±0.6
$GalC_5S$-Au-SC_5DO3A-Gd	18.0±0.3	4.1±0.8
$ManC_5S$-Au-SC_5DO3A-Gd	15.5±0.9	3.8±0.9
cellobioseC_5S-Au-SC_5DO3A-Gd	16.6±0.9	0.2±0.2
maltoseC_5S-Au-SC_5DO3A-Gd	14.7±0.6	0.8±0.4
$LacC_5S$-Au-SC_5DO3A-Gd	17.0±0.8	3.8±0.7
Dotarem®	3.0±0.2	3.6±0.8

Figure 1.8: *A) T_1-weighted MR images (phantoms) of $GlcC_xS$-Au-SC_{11}DO3A-Gd, glycoC_5S-Au-SC_{11}DO3A-Gd, glycoC_5S-Au-SC_5DO3A-Gd GNPs and Dotarem® at different concentrations, acquired at 11.7 T and 25 ºC in water. B) Longitudinal relaxivities values of $GlcC_xS$-Au-SC_{11}DO3A-Gd, glycoC_5S-Au-SC_{11}DO3A-Gd, glycoC_5S-Au-SC_5DO3A-Gd GNPs and Dotarem® in water at 1.41 T and 37 ºC and 11.7 T and 25 ºC.*

The results obtained with Dotarem® and GNPs at 11.7 T (500 MHz) showed that, at the same Gd(III) concentration, Dotarem® has better T_1 value than the GNPs while at 1.41 T (60 MHz) the GNPs are better contrast agents. The image-based r_1 of Dotarem® at 11.7 T was 3.6 $mM^{-1}s^{-1}$, while r_1 of paramagnetic GNPs at this magnetic field suffer a dramatic decrease (see Figure 1.8-B). The maintenance of relaxivity of Dotarem® at 11.7 T respect to 1.41 T indicates a scarce dependence of field strength, as expected for small molecular T_1-contrast agents. [22] The considerable decrease in T_1-relaxivity at 11.7 T (around 70%) for GNPs is expected for these types of macromolecules. [23]

3.2 *Preparation of Gd-based paramagnetic gold glyconanoparticle with DOTA-N-(2-aminoethyl)ethanamide Gd(III)-complex derivatives (HSC_{11}-EdA-DOTA-Gd or HSC_{11}-EdA-DOTA-Gd).*

A key feature of Gd-based probes is their thermodynamic stability and their rate of decomplexation/transmetallation (kinetic stability). [24] For this reason, all Gd-based contrast agents in clinical use are nine-coordinated complexes forming the Gd 8 bonds with the multidentate ligand and only one bond with a water molecule. Gd(III) complexes with macrocyclic DO3A-like heptadentate ligands are generally less stable than complexes of analogous DOTA-*N*-(2-aminoethyl)ethanamide derivatives and the dissociation rate is about two orders of magnitude higher for $Gd(DO3A)(H_2O)_2$ complex than for $Gd(DOTA)(H_2O)$ complex.[25] To reduce the toxicity and have in hand GNPs with potentiality for clinical use, the chelating agent DOTA-*N*-(2-aminoethyl)ethanamide was chosen. Starting from DOTA-*N*-(2-aminoethyl)ethanamide DOTA-EdA-C_xSH with eleven or five carbon atoms chain were prepared by using a peptidic coupling. [26]

---

[22] P. Caravan, C. T. Farrar, L. Frullano and R. Uppal, *Contrast Media Mol. Imaging,* **2009**, 4 89–100 (Influence of molecular parameters and increasing magnetic field strength on relaxivity of gadolinium- and manganese-based T1 contrast agents)

[23] Y. T. Lim, M. Y. Cho, B. S. Choi, J. M. Lee and B. H. Chung, *Chem. Commun*., **2008**, 4930–4932 (Paramagnetic gold nanostructures for dual modal bioimaging and phototherapy of cancer cells)

[24] S, Laurent, L. Vander Elst, F.M.A. Copoix and R. Muller, *Invest. Radiol*., **2001**, 36, 115-122 (Stability of MRI Paramagnetic Contrast Media. A Proton Relaxometric Protocol for Transmetallation Assessment)

[25] C. Thakral, J. Alhariri and J. L. Abraham, *Contrast Media Mol Imaging,* **2007**, 2, 199-205 (Long-term retention of gadolinium in tissues from nephrogenic systemic fibrosis patient after multiple gadolinium-enhanced MRI cases:case report and implications)

[26] L.M. De Leon-Rodriguez, S. Viswanathan and A. D. Sherry *Contrast, Media Mol. Imaging*, **2010**, 5, 121–125 (Improved synthesis of DOTA tetraamide ligands for lanthanide(III) ions: A tool for increasing the repertoire of potential PARACEST contrast agents for MRI and/or fluorescent sensors).

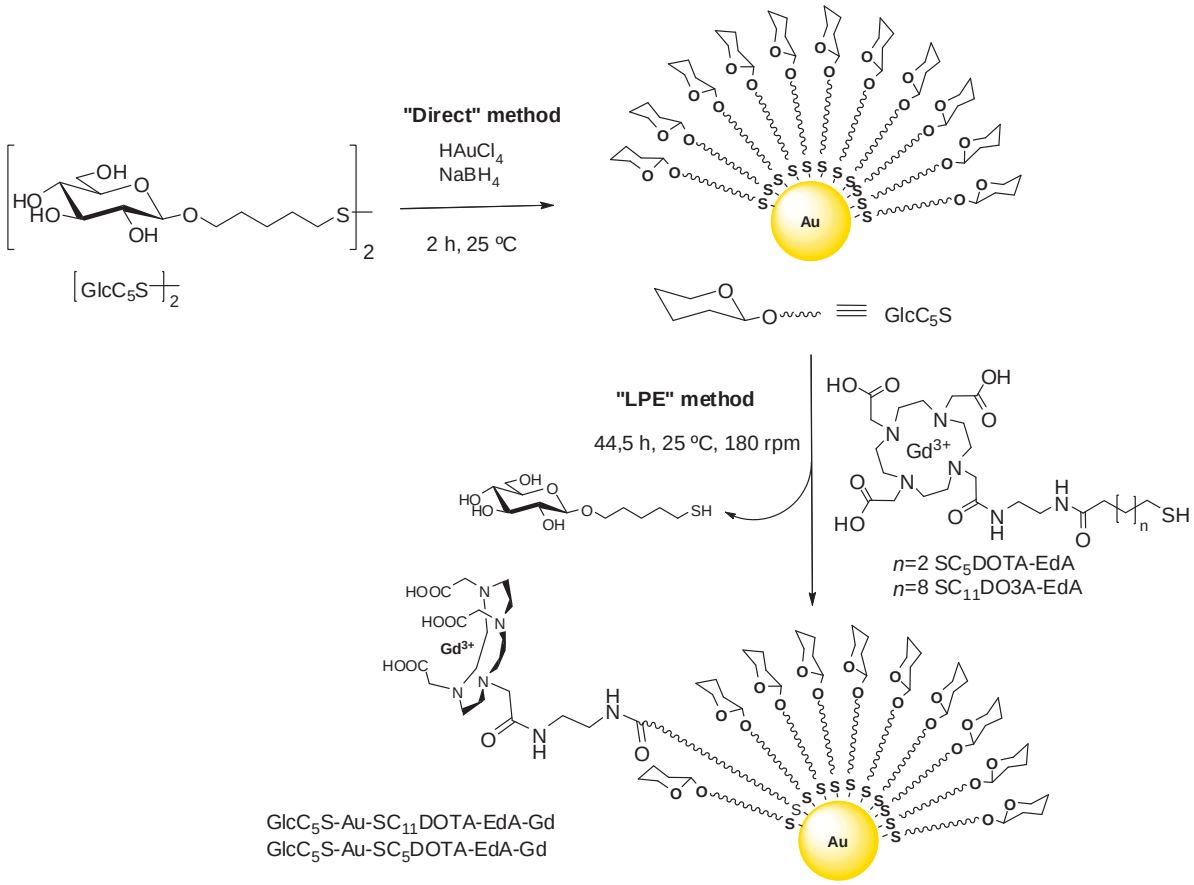

Scheme 1.13: *Synthesis of paramagnetic Gd-based gold glyconanoparticles (GNPs) by Ligand Place Exchange (LPE) of 100% sugar-coated gold GNPs and DOTA-EdA-Gd complexes.*

The Gd-complexes were prepared as explained in paragraph **1.3.** (*Synthesis of DO3A and DOTA-EdA derivatives)*. The Gd-based GNPs (Scheme 1.13) prepared with these new ligands were synthesized starting form $GlcC_5S$-Au GNPs following the LPE method describe before in paragraph **3** (Preparation of Gd-based paramagnetic gold glyconanoparticles by ligand place exchange method).

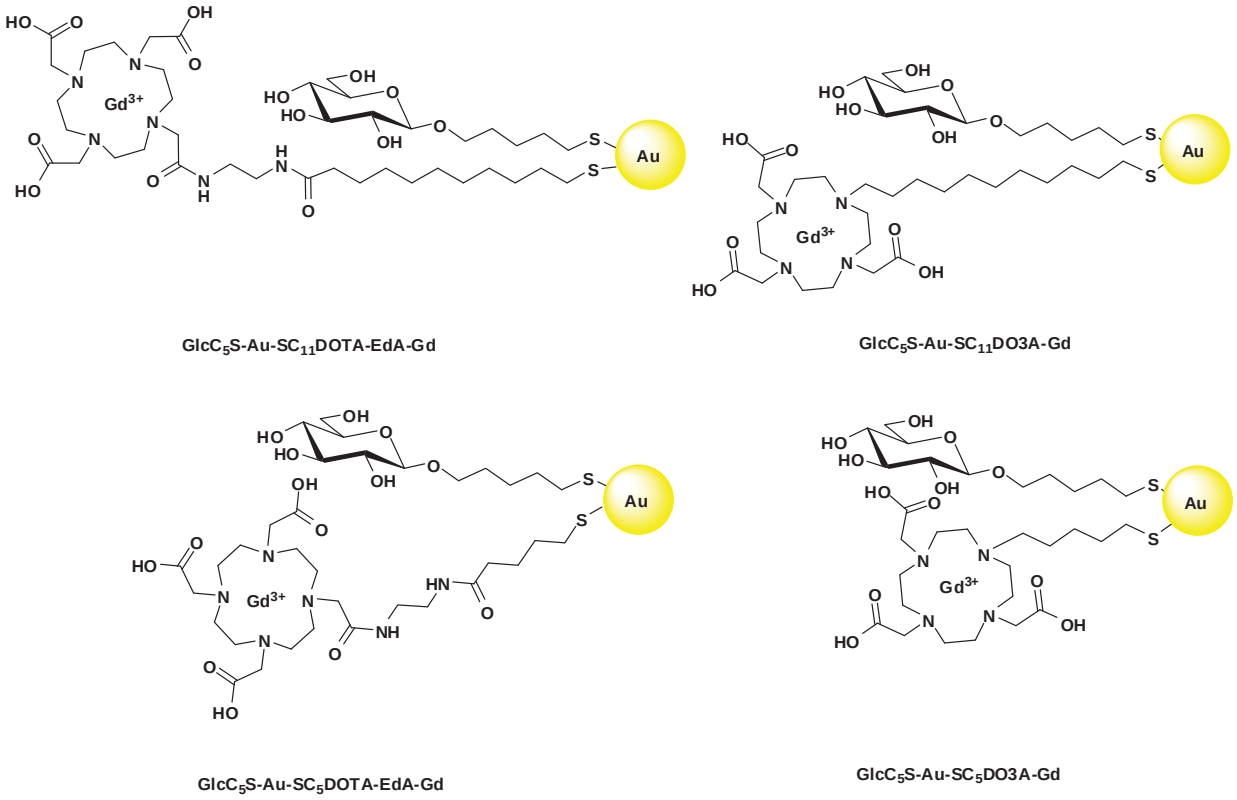

Figure 1.9: *$GlcC_5S$-Au-SC_{11}DOTA-EdA-Gd, $GlcC_5S$-Au-SC_{11}DO3A-Gd, $GlcC_5S$-Au-SC_5DOTA-EdA-Gd and $GlcC_5S$-Au-SC_5DO3A-Gd GNPs.*

Relaxivities. The relaxivity values obtained for $GlcC_5S$-Au-SC_{11}DOTA-EdA-Gd GNP were r_1= 18.4 $(smM)^{-1}$ and r_2= 31.1 $(smM)^{-1}$ and for $GlcC_5S$-Au-SC_5DOTA-EdA-Gd were r_1= 4.5 $(smM)^{-1}$ and r_2= 7.4 $(smM)^{-1}$ (Table 1.8). The amount of Gd found (3.6 % for $GlcC_5S$-Au-SC_{11}DOTA-EdA-Gd and 3.6 % for $GlcC_5S$-Au-SC_5DOTA-EdA-Gd) is in the range of that found for the other GNPs using the following conditions: 1.1 equivalents of the chelant, 44 hours of incubation, 180 rpm and 25 ºC.

Table 1.8: *Longitudinal and transversal relaxivities of $GlcC_5S$-Au-SC_{11}DOTA-EdA-Gd, $GlcC_5S$-Au-SC_{11}DO3A-Gd GNPs.*

GNPs	r_1 ($s^{-1}mM^{-1}$)	r_2 ($s^{-1}mM^{-1}$)	% Gd
$GlcC_5S$-Au-SC_{11}DOTA-EdA-Gd	18.4±0.9	31.1±0.9	3.6±0.3
$GlcC_5S$-Au-SC_{11}DO3A-Gd	7.4±0.7	11.9±0.4	4.7±0.1
$GlcC_5S$-Au-SC_5DOTA-EdA-Gd	4.5±0.9	7.4±0.8	3.6±0.2
$GlcC_5S$-Au-SC_5DO3A-Gd	16.9±0.4	27.9±0.8	3.1±0.2

The r_1 of $GlcC_5S$-Au-SC_{11}DOTA-EdA-Gd is 3 times higher than r_1 of $GlcC_5S$-Au-SC_{11}DO3A-Gd (Table 1.7). However, in the case of $GlcC_5S$-Au-SC_5DOTA-EdA-Gd and $GlcC_5S$-Au-SC_5DO3A-Gd the values are just the opposite: the r_1 of $GlcC_5S$-Au-SC_5DO3A-Gd is 4 times the the r_1 of $GlcC_5S$-Au-SC_5DOTA-EdA-Gd. The difference between these GNPs is the macrocyclic chelate (Figure 1.9). In $GlcC_5S$-Au-SC_{11}DOTA-EdA-Gd and $GlcC_5S$-Au-SC_5DOTA-EdA-Gd the number of water molecules coordinated to each Gd centre (q) is 1 whereas in $GlcC_5S$-Au-SC_{11}DO3A-Gd and $GlcC_5S$-Au-SC_5DO3A-Gd is 2. Taken this into account, the relaxivity for $GlcC_5S$-Au-SC_{11}DO3A-Gd and $GlcC_5S$-Au-SC_5DO3A-Gd should be higher than in the case of DOTA-EdA-Gd GNPs, because incrementing the number of q the relaxivity increases. In the case of $GlcC_5S$-Au-SC_5DO3A-Gd and $GlcC_5S$-Au-SC_5DOTA-EdA-Gd the relaxivity of $GlcC_5S$-Au-SC_5DO3A-Gd is higher than the relaxivity of $GlcC_5S$-Au-SC_5DOTA-EdA-Gd, and it seems that the number of water molecules exchanging with the Gd(III) is the parameter which governs the relaxivity. However, an opposite values are obtained for $GlcC_5S$-Au-SC_{11}DO3A-Gd and $GlcC_5S$-Au-SC_{11}DOTA-EdA-Gd. It could be that the values of the rotational correlation time (τ_R) and the residence lifetime (τ_m) of the Gd complexes influence in different way the relaxativity values..

3.3 *Discussion.*

The set up of a robust method based on the ligand place exchange (LPE) for the preparation of Gd-based paramagnetic gold glyconanoparticles assure the reproducibility of GNPs as MRI probes. The main advantage of the LPE method herein described is that the amount of Gd(III) inserts on the gold nanoparticles depends on the number of exchanged Gd-complexes. The exchange is the same as far as the reaction condition are constant. This also avoids the need of extensive washings of the nanoparticles to eliminate the free Gd cations and, for nanoparticles bearing biomolecules like carbohydrates, help to overcome the possible coordination of Gd(III) by the hydroxy groups of the sugars.

Keeping the same incubation conditions for the exchange reaction, the amount of HSC_{11}DO3A-Gd or HSC_5DO3A-Gd present in each GNP is the same inside the error (Tables 1.5-1.7) and, thus, the values of r_1 and r_2 must not change, if other factors (τ_R, τ_M, q) are maintained constant (see Introduction).

The amount of Gd(III) in each GNP is reproducible and slightly higher than the one obtained using the direct synthesis. [5] The percentages values of Gd are in the range ~3-5% with the exception of cellobiose-derivatives which is lower (2.7 %) (Table 1.5-1.7), while most of the GNPs prepared by the "direct" method had a final Gd(III) content between ~0.5-2%. [5] In

general, the current results show that incubation of the DO3A-derivatives with $GdCl_3$ in pH-controlled conditions before incubation with the preformed GNPs allows a better control of the gadolinium amount in the GNPs. In place exchange reaction the ligand exchange takes place preferently on gold atoms in edge and vertice positions which are more reactive that the atoms on terrace sites. [17] It is supposed that thiol-for-thiol exchange onto the pre-formed GNPs prevalently occurs at these positions of the gold nanoclusters. This may have implications on the presentation of the ligands on the cluster which is probably different respect to the one obtained with the direct synthesis [5], which could explain the different value of r_1 for the nanoparticles in spite of they contain the same precent of Gd (Table 1.8).

In the five GNPs bearing glucose derivatives $GlcC_xS$-Au-SC_{11}DO3A-Gd, the amount of Gd(III) and the relaxivity values are almost the same (~ 7 $s^{-1}mM^{-1}$, Table 1.5). In all these cases the Gd-complex protrudes above the sugar moiety, being free to move (Figure 1.10) so that no differences in τ_R, τ_M and q values are expected.

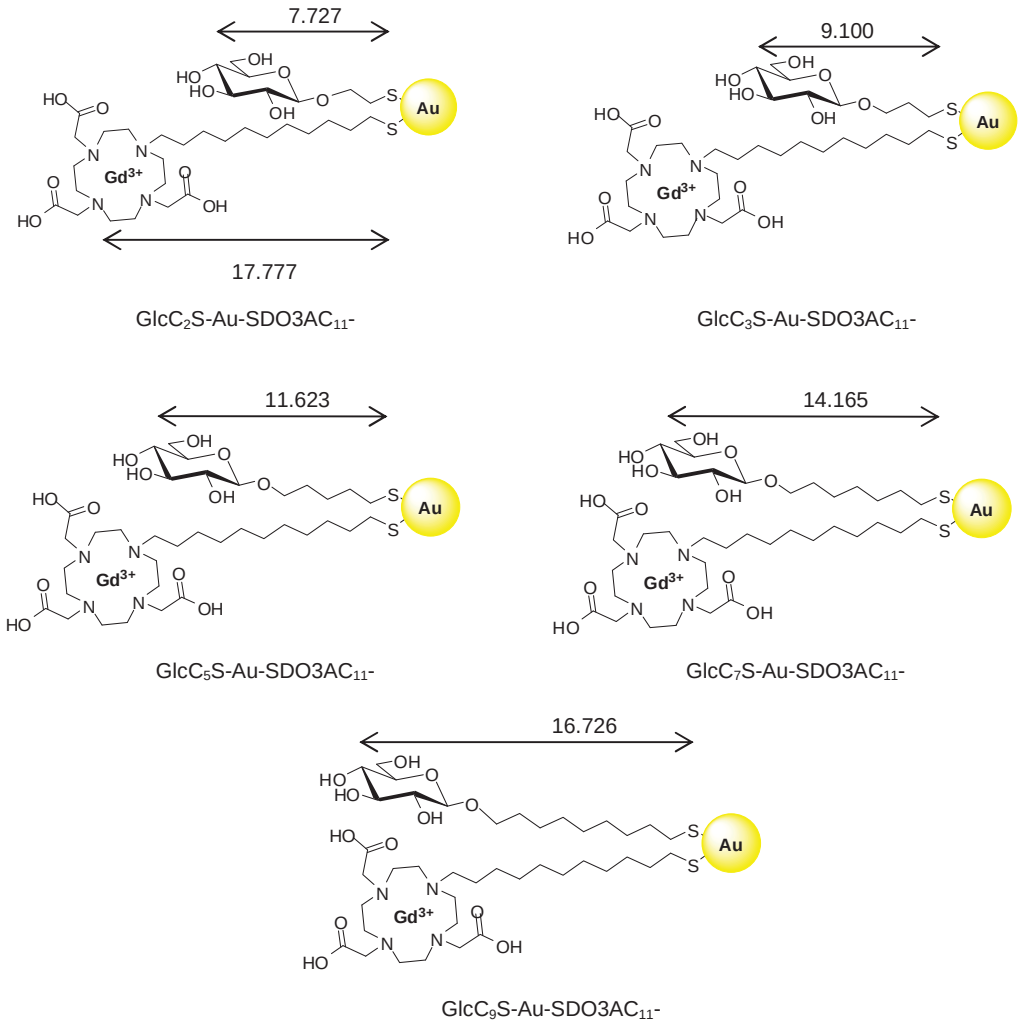

Figure 1.10: *Longitude of the different ligands in $GlcC_xS$-Au-SC_{11}DO3A-Gd GNPs taken from the sulphur atoms to either the C-4 atom of the sugars or to the N-4 of the aza-cyclo derivative. NOTE: GNPs are not drawn in scale in order to a better visualization.*

A similar situation also takes place in the GNPs bearing mannose and galactose and the HSC_{11}DO3A-Gd complex, with relaxivity values between 7.4-9.7 $s^{-1}mM^{-1}$ (Table 1.6). However, in the monosaccharide series where the chelant and the sugars have the same longitude (C5), the proximity of the sugars may contribute to immobilize the DO3A-Gd complex and the relaxivity r_1 values are about the double (range 15.5-18.0 $s^{-1}mM^{-1}$) than those obtained for the monosaccharideC_5S-Au-SC_{11}DO3A-Gd GNPs (7.4-9.7 $s^{-1}mM^{-1}$) (Figure 1.11). All GNPs functionalized with disaccharides and Gd-complexes (Figure 1.11) show r_1 values in the same range (11.2-12.9 $s^{-1}mM^{-1}$ and 14.7-17.0 $s^{-1}mM^{-1}$) .The blocking effect due to the packing of the glycoconjugates towards the Gd-chelate derivatives having similar length may enhance the rigidity of the chelate, contribute to slow the rotation of Gd-complex, and be thus responsible for the improvement of the Gd(III) relaxivity. These results are in agreement with our previous finding that the relative position of the sugar moiety respect to the paramagnetic ion seems to play a role in tuning the relaxivity. [5]

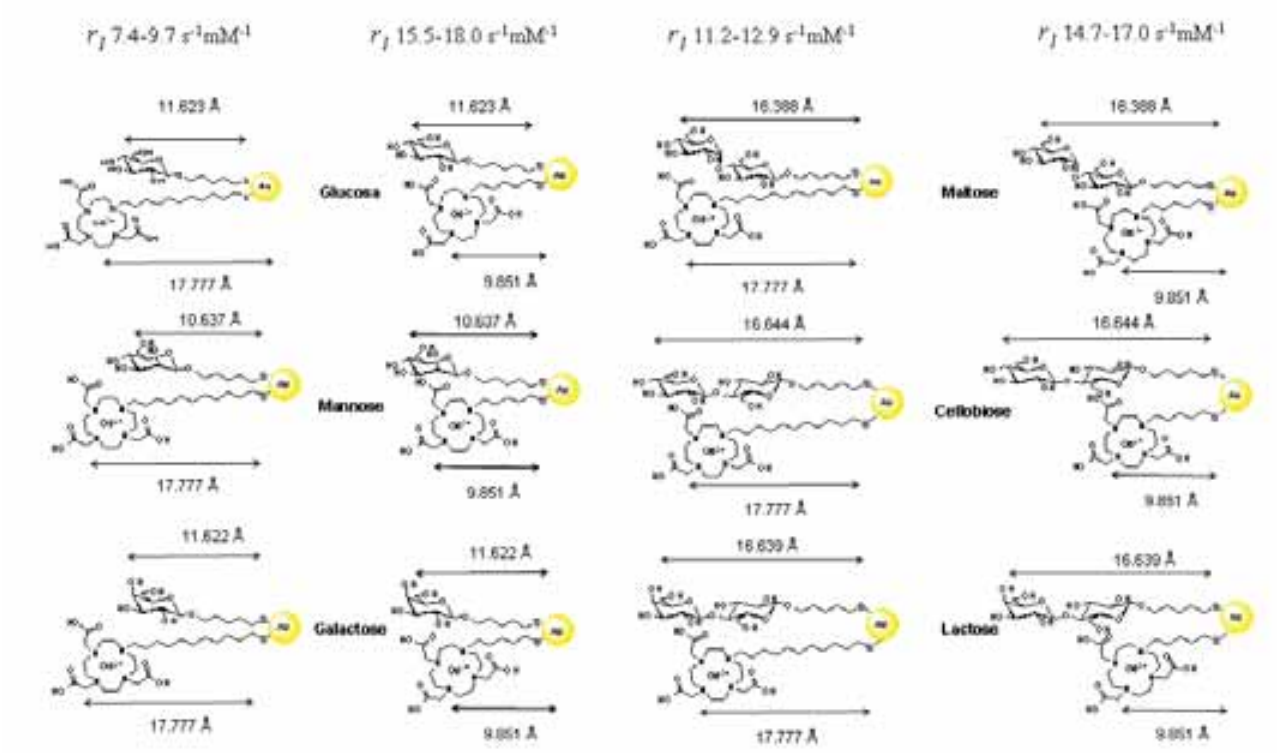

Figure 1.11: *Longitude of the different ligands in glycoC_xS-Au-SC_{11}DO3A-Gd and glycoC_xS-Au-SC_5DO3A-Gd GNPs taken from the sulphur atoms to either the C-4' atom of the sugars or to the N-4 of the aza-cyclo derivative. NOTE: GNPs are not draw in scale in order to a better visualization.*

The relaxivity values of the GNP synthesized in this Thesis, measured at 1.41 T(60 MHz) range from 6.3 to 18.0 $s^{-1}mM^{-1}$. All of them showed better values than the commercial agent Dotarem® (r_1= 3.0 $s^{-1}mM^{-1}$). When the relaxivity of GNPs was measured at higher fields (11.7 T, 500 MHz),

the r_1 of Gd-based paramagnetic GNPs decreased around 70%, while the relaxivity value of Dotarem® is maintained (Figure 1.8B), as it is expected for small molecules. Macromolecules are field-dependent and their relaxivity decreases when the field increases. [21] This represents a disadvantage for GNPs as macromolecules and the reason why in the MRI phantoms at 11.7 T, Dotarem® showed brighter contrast than the GNPs. However, these results do not necessarly correlated with the results in vivo. In fact, paramagnetic GNPs incorporating monosaccharides are able to cause a selective, hiperintensive signal in different cell lines, while Dotarem are not able to increase the contrast of them, or glucose incorporating GNPs are as good contrast agents for imaging *in vivo* glioma in mice than Dotarem® (see Chaper 2 and 3). In addition, gold glyconanoparticles offer a platform for simultaneous introduction of a variety of molecules (peptides, fluorescence probes…) for having targeted, multimodal and multifunctional probes or singular properties to reach easely the brain. The original idea to introduce glucose into the GNPs was to facilitate the crossing of the blood brain barrier (BBB) and to better imaging glioma in its early stage.

Sugars have also the capacity to confer biocompatibility to nanomaterials. In our experience, all gold and magnetic glyconanoparticles tested up to day have not shown any cytotoxycity at concentration up to 100 μg/mL. Cytotoxicity assays have been carried out in GL261 glioma cells with the GNPs prepared in this Thesis. The results are reported in chapter 2.

4. Conclusions

Multivalent Gd-based paramagnetic gold glyconanoparticles have been designed as MRI probes and prepared using two different methods: "direct" synthesis and ligand place exchange (LPE) reactions. The latter method showed the best results in terms of increased Gd(III) content and reproducibility. Using LPE method, a small library of paramagnetic GNPs has been prepared by systematic variation of the sugar nature and the length of the linkers, to rationalize the changes observed in the relaxivity values.

The small size (2–4 nm) of the GNPs and the coating of carbohydrates make them highly stable in water or in buffer and non-toxic to cells. Differences up to the double in relaxivity values can be obtained by changing the nature of the sugar and the relative position of the sugar moiety with respect to the paramagnetic ion.

In the following chapters, the application of selected glyconanoparticles as T_1-reporters of cellular receptors (Chapter 2) and the results obtained with $GlcC_5S$-Au-SC_{11}DO3A-Gd GNP as MRI

probe for imaging *in vivo* glioma in mice and its biodistribution and toxicity profile will be presented (Chapter 3).

5. Experimental part

General. All chemicals were purchased as reagent grade from Sigma-Aldrich and were used without further purification. UV-Vis spectra were carried out with a Beckman Coulter DU 800 spectrometer. Infrared spectra (IR) were recorded from 4000 to 500 cm^{-1} with a JASCO FT/IR 410 model spectrometer: solids were pressed into a KBr plate and oils were subjected to attenuated total reflection (ATR). ^{1}H-NMR and ^{13}C-NMR spectra were recorded Bruker AVANCE (500 MHz) spectrometer. Chemical shifts (δ) are given in ppm relative to the residual signal of the solvent used. Coupling constants (*J*) are reported in Hz. Splitting patterns are described by using the following abbreviations: br, broad; s, singlet; d, doublet; t, triplet; q, quartet; m, multiplet. Mass spectra were carried out with an Esquire 6000 ESIIon Trap from Bruker Daltonics. High resolution mass spectra (HR-MS) were obtained using the matrix-assisted laser desorption/ionization (MALDI) technique with a 4700 Proteomics Analyzer (Applied Biosystems) with MALDI-time-of-flight (TOF) configuration. For transmission electron microscopy (TEM) examinations, a single drop (1 μL) of the aqueous solution (ca. 0.1 mg/mL in milliQ water) of the gold glyconanoparticles (GNPs) was placed onto a copper grid coated with a carbon film (Electron Microscopy Sciences). The grid was left to dry in air for several hours at room temperature. TEM analysis was carried out in a Philips JEOL JEM-2100F working both at 200 kV. The average diameter and number of gold atoms of the GNPs was deduced according to a previous work. [27] House distilled water was further purified using a Milli-Q reagent grade water system (Millipore).

Synthesis of spacers:

11-(*S*-acetyl)mercaptoundecan-1-ol (1, AI002):

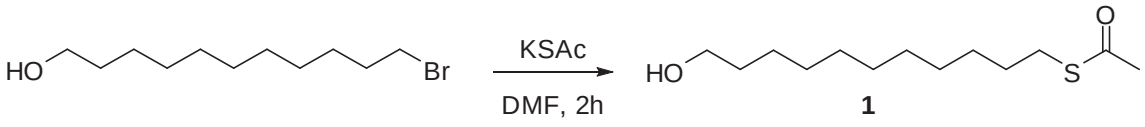

A solution of 11-bromoundecanol (10.0 g, 39.8 mmol, 1.0 eq.) and potassium thioacetate (5.5 g, 48.2 mmol, 1.2 eq.) in DMF (50 mL) was stirred at room temperature for 2 hours. The reaction mixture was diluted in AcOEt (100 mL) and then washed with water (3 x 50 mL). The organic phase was dried over anhydrous Na_2SO_4, filtered and concentrated. The resulting product was

[27] M. J. Hostetler, J. E. Wingate, C.-J. Zhong, J. E. Harris, R. W. Vachet, M. R. Clark, J. D. Londono, S. J. Green, J. J. Stokes, G. D. Wignall, G. L. Glish, M. D. Porter, N. D. Evans, R. W. Murray, *Langmuir* **1998**, *14*, 17-30.

purified by column chromatography (d = 8 cm; h = 14 cm) using AcOEt/Hexane 1/4 as eluent to give the corresponding 11-(*S*-acetyl)mercaptoundecan-1-ol (**1**) (6.77 g, 27.5 mmol, 70%) as a yellow-white solid. This compound was previously reported in the literature. [7]

Rf = 0.22 (AcOEt/Hexane 1/4).

^{1}H NMR ($CDCl_3$, 500 MHz) δ 3.64 (bt, 2H, *J* ~ 6.4 Hz, H-1), 2.86 (t, 2H, *J* = 7.4 Hz, H-11), 2.32 (s, 3H, SAc), 1.58-1.53 (m, 4H, H-2 and H-10), 1.36-1.27 (m, 14H, H-3 – H-9). OH signal not detected.

11-Triphenylmethylmercaptoundecan-1-ol (5, AI009):

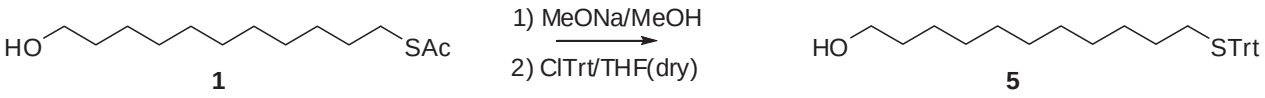

A solution of 11-(*S*-acetyl)mercaptoundecan-1-ol (**1**) [7] (2.0 g, 8.1 mmol, 1.0 eq.) and a catalytic amount of MeONa in MeOH (60 mL) was stirred under argon atmosphere for 1 hour. The product was concentrated and then dissolved in dry THF (30 mL). Tritylchloride (3.4 g, 12.2 mmol, 1.5 eq.) was added under argon atmosphere and the mixture was stirred for 15 hours. After concentration, the resulting product was purified by column chromatography (d = 4 cm; h= 10.5 cm) using AcOEt/Hexane 1/4 as eluent to give the corresponding alcohol (2.0 g, 4.2 mmol, 52%) as a transparent oil. The ^{1}H NMR was in agreement with the data reported in the literature for the same compound. [9]

Rf = 0.36 (AcOEt/Hexan 1/4).

^{1}H NMR ($CDCl_3$, 500 MHz) δ 7.42-7.20 (m, 15H, Trt), 3.63 (t, 2 H, *J* = 6.6 Hz), 2.13 (t, 2H, J= 7.4 Hz), 1.59-1.53 (m, 2H), 1.42-1.14 (m, 16H, CH_2CH_2 and OH).

1-bromo-11-triphenilmethylmercaptoundecane (2, AI010):

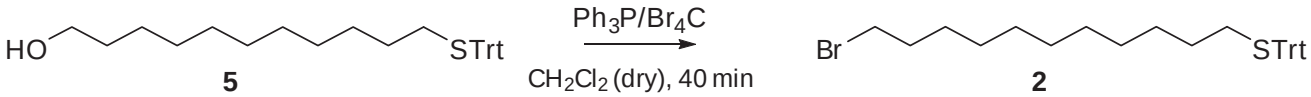

Triphenylphosphine (2.75 g, 10.50 mmol, 2.50 eq.) was added under argon atmosphere to a solution of 11-triphenylmethylmercaptoundecan-1-ol (**5**) (2.0 g, 4.2 mmol, 1.0 eq.) in CH_2Cl_2 dry (50 mL). Then, tetrabromomethane (3.48 g, 10.50 mmol, 2.50 eq.) was added slowly as the

reaction is exothermic. The mixture was stirred for 40 minutes under argon atmosphere. The reaction mixture was concentrated. The resulting product was purified by column chromatography (d = 4 cm; h = 16 cm) using AcOEt/Hexane 1/40 as eluent to give 1-bromo-11-triphenilmethylmercaptoundecane (**2**) (1.42 g, 2.62 mmol, 63%).

Rf =0.51 (AcOEt/Hexan 1/40).

^{1}H NMR ($CDCl_3$, 500 MHz) δ 7.43-7.20 (m, 15H, Trt), 3.42 (t, 2 H, H-1, J = 6.9 Hz), 2.15 (t, 2H, H-11 *J*= 7.4 Hz), 1.86 (q, 2H, H-10 *J*= 7.4, 14.4 Hz), 1.56-0.85 (m, 16H, H-2 – H-9).

^{13}C NMR ($CDCl_3$, 100 MHz) δ 144.9 (C1- Trt), 129.5 (C3-Tr), 127.7 (C2-Tr), 126.4 (C4-Tr), 68.7 (–*C*Ph_3), 36.3 (-*C*H_2CH_2Br), 35.1 (-*C*H_2Br), 34.3 (*C*H_2CH_2STr), 31.8, 31.7, 31.5, 31.4, 31.3, 31.1, 30.9, 30.5 (-*C*H_2*C*H_2-).

11-(*S*-acetyl)mercaptoundecanoic acid (3, AI160):

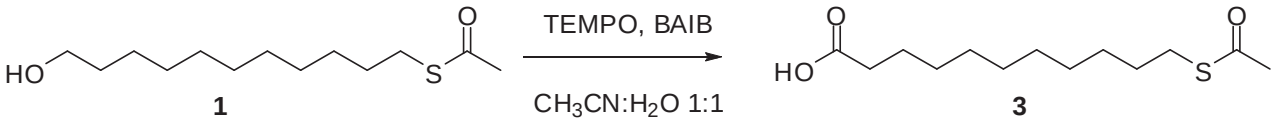

11-(*S*-acetyl)mercaptoundecan-1-ol (**1**) (67 mg, 0.27 mmol, 1.0 eq.) was dissolved in 0.5 mL of CH_3CN and, then, 0.5 mL of H_2O was added. BAIB (362 mg, 1.09 mmol, 4.0 eq.) and TEMPO (13 mg, 0.08mmol, 0.3 eq.) were added and the mixture was stirred at room temperature for 5 hours. The reaction was quenched with $Na_2S_2O_3$ (15 mL), the aqueous phase was acidified with HCl 1M and it was extracted with ACOEt (4x25 mL). The organic phase was dried over Na_2SO_4, filtered and concentrated. The resulting product was purified by column chromatography using AcOEt/Hexane 1/3 as eluent to give the corresponding acid **3** (43 mg, 0.165 mmol, 61%).

Rf =0.34 (AcOEt /Hexane 1/3).

^{1}H NMR ($CDCl_3$, 500 MHz) δ 2.85 (t, 2 H, -CH_2S, *J* = 7.4 Hz), 2.34 (t, 2H, HOOCCH_2- *J*= 7.5 Hz), 2.32 (s, 3H, SCOCH_3), 1.65-1.60 (m, 2H,-CH_2CH_2-), 1.57-1.52 (m, 2H,-CH_2CH_2-), 1.34-1.27 (m, 12H, -CH_2CH_2-).

MS (ESI) *m/z* 519.3 $[2M-H]^-$. Calculated MS *m/z* 260.1 [M]

1-bromo-5-triphenilmethylmercaptopentane (6, MMS040):

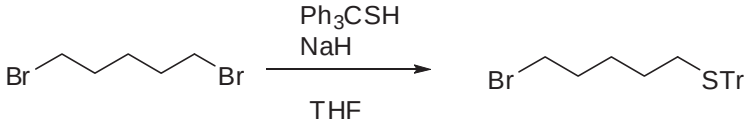

In a three necked flask a solution of triphenylmethanethiol (885 mg, 3.2 mmol, 1 eq.) in dry THF (20 mL) and a solution of 1,5-dibromopenthane (445 μL, 3.27 mmol, 1 eq.) in dry THF were added, drop by drop (0.5 mL/min), simultaneously and under argon atmosphere over a suspension of sodium hydride (NaH) (383 mg, 9.6 mmol, 3eq., 60% in mineral oil). The mixture was stirred 16 hours at 25 ºC, filtered and concentrated. The crude was filtered over a silica gel filter (11 g, 2x11 cm column) using AcOEt/Hexan 100/1 as eluent. It was recristalized in hexane (561 mg, 1.32 mmol, 41%).

^{1}H NMR ($CDCl_3$, 300 MHz) δ 7.44-7.19 (m, 15H, Trt), 3.31 (t, 2 H, *J* = 6.8 Hz, C*H*$_2$Br), 2.17 (t, 2H, *J*= 7.0 Hz, -C*H*$_2$SPh), 1.70-1.67 (m, 2H, -C*H*$_2$CH$_2$Br), 1.43-1.35 (m, 4H,-C*H*$_2$CH$_2$SPh and -C*H*$_2$CH$_2$CH$_2$Br).

^{13}C NMR ($CDCl_3$, 75 MHz) δ 144.9 (3C, C1- Trt), 129.5 (6C, C3-Tr), 127.8 (6C, C2-Tr), 126.5 (3C, C4-Tr), 66.5 (–*C*Ph$_3$), 33.5 (-*C*H$_2$Br), 32.2 (-*C*H$_2$CH$_2$Br), 31.6 (*C*H$_2$STr), 27.8, 27.5.

IR (KBr): 3061, 2957, 2936, 2852, 1591, 1485, 1442 cm^{-1}.

MS (ESI) *m/z* (rel. Int.) 449 [M+Na]$^+$ (100), 243 [CPh$_3$]$^+$ (29). Calculated MS *m/z* 149.0 [M]

5-(*S*-acetyl)mercaptopentanoic acid (4, AI176):

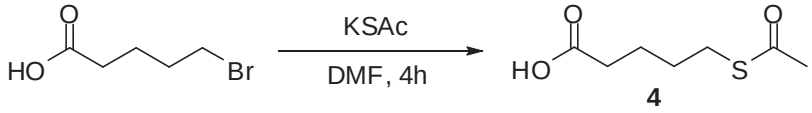

4

A solution of 4-bromopentanoic acid (1 g, 5.8 mmol, 1.0 eq.) and potassium thioacetate (788 mg, 6.9 mmol, 1.2 eq.) in DMF (12 mL) was stirred at room temperature for 4 hours. The reaction mixture was diluted in AcOEt (20 mL) and then was washed with water (6 x 25 mL). The organic phase was dried over anhydrous $MgSO_4$, filtered and concentrated. The resulting product was purified by column chromatography using AcOEt/Hexane 5/5 as eluent to give the corresponding 5-(*S*-acetyl)mercaptopentanoic acid (**4**) (648 mg, 3.7 mmol, 65%). Rf =0.46 (AcOEt/Hexane 5/5).

^{1}H NMR ($CDCl_3$, 500 MHz) δ 2.81 (t, 2 H, -C*H*$_2$S, *J* = 7.2 Hz), 2.31 (t, 2H, HOOCC*H*$_2$- *J*= 7.1 Hz), 2.26 (s, 3H, SCOC*H*$_3$), 1.66-1.60 (m, 2H,-CH$_2$CH$_2$-), 1.59-1.55 (m, 2H,-CH$_2$CH$_2$-).

^{13}C NMR ($CDCl_3$, 500 MHz) δ 195.7 (1C, -*C*OCH_3), 179.2 (1C, -*C*OOH), 33.2 (1C, -*C*H_2COOH), 30.3 (1C, *C*H_3), 28.6, 28.3 (2C, -CH_2SAc, -CH_2CH_2SAc), 23.4 (1C, -*C*H_2CH_2COOH).

IR (KBr): 2936, 1693, 1428, 1234, 1138, 1105, 969, 926 cm^{-1}.

MS (ESI) *m/z* 199.0 $[M+Na]^+$. Calculated MS *m/z* 176.1 [M]

Synthesis of neoglycoconjugates:

Peracetylated glycosides were used as starting materials, except for lactose which was perbenzoylated. The thiol-protected monosaccharides and cellobioside bearing an *S*-acetyl-ending five carbon-atoms linker were obtained after radical addition of thioacetic acid to the double bond of the corresponding peracetylated *n*-pentenyl glycosides derivatives. [28] Following a similar strategy, the peracetylated allyl glucoside was elongated to its *S*-acetyl derivative. 7-Bromoheptan-1-ol and 9-bromononan-1-ol were used as acceptors for the insertion of longer aliphatic linkers into peracetylated glucose and nucleophilic displacement of bromide with potassium thioacetate afforded the corresponding *S*-acetyl derivatives. Octaacetylated maltoside was directly glycosylated with 5-hydroxy-1-(*S*-acetyl) mercaptopentane. All these glycosides were obtained with a synthetic approach based on Fisher glycosylation, except for cellobiose which was used as glycosyl bromide in a classic Köenigs-Knorr reaction. On the other hand, anomeric trichloroacetimidates were used as glycosyl donors to obtain lactose- and glucose-conjugates with five and two carbon-atoms linkers by using pent-4-en-1-ol and 2-bromoethanol as acceptors, respectively. Methanolysis was used as final step to deprotect the *S*-acetyl and *O*-acetyl (*O*-benzoyl in the case of $LacC_5SH$) protecting groups.

[28] T. Buskas, E. Söderberg, P. Konradsson and B. Fraser-Reid, *J. Org. Chem.*, **2000**, 65, 958 (Use of *n*-Pentenyl Glycosides as Precursors to Various Spacer Functionalities).

Trichloroacetimidate of 2, 3, 4, 6-tetra-*O*-acetyl-D-glucopyranose

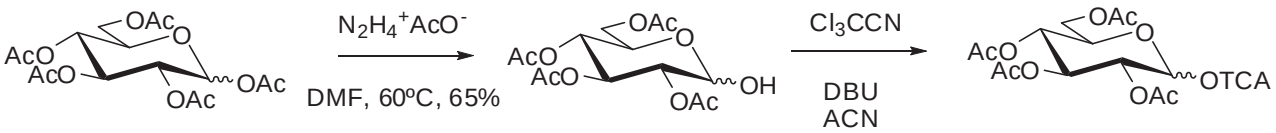

2, 3, 4, 6-tetra-*O*-acetyl-D-glucopyranose: Hydrazine acetate ($N_2H_4^+AcO^-$) (11.6 g, 126.1 mmol, 1.5 eq.) was added in several portions to a solution of acetylated glucose (32.8 g, 84.1 mmol, 1 eq.) in DMF (90 mL). The reaction was stirred at 60 ºC and controlled by TLC until a new product with lower Rf appeared. The crude was diluted with AcOEt (200 mL) and washed with water (3x60 mL). The organic phase was purified by column chromatography using AcOEt/Hexane 1/2 as an eluent to give an amorphous solid (19.4 g, 55.7 mmol, 65%). [10]

^{1}H NMR ($CDCl_3$, 300 MHz) δ 5.53 (t, 1H, *J*= 9.9 Hz), 5.46 (d, 1H, *J*= 3.6 Hz), 5.07 (t, 1H, *J*= 9.6 Hz), 4.89 (dd, 1H, *J*= 3.6, 10.2 Hz), 4.29-4.20 (m, 2H), 4.1-4.10 (m, 1H), 2.09 (s, 3H, OAc), 2.08 (s, 3H, OAc), 2.03 (s, 3H, OAc), 2.01 (s, 3H, OAc).

Trichloroacetimidate of 2, 3, 4, 6-tetra-*O*-acetyl-D-glucopyranose: Cl_3CCN (39.4 g, 272.9 mmol, 15 eq.) was added to 2, 3, 4, 6-tetra-*O*-acetyl-D-glucopyranose (19 g, 54.6 mmol, 1 eq.) in CH_2Cl_2 (50 mL). The mixture was stirred for 2 hours, it was concentrated and purified by column chromatography using AcOEt:Hexane 1/2 as an eluent (22 g, 46.2 mmol, 84 %). [10]

^{1}H NMR ($CDCl_3$, 300 MHz) δ 8.71 (s, 1H, NH), 5.85 (d, 1H, *J*=6.8 Hz), 5.26 (d, 1H, *J*=6.8 Hz), 5.21-5.15 (m, 1H), 4.28 (dd, 1H, *J*=3.9, 12.5 Hz), 4.14-4.06 (m, 1H,), 3.90-3.87 (m, 1H), 2.05 (s, 3H, OAc), 2.01-1.98 (s, 9H, 3xOAc)

2,2'-dithio bis[ethyl β-D-glucopyranoside] [GlcC$_2$S]$_2$

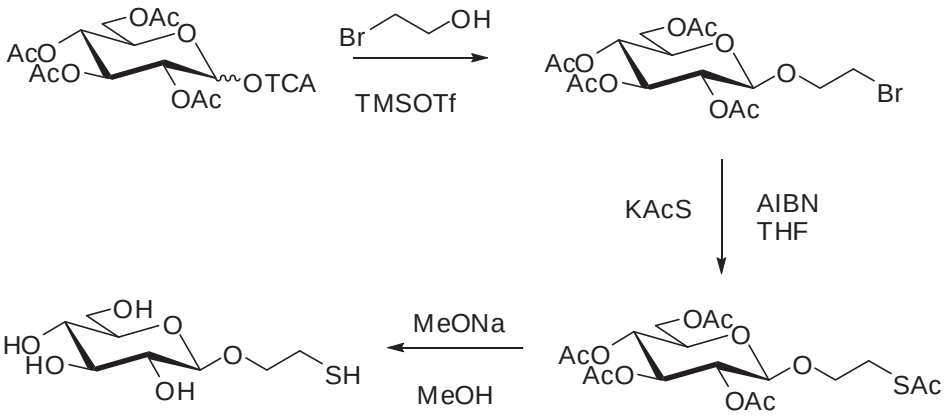

2-bromo-ethyl-(2, 3, 4, 6-tetra-*O*-acetyl-β-D-glucopyranoside): TMSOTf (0.04 eq.) was added to a solution of the trichloroacetimidate (11.1 g, 23.1 mmol, 1 eq.) and the commercial acceptor 2-bromoethanol (8.6 g, 69.3 mmol, 1.5 eq.) at room temperature and under argon atmosphere. The mixture was stirred 30 minutes, concentrated and purified by column chromatography using AcOEt/Hexane 1/2 as an eluent (6.6 g, 14.5 mmol, 63 %). [10]

^{1}H NMR (CDCl$_3$, 300 MHz) δ 5.20 (t, 1H, *J*= 9.5 Hz), 5.1-4.9 (m, 2H), 4.55 (d, 1H, *J*= 7.9 Hz,H1), 4.24 (dd, 1H, *J*=4.8, 12.3 Hz), 4.18-4.09 (m, 2H), 3.84-3.75 (m, 1H), 3.72-3.66 (m, 1H), 3.46-3.41 (m, 2H), 2.07 (s, 3H, OAc), 2.04 (s, 3H,OAc), 2.00 (s, 3H, OAc), 1.99 (s, 3H, OAc).

2-thioacetyl-ethyl-(2, 3, 4, 6-tetra-*O*-acetyl-β-D-glucopyranoside): Potassium thioacetate (4.96 g, 43.5 mmol, 3 eq.) was added to a solution of 2-bromo-ethyl-(2, 3, 4, 6-tetra-O-acetyl-β-D-glucopyranoside (6.6 g, 14.5 mmol, 1 eq.) in DMF (60 mL). The reaction mixture was stirred at 60ºC for 12 hours, concentrated and purified by column chromatography using AcOEt/Hexane 1/2 as an eluent (6.18 g, 13.7 mmol, 95 %). [10]

^{1}H NMR (CDCl$_3$, 300 MHz) δ 5.09 (t, 1H, *J*= 9.5 Hz), 4.97 (t, 1H, *J*= 9.9 Hz), 4.87 (t, 1H, *J*= 9.3 Hz), 4.44 (d, 1H, *J*=7.9 Hz, H1), 4.15 (dd, 1H, *J*=4.8, 12.3 Hz), 4.04-4.00 (m, 1H), 3.89-3.83 (m, 1H), 3.64-3.60 (m, 1H), 3.55-3.49 (m, 1H), 3.05-2.89 (m, 2H, C*H*$_2$SAc), 2.23 (s, 3H, CH$_3$COS), 1.97 (s, 3H, OAc), 1.96 (s, 3H, OAc), 1.92 (s, 3H, OAc), 1.90 (s, 3H, OAc).

2,2'-dithio bis[ethyl β-D-glucopyranoside] [GlcC$_2$S]$_2$: 2-thioacetyl-ethyl-(2, 3, 4, 6-tetra-O-acetyl-β-D-glucopyranoside) (6 g, 13.3 mmol, 1 eq.) was dissolved in dry MeOH (25 mL) and 1 equivalent of methanolic solution of NaOMe 1N was added (13.3 mL, 13.3 mmol). The reaction was stirred for 24 hours open to the air in order to complete the oxidation of the thiol group. The

mixture was neutralized with Amberlist IR-120 resins, filtered and concentrated. A mixture of thiol and disulfide (mayor product) was obtained (3.3 g, 6.9 mmol, quantitative). [10]

Rf =0.50 (CH_2Cl_2/MeOH 7/3).

^{1}H NMR (D_2O, 400 MHz) δ 4.54 (d, 1H, J=7.9 Hz, H1), 4.09-3.97 (m, 2H), 3.90-3.84 (m, 1H,), 3.76 (dd, 1H, J=5.8, 12.3 Hz), 3.56-3.40 (m, 3H), 3.33 (t, 1H, J=8.1 Hz), 2.82 (t, 2H, J=6.3 Hz, C*H*$_2$S-).

^{13}C-NMR (D_2O, 100MHz) δ 102.3 (C1), 75.9 (C5), 75.7 (C2), 73.1 (C3), 71.7 (C4), 39.9 (C6), 60.7 (C7), 23.4 (C8).

MS (ESI) *m/z* 263 (100) $[M+Na]^+$ Calculated MS *m/z* 240.1 [M]

2,2'-dithio bis[propyl β-D-glucopyranoside][GlcC$_3$S]$_2$

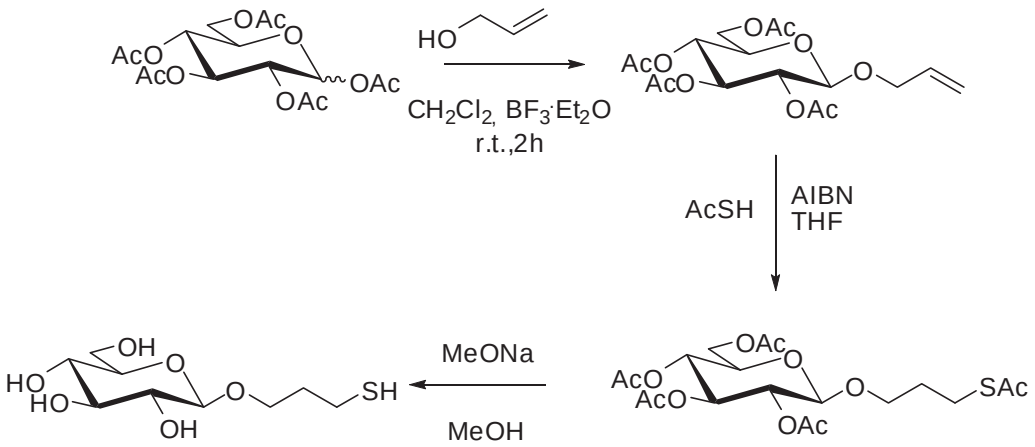

1-propenyl 2, 3, 4, 6-tetra-*O*-acetyl-β-D-glucopyranoside (MME142): 2-propen-1-ol (1.83 g, 31.5 mmol, 3 eq.) and trifluoroboroetherate ($BF_3{\cdot}Et_2O$) (7.5 g, 52.2 mmol, 5 eq.) were added to a solution of peracetylated glucose (4.1 g, 10.5 mmol, 1 eq.) in dry CH_2Cl_2 (30 mL). The reaction mixture was stirred for 2 hours, quenched with $NaHCO_3$ and purified by column chromatography using AcOEt/Hexane 1/3 as an eluent (2.27 g, 5.64 mmol, 56 %). [11]

Rf =0.30 (AcOEt/Hexane 1/2).

^{1}H NMR ($CDCl_3$, 500 MHz) δ 5.85 (m, 1H, -C*H*=CH_2), 5.26 (m, 2H, -CH=C*H*$_2$), 5.20 (m, 1H, H3), 5.09 (t, 1H, *J*=9.6 Hz, H4), 5.02 (dd, 1H, *J*=7.9, 9.5 Hz, H2), 4.55 (d, 1H, *J*=7.9 Hz, H1), 4.36-4.31 (m, 1H, -C*H*$_2$CHCH_2), 4.25 (q, 1H, *J*=4.7, 12.3 Hz, H6), 4.15-4.07 (m, 2H, H6, -C*H*$_2$CHCH_2), 3.68 (m, 1H, H5), 2.08 (s, 3H, OAc), 2.04 (s, 3H, OAc), 2.01 (s, 3H, OAc), 2.00 (s, 3H, OAc).

1-thioacetylpropyl 2, 3, 4, 6-tetra-*O*-acetyl-β-D-glucopyranoside (MME144): Thioacetic acid (1.48 g, 19.48 mmol, 4 eq.) and a catalytic amount of AIBN were added to a solution of 1-propenyl-2, 3, 4, 6-tetra-O-acetyl-β-D-glupyranoside (1.89 g, 4.87 mmol, 1 eq.) in dry THF (40 mL). The reaction mixture was stirred for 24 hours at 80ºC with reflux, controlled by NMR, concentrated and purified by column chromatography usung AcOEt/Hexane 1/3 as an eluent (1.91 g, 4.11 mmol, 84 %). [11]

^{1}H NMR ($CDCl_3$, 500 MHz) δ 5.17 (t, 1H, *J*=9.5 Hz, H3), 5.04 (t, 1H, *J*=9.9 Hz, H4), 4.94 (dd, 1H, *J*=7.9, 9.5 Hz, H2), 4.47 (d, 1H, *J*=7.9 Hz, H1), 4.22 (q, 1H, *J*=4.8, 12.2 Hz, H6), 4.10 (m, 1H, H6), 3.90-3.86 (m, 1H, -OCH_2CH_2-), 3.69-3.66 (m, 1H, H5), 3.54-3.49 (m, 1H, -OCH_2CH_2-), 2.87 (m, 2H, -CH_2S), 2.29 (s, 3H, SAc), 2.06 (s, 3H, OAc), 2.03 (s, 3H, OAc), 1.99 (s, 3H, OAc), 1.97 (s, 3H, OAc), 1.88-1.74 (m, 2H, -CH_2-).

2,2'-dithio bis[propyl β-D-glucopyranoside] [GlcC_3S]$_2$ (MME147)**:** 1-thioacetylpropenil-2, 3, 4, 6-tetra-O-acetyl-β-D-glupiranoside (450 mg, 0.969 mmol, 1 eq.) was dissolved in MeOH (5 mL) and NaOMe was added (10 mg, 0.19 mmol, 0.2 eq.). The reaction was stirred for 16 hours open to the air in order to complete the oxidation of the thiol group. The mixture was neutralized with Amberlist IR-120 resins, filtered and concentrated. A mixture of thiol and disulfide was obtained as yellow oil (243 mg, 0.956 mmol, 98%). [11]

^{1}H NMR (CD_3OD, 500 MHz) δ 4.26 (d, 1H, *J*=7.8 Hz, H1), 4.02-3.96 (m, 1H), 3.88-3.84 (m, 1H), 3.70-3.64 (m, 2H), 3.27 (m, 2H), 3.19-3.14 (m, 1H), 2.82 (t, 2H, *J*=7.1 Hz, CH_2S-S) and 2.6 (t, 2H, *J*=7.1 Hz, CH_2SH), 2.00 (m, 1H, -CH_2C$H_2$$CH_2$), 1.88 (m, 1H, -$CH_2CH_2$$CH_2$).

2,2'-dithio bis[pentyl β-D-glucopyranoside] [GlcC_5S]$_2$

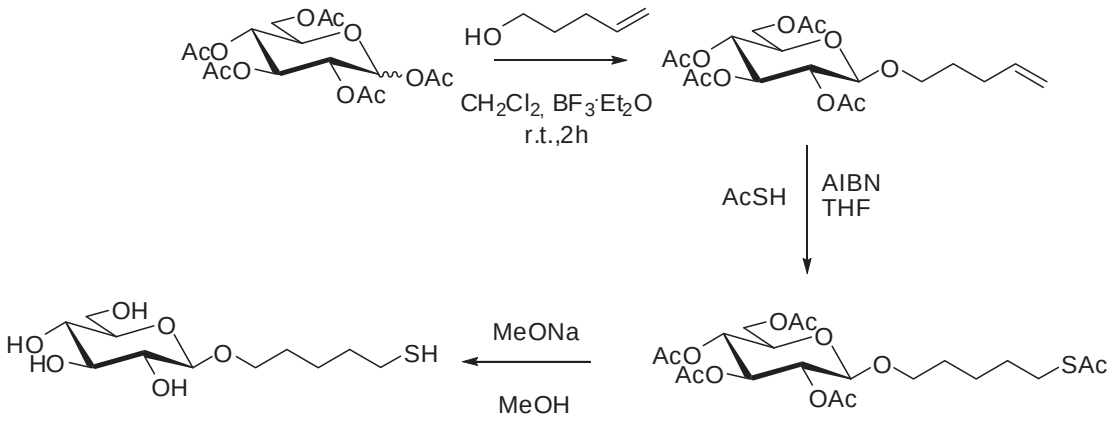

1-pentenyl 2, 3, 4, 6-tetra-*O*-acetyl-β-D-glucopyranoside (FC001): 4-penten-1-ol (3.53 g, 41.0 mmol, 4 eq.) and trifluoroboroetherate ($BF_3{\cdot}Et_2O$) (7.27 g, 51.25 mmol, 5 eq.) were added to a solution of acetylated glucose (4 g, 10.25 mmol, 1 eq.) in dry CH_2Cl_2 (30 mL). The reaction mixture was stirred for 2 hours, concentrated and purified by column chromatography using a gradient of AcOEt/Hexane (from 20 to 50%) as an eluent (2.83 g, 6.79 mmol, 66 %). [8]

Rf =0.37 (AcOEt/Hexane 1/2).

^{1}H NMR ($CDCl_3$, 500 MHz) δ 5.80 (m, 1H, C*H*=CH_2), 5.22 (t, 1H, *J*=9.5 Hz, H3), 5.11 (t, 1H, *J*=10.0 Hz, H4), 5.00 (m, 3H, H2, CH=CH_2), 4.51 (d, 1H, *J*=8.0 Hz, H1), 4.28 (dd, 1H, *J*=4.5, 12.0 Hz, H6), 4.16 (dd, 1H, *J*=2.5, 12.5 Hz, H6'), 3.91 (m, 1H, -CH_2O-), 3.7 (m, 1H, H5), 3.51 (m, 1H, -CH_2O-), 2.2-2.0 (m, 14H, CH_3CO, -C$H_2$$CH_2$$CH_2$), 1.66 (m, 1H, -$CH_2CH_2$$CH_2$).

1-thioacetylpentyl 2, 3, 4, 6-tetra-*O*-acetyl-β-D-glucopyranoside (FC002): Thioacetic acid (0.59 g, 7.78 mmol, 4 eq.) and a catalytic amount of AIBN were added to a solution of 1-pentenyl-2, 3, 4, 6-tetra-O-acetyl-β-D-glupiranoside (0.81 g, 1.95 mmol, 1 eq.) in dry THF (20 mL). The reaction mixture was stirred for 24 hours at 80ºC with reflux, controlled by NMR, concentrated and purified by column chromatography using a gradient of AcOEt/Hexane (from 20 to 40%) as an eluent(0.918 g, 1.92 mmol, 96 %). [8]

^{1}H NMR ($CDCl_3$, 500 MHz) δ 5.21 (t, 1H, *J*=9.5 Hz, H3), 5.09 (t, 1H, *J*=10.0 Hz, H4), 4.99 (t, 1H, *J*=8.0 Hz, H2), 4.50 (d, 1H, *J*=8.0 Hz, H1), 4.27 (dd, 1H, *J*=4.5, 12.0 Hz, H6), 4.15 (dd, 1H, *J*=4.5, 12.0 H6'), 3.87 (m, 1H, -CH_2O-), 3.7 (m, 1H, H5), 3.50 (m, 1H, -CH_2O-), 2.87 (t, 2H, *J*=7.0 Hz, CH_2S-), 2.33 (s, 3H, CH_3S), 2.2-2.0 (m, 12H, CH_3CO), 1.66-1.35 (m, 6H, CH_2CH_2CH_2).

2,2'-dithio bis[pentyl β-D-glucopyranoside] [GlcC$_5$S]$_2$ (FC003)**:** 1-thioacetylpentyl-2, 3, 4, 6-tetra-O-acetyl-β-D-glupiranoside (2.98 mg, 6.24 mmol, 1 eq.) dissolved in dry MeOH (20 mL) and 1 equivalent of methanolic solution of NaOMe 1N was added (6.24 mmol, 1 eq.). The reaction was stirred for 30 minutes open to the air in order to complete the oxidation of the thiol group. The mixture was neutralized with Amberlist IR-120 resins, filtered and concentrated. The disulfide (mayor product) was obtained (1.47 g, 5.21mmol, 84%) as a yellow syrup. [8]

^{1}H NMR (CD$_3$OD, 500 MHz) δ 4.26 (d, 1H, *J*=7.8 Hz, H1), 4.05-3.78 (m, 2H, H5, H6b), 3.7-3.5 (m, 2H, H4, H6a), 3.5-3.2 (m, 3H, H3, -C*H*$_2$O-), 3.18 (t, 1H, *J*=8.1 Hz, H2), 2.52 (t, 2H, *J*=6.9 Hz, C*H*$_2$S), 1.8-1.4 (m, 6H, C*H*$_2$C*H*$_2$C*H*$_2$).

2,2'-dithio bis[heptyl β-D-glucopyranoside] [GlcC$_7$S]$_2$

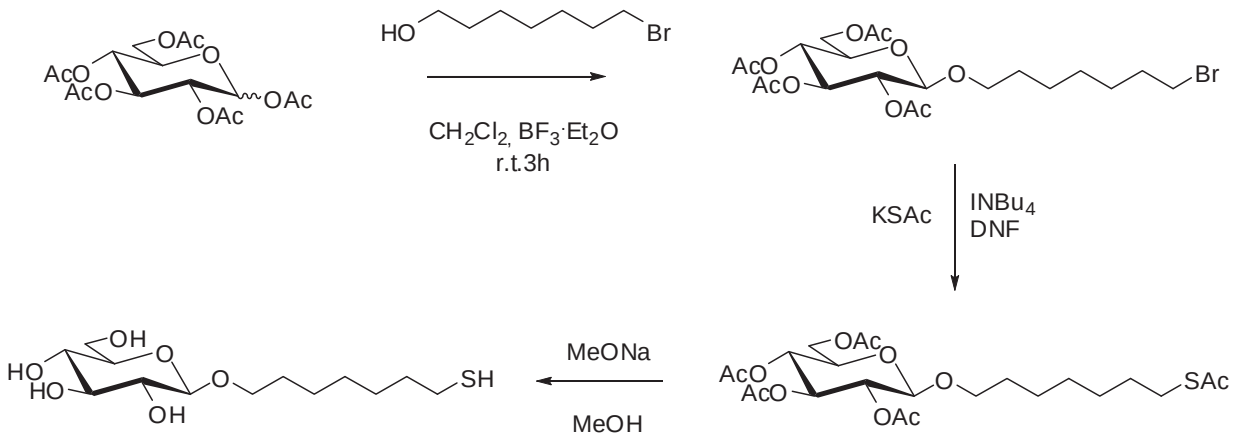

7-bromo-heptyl 2, 3, 4, 6-tetra-*O*-acetyl-β-D-glucopyranoside (MME137): 7-bromo-1-heptanol (585 mg, 3 mmol, 3 eq.) and trifluoroboroetherate ($BF_3{\cdot}Et_2O$) (709.7 mg, 5 mmol, 5 eq.) were added to a solution of acetylated glucose (390.34 mg, 1 mmol, 1 eq.) in dry CH_2Cl_2 (5 mL). The reaction mixture was stirred for 3 hours, quenched with $NaHCO_3$, washed with CH_2Cl_2 (2x10 mL) and water (1x10 mL), dried over Na_2SO_4, filtered, concentrated and purified by column chromatography using AcOEt/Hexane 1/2 as an eluent (162 mg, 0.308 mmol, 31 %).

Rf =0.32 (AcOEt/Hexane 1/2).

^{1}H NMR (CDCl$_3$, 500 MHz) δ 5.17 (t, 1H, *J*=9.5 Hz, H3), 5.05 (t, 1H, *J*=9.5 Hz, H4), 4.94 (dd, 1H, *J*=7.9, 9.5 Hz, H2), 4.46 (d, 1H, *J*=7.9 Hz, H1), 4.23 (q, 1H, *J*=4.7, 12.3 Hz, H6), 4.10 (m, 1H, H6), 3.86-3.81 (m, 1H, -OC*H*$_2$CH$_2$), 3.68-3.64 (m, 1H, H5), 3.46-3.42 (m, 1H, -OC*H*$_2$CH$_2$), 3.37 (t, 2H, *J*=6.8 Hz, -C*H*$_2$Br), 2.05 (s, 3H, OAc), 2.01 (s, 3H, OAc), 1.99 (s, 3H, OAc) , 1.97 (s,

3H, OAc), 1.81 (m, 2H, -$CH_2CH_2CH_2CH_2CH_2$-), 1.57-1.49 (m, 2H, -$CH_2CH_2CH_2CH_2CH_2$-), 1.42-1.36 (m, 2H, -$CH_2CH_2CH_2CH_2CH_2$-), 1.33-1.26 (m, 4H, -$CH_2CH_2CH_2CH_2CH_2$-).

1-thioacetylheptyl 2, 3, 4, 6-tetra-*O*-acetyl-β-D-glupyranoside (MME140): A catatlytic amount of tetrabutyl ammonium iodide ($INBu_4$) was added to a solution of 7-bromo-hepty-l-2, 3, 4, 6-tetra-O-acetyl-β-D-glupiranoside (162 mg, 0.308 mmol, 1eq.) and potassium thioacetate (KSAc) (105 mg, 0.923 mmol, 3 eq.) in dry DMF (2 mL). The reaction mixture was stirred 24 hours at 60ºC, diluted with AcOEt (10 mL), washed with water (4x10 mL), dried over Na_2SO_4, filtered, concentrated and purified by column chromatography using AcOEt/Hexane 1/2 as an eluent (143 mg, 0.275 mmol, 89 %).

Rf =0.33 (AcOEt/Hexane 1/2).

^{1}H NMR ($CDCl_3$, 500 MHz) δ 5.15 (t, 1H, *J*=9.6 Hz, H3), 5.03 (t, 1H, *J*=9.6 Hz, H4), 4.93 (dd, 1H, *J*=8.0, 9.6 Hz, H2), 4.44 (d, 1H, *J*=8.0 Hz, H1), 4.22 (q, 1H, *J*=12.3, 4.7 Hz, H6), 4.08 (q, 1H, *J*=2.8, 12.3 Hz, H6), 3.83-3.79 (m, 1H, O*C*H_2CH_2), 3.66-3.63 (m, 1H, H5), 3.44-3.39 (m, 1H, O*C*H_2CH_2), 2.80 (t, 2H, *J*=7.3 Hz, *C*H_2SAc), 2.27(s, 3H, SAc), 2.04 (s, 3H, OAc), 1.99 (s, 3H, OAc), 1.97 (s, 3H, OAc), 1.95 (s, 3H, OAc), 1.54-1.48 (m, 4H, -*C*H_2CH_2SAc and OCH_2C*H*$_2$-), 1.31-1.22 (m, 6H, -*C*H_2*C*H_2*C*H_2-).

^{13}C NMR ($CDCl_3$, 125 MHz) δ 195.8 (COS), 170.5, 170.2, 169.3, 169.1 (CO), 100.7 (C1), 72.7 (C3), 71.6 (C2), 71.2 (C5), 69.9 (C4), 68.4 (-O*C*H_2-), 61.9 (C6), 30.5 (*C*H_3COS), 29.3 (-*C*H_2S-), 29.1 (-$CH_2CH_2CH_2CH_2CH_2$-), 28.9 (-$CH_2CH_2CH_2CH_2CH_2$-), 28.6 (-$CH_2CH_2CH_2CH_2CH_2$-), 28.5 (-$CH_2CH_2CH_2CH_2CH_2$-), 25.5 (-$CH_2CH_2CH_2CH_2CH_2$-), 20.6, 20.5, 20.4, 20.4 (CH_3).

2,2'-dithio bis[heptyl β-D-glucopyranoside] [GlcC_7S]$_2$ (MME143)**:** 1-thioacetylheptanyl-2, 3, 4, 6-tetra-*O*-acetyl-β-D-glupyranoside (143 mg, 0.275 mmol, 1 eq.) was dissolved in MeOH (3 mL) and NaOMe was added (15 mg, 0.275 mmol, 1 eq.). The reaction was stirred for 20 hours open to the air in order to complete the oxidation of the thiol group. The mixture was neutralized with Amberlist IR-120 resins, filtered and concentrated. A mixture of thiol and disulfide was obtained as yellow oil (71 mg, 0.228 mmol, 83%).

^{1}H NMR (CD_3OD, 500 MHz) δ 4.24 (dd, 1H, *J*=2.2, 7.8 Hz, H1), 3.93-.3.85 (m, 2H, H6 and –O*C*H_2CH_2-), 3.66 (m, 1H, H6), 3.57-3.51 (m, 1H, –O*C*H_2CH_2-), 3.35 (m, 1H, H3), 3.29-3.24 (m, 2H, H4 and H5), 3.17 (m, 1H, H2), 2.68 (t, 2H, *J*=7.2 Hz, *C*H_2S-S) and 2.49 (t, 2H, *J*=7.2 Hz, *C*H_2SH), 1.71-1.57 (m, 4H, -*C*H_2CH_2SH and OCH_2C*H*$_2$-), 1.45-1.31 (m, 6H, -*C*H_2*C*H_2*C*H_2-).

^{13}C NMR (CD_3OD, 500 MHz) δ 104.3 (C1), 78.0 (C3), 77.8 (C4 or C5), 75.0 (C2), 71.6 (C4 or C5), 70.8 (-O*C*H_2-), 62.7 (C6), 39.7 (-*C*H_2S-S-), 30.6 (-$CH_2CH_2CH_2CH_2CH_2$-), 30.1 (-

$CH_2CH_2CH_2CH_2CH_2$-), 29.9 (-$CH_2CH_2CH_2CH_2CH_2$-), 29.4 (-$CH_2CH_2CH_2CH_2CH_2$-), 29.3 (-$CH_2CH_2CH_2CH_2CH_2$-), 24.9 (CH_2SH).

MS (ESI) *m/z* 641.258 $[M+Na]^+$ (disulfure). Calculated MS *m/z* 310.2 [M]

2,2'-dithio bis[nonyl β-D-glucopyranoside] [$GlcC_9S]_2$

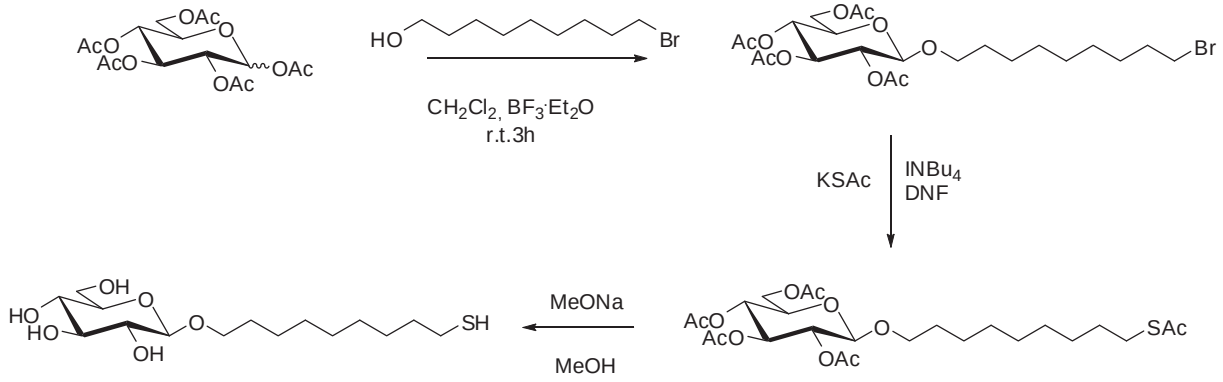

9-bromo-nonyl 2, 3, 4, 6-tetra-*O*-acetyl-β-D-glucopyranoside (MME136): 9-bromo-1-nonanol (669 mg, 3 mmol, 3 eq.) and trifluoroboroetherate ($BF_3{\cdot}Et_2O$) (709.7 mg, 5 mmol, 5 eq.) were added to a solution of acetylated glucose (390.34 mg, 1 mmol, 1 eq.) in dry CH_2Cl_2 (5 mL). The reaction mixture was stirred for 2 hours, quenched with $NaHCO_3$, washed with CH_2Cl_2 (2x10 mL) and water (1x10 mL), dried over Na_2SO_4, filtered, concentrated and purified by column chromatography using AcOEt/Hexane 1/2 as an eluent (187 mg, 0.34 mmol, 34 %).

Rf =0.32 (AcOEt/Hexane 1/2).

^{1}H NMR ($CDCl_3$, 500 MHz) δ 5.16 (t, 1H, *J*=9.6 Hz, H3), 5.05 (t, 1H, *J*=9.6 Hz, H4), 4.94 (dd, 1H, *J*=8.0, 9.6 Hz, H2), 4.45 (d, 1H, *J*=8.0 Hz, H1), 4.23 (dd, 1H, *J*=4.7, 12.3 Hz, H6), 4.09 (dd, 1H, *J*=2.4, 12.3 Hz, H6), 3.85-3.81 (m, 1H, -OCH_2-), 3.67-3.64 (m, 1H, H5), 3.45-3.41 (m, 1H, -OCH_2-), 3.37 (t, 2H, *J*= 6.8 Hz, -CH_2Br), 2.05 (s, 3H, OAc), 2.00 (s, 3H, OAc), 1.99 (s, 3H, OAc), 1.97 (s, 3H, OAc), 1.81 (m, 2H, -C$H_2$$CH_2$Br), 1.56-1.47 (m, 2H, -$OCH_2CH_2$-), 1.41-1.35 (m, 2H, -C$H_2$$CH_2$$CH_2$Br), 1.30-1.21 (m, 8H, -CH_2CH_2CH_2CH_2-).

^{13}C NMR ($CDCl_3$, 125 MHz) δ 170.8, 170.4, 170.3, 168.7 (CO), 95.8 (C1), 71.1, 70.4, 68.9, 68.8, 67.2, 62.1 (C6), 34.1, 32.9, 29.5, 29.3, 28.8, 28.2, 26.1, 20.9, 20.8, 20.7.

MS (ESI) *m/z* 575.142 $[M+Na]^+$ Calculated MS *m/z* 552.2 [M]

1-thioacetylnonyl 2, 3, 4, 6-tetra-*O*-acetyl-β-D-glucopyranoside (MME138): A catatlytic amount of tetrabutyl ammonium iodide ($INBu_4$) was added to a solution of 9-bromo-nonyl-l-2, 3, 4, 6-tetra-O-acetyl-β-D-glupiranoside (187 mg, 0.34 mmol, 1eq.) and potassium thioacetate (KSAc) (116 mg, 1.02 mmol, 3 eq.) in dry DMF (2 mL). The reaction mixture was stirred 24 hours at 60ºC, diluted with AcOEt (10 mL), washed with water (4x10 mL), dried over Na_2SO_4, filtered, concentrated and purified by column chromatography using AcOEt/Hexane 1/2 as an eluent (163 mg, 0.297 mmol, 87 %).

Rf =0.33 (AcOEt/Hexane 1/2).

^{1}H NMR ($CDCl_3$, 500 MHz) δ 5.18 (t, 1H, *J*=9.5 Hz, H3), 5.06 (t, 1H, *J*=9.8 Hz, H4), 4.95 (dd, 1H, *J*=8.0, 9.6 Hz, H2), 4.46 (d, 1H, *J*=8.0 Hz, H1), 4.24 (dd, 1H, *J*=4.7, 12.3 Hz, H6), 4.10 (dd, 1H, *J*=2.4, 12.3 Hz, H6), 3.85-3.81 (m, 1H, -OC*H*$_2$-), 3.68-3.65 (m, 1H, H5), 3.46-3.42 (m, 1H, -OC*H*$_2$-), 2.83 (t, 2H, *J*= 7.4 Hz, -C*H*$_2$SAc), 2.29 (s, 3H, SAc), 2.06 (s, 3H, OAc), 2.01 (s, 3H, OAc), 2.00 (s, 3H, OAc), 1.98 (s, 3H, OAc), 1.56-1.50 (m, 4H, -OCH$_2$C*H*$_2$- and -C*H*$_2$CH$_2$CH$_2$SAc), 1.33-1.24 (m, 10H, -C*H*$_2$C*H*$_2$C*H*$_2$C*H*$_2$C*H*$_2$-).

2,2'-dithio bis[nonyl β-D-glucopyranoside] [$GlcC_9S]_2$ (MME139)**:** 1-thioacetylnonyl-2, 3, 4, 6-tetra-O-acetyl-β-D-glupiranoside (163 mg, 0.297 mmol, 1 eq.) was dissolved in MeOH (3 mL) and NaOMe was added (16 mg, 0.3 mmol, 1 eq.). The reaction was stirred for 24 hours open to the air in order to complete the oxidation of the thiol group. The mixture was neutralized with Amberlist IR-120 resins, filtered and concentrated. A mixture of thiol and disulfide was obtained as yellow oil (57 mg, 0.168 mmol, 57%).

^{1}H NMR ($CDCl_3$-CD_3OD, 500 MHz) δ 4.25 (d, 1H, *J*=8.0 Hz, H1), 3.89-3.83 (m, 2H, H6 and –OC*H*$_2$CH$_2$-), 3.71 (dd, 1H, *J*=5.0, 12.0 Hz, H6), 3.52 (m, 1H, –OC*H*$_2$CH$_2$-), 3.36 (m, 2H, H3 and H4), 3.27-3.24 (m, 1H, H5), 3.20 (m, 1H, H2), 2.65 (t, 2H, *J*=7.2 Hz, C*H*$_2$S-S) and 2.47 (t, 2H, *J*=7.2 Hz, C*H*$_2$SH), 1.67-1.53 (m, 4H, OCH$_2$C*H*$_2$- and -C*H*$_2$CH$_2$CH$_2$S), 1.38-1.25 (m, 10H, -C*H*$_2$C*H*$_2$C*H*$_2$C*H*$_2$C*H*$_2$-).

^{13}C NMR (CD_3OD, 500 MHz) δ 104.3 (C1), 78.1 (C3), 77.9 (C4 or C5), 75.1 (C2), 71.6 (C4 or C5), 70.8 (-O*C*H$_2$-), 62.7 (C6), 39.7 (-*C*H$_2$S-S-), 30.7, 30.6, 30.5, 30.3, 30.2 and 29.4 (-*C*H$_2$-), 27.1 (*C*H$_2$SH).

MS (ESI) *m/z* 697.320 $[M+Na]^+$ (disulfure). Calculated MS *m/z* 338.2 [M]

2,2'-dithio bis[pentyl β-D-galactopyranoside] [GalC_5S]$_2$

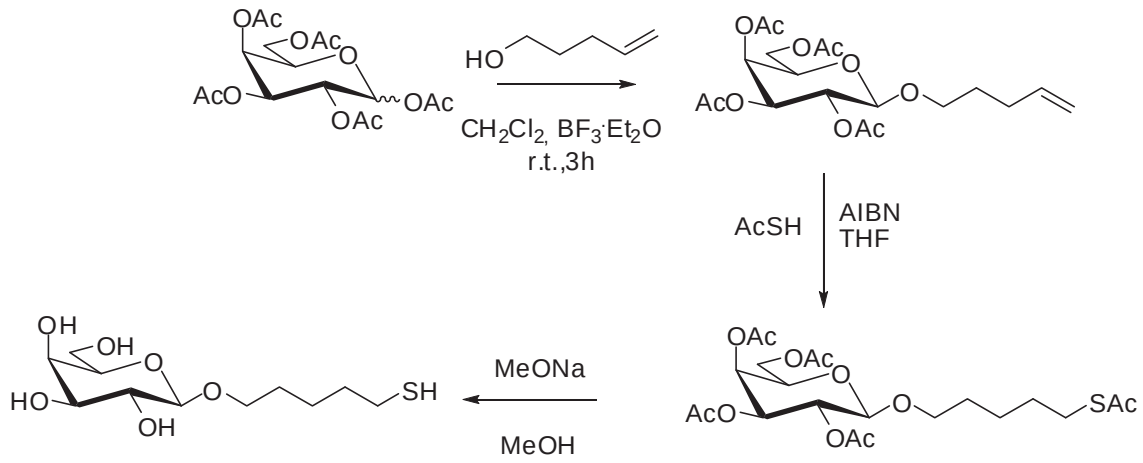

1-pentenyl 2, 3, 4, 6-tetra-*O*-acetyl-β-D-galactopyranoside (MME173): 4-penten-1-ol (3.53 g, 41.0 mmol, 4 eq.) and trifluoroboroetherate ($BF_3{\cdot}Et_2O$) (7.27 g, 51.25 mmol, 5 eq.) were added to a solution of acetylated galactose (4 g, 10.25 mmol, 1 eq.) in dry CH_2Cl_2 (30 mL). The reaction mixture was stirred for 3 hours, quenched with $NaHCO_3$ and extracted with water (3x100 mL). The organic phase was dried over Na_2SO_4, concentrated and purified by column chromatography using a gradient of AcOEt/Hexane (from 15 to 50%) as an eluent (2.35 g, 5.64 mmol, 55 %).

Rf = 0.45 (AcOEt/Hexane 1/2).

^{1}H NMR ($CDCl_3$, 500 MHz) δ 5.78 (m, 1H, C*H*=CH_2), 5.38 (m, 1H, H4), 5.11 (dd, 1H, *J*=10.5, 7.9 Hz, H2), 5.00-4.90 (m, 3H, H3, CH=CH_2), 4.51 (d, 1H, *J*=7.9 Hz, H1), 4.14 (m, 2H, H6,H6'), 3.90 (m, 2H, -CH_2O-), 3.50 (m, 1H, H5), 2.15 (s, 3H, CH_3CO), 2.12-2.07 (m, 4H, -CH_2CH_2-), 2.05 (s, 3H, CH_3CO), 2.04 (s, 3H, CH_3CO), 1.98 (s, 3H, CH_3CO), 1.69 (m, 2H, CH_2CH_2CH=CH_2).

1-thioacetylpentyl 2, 3, 4, 6-tetra-*O*-acetyl-β-D-galactopyranoside (MME175): Thioacetic acid (1.7 g, 22.56 mmol, 4 eq.) and a catalytic amount of AIBN were added to a solution of 1-pentenyl-2, 3, 4, 6-tetra-O-acetyl-β-D-galactopyranoside (2.35 g, 5.64 mmol, 1 eq.) in dry THF (40 mL). The reaction mixture was stirred for 24 hours at 80ºC with reflux, controlled by NMR, concentrated and purified by *Biotage* using a gradient of AcOEt/Hexane (from 0 to 80%) as an eluent (2.29 g, 4.79 mmol, 85 %).

Rf = 0.26 (AcOEt/Hexane 1/2).

^{1}H NMR ($CDCl_3$, 500 MHz) δ 5.38 (d, 1H, *J*=3.3 Hz, H4), 5.19 (dd, 1H, *J*=10.4, 7.9 Hz, H2), 5.00 (dd, 1H, *J*=10.4, 3.3 Hz, H3), 4.44 (d, 1H, *J*=8.0 Hz, H1), 4.19-4.09 (m, 2H, H6, H6'), 3.90-3.85 (m, 2H, OCH_2, H5), 3.49-3.44 (m, 1H, OCH_2), 2.85 (t, 2H, *J*=7.3 Hz, CH_2SAc), 2.32 (s, 3H, SAc), 2.14 (s, 3H, OAc), 2.05 (s, 3H, OAc), 2.04 (s, 3H, OAc), 1.98 (s, 3H, OAc), 1.63-1.54 (m, 4H, -CH_2CH_2-), 1.46-1.34 (m, 2H, -CH_2-).

^{13}C NMR (CD_3OD, 125 MHz) δ 195.8 (COS), 170.3, 170.2, 170.1, 169.3 (CO), 101.2 (C1), 70.9 (C3), 70.5 (C5 or OCH_2), 69.7 (C5 or OCH_2) , 68.8 (C2), 67.0 (C4), 61.2 (C6), 30.6 (CH_3COS), 29.1 (-CH_2S-), 28.9 (-CH_2CH_2CH_2-), 28.8 (-CH_2CH_2CH_2-), 25.0 (-CH_2CH_2CH_2-), 20.7, 20.6, 20.5, 20.5 (CH_3).

2,2'-dithio bis[pentyl β-D-galactopyranoside] [GalC_5S]$_2$ (AI168)**:** 1-thioacetylpentyl-2, 3, 4, 6-tetra-O-acetyl-β-D-glupiranoside (1.9 mg, 3.86 mmol, 1 eq.) dissolved in dry MeOH (20 mL) and NaOMe was added (0.2 g, 3.86 mmol, 1 eq.). The reaction was stirred overnight under argon. The mixture was filtered and concentrated. A mixture of the disulfide (mayor product) and the thiol was obtained (931 mg, 3.30 mmol, 87%).

^{1}H NMR (CD_3OD, 500 MHz) δ 4.42 (d, 1H, *J*=7.9 Hz, H1), 3.94-3.75 (m, 2H, H5, H6), 3.77-3.70 (m, 2H, H4, H6), 3.58-3.45 (m, 4H, H3, H2, - OCH_2), 2.70 (t, 2H, *J*=7.3 Hz, CH_2S-S), 2.48 (t, 2H, *J*=7.3 Hz, CH_2SH), 1.74-1.56 (m, 4H, -CH_2CH_2-), 1.52-1.44 (m, 2H, -CH_2-).

5,5'-Dithio bis (pentyl-β-D-mannopyranoside) [ManC_5S]$_2$

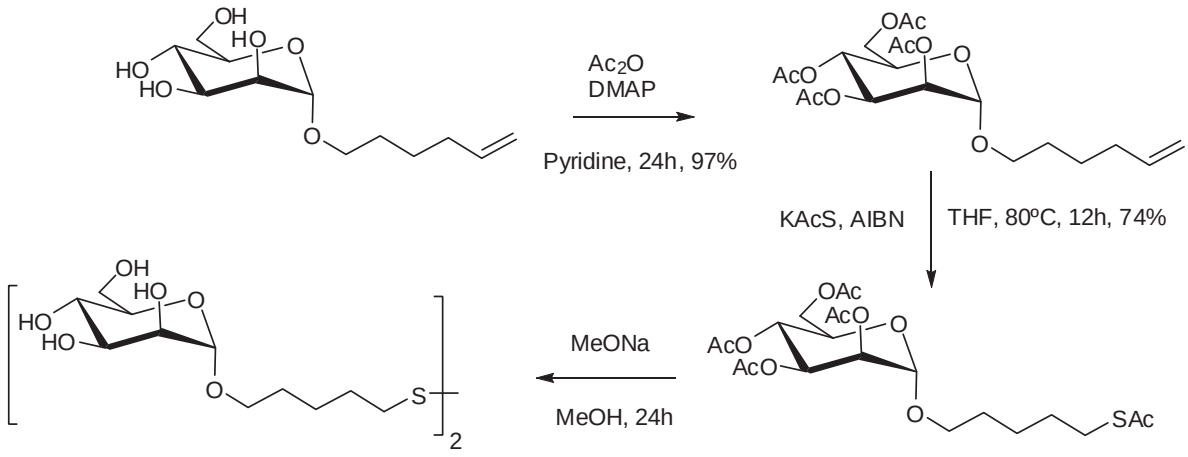

4-Pentenyl tetra-*O*-acetyl-β-D-mannopyranoside (FC016): Acetic anhydride (3.3 mL, 34.9 mmol, 9 equiv.) and a catalytic amount of dimethylaminopyridine (DMAP) were added to a stirred solution of pent-4-enyl β-D-mannopyranoside (0.956 g, 3.85 mmol, 1 equiv.) in pyridine

5.5 mL). The solution was stirred overnight, diluted with AcOEt (20 mL) and washed with water (20 mL), HCl 10% (20 mL) and a saturated solution of $NaHSO_4$ (20 mL). The organic layer was dried over $NaSO_4$, filtered and concentrated. The crude product was purified by column chromatography using CH_2Cl_2/MeOH 19/1 as an eluent to afford the product as a syrup (1.56 g, 3.73 mol, 97%). [8]

Rf=0.37 (Hexane/ AcOEt 1/1)

^{1}H NMR (CD_3OD, 300 MHz): δ 5.89-5.71 (m, 1H; CH=), 5.36-5.24 (m, 3H), 5.11-4.63 (m, 2H; =CH2), 4.79 (s, 1H; H-1), 4.34-4.21 (m, 1H; H6), 4.09 (m, 1H; H6), 4.04-4.39 (m, 1H; H5), 3.76-3.62 (m, 1H; OC*H*$_2$CH$_2$), 3.52-3.39 (m, 1H; OC*H*$_2$CH$_2$), 2.15 (s, 3H; OAc), 2.10 (s, 3H; OAc), 2.04 (s, 3H; OAc), 1.99 (s,3H; OAc), 1.74-1.62 (m, 4H).

5-Thioacetylpentyl tetra-*O*-acetyl-β-D-mannopyranoside (FC017): Thioacetic acid (4 equiv.) and a catalytic amount of AIBN were added to a solution of pent-4-enyl tetra-O-acetyl-a-D-mannopyranoside (800 mg, 1.92 mmol, 1 equiv.) in THF (20 mL). The mixture was refluxed for 12 h. The crude reaction was concentrated and purified by column chromatography using CH_2Cl_2/MeOH 19/1 as an eluent to afford the product as a syrup (0.7 g, 1.42 mmol, 74%). [8]

Rf=0.30 (Hexane/AcOEt 1/1)

^{1}H NMR (CD_3OD, 300 MHz): δ 5.36-5.22 (m, 3H), 4.79 (s, 1H; H-1), 4.28 (dd, *J*=5.1, 12.0 Hz, 1H; H6), 4.17-4.05 (m, 1H; H6), 4.03-3.92 (m, 1H; H5), 3.77-3.59 (m, 1H; OC*H*$_2$CH$_2$), 3.54-3.37 (m, 1H; OC*H*$_2$CH$_2$), 2.87 (t, *J*=6.9 Hz, 2H; C*H*$_2$SAc), 2.32 (s, 3H; SAc), 2.15 (s, 3H; OAc), 2.10 (s, 3H; OAc), 2.04 (s, 3H; OAc), 2.00 (s, 3H; OAc), 1.74-1.50 (m, 6H).

5,5'-Dithio bis (pentyl-β-D-mannopyranoside) [ManC_5S]$_2$ (FC018): 0.7 mL of a NaOMe solution (1 N in MeOH) was added to a solution of 5-thioacetylpentyl tetra-O-acetyl-a-D-mannopyranoside (0.493 g, 1.0 mmol, 1 equiv.) in MeOH (12 mL). The reaction was stirred under argon atmosphere over 2 h. The reaction was neutralized by Amberlist IR-120 resin, filtered and evaporated. The product was obtained as a syrup, mixture of disulfide and thiol (282 mg, 1.0 mmol, quantitative). [8]

^{1}H NMR (CD_3OD, 500 MHz): δ 4.75 (s, 1H; H1), 3.83 (dd, *J*=2.0, 11.5 Hz, 1H; H6), 3.80-3.42 (m, 7H), 2.71 (t, *J*=7.5 Hz, 1H; C*H*$_2$S-S); 2.52 (t, *J*=7.5 Hz, 1H; C*H*$_2$SH), 1.77-1.45 (m, 6H).

^{13}C NMR (CD_3OD, 500 MHz): δ 99.7 (C1), 72.8, 70.8, 70.5, 66.8, 61.1, 59.7 (C6), 37.8 (CH_2S-S), 33.2, 28.4, 28.2, 24.4, 23.1 (CH_2SH).

5, 5'-Dithiobis[pentyl(α-D-glucopyranosyl) (1→4)-β-D-glucopyranoside] [MaltoseC$_5$]$_2$

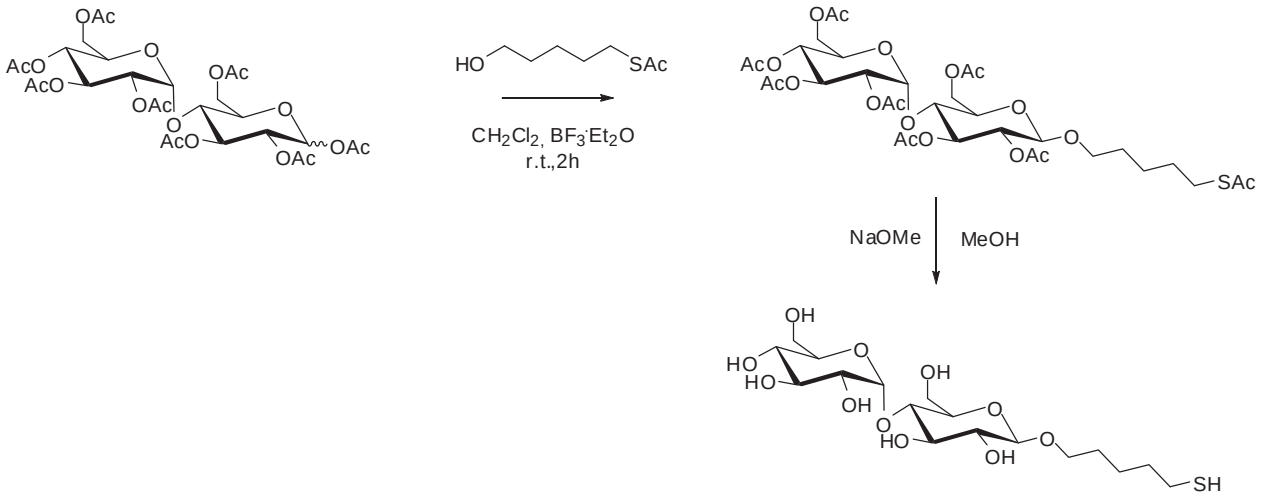

5-Thioacetylpentyl 2, 3, 4, 6-tetra-*O*-acetyl- α-D-glucopyranosyl (1→4) 2, 3, 6-tri-*O*-aceyl-β-D-glucopyranoside (MME102): A solution of acetylated maltose (1323 mg, 1.95 mmol, 1.0 eq.) in dry CH_2Cl_2 (25 mL) was added 5-thioacetylpentan-1-ol (950 mg, 5.85 mmol, 3 eq.) under argon atmosphere, as well as $BF_3{\cdot}Et_2O$ (1522 mL, 10.7 mmol, 5.5 eq.). The mixture was stirred for 2 hours and concentrated. The resulting product was purified by column chromatography using Hexane/AcOEt 1.5/1 as an eluent to give the corresponding neoglycoconjugate (830 mg, 1.06 mmol, 55%). [14]

Rf=0.26 (Hexane/AcOEt 1.5/1)

^{1}H NMR (CDCl$_3$, 500 MHz) δ 5.41 (d, 1H, *J* = 4.0 Hz, H-1´); 5.36 (t, 1H, *J* = 10.1 Hz, H-3´); 5.24 (t, 1H, *J* = 9.5 Hz, H-3); 5.05 (t, 1H, *J* = 10.1 Hz, H-4´); 4.85 (dd, 1H, *J* = 10.1, 4.0 Hz, H-2´); 4.81 (dd, 1H, *J* = 9.5, 7.9 Hz, H-2); 4.50 (d, 1H, *J* = 7.9 Hz, H-1); 4.47 (dd, 1H, *J* = 12.1, 2.7 Hz, H-6a); 4.24 (dd, 1H, *J* = 12.4, 3.9 Hz, H-6´a); 4.22 (dd, 1H, *J* = 12.1, 4.4 Hz, H-6b); 4.04 (dd, 1H, *J* = 12.4, 2.2 Hz, H-6´b); 3.99 (t, 1H, *J* = 9.5 Hz, H-4); 3.97-3.94 (m, 1H, H-5´); 3.86-3.81 (m, 1H, OC*H*$_2$CH$_2$); 3.70-3.65 (m, 1H, H-5); 3.49-3.45 (m, 1H, OC*H*$_2$CH$_2$); 2.84 (t, 2H, *J* = 7.9 Hz, C*H*$_2$SAc); 2.32 (s, 3H, SAc); 2.14 (s, 3H, OAc); 2.10 (s, 3H, OAc); 2.04 (s, 3H, OAc); 2.02 (s, 6H, 2xOAc); 2.00 (s, 6H, 2xOAc); 1.62-1.54 (m, 4H, C*H*$_2$CH$_2$SAc and OCH$_2$C*H*$_2$); 1.44-1.34 (m, 2H, C*H*$_2$CH$_2$CH$_2$SAc).

5, 5'-Dithiobis[pentyl(α-D-glucopyranosyl) (1→4)-β-D-glucopyranoside] [MaltoseC$_5$]$_2$ (MME108): 5-thioacetylpenthyl-2, 3, 4, 6-tetra-O-acetyl- α-D-glucopyranosyl (1→4) 2, 3,-tri- O-acetyl-β-D-glucopyranoside (830 mg, 1.06 mmol, 1 eq.) was dissolved in MeOH (15 mL) and NaOMe was added (57 mg, 1.06 mmol, 1 eq.). The reaction was stirred for 4 hours open to the air

in order to complete the oxidation of the thiol group. The mixture was quenched with HCl 0.1N up to pH=7 and concentrated. In order to take off the salts the product was passed through a Sephadex (MeOH/CH_2Cl_2). A mixture of thiol and disulfide was obtained as yellow oil (470 mg, 1.057 mmol, quantitative).

^{1}H NMR (CD_3OD, 500 MHz) δ 5.19 (d, 1H, *J*=3.3 Hz, H1´), 4.30 (d, 1H, *J*=7.7 Hz, H1), 3.95-3.82 (m, 4H, H6´, H6, H5´, H5), 3.73-3.54 (m, 6H, H6´, H6, H4´, H4, H3´, H3), 3.48 (dd, 1H, *J*=9.6, 3.3 Hz, H2´), 3.40 (m, 1H, H2), 3.33-3.24 (m, 2H, -OC*H*$_2$), 2.73 (t, 2H, *J*=7.20 Hz, -C*H*$_2$S-S-), 2.53 (t, 2H, *J*=7.0 Hz, C*H*$_2$SH), 1.77-1.66 (m, 4H, -C*H*$_2$CH$_2$C*H*$_2$-), 1.52 (m, 2H, -CH$_2$C*H*$_2$CH$_2$-).

^{13}C NMR (CD_3OD, 500 MHz) δ 104.38, 102.96 (C1, C1´), 81.39, 77.93, 76.65, 75.14, 74.83, 74.76, 74.23, 71.56, 70.72, 62.81, 62.26 (C6, C6´), 39.75, 30.42, 30.12, 26.02.

MS (ESI) *m/z* 909.3026 $[M+Na]^+$ (disulfure). Calculated MS *m/z* 444.2 [M]

5, 5'-Dithiobis[pentyl(β-D-glucopyranosyl) (1→4)-β-D-glucopyranoside] [CellobioseC$_5$]$_2$

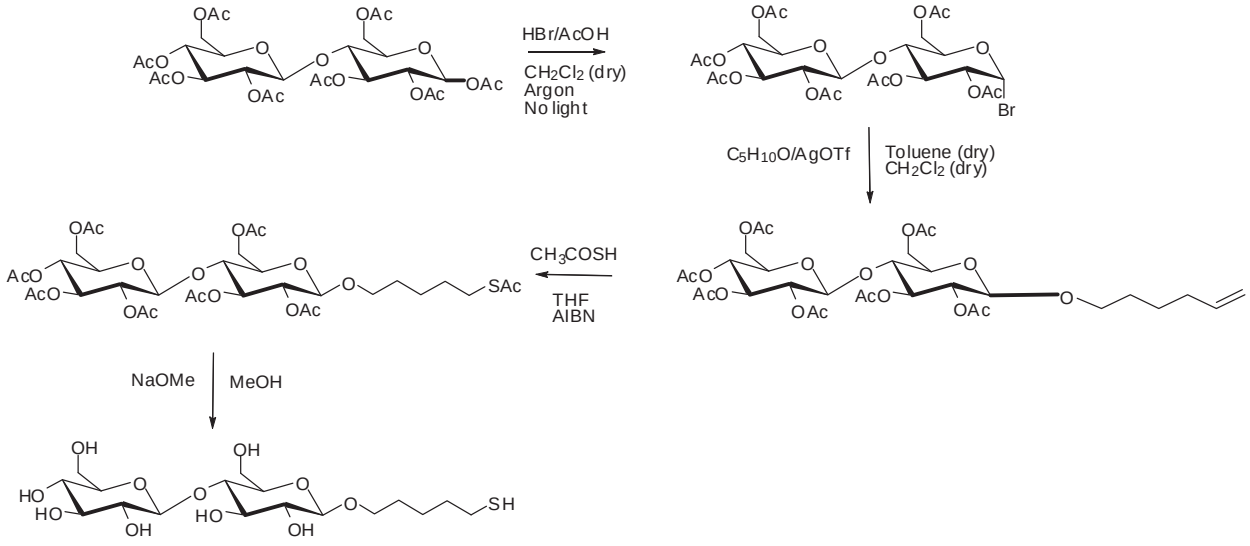

1-bromo-2, 3, 4, 6-tetra-*O*-acetyl-β-D-glucopyranosyl (1→4) 2, 3,6-tri-*O*-aceyl-β-D-glucopyranoside (AI059, MME112): Cellobiose (7.0 g, 10.32 mmol, 1.0 eq.) was dissolved in dry CH_2Cl_2 (30 mL) under argon atmosphere and HBr/AcOH (10.3 mL, 56.76 mmol, 5.5 eq.) was added. The solution was stirred 1 hour under argon atmosphere and in dark. The mixture was diluted with 50 mL of CH_2Cl_2 and neutralized with saturated Na_2CO_3 until the pH was around 7. 100 mL of CH_2Cl_2 were added and the solution was extracted with saturated Na_2CO_3 (200 mL x

3) and water (100 mL). The organic phase was dried over Mg_2SO_4, filtered and concentrated to give the corresponding product (6.92 g, 9.89 mmol, 96%) as a white solid.

R_f =0.50 (AcOEt/Hexan 4/1).

^{1}H NMR ($CDCl_3$, 500 MHz) δ 6.52 (d, 1H, *J* = 4.1 Hz, H-1); 5.53 (t, 1H, *J* =9.7 Hz, H-3); 5.15 (t, 1H, *J* = 9.3 Hz, H-3´); 5.07 (t, 1H, *J* = 9.3 Hz, H-4´); 4.93 (dd, 1H, *J* = 9.3, 8.1 Hz, H-2´); 4.76 (dd, 1H, *J* = 9.7, 4.1 Hz, H-2); 4.54 (d, 1H, *J* = 8.1 Hz, H-1´); 4.54-4.51 (m, 1H, H-6b); 4.36 (dd, 1H, *J* = 12.5, 4.4 Hz, H-6´b); 4.21-4.15 (m, 2H, H-5 and H-6a); 4.04 (dd, 1H, *J* = 12.5, 2.2 Hz, H-6´a); 3.83 (t, 1H, *J* = 9.7 Hz, H-4); 3.67 (dd, 1H, *J* = 9.3, 4.4, 2.2 Hz, H-5´); 2.13 (s, 3H, OAc); 2.08 (s, 6H, 2xOAc); 2.04 (s, 6H, 2xOAc); 2.01 (s, 3H, OAc); 1.98 (s, 3H, OAc).

4-Pentenyl 2, 3, 4, 6-tetra-*O*-acetyl-β-D-glucopyranosyl (1→4) 2, 3,6-tri-*O*-aceyl-β-D-glucopyranoside (AI060): A solution of 1-bromo-2, 3, 4, 6-tetra-*O*-acetyl- β-D-glucopyranosyl (1→4) 2, 3,6-tri- O-aceyl- β-D-glucopyranoside (6.9 g, 9.9 mmol, 1.0 eq.) and 4-penten-1-ol (2.2 mL, 21.76 mmol, 2.2 eq.) in dry CH_2Cl_2 (80 mL) was stirred 30 minutes in the presence of acetonated molecular sieves (4 Å powder) under argon atmosphere and in dark. In the meantime, AgOTf (3.5 g, 13.6 mmol, 1.4 eq.) was kept under argon atmosphere and dry toluene (30 mL) was added. All the AgOTf was solubilised after stirring. The flask with the first reaction was put at 0º C (ice bath) and AgOTf solution was added drop by drop. The reaction was left from 0º C to room temperature on its own for 2 hours 30 minutes but it seemed that it was not completed (TLC control). More AgOTf (1.3 g, 4.9 mmol, 0.5 eq.) in dry toluene (11.5 mL) and 4-penten-1-ol (0.5 mL, 4.9 mmol, 0.5 eq.) were added and the reaction was stirred for 2 hours and 30 minutes. The TLC was similar to the other one. The mixture was filtered over Cellite with CH_2Cl_2 and concentrated. The resulting product was purified by column chromatography (d = 8 cm; h = 15 cm) using a gradient of Hexane/AcOEt (fron 10% to 100%) as an eluent, but α and β neoglycoconjugates were in the same fractions. This fractions were purified again by *Biotage* (clumn: 40+M) to give the corresponding α and β neoglycoconjugates.

R_f =0.32 (AcOEt/Hexan 1/1).

^{1}H NMR (AI060-β-F1-88, $CDCl_3$, 500 MHz) δ 5.81-5.73 (m, 1H, C*H*CH_2), 5.19-5.12 (m, 2H, H-3 and H-3'), 5.06 (t, 1H, H-4´, *J*= 9.7 Hz), 5.02-4.87 (m, 2H, H-2 and H-2´), 4.52-4.49 (m, 2H, H-1´ and H-6_b), 4.44 (d, 1H, H-1, *J*= 8.0 Hz), 4.36 (dd, 1H, H-6´$_b$, *J*= 8.0, 4.4 Hz), 4.09 (dd, 1H, H-6_a, *J*= 6.9, 5.0 Hz), 4.04 (dd, 1H, H-6´$_a$, *J*= 10.4, 2.0 Hz), 3.87-3.81 (m, 1H, C*H*$_2$O), 3.76 (t, 1H, H-4, *J*= 9.5 Hz), 3.67-3.63 (m, 1H, H-5´), 3.59-3.56 (m, 1H, H-5), 3.49-3.44 (m, 1H, C*H*$_2$O), 2.12 (s, 3H, OAc), 2.08 (s, 3H, OAc), 2.03 (s, 3H, OAc), 2.02 (s, 3H, OAc), 2.01 (s, 3H, OAc), 2.00 (s, 3H, OAc), 1.98 (s, 3H, OAc), 1.72-1.62 (m, 2H, CH_2CH_2).

^{1}H NMR (AI060-α-F2-88, $CDCl_3$, 500 MHz) δ 5.84-5.76 (m, 1H, C*H*CH_2), 5.65 (d, 1H, H-1, *J*= 5.2 Hz), 5.55-5.54 (m, 1H, H-3), 5.2 (t, 1H, H-3´, *J*= 9.5 Hz), 5.12 (t, 1H, H-4´, *J*= 9.8 Hz), 5.04-4.96 (m, 3H, H-2´ and CHCH_2), 4.68 (d, 1H, H-1´, *J*= 8.1 Hz), 4.33-4.31 (m, 1H, H-2), 4.27-4.22 (m, 2H, H-6_a and H-6´$_a$), 4.16-4.07 (m, 2H, H-6_b and H-6´$_b$), 3.86-3.82 (m, 1H, H-5), 3.78-3.75 (m, 1H, H-5´), 3.63 (d, 1H, H-4´, *J*= 9.6 Hz), 3.49 (t, 2H, CH_2O, *J*= 6.5 Hz), 2.12 (s, 5H, OAc and CHCH_2), 2.10 (s, 3H, OAc), 2.09 (s, 3H, OAc), 2.05 (s, 3H, OAc), 2.02 (s, 3H, OAc), 2.00 (s, 3H, OAc), 1.67-1.62 (m, 2H, CH_2CH_2).

5-Thioacetylpentyl 2, 3, 4, 6-tetra-*O*-acetyl- β-D-glucopyranosyl (1→4) 2, 3, 6-tri- *O*-aceyl- β-D-glucopyranoside (AI061, MME115): Pent-4-enyl 2, 3, 4, 6-tetra-O-acetyl- β-D-glucopyranosyl (1→4) 2, 3,6-tri- O-aceyl- β-D-glucopyranoside (250 mg, 0.354 mmol, 1 eq.) was dissolved in THF (10 mL). Thiolacetic acid (0.1 mL, 1.392 mmol, 4 eq.) and a catalytic amount of AIBN (2 spatula) were added and the mixture was stirred to reflux (86ºC) for 5 hours. The mixture was concentrated and it was purify by *Biotage* (column: 40+M) using a gradient of AcOEt/Hexane to give the corresponding product (269 mg, 0.345 mmol, 97%).

R_f =0.38 (AcOEt/Hexan 1/1).

^{1}H NMR ($CDCl_3$, 500 MHz) δ 5.21 (t, 1H, *J*=9.5 Hz), 5.17 (t, 1H, *J*=9.5 Hz), 5.00 (t, 1H, *J*=9.8 Hz), 4.71 (d, 1H, *J*=8.0 Hz, H1'), 4.58 (d, 1H, *J*=8.0 Hz, H1), 4.51 (m, 1H), 4.40 (dd, 1H, *J*=12.6, 4.4 Hz), 4.15 (m, 1H), 4.05 (m, 1H), 3.90-3.86 (m, 1H), 3.85-3.79 (m, 2H), 3.74-3.71 (m, 1H), 3.54-3.49 (m, 1H), 4.44 (m, 1H), 3.16 (m, 1H), 2.86 (t, 2H, 7.1 Hz, CH_2SAc), 2.30 (s, 3H, SAc), 2.11 (s, 3H, OAc), 2.06 (s, 3H, OAc), 2.03 (s, 3H, OAc), 2.02 (s, 3H, OAc), 2.02 (s, 3H, OAc), 1.99 (s, 3H, OAc), 1.94 (s, 3H, OAc), 1.56 (m, 4H), 1.43-1.36 (m, 2H).

5, 5'-Dithiobis[pentyl(β-D-glucopyranosyl) (1→4)-β-D-glucopyranoside] [CellobioseC_5]$_2$ (AI062, MME118): 5-Thioacetylpenthyl-2, 3, 4, 6-tetra-O-acetyl- β-D-glucopyranosyl (1→4) 2, 3, 6-tri- O-aceyl- β-D-glucopyranoside (269 mg, 0.345 mmol, 1 eq.) was dissolved in MeOH (30 mL) and then sodium methoxide (37.27 mg, 0.69 mmol, 2 eq.) was added. The reaction mixture was stirred for 24 hours (NMR control) and it was neutralized with Amberlist IR-120 resins, filtered and concentrated. The product was cleaned with diethyl ether.

^{1}H NMR (CD_3OD, 500 MHz) δ 4.41 (d, 1H, *J*=7.7 Hz, H1'), 4.28 (d, 1H, *J*=7.7 Hz, H1), 3.88 (m, 4H, H6´, H6, H5´, H5), 3.59-3.48 (m, 4H, H6´, H6, H4´, H4), 3.38 (m, 3H, H3´, H3, H2´), 3.25-3.21 (m, 3H, H2, -OCH_2), 2.70(t, 2H, *J*=7.2 Hz, CH_2S-S), 2.50 (t, 2H, *J*=7.3 Hz, CH_2SH), 1.74-1.63 (m, 4H, -CH_2CH_2-), 1.50 (m, 2H, -CH_2-).

^{13}C NMR (CD_3OD, 500 MHz) δ 104.65, 104.25 (C1, C1´), 80.82, 78.15, 77.89, 76.48, 74.97, 74.88, 71.42, 70.72, 62.47, 61.94 (C6, C6´), 39.74, 30.40, 30.10, 26.00, 25.89.

MS (ESI) *m/z* 909.3046 $[M+Na]^+$ (disulfure). Calculated MS *m/z* 444.2 [M]

5,5'-dithiobis[pentyl-α-D-galactopyranosyl](1→4)-β-D-glucopyranoside [$LacC_5S]_2$

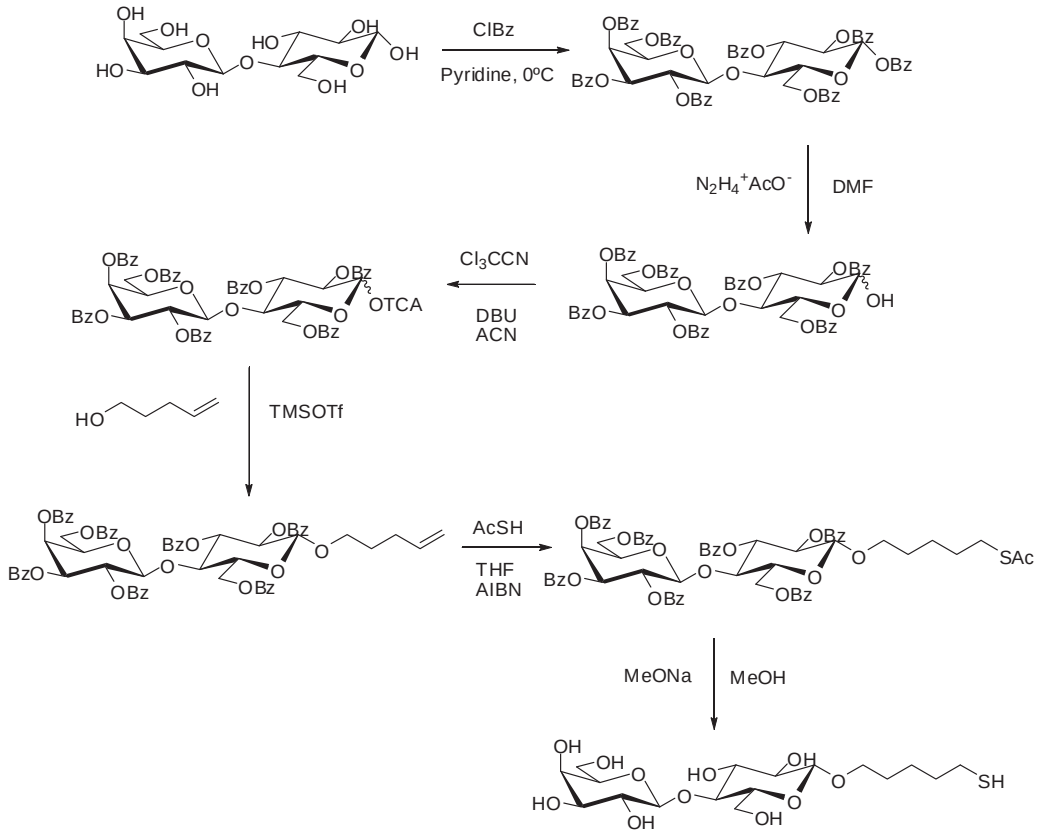

Benzoyl 2, 3, 4, 6-tetra-*O*-benzoyl-β-D-galactopyranosyl (1→4) 1, 2, 3, 6-tetra-*O*-benzoyl-α-D-glucopyranoside: Benzoyl chloride (BzCl) (40 mL, 332 mmol, 12 eq.) and a catalytic amount of DMAP were added, at 0ºC, to a solution of lactose (10 g, 27.7 mmol, 1 eq.) in pyridine (100mL). The mixture was stirred 24 hours, diluted in AcOEt (500 mL) and extracted with water (1x100 mL), HSO_4 2N (1x100 mL) and sodium bicarbonate (1x100 mL). The organic phase was dried over Na_2SO_4, filtered, concentrated and purified by column chromatography using AcOEt/Hexane 1/1 as an eluent (32 g, 27.7 mmol, quantitative). [7]

Rf= 0.5 (AcOEt/Hexane 1/1)

^{1}H NMR ($CDCl_3$, 300 MHz) δ 7.72-7.17 (m, 40H, Bz), 6.76 (d, 1H, *J*=3.6 Hz, H1), 6.21 (dd, 1H, *J*=10.2, 9.0 Hz, H3), 5.80-5.74 (m, 2H, H2´, H4´), 5.62 (dd, 1H, *J*=10.2, 3.6 Hz, H2), 5.39 (dd,

1H, *J*=10.2, 3.3 Hz, H3´), 4.96 (d, 1H, *J*=7.8 Hz, H1´), 4.56 (s, 2H, H6a, H5b), 4.40 (t, 1H, *J*=9.0 Hz, H4), 4.31 (m, 1H, H6´), 3.92 (m, 1H, H6´), 3.83-3.73 (m, 2H, H5, H5´).

2, 3, 4, 6-tetra-*O*-benzoyl-β-D-galactopyranosyl (1→4) 2, 3, 6-tri-*O*-benzoyl-α-D-glucopyranose: Hydrazine acetate ($N_2H_4^+AcO^-$) (2.35 g, 25.55 mmol, 1.5 eq.) was added in several portions to a solution of benzoylated lactose (20 g, 17.04 mmol, 1 eq.) in DMF (50 mL). The reaction was stirred at 60ºC and controlled by TLC until a new product with lower Rf appeared. The crude was diluted with AcOEt (200 mL) and washed with water (3x60 mL). The organic phase was purified by column chromatography using AcOEt/Hexane 1/2 as an eluent to give an amorphous solid (11 g, 10.28 mmol, 74%). [7]

^{1}H NMR ($CDCl_3$, 300 MHz) δ 8.07-7.25 (m, 35H, Bz), 6.14 (t, 1H, *J*=9.6 Hz, H3), 5.77-5.68 (m, 2H, H2´, H4'), 5.62 (d, 1H, *J*=3.6 Hz, H1), 5.40 (dd, 1H, *J*=10.3, 3.4 Hz, H2), 5.24 (dd, 1H, *J*=7.2, 3.6 Hz, H3´), 4.94 (d, 1H, *J*=7.8 Hz, H1´), 4.59 (m, 1H, H6a), 4.51 (dd, 1H, *J*=9.1, 3.3 Hz, H6b), 4.24 (t, 1H, *J*=9.6 Hz, H4), 3.94-3.67 (m, 2H, H5, H5´).

Trichloroacetimidate of 2, 3, 4, 6-tetra-*O*-benzoyl-β-D-galactopyranosyl (1→4) 2, 3, 6-tri-*O*-benzoyl-D-glucopyranosile: Cl_3CCN (15.46 mL, 154 mmol, 15 eq.) and 2 mL of DBU in dry CH_2Cl_2 (5 mL) were added to 2, 3, 4, 6-tetra-O-benzoyl-β-D-galactopyranosyl (1→4) 2, 3, 6-tri-O-benzoyl-α-D-glucopyranose (11 g, 10.28 mmol, 1 eq.) in dry CH_2Cl_2 (40 mL). The mixture was stirred for 2 hours, diluted in AcOEt (200 mL) and extracted with water (3x60 mL). The organic phase was dried over Na_2SO_4, filtered, concentrated and purified by column chromatography using AcOEt/Hexane 1/2 as an eluent (10 g, 8.31 mmol, 81 %). [7]

^{1}H NMR ($CDCl_3$, 500 MHz) δ 8.56 (s, 1H, NH), 8.03-7.16 (m, 35H, Bz), 6.70 (d, 1H, *J*=3.6 Hz, H1), 6.15 (m, 1H, H3), 5.74 (m, 2H, H2´, H4´), 5.54 (dd, 1H, *J*=10.3, 3.4 Hz, H2), 5.39 (dd, 1H, *J*=7.2, 3.6 Hz, H3´), 4.94 (d, 1H, *J*=7.8 Hz, H1´), 4.57 (m, 2H, H6a, H6b), 4.34 (m, 2H, H6´a, H6´b), 4.24 (t, 1H, *J*=9.6 Hz, H4), 3.92-3.67 (m, 2H, H5, H5´).

1-pentenyl-2, 3, 4, 6-tetra-*O*-benzoyl-α-D-galactopyranosyl (1→4) 2, 3, 6-tri-*O*-benzoyl-β-D-glucopyranoside: TMSOTf (0.08 eq.) was added to a solution of the trichloroacetimidate (7 g, 5.82 mmol, 1 eq.) and 4-penten-1-ol (1.26 g, 14.66 mmol, 2.5 eq.) in dry CH_2Cl_2 (60 mL) at room temperature and under argon atmosphere. The mixture was stirred 30 minutes, diluted CH_2Cl_2 and washed with water.The organic phase was concentrated and purified by column chromatography using AcOEt/Hexane 1/3 as an eluent (2.6 g, 2.03 mmol, 70 %). [7]

^{1}H NMR ($CDCl_3$, 300 MHz) δ 8.08-7.10 (m, 35H, Bz), 5.77 (t, 1H, *J*=10.0 Hz, H3), 5.70-5.67 (m, 2H, H2´, H4´), 5.6 (m, 1H, C*H*=CH_2), 5.45 (t, 1H, *J*=8.5 Hz, H2), 5.38 (dd, 1H, *J*=10.5, 3.0 Hz, H3´), 4.84 (d, 1H, *J*=7.5 Hz, H1), 4.78 (m, 2H, CH=CH_2), 4.67 (d, 1H, H1´), 4.57 (dd, 1H, *J*=12.0, 4.2 Hz, H6), 4.47 (dd, 1H, *J*=12.0, 4.5 Hz, H6´), 4.25 (t, 1H, *J*=9.5 Hz, H4), 3.90-3.78 (m, 3H), 3.78-3.60(m, 2H), 3.45 (m, 1H), 1.95 (m, 2H), 1.54 (m, 4H).

^{13}C NMR ($CDCl_3$, 75 MHz) δ 165.9, 165.7, 165.5, 164.0 (Bz), 137.9 (-*C*H=CH_2), 133.9, 133.8, 133.7, 133.6, 133.5, 130.2, 130.0, 129.9, 129.7, 129.6, 129.0, 128.9, 128.8, 128.7, 128.6 (CH=*C*H_2), 115.2 (-CH*C*H_2), 101.4, 101.2, (C1, C1´), 73.3, 73.2, 72.0, 71.7, 70.2, 69.7, 67.8, 62.7, 61.3 (C6, C6´), 30.4, 30.0, 28.7 (CH_2CH_2).

1-thioacetylpentyl 2, 3, 4, 6-tetra-*O*-benzoyl-α-D-galactopyranosyl (1→4) 2, 3, 6-tri-*O*-benzoyl-β-D-glucopyranoside: 1-pentenyl-2, 3, 4, 6-tetra-*O*-benzoyl-α-D-galactopyranosyl (1→4) 2, 3, 6-tri-*O*-benzoyl-β-***D***-glucopyranoside (5.69 g, 4.99 mmol, 1 eq.) was dissolved in THF (30 mL). Thiolacetic acid (1.42 mL, 19.9 mmol, 4 eq.) and a catalytic amount of AIBN (2 spatula) were added and the mixture was stirred to reflux (86ºC) for 24 hours. The mixture was concentrated and it was purified by column chromatography using AcOEt/Hexane 1/3 as an eluent to give the corresponding product (5.8 g, 4.78 mmol, 95%). [7]

^{1}H NMR ($CDCl_3$, 300 MHz) δ 8.1-7.05 (m, 35H, Bz), 5.79 (t, 1H, *J*=10.0 Hz, H3), 5.76-5.66 (m, 2H, H2, H4), 5.44 (t, 1H, *J*=8.0Hz), 5.35 (dd, 1H, *J*=10.0, 3.0 Hz, H3´), 4.86 (d, 1H, *J*=7.9 Hz, H1), 4.66 (d, 1H, *J*=8.1 Hz, H1´), 4.59 (m, 1H), 4.45 (dd, 1H, *J*=12.0, 3.9 Hz), 4.24 (t, 1H, *J*=9.5 Hz), 3.95-3.78 (m, 3H), 3.78-3.60 (m, 2H), 3.45 (m, 1H), 2.55 (m, 2H, -CH_2S-), 2.25 (s, 3H, SAc), 1.5-1.2 (m, 6H, -CH_2CH_2CH_2-).

^{13}C NMR ($CDCl_3$, 75 MHz) δ 196.2 (COS), 166.2, 165.9, 165.8, 165.6, 165.5, 165.2 (Bz), 133.7, 130.1, 130.0, 101.5, 101.3 (C1,C1´), 73.4, 73.3, 72.1, 71.8, 70.3, 67.9, 62.8, 61.5 (C6, C6´), 31.0, 29.4, 29.1, 25.4 (CH_2CH_2).

5,5'-dithiobis[pentyl-α-D-galactopyranosyl](1→4)-β-D-glucopyranoside [$LacC_5S]_2$: 1-thioacetylpentyl-2, 3, 4, 6-tetra-*O*-benzoyl-α-D-galactopyranosyl (1→4) 2, 3, 6-tri-*O*-benzoyl-β-***D***-glucopyranoside (2.86 g, 2.35 mmol, 1 eq.) dissolved in dry MeOH (40 mL) and 2 equivalent of methanolic solution of NaOMe 1N was added (4.7 mmol, 1 eq.). The reaction was stirred for 24 hours open to the air in order to complete the oxidation of the thiol group. The mixture was neutralized with Amberlist IR-120 resins, filtered and concentrated. The residue was washed several times with ether (15 mL) in order to take off the methyl benzoate. A mixture of the

disulfide (mayor product) and the thiol was obtained (538 mg, 0.6 mmol, 52%) as a white solid. [7]

^{1}H NMR (D_2O, 500 MHz) δ 4.29 (t, 2H, *J*=8.4 Hz, H1, H1´), 3.8-3.7 (m, 2H), 3.7-3.3 (m, 10H), 3.1 (m, 2H, -C*H*$_2$OH), 2.6 (t, 2H, *J*=7.2 Hz, -C*H*$_2$SH), 1.65-1.4 (m, 4H, C*H*$_2$C*H*$_2$), 1.4-1.2 (m, 2H, CH_2CH_2).

^{13}C NMR (D_2O, 75 MHz) δ 103.2, 102.3 (C1, C1´), 78.6, 75.0, 74.7, 73.1, 72.8, 71.2, 70.7, 68.8, 61.3, 60.3 (C6, C6´), 38.4, 28.7, 28.4, 24.3.

Synthesis of DO3A and DO3A-amide derivatives:

1, 4, 7,-tris(carboxymehyl)-10-(11-mercaptoundecyl)-1, 4, 7, 10-tetraazacyclododecane ($DO3AC_{11}SH$)

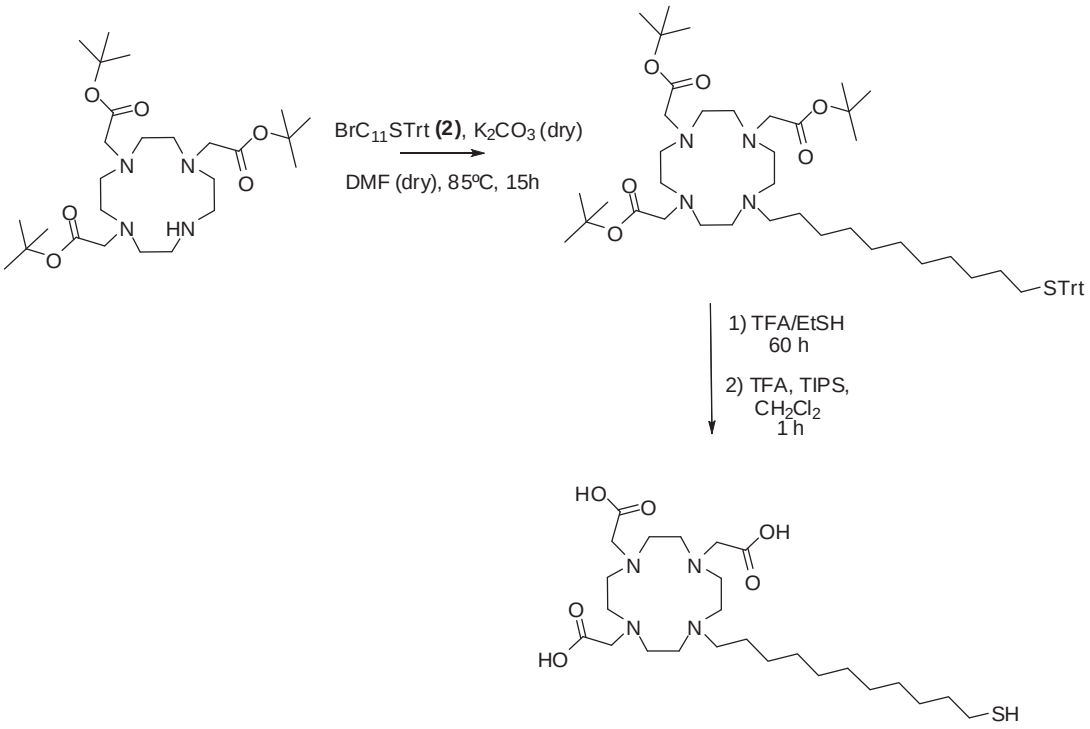

1, 4, 7,-tris(tertbutylacetate)-10-(11-thiotriphenylundecyl)-1, 4, 7, 10-tetraazacyclododecane (AI011): K_2CO_3 anhydrous (400.0 mg, 2.9 mmol, 3.0 eq.) was added to a solution of DO3A^{t}Bu (500.0 mg, 1.0 mmol, 1.0 eq.) in DMF dry (12.5 mL). Then, the linker (791.0 mg, 1.5 mmol, 1.5 eq.) was added and the mixture was stirred under argon atmosphere at 85 ^{o}C for 15 hours. After concentrating, the resulting product was purify by column chromatography (d = 3 cm; h = 11 cm) using CH_2Cl_2/MeOH 9/1 as an eluent to give the corresponding $DO3AC_{11}S$ (963 mg).

Rf =0.47 (CH_2Cl_2/MeOH 9/1).

^{1}H NMR ($CDCl_3$, 500 MHz) δ 7.50-7.20 (m, 15H, Ph), 3.70-2.20 (m, 24H, -NC*H*$_2$-), 2.12 (t, 2H, J=7.2 Hz, -C*H*$_2$SPh), 1.60-1.30 (m, 27H, *tert*-butil), 1.30-1.10 (m, 17H, -CH_2-).

^{13}C-NMR (75MHz, CDCl3) δ 169.7 (*C*OO^{t}Bu), 144.8, 129.4, 127.6 and 126.3 (4 *C*-Ph), 81.6 (-*C*CH_3) 66.2 (-*C*Ph_3), 56.7 (-*C*H_2N-), 52.5 (-N*C*$H_2CH_2CH_2$-), 52.5-50.1 (-N*C*H_2*C*H_2N-), 47.6 (-N*C*H_2CH_2N-), 31.8 (-*C*H2S-), 29.6, 29.5, 29.4, 29.3, 29.1, 28.9, 28.6, 27.4, 27.3, 26.3 (-CH_2CH_2).

MS (ESI) m/z: 943 $[M+H]^+$. Calculated MS *m/z* 942.6 [M]

1, 4, 7,-tris(carboxymethyl)-10-(11-mercaptoundecyl)-1, 4, 7, 10-tetraazacyclododecane (AI012): Trifluoroacetic acid (TFA) (15.7 mL, 204 mmol, 200 eq.) was added to a solution of DO3A^{t}Bu/linker (963.0 mg, 1.0 mmol, 1.0 eq.) in ethanethiol (EtSH) (51 mL) and it was stirred for 60 hours. The reaction mixture was concentrated and, then, CH_2Cl_2 (28 mL), trifluoroacetic acid (TFA) (3 mL) and triisopropylsilyl (TIPS) (3 mL) were added (to capture the carbocation formed during the reaction). The mixture was stirred for 1 hour and concentrated. The concentrated product was dissolved in CH_2Cl_2/MeOH 1/1 (3 mL) and it was added into Et_2O (500 mL) to give a precipitated white solid (it was leave overnight). This product was dissolved in CH_2Cl_2/MeOH 1/1 (40 mL), concentrated and freeze-dried (608 mg, 0.9 mmol, 89%).

^{1}H NMR (D_2O, 500 MHz) δ 3.75-3.03 (m, 22H, -CH_2-ciclen), 2.64 (s, 2H, -CH_2-S-S- CH_2), 2.46 (t, 2H, J= 7.4 Hz), 1.62-1.48 (m, 2H, CH_2-CH_2-N-), 1.23-1.21 (m, 18H, -CH_2-).

^{13}C-NMR (75MHz, DMSO, 80ºC) δ 173.8 (*C*OOH), 57.1 (-*C*H_2-COOH) 54.3, 53.4, 51.8, 51.1 (-N*C*H_2*C*H_2N-) 32.7 (-*C*H_2S-), 31.4, 30.7, 30.4, 30.3, 29.6, 29.0 (- CH_2CH_2-).

IR (KBr) 3417, 2925, 2853, 1637, 1406, 1203 cm-1;

MS (ESI) m/z: 531 $[M-H]^-$. Calculated MS *m/z* 532.3 [M]

1, 4, 7,-tris(carboxymethyl)-10-(5-mercaptopentyl)-1, 4, 7, 10-tetraazacyclododecane (DO3AC$_5$SH)

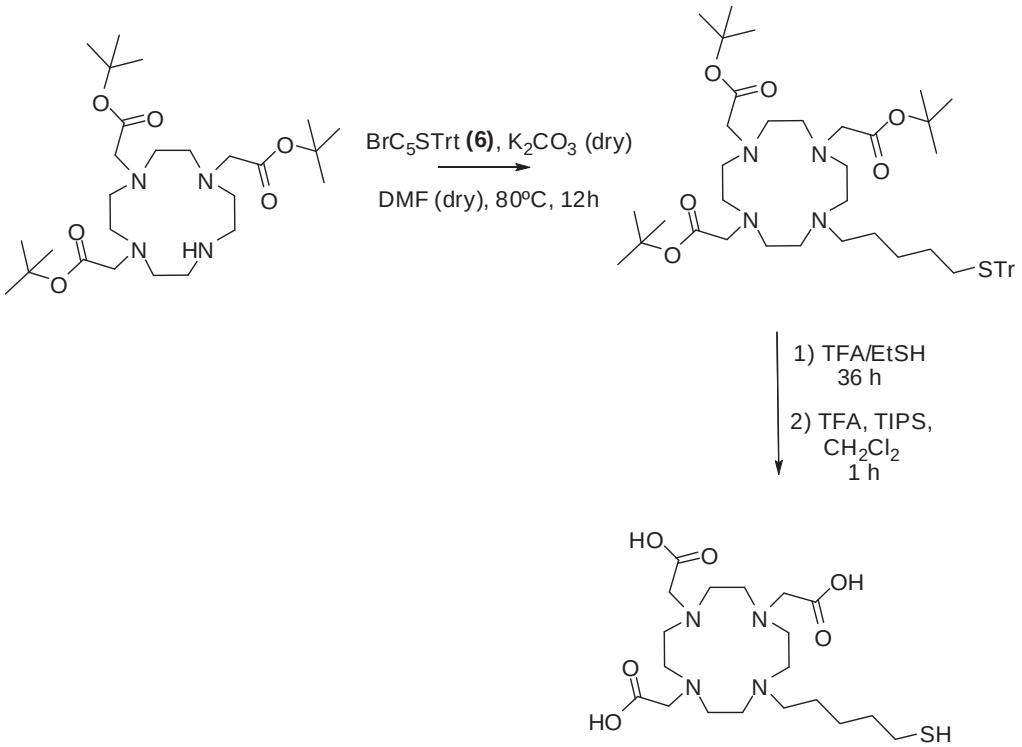

1, 4, 7,-tris(tertbutilacetate)-10-(5-thiotriphenylpentyl)-1, 4, 7, 10-tetraazacyclododecane (MMS115): K_2CO_3 (95 mg, 0.69 mmol, 3 eq.) was added to a solution of DO3A^{t}Bu (118 mg, 0.23 mmol, 1.0 eq.) in DMF (3 mL). Then, the linker (146 mg, 0.34 mmol, 1.4 eq.) dissolved in DMF (1.5 mL) was added drop by drop and the mixture was stirred with refrigeration at 80 ^{o}C for 12 hours. The reaction mixture was diluted with CH_2Cl_2, filtered and concentrated. The resulting product was purified by column chromatography using a gradient of CH_2Cl_2/MeOH (from 0% to 5%) to give DO3AC$_5$SH (179 mg, 0.21 mmol, 91 %).

^{1}H NMR (CDCl$_3$, 500 MHz) δ 7.37-7.19 (m, 15H, Ph), 3.50-2.20 (ma, 24H, -NC*H*$_2$-), 2.13 (t, 2H, *J*=7.1 Hz, -C*H*$_2$SPh), 1.45 (s, 18H), 1.43 (s, 9H), 1.41-1.34 (m, 2H, -C*H*$_2$-CH$_2$STr), 1.33-1.24 (m, 4H, -C*H*$_2$-CH$_2$SPh and -C*H*$_2$-CH$_2$CH$_2$N-).

^{13}C NMR (CDCl$_3$, 100 MHz) δ 173.5 (*C*O*t*Bu), 172.7 (2C, *C*O*t*Bu), 144.9 (3C, C1-Ph), 129.5 (6C, C3-Ph), 127.8 (6C, C2-Ph), 126.5 (3C, C4-Ph), 82.6 and 82.3 (3C, COO*C*(CH$_3$)$_3$), 66.4 (–*C*Ph$_3$), 56.4, 55.8 and 54.1 (4C, -N*C*H$_2$COO*t*Bu and –N*C*H$_2$CH$_2$CH$_2$-),50.3 (broad signal (8C, t), -NCH$_2$*C*H$_2$N-) 31.9 (-*C*H$_2$STr), 31.6 (*C*H$_2$STr), 28.5 (-*C*H$_2$CH$_2$STr), 27.9, 27.8.

IR (KBr): 3084, 3058, 2957, 2931, 2852, 1723, 1456, 1393, 1368 cm^{-1}.

1, 4, 7,-tris(carboxymethyl)-10-(5-mercaptopentyl)-1, 4, 7, 10-tetraazacyclododecane (MME014): Trifluoroacetic acid (TFA) (3.2, 42 mmol, 200 eq.) was added to a solution of

DO3A^{t}Bu/linker (179 mg, 0.21 mmol, 1 eq.) in ethanothiol (EtSH) (10 mL) and it was stirred for 36 hours. Triisopropylsilane (TIPS) (430 uL, 21 mmol, 100 eq.) was added (to capture the carbocation formed during the reaction) and the mixture was stirred for 1 hour. The crude was concentrated, the obtained product was dissolved in CH_2Cl_2/MeOH 1/1 and it was added into cold Et_2O (overnight). The obtained product was freeze-dried (85 mg, 0.189 mmol, 90%).

^{1}H NMR (D_2O, 500 MHz) δ 4.05-4.03 (bs, 2H, -NC*H*$_2$COOH), 3.67-3.43 (m, 12H, -NC*H*$_2$-), 3.30 (t, 2H, *J*= 7.1 Hz, -NC*H*$_2$CH$_2$CH$_2$-), 3.21-3.02 (m, 8H, -NC*H*$_2$-), 2.78 (t, 2H, *J*= 7.0 Hz, -C*H*$_2$S), 1.81-1.74 (m, 4H, -C*H*$_2$-CH$_2$S and -CH$_2$C*H*$_2$CH$_2$N-), 1.51-1.49 (m, 2H, -C*H*$_2$-CH$_2$CH$_2$N-)

^{13}C NMR (D_2O, 500 MHz) δ 174.3 (*C*OOH), 55.9 (-N*C*H$_2$COOH), 54.3 (–N*C*H$_2$CH$_2$CH$_2$-), 53.1, 51.7, 49.9, 48.9, 48.4 and 48.1 (-NCH$_2$*C*H$_2$N- and –NCH$_2$COOH), 37.4 (-*C*H$_2$S-), 27.7 (-*C*H$_2$CH$_2$S-), 24.6 (-*C*H$_2$CH$_2$CH$_2$N-), 22.4 (-CH$_2$*C*H$_2$CH$_2$N-)

IR (KBr): 3550-3250, 2928, 2853, 1683, 1409, 1203, 1133 cm^{-1}.

MS (ESI) *m/z* 449.2 [M+H]$^{+}$. Calculated MS *m/z* 448.2 [M]

2, 2', 2''-(10-(2-(2-(11-mercaptoundecanamido)ethylamino)2-oxoethyl)- 1, 4, 7, 10-tetraazacyclododecane-1, 4, 7-triyl)triacetic acid [DOTA-EdA-C$_{11}$SH (EdA=ethylene diamide)]

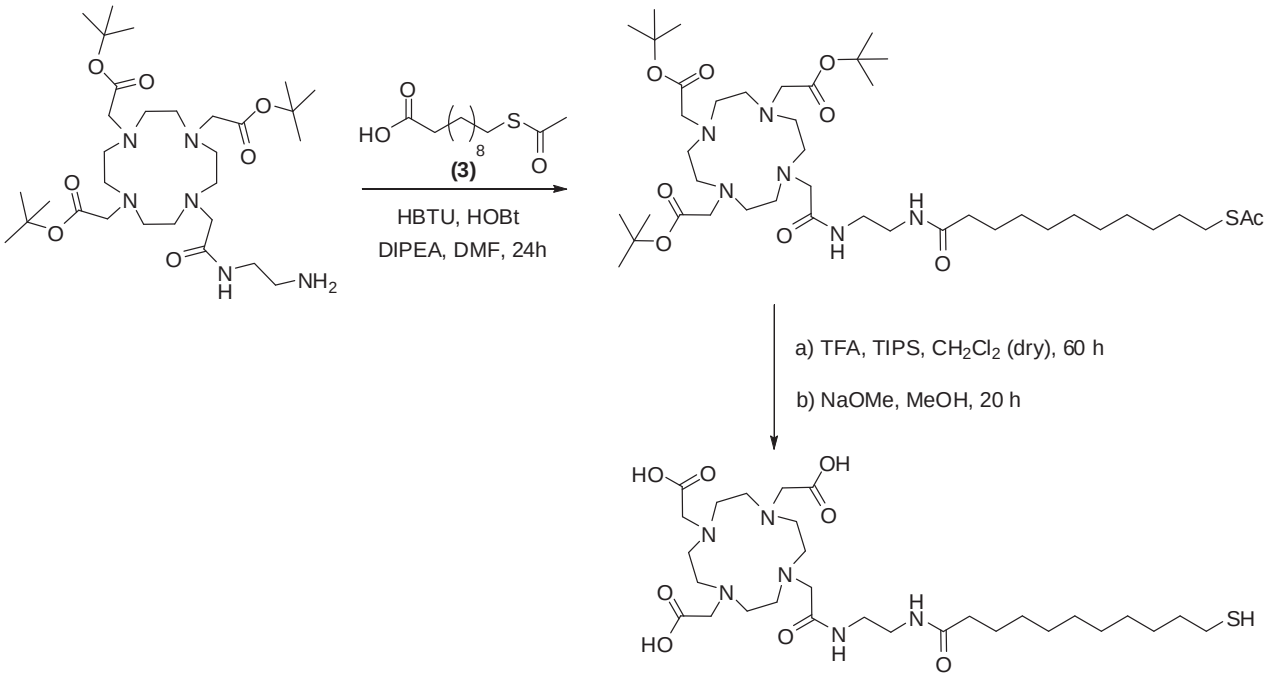

***Tert*-butil 2, 2', 2''-(10-(2-(2-(11-(acetylthio)undecanamido)ethylamino)-2-oxoethyl)-1, 4, 7, 10-tetraazacyclododecane-1, 4, 7-triyl)triacetate (AI159)**: HOBt (67 mg, 0.432 mmol, 1.5 eq.) was added to a solution of 11-(*S*-acetyl)mercaptoundecanoic acid (**3**) (75 mg, 0.288 mmol, 1 eq.) in 2 mL of DMF. After 5 minutes HBTU (164 mg, 0.432 mmol, 1.5 eq.) was added. In another flask, DIPEA (74 mg, 0.576 mmol, 2 eq.) was added to a solution of DO3A^{t}Bu-*N*-(2-aminoethyl)ethanamide (195 mg, 0.317 mmol, 1.1 eq.) in 2 mL DMF. Both mixtures were stirred separately for 1 hour, then the DO3A^{t}Bu-*N*-(2-aminoethyl)ethanamide solution was added to the activated acid mixture and the reaction was stirred for 24 hours. The reaction was quenched with 5 mL of AcOEt and it was extracted with NH_4Cl (5x10 mL). The organic phase was washed first with NaOH 5M (2x5 mL) and afterwards with H_2O (3x5 mL). It was dried over Na_2SO_4, filtered and concentrated. The resulting product was purified by column chromatography using a gradient of CH_2Cl_2/MeOH (from 0% to 20%) to give DOTA-EdA-C_{11}SAc (112 mg, 0.131 mmol, 46%).

Rf =0.56 (CH_2Cl_2/MeOH 95/5).

^{1}H NMR ($CDCl_3$, 500 MHz) δ 6.74 (s, 1H, -N*H*-), 6.48 (s, 1H, -N*H*-), 3.41-2.00 (bm, 24H, -CH_2- ciclen), 3.31 (s, 4H, -NHCH_2CH_2NH-), 2.84 (t, 2H, *J*=7.3 Hz, -CH_2S-), 2.30 (s, 3H, SAc), 2.18 (t, 2H, *J*= 7.5 Hz, -NHCO-C$H_2$$CH_2$-), 1.60-1.50 (m, 2H, -C$H_2$$CH_2$S-), 1.44 (s, 9H, ^{t}Bu), 1.43 (s, 18H, ^{t}Bu), 1.32-1.23 (m, 14H, -CH_2-).

^{13}C NMR ($CDCl_3$, 500 MHz) δ 196.1 (1C, -S*C*OCH_3), 174.6, 172.5 and 171.9 (5C, 3 x -*C*OO-, 2 x -*C*ON-), 81.9 (3C, COO*C*(CH_3)$_3$), 55.8, 55.7 and 55.6, 39.9 and 39.2 (2C, -NH*C*H_2*C*H_2NH-), 36.3 (1C, -NHCO*C*$H_2$$CH_2$-), 30.6 (1C, -SCO*C*$H_3$), 29.4, 29.3, 29.2 (9C, -(*C*H_2)$_8$*C*H_2SAc), 28.8 and 27.9 (9C, COOC(*C*H_3)$_3$), 25.8 (1C, -NHCOCH_2*C*H_2).

MS (ESI) *m/z* 858.5 $[M+2H]^+$. Calculated MS *m/z* 856.6 [M]

2, 2', 2''-(10-(2-(2-(11-mercaptoundecanamido)ethylamino)2-oxoethyl)- 1, 4, 7, 10-tetraazacyclododecane-1, 4, 7-triyl)triacetic acid (AI167): Trifluoroacetic acid (TFA) (3.6 mL, 46.6 mmol, 200 eq.) and TIPS (0.67 mL, 3.3 mmol, 14 eq.) were added to a solution of protected DOTA-EdA/linker (200 mg, 0.23 mmol, 1 eq.) dry CH_2Cl_2 (10 mL) and it was stirred at room temperature for 60 hours. Diethylether (20 mL) was added to the mixture and it was left overnight in order to obtain a precipitate. The precipitate was clean several times with diethylether. The product was dissolved in MeOH (20 mL) and a catalytic amount of NaOMe was added. The reaction was stirred at room temperature for 20 hours under argon, concentrated and clean with a Sephadex (MeOH/H_2O 9/1). The obtained product was dissolved in water and freeze-dried (99.1 mg, 0.15 mmol, 70%).

^{1}H NMR (CD_3OD, 500 MHz) δ 3.61-3.23 (m, 4H, -NHCH_2CH_2NH-), 3.41-2.00 (bm, 24H, -CH_2-ciclen), 2.68 (t, 2H, *J*=7.2 Hz, -CH_2S-), 2.21 (t, 2H, *J*=7.5 Hz, -NHCOCH_2CH$_2$-), 1.70-165 (m, 2H, -CH_2CH$_2$S-), 1.63-1.57 (m, 2H, -NHCOCH$_2$CH_2-), 1.45-1.38 (m, 2H, -CH_2CH$_2$CH$_2$S-), 1.32 (s, 10H, -CH_2CH_2CH_2CH_2CH_2-).

^{13}C NMR (CD_3OD, 500 MHz) δ 179.4, 176.8 and 175.3 (5C, 3 x -*C*OO-, 2 x -*C*ON-), 60.8, 60.7 and 60.6, (3 x -*C*H$_2$COOH), 58.1, 40.7, 39.8, 37.3, 30.7, 30.6, 30.5, 30.4, 30.3, 30.2, 29.6, 29.4.

IR (KBr): 3439, 2926, 2847, 1596, 1403, 1321, 1093, 1014, 976, 925, 602 cm^{-1}.

MS (MALDI) *m/z* 648.1 $[M+2H]^+$. Calculated MS *m/z* 646.4 [M]

2, 2', 2''-(10-(2-(2-(5-mercaptopentanamido)ethylamino)2-oxoethyl)- 1, 4, 7, 10-tetraazacyclododecane-1, 4, 7-triyl)triacetic acid [DOTA-EdA-C_5SH (EdA=ethylene diamide)]

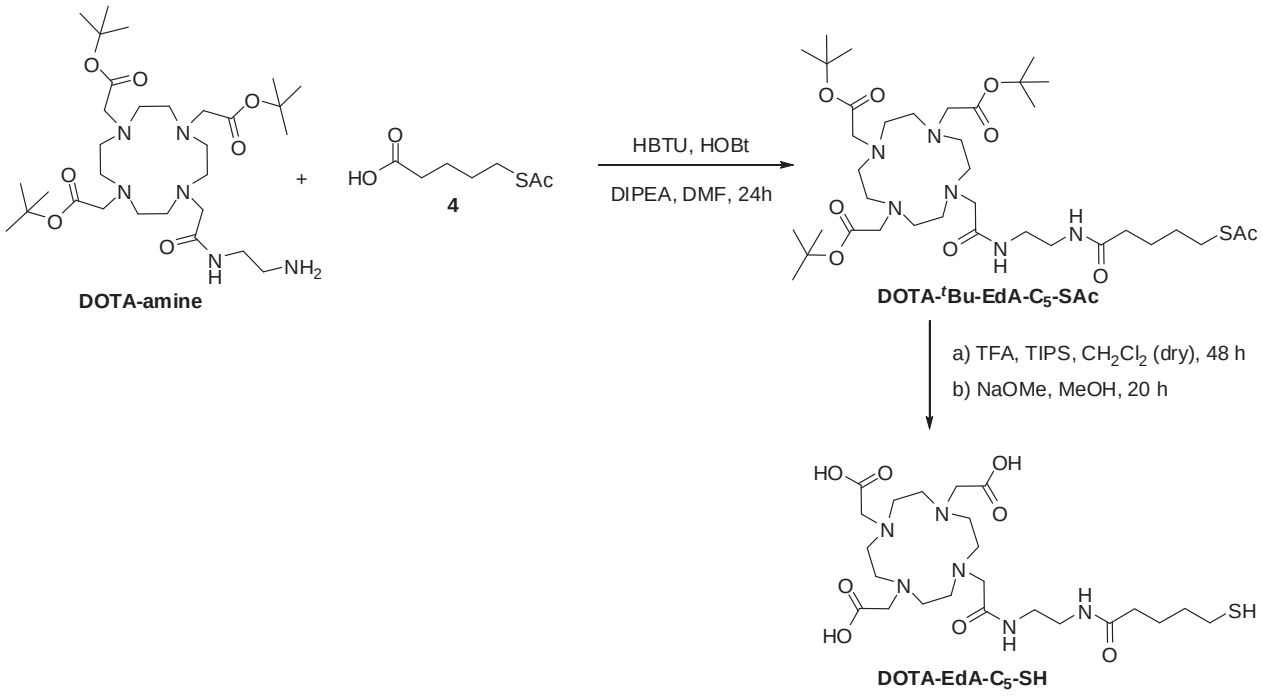

***Tert*-butil 2, 2', 2''-(10-(2-(2-(5-(acetylthio)pentanamido)ethylamino)-2-oxoethyl)-1, 4, 7, 10-tetraazacyclododecane-1, 4, 7-triyl)triacetate (AI177)**: HOBt (133 mg, 0.84 mmol, 1.5 eq.) was added to a solution of 5-(*S*-acetyl)mercaptopentanoic acid (**4**) (100 mg, 0. 56 mmol, 1 eq.) in 5 mL of DMF. After 5 minutes HBTU (319 mg, 0.84 mmol, 1.5 eq.) were added. In other flask, DIPEA (145 mg, 1.12 mmol, 2 eq.) was added to a solution of DO3A^{t}Bu-*N*-(2-aminoethyl)ethanamide (381 mg, 0.62 mmol, 1.1 eq.) in 8 mL DMF. Both mixtures were stirred

separately for 1 hour, then DO3A^{t}Bu-*N*-(2-aminoethyl)ethanamide solution was added to the acid mixture and the reaction was stirred for 24 hours. The reaction was quenched with 20 mL of AcOEt and it was extracted with NH_4Cl (4x20 mL). The organic phase was washed first with NaOH 5M (3x20 mL) and afterwards with H_2O (1x20 mL). It was dried over $MgSO_4$, filtered and concentrated. The resulting product was purified by column chromatography using a gradient of CH_2Cl_2/MeOH (from 0% to 20%) to give the corresponding DOTA-EdA-C_{11}SAc (200 mg, 0.259 mmol, 46%).

Rf =0.46 (CH_2Cl_2/MeOH 90/10).

^{1}H NMR ($CDCl_3$, 500 MHz) δ 7.07 (s, 1H, -N*H*-), 6.80 (s, 1H, -N*H*-), 3.42-3.31 (m, 4H, -NHCH_2CH_2NH-), 3.04-3.02 (m, 2H, NHCO-CH_2CH$_2$-), 2.91-2.89 (m, 2H, -CH_2SAc), 2.32 (s, 3H, SAc), 2.30-2.27 (m, 2H, HNOCH_2-), 3.62-2.00 (bm, 22H, -CH$_2$-ciclen), 1.76-1.60 (m, 4H, -CH_2CH_2S-), 1.47 (d, 27H, *J*=6.8 Hz, ^{t}Bu).

^{13}C NMR ($CDCl_3$, 500 MHz) δ 196.1 (1C, -S*C*OCH$_3$), 173.8, 172.3, 171.8 (5C, 3 x -*C*OO-, 2 x -*C*ON-), 82.1 (3C, COO*C*(CH$_3$)$_3$), 55.8, 55.7 and 55.6, 39.7 and 39.1(2C, -HN*C*H$_2$*C*H$_2$NH-), 35.6 (1C, NHCO*C*H$_2$CH$_2$-), 30.6 (1C, -SCO*C*H$_3$), 29.0 and 28.9 (2C,-*C*H$_2$*C*H2SAc), 28.1 and 27.9 (9C, COOC(*C*H$_3$)$_3$), 24.8 (HNCOCH$_2$*C*H$_2$-).

IR (KBr): 3426, 2977, 2932, 2821, 1729, 1678, 1541, 1369, 1229, 1164, 1107, 842 cm^{-1}.

MS (ESI) *m/z* 795.5 [M+Na]$^{+}$. Calculated MS *m/z* 772.5 [M]

2, 2', 2''-(10-(2-(2-(5-mercaptopentanamido)ethylamino)2-oxoethyl)- 1, 4, 7, 10-tetraazacyclododecane-1, 4, 7-triyl)triacetic acid (AI178): Trifluoroacetic acid (TFA) (3.2 mL, 41.2 mmol, 200 eq.) and TIPS (0.59 mL, 2.9 mmol, 14 eq.) were added to a solution of protected DOTA-EdA/linker (160 mg, 0.21 mmol, 1 eq.) dry CH_2Cl_2 (10 mL) and it was stirred at room temperature for 48 hours. Diethylether (20 mL) was added to the mixture and it was left overnight in order to obtain a precipitate. The precipitate was clean several times with diethylether. The product was dissolved in MeOH (20 mL) and a catalytic amount of NaOMe was added. The reaction was stirred at room temperature for 20 hours under argon, concentrated, dissolved in water and freeze-dried (99.0 mg, 0.177 mmol, 90%).

^{1}H NMR (CD_3OD, 500 MHz) δ 3.57 (s, 2H, -NHCH$_2$CH_2NH-), 3.55 (s, 2H, -NHCH_2CH$_2$NH-), 2.97-2.55 (bm, 14H, -CH$_2$-ciclen), 2.52 (m, 2H, -CH_2S-), 2.45-2.04 (m, 14H, -NHCOCH_2CH$_2$-, -CH$_2$-ciclen), 1.75-166 (m, 4H, -CH_2CH$_2$S-).

^{13}C NMR (CD_3OD, 500 MHz) δ 179.8, 175.3, 170.4 (5C, 3 x -*C*OO-, 2 x -*C*ON-), 60.6, 60.5, 60.3, (3 x -*C*H$_2$COOH), 58.1, 52.9 39.3, 39.2, 36.7, 28.9, 25.8, 25.7, 24.7.

IR (KBr): 3448, 2962, 2854, 1686, 1592, 1409, 1333, 1206, 1137, 803, 724, 610 cm^{-1}.

MS (MALDI) *m/z* 585.3 $[M+Na]^+$. Calculated MS *m/z* 562.3 [M]

Incubation of DO3AC$_x$SH and DOTA-EdA-CxSH derivatives with Gd (III)

1, 4, 7,-tris(carboxymehyl)-10-(11-mercaptoundecyl)-1, 4, 7, 10-tetraazacyclododecane-Gd (Gd-DO3AC$_{11}$SH): DO3AC$_{11}$SH derivatives was incubated with 0.9 equivalents of 0.1 M solution of $GdCl_3$ in HEPES buffer (pH=7.4).

IR (KBr): 3452, 2926, 2853, 1592, 1397 cm^{-1}

^{17}O: $q = 2.0 \pm 0.2$.

1, 4, 7,-tris(carboxymethyl)-10-(5-mercaptopentyl)-1, 4, 7, 10-tetraazacyclododecane-Gd (Gd-DO3AC$_5$SH): DO3AC$_5$SH derivatives was incubated with 0.9 equivalents of 0.1 M solution of $GdCl_3$ in HEPES buffer (pH=7.4).

IR (KBr): 3550-3250, 2928, 2853, 1588, 1397 cm^{-1}

^{17}O: $q = 2.1 \pm 0.2$.

2, 2', 2''-(10-(2-(2-(11-mercaptoundecanamido)ethylamino)2-oxoethyl)- 1, 4, 7, 10-tetraazacyclododecane-1, 4, 7-triyl)triacetic acid-Gd (Gd-DOTA-EdA-C$_{11}$SH): DOTA-EdA-C$_{11}$SH derivatives was incubated overnight at 70ºC with 0.9 equivalents of 0.1 M solution of $GdCl_3$ in HEPES buffer (pH=7.4).

IR (KBr): 3445, 2926, 2853, 1596, 1403 cm^{-1}.

^{17}O: $q \sim 1.2 \pm 0.2$.

MS (MALDI) *m/z* 1764.8 $[M+Gd^{3+}]^+$ (disulfure). Calculated MS *m/z* 1764.5 $[M+Gd^{3+}]^+$ (disulfure).

2, 2', 2''-(10-(2-(2-(5-mercaptopentanamido)ethylamino)2-oxoethyl)- 1, 4, 7, 10-tetraazacyclododecane-1, 4, 7-triyl)triacetic acid-Gd (Gd-DOTA-EdA-C$_5$SH): DOTA-EdA-C$_5$SH derivatives was incubated overnight at 70ºC with 0.9 equivalents of 0.1 M solution of $GdCl_3$ in HEPES buffer (pH=7.4).

IR (KBr): 3452, 2967, 2851, 1588, 1410 cm^{-1}.

^{17}O: $q \sim 1.1 \pm 0.2$.

MS (MALDI) *m/z* 1596. $[M+Gd^{3+}]^+$ (disulfure). Calculated MS *m/z* 1596.3 $[M+Gd^{3+}]^+$ (disulfure).

Synthesis of 100% sugar-coated glyconanoparticles

General procedure: A 0.025 M solution (1 eq.) of $HAuCl_4$ in MilliQ water was added to a 0.012 M solution (3 eq.) of the glycoconjugate. A freshly prepared 1M solution (27 eq.) of $NaBH_4$ was then added and the reaction mixtures were stirred for 2 hours in the shaker. Afterwards the supernatant was taken off. The residue was dissolved in MilliQ water and purified by dyalisis (MWCO=10000) during 4 days, then, the nanoparticles were freeze-dried.

$GlcC_2S$-Au glyconanoparticles (DAP284): A 0.012 M solution of $GlcC_2SH$ (40 mg, 0.168 mmol, 3 eq.) in MeOH (16.4 mL) was placed in 4 flasks (4.1 mL each). A 0.025 M solution of $HAuCl_4$ (9.5 mg, 0.028 mmol, 1 eq.) in MilliQ water was added to each flask (0.28 mL each). A freshly prepared 1M solution of $NaBH_4$ (28.5 mg, 0.756 mmol, 27 eq.) was then added in 4 times (189 μL in each batch) as the reaction is exothermic. The reaction mixtures were stirred for 2 hours in the shaker. The supernatant was taken off from the batches. The residue was dissolved in MilliQ water and purified by dyalisis (MWCO=10000) during 4 days. After liophilization 7.1 mg of a black solid was obtained.

TEM: 1.7 ± 0.2 nm.

IR (KBr): 3430 (broad band), 2917, 2848, 1078 cm^{-1}

UV: No surface plasmon band.

^{1}H NMR (D_2O, 500 MHz) δ 4.53 (bs, 1H, H1), 4.29-3.49 (bm, 8H, OCH_2, H2, H3, H4, H5, H6a, H6b). CH_2S not detected presumably due to gold quenching.

Elemental analysis found: C 16.94 %, H 2.93 %, S 5.74 %.

Elemental analysis calculated for: $Au_{201}(C_8H_{16}O_6S)_{121}$

C 16.93 %, H 2.84 %, S 5.65 %.

$GlcC_3S$-Au glyconanoparticles (AI099): A 0.012 M solution of $GlcC_3SH$ (50 mg, 0.197 mmol, 3 eq.) in MeOH (16.4 mL) was placed in 5 flasks (3.3 mL each). A 0.025 M solution of $HAuCl_4$ (22.26 mg, 0.066 mmol, 1 eq.) in MilliQ water was added to each flask (0.53 mL each). A freshly prepared 1M solution of $NaBH_4$ (66.92 mg, 1.77 mmol, 27 eq.) was then added in 4 times (354 μL in each batch) as the reaction is exothermic. The reaction mixture was stirred for 2 hours in the shaker. The supernatant was taken off from the batches. The residue was dissolved in MilliQ water and purified by dyalisis (MWCO=10000) during 4 days. After liophilization 9.2 mg of a black solid was obtained.

TEM: 2.1± 0.3 nm.

IR (KBr): 3401 (broad band), 2914, 2857, 1071 cm^{-1}

UV: λ= 526 nm, surface plasmon band.

^{1}H NMR (D_2O, 500 MHz) δ 4.46 (bdd, 1H, H1), 4.10-3.23 (bm, 8H, OCH_2, H2, H3, H4, H5, H6a, H6b), 2.16 (bs, -CH_2). CH_2S not detected presumably due to gold quenching.

Elemental analysis found: C 7.76 %, H 1.51 %, S 3.90 %.

Elemental analysis calculated for: $Au_{314}(C_9H_{17}O_6S)_{53}$

C 7.72%, H 1.30%, S 2.29%.

GlcC_5S-Au glyconanoparticles (AI084): A 0.012 M solution of GlcC_5SH (120 mg, 0.425 mmol, 3 eq.) in MeOH (35.4 mL) was placed in 4 flasks (8.8 mL each). A 0.025 M solution of $HAuCl_4$ (48.25 mg, 0.142 mmol, 1 eq.) in MilliQ water was added to each flask (1.42 mL each). A freshly prepared 1M solution of $NaBH_4$ (145.0 mg, 3.83 mmol, 27 eq.) was then added in 4 times (958 μL in each batch) as the reaction is exothermic. The reaction mixture was stirred for 2 hours in the orbitalical shaker. The supernatant was taken off from the batches. The residue was dissolved in MilliQ water and purified by dyalisis (MWCO=10000) during 4 days. After liophilization 23 mg of a black solid was obtained.

TEM: double distribution 1.2 ± 0.2 nm (77%) and 4.9 ± 0.6 nm (23%).

IR (KBr): 3417 (broad band), 2917, 2847, 1071 cm^{-1}

UV: λ= 525 nm, surface plasmon band.

^{1}H NMR (D_2O, 500 MHz) δ 4.44 (bsd1H, 1H), 4.00-3.24 (bm, 8H, OCH_2, H2, H3, H4, H5, H6a, H6b), 2.00-1.50 (bm, 6H, -CH_2-). CH_2S not detected presumably due to gold quenching.

Elemental analysis found: C 22.07 %, H 3.95 %, S 4.51 %.

Elemental analysis calculated for: $Au_{140}(C_{11}H_{21}O_6S)_{87}$

C 22.04 %, H 3.70 %, S 5.35 %.

GlcC_7S-Au glyconanoparticles (AI100): A 0.012 M solution of GlcC_7SH (40 mg, 0.129 mmol, 3 eq.) in MeOH (10.7 mL) was placed in 3 flasks (3.6 mL each). A 0.025 M solution of $HAuCl_4$ (14.61 mg, 0.043 mmol, 1 eq.) in MilliQ water was added to each flask (0.573 mL each). A freshly prepared 1M solution of $NaBH_4$ (43.89 mg, 1.16 mmol, 27 eq.) was then added in 4 times (387 μL in each batch) as the reaction is exothermic. The reaction mixture was stirred for 2 hours in the shaker. The supernatant was taken off from the batches. The residue was dissolved in MilliQ water and purified by dyalisis (MWCO=10000) during 4 days. After liophilization 9.5 mg of a black solid was obtained.

TEM: 1.9 ± 0.3 nm.

IR (KBr): 3433 (broad band), 2920, 2850, 1071 cm^{-1}

UV: λ= 520 nm, surface plasmon band.

^{1}H NMR (D_2O, 500 MHz) δ 4.44 (d, 1H, H1), 3.95-3.20 (bm, 8H, OCH_2, H2, H3, H4, H5, H6a, H6b), 1.78-1.23 (bm, 10H, -CH_2-). CH_2S not detected presumably due to gold quenching.

Elemental analysis found: C 23.59%, H 3.94%, S 4.95%.

Elemental analysis calculated for: $Au_{225}(C_{13}H_{25}O_6S)_{126}$

C 23.58%, H 3.96%, S 4.84%.

$GlcC_9S$-Au glyconanoparticles (AI102): A 0.012 M solution of $GlcC_9SH$ (30 mg, 0.089 mmol, 3 eq.) in MeOH (7.4 mL) was placed in 3 flasks (2.5 mL each). A 0.025 M solution of $HAuCl_4$ (10 mg, 0.029 mmol, 1 eq.) in MilliQ water was added to each flask (0.387 mL each). A freshly prepared 1M solution of $NaBH_4$ (30.17 mg, 0.80 mmol, 27eq.) was then added in 4 times (267 μL in each batch) as the reaction is exothermic. The reaction mixture was stirred for 2 hours in the shaker. The supernatant was taken off from the batches. The residue was dissolved in MilliQ water and purified by dyalisis (MWCO=10000) during 4 days. After liophilization 8.5 mg of a black solid was obtained.

TEM: 2.1 ± 0.3 nm.

IR (KBr): 3430 (broad band), 2920, 2847, 1071 cm^{-1}

UV: λ= 519 nm, surface plasmon band.

^{1}H NMR (D_2O, 500 MHz) δ 4.42 (d, 1H, H1), 3.95-3.31 (bm, 8H, OCH_2, H2, H3, H4, H5, H6a, H6b), 1.83-1.23 (bm, 12H, -CH_2-). CH_2S not detected presumably due to gold quenching.

Elemental analysis found: C 24.07 %, H 3.95%, S 4.51%.

Elemental analysis calculated for: $Au_{314}(C_{15}H_{29}O_6S)_{150}$

C 24,00 %, H 4,03 %, S 4.27 %.

$ManC_5S$-Au glyconanoparticles (AI111): A 0.012 M solution $ManC_5SH$ (40 mg, 0.142 mmol, 3 eq.) in MeOH (11.8 mL) was placed in 3 flasks (3.9 mL each). A 0.025 M solution of $HAuCl_4$ (16 mg, 0.047 mmol, 1 eq.) in MilliQ water was added to each flask (0.627 mL each). A freshly prepared 1M solution of $NaBH_4$ (48.3 mg, 1.3 mmol, 27 eq.) was then added in 4 times (433 μL in each batch) as the reaction is exothermic. The reaction mixture was stirred for 2 hours in the shaker. The supernatant was taken off from the batches. The residue was dissolved in MilliQ water and purified by dyalisis (MWCO=10000) during 4 days. After liophilization 7.8 mg of a brown solid was obtained.

TEM: 2.1 ± 0.3 nm.

IR (KBr): 3420 (broad band), 2923, 2847, 1093cm^{-1}

UV: λ= 520 nm, surface plasmon band.

^{1}H NMR (D_2O, 500 MHz) δ 3.89-3.49 (bm, 8H, OCH_2, H2, H3, H4, H5, H6a, H6b), 1.89-1.02 (bm, 6H, -CH_2-). CH_2S not detected presumably due to gold quenching. Anomemeric proton not detected due to water suppression pulse in NMR.

Elemental analysis found: C 18.82 %, H 3.17 %, S 5.20 %.

Elemental analysis calculated for: $Au_{314}(C_{11}H_{21}O_6S)_{148}$

18.87 % of C, 3.17 % of H, 4.58 % of S.

CellobioseC_5S-Au glyconanoparticles (AI112): A 0.012 M solution CellobioseC_5SH (40 mg, 0.090 mmol, 3 eq.) in MeOH (7.5 mL) was placed in 2 flasks (3.8 mL each). A 0.025 M solution of $HAuCl_4$ (10.2 mg, 0.03 mmol, 1 eq.) in MilliQ water was added to each flask (0.6 mL each). A freshly prepared 1M solution of $NaBH_4$ (30.6 mg, 0.81 mmol, 27 eq.) was then added in 4 times (405 μL in each batch) as the reaction is exothermic. The reaction mixture was stirred for 2 hours in the shaker. The supernatant was taken off from the batches. The residue was dissolved in MilliQ water and purified by dyalisis (MWCO=10000) during 4 days. After liophilization 8.0 mg of a black solid was obtained.

TEM: 2.0 ± 0.1 nm.

IR (KBr): 3420 (broad band), 2917, 2850, 1074 cm^{-1}

UV: λ= 520 nm, surface plasmon band.

^{1}H NMR (D_2O, 500 MHz) Broad signals.

Elemental analysis found: C 15.83 %, H 2.70 %, S 3.79 %.

Elemental analysis calculated for: $Au_{314}(C_{17}H_{31}O_{11}S)_{73}$

C 15.81 %, H 2.50 %, S 2.48 %.

GalC_5S-Au glyconanoparticles (AI113): A 0.012 M solution GalC_5SH (40.6 mg, 0.144 mmol, 3 eq.) in MeOH (12 mL) was placed in 3 flasks (4 mL each). A 0.025 M solution of $HAuCl_4$ (16.3 mg, 0.048 mmol, 1 eq.) in MilliQ water was added to each flask (0.640 mL each). A freshly prepared 1M solution of $NaBH_4$ (49.2 mg, 1.3 mmol, 27 eq.) was then added in 4 times (433 μL in each batch) as the reaction is exothermic. The reaction mixture was stirred for 2 hours in the shaker. The supernatant was taken off from the batches. The residue was dissolved in MilliQ water and purified by dyalisis (MWCO=10000) during 4 days. After liophilization 10.4 mg of a brown solid was obtained.

TEM: 1.8 ± 0.1 nm.

IR (KBr): 3420 (broad band), 2920, 2850, 1074 cm^{-1}

UV: No surface plasmon band.

^{1}H NMR (D_2O, 500 MHz) δ 4.40 (bd, 1H, H1), 3.95-3.54 (bm, 8H, OCH_2, H2, H3, H4, H5, H6a, H6b), 2.04-1.48 (bm, 6H, -CH_2-). CH_2S not detected presumably due to gold quenching.

Elemental analysis found: C 19.13 %, H 3.19 %, S 5.54 %.

Elemental analysis calculated for: $Au_{201}(C_{11}H_{21}O_6S)_{97}$

C 19.16 %, H 3.07 %, S 4.65 %.

LacC_5S-Au glyconanoparticles (AI114): A 0.012 M solution LacC_5SH (39.6 mg, 0.089 mmol, 3 eq.) in MeOH (7.4 mL) was placed in 2 flasks (3.7 mL each). A 0.025 M solution of $HAuCl_4$ (10.2 mg, 0.030 mmol, 1 eq.) in MilliQ water was added to each flask (0.6 mL each). A freshly prepared 1M solution of $NaBH_4$ (30.3 mg, 0.801 mmol, 27 eq.) was then added in 4 times (400 μL in each batch) as the reaction is exothermic. The reaction mixture was stirred for 2 hours in the shaker. The supernatant was taken off from the batches. The residue was dissolved in MilliQ water and purified by dyalisis (MWCO=10000) during 4 days. After liophilization 9.9 mg of a clear solid was obtained.

TEM: 2.0 ± 0.3 nm.

IR (KBr): 3404 (broad band), 2920, 2853, 1071 cm^{-1}

UV: No surface plasmon band.

^{1}H NMR (D_2O, 500 MHz) δ 4.54 (bs, 2H, H1, H1'), 4.15-3.37 (bm, 14H, OCH_2, H2', H3', H4', H5', H6'a, H6'b, H2, H3, H4, H5, H6a, H6b), 2.29-1.45 (bm, 6H, -CH_2-). CH_2S not detected presumably due to gold quenching.

Elemental analysis found: C 22.84 %, H 3.85 %, S 5.06 %.

Elemental analysis calculated for: $Au_{314}(C_{17}H_{31}O_{11}S)_{138}$

C 22.87 %, H 3.61 %, S 3.59 %.

MaltoseC_5S-Au glyconanoparticles (AI115): A 0.012 M solution MaltoseC_5SH (30 mg, 0.067 mmol, 3 eq.) in MeOH (5.6 mL) was placed in 2 flasks (2.8 mL each). A 0.025 M solution of $HAuCl_4$ (7.5 mg, 0.022 mmol, 1 eq.) in MilliQ water was added to each flask (0.44 mL each). A freshly prepared 1M solution of $NaBH_4$ (22.8 mg, 0.603 mmol, 27 eq.) was then added in 4 times (302 μL in each batch) as the reaction is exothermic. The reaction mixture was stirred for 2 hours in the shaker. The supernatant was taken off from the batches. The residue was dissolved in MilliQ water and purified by dyalisis (MWCO=10000) during 4 days. After liophilization 6.7 mg of a brown solid was obtained.

TEM: 2.1 ± 0.3 nm.

IR (KBr): 3423 (broad band), 2917, 2847, 1071 cm^{-1}

UV: λ= 520 nm, surface plasmon band.

^{1}H NMR (D_2O, 500 MHz) δ 5.45 (bs, 1H, H1'), 4.53 (bs, 1H, 1H), 4.16-3.64 (bm, 14H, OCH_2, H2', H3', H4', H5', H6'a, H6'b, H2, H3, H4, H5, H6a, H6b), 1.90-1.46 (bm, 6H, -CH_2-). CH_2S not detected presumably due to gold quenching.

Elemental analysis found: C 24.52 %, H 3.95 %, S 3.45 %.

Elemental analysis calculated for: $Au_{314}(C_{17}H_{31}O_{11}S)_{159}$

C 24.50 %, H 3.87 %, S 3.85 %.

Preparation of glyconanoparticles (GNPs) incorporating DO3A derivates by LPE

General procedure: Gold GNPs (1 eq. of the sugar) were dissolved in MilliQ water and previously prepared Gd-DO3AC_xSH solution was added (1.1 eq.). The mixture was stirred in the shaker for 44 hours at 25ºC and 180 r.p.m. in order to the exchange takes place. The solution was filtered with "*Amicon"* filters (M_w=10000 or 5000 g/mol) until NMR of the washing water showed no Gd-DO3AC_xSH. The nanoparticle was dissolved in MilliQ water and they were freeze-dried.

GlcC_2S-Au-SC_{11}DO3A-Gd glyconanoparticles (AI107): The GlcC_2S-Au glyconanoparticle (5.35 mg, 0.077 μmol, 9.52 μmol of glucose, 1 eq. of glucose) was dissolved in 5 mL of MilliQ water and previously prepared DO3AC_{11}-Gd^{3+} solution (5.1 mg, 9.57 μmol, 1.1 eq., 95.7 μL of Gd^{3+} solution) was added. After 44 hours of incubation at 25ºC, 6.84 mg of AI107 were obtained.

TEM: 1.8 ± 0.2 nm.

UV: No surface plasmon band.

IR (KBr): 3411 (broad band), 2923, 2851, 1594, 1400, 1078 cm^{-1}

^{1}H NMR (D_2O, 500 MHz) δ 4.54 (bs, 1H, H1), 4.19-3.15 (bm, 30H, -CH_2-ciclen, OCH_2, H2, H3, H4, H5, H6a, H6b), 1.71-1.30 (bm, 20H, -CH_2-).

ICP: Gd 3.38% and S 6.69%.

$Au_{201}(C_8H_{15}O_6S)_{107}(C_{25}H_{47}N_4O_6S)_{16}Gd_{16}$ (Au 51.87 %, Gd 3.30% and S 5.17 %).

r_1= 7.08 $(smM)^{-1}$

r_2= 11.01 $(smM)^{-1}$

GlcC_3S-Au-SC_{11}DO3A-Gd glyconanoparticles (AI106): The GlcC_3S-Au glyconanoparticle (4.60 mg, 0.241 μmol, 3.37 μmol of glucose, 1 eq. of glucose) was dissolved in 5 mL of MilliQ

water and previously prepared DO3AC$_{11}$-Gd^{3+} solution (2.0 mg, 3.75 μmol, 1.1 eq., 37.5 μL of Gd^{3+} solution) was added. After 44 hours of incubation at 25ºC, 4.09 mg of AI106 were obtained.

TEM: 1.9± 0.3 nm.

UV: λ= 520 nm, surface plasmon band.

IR (KBr): 3420 (broad band), 2920, 2847, 1597, 1078 cm^{-1}

^{1}H NMR (D_2O, 500 MHz) δ broad signal due to Gd ion. Unable to be assigned.

ICP: Gd 3.34% and S 5.26 %.

$Au_{314}(C_9H_{17}O_6S)_{20}(C_{25}H_{47}N_4O_6S)_{33}Gd_{33}$ (Au 74.85 %, Gd 3.14% and S 2.08 %).

r_1= 6.34 (smM)$^{-1}$

r_2= 10.52 (smM)$^{-1}$

GlcC$_5$S-Au-SC$_{11}$DO3A-Gd glyconanoparticles (AI101): The GlcC$_5$S-Au glyconanoparticle (8.15 mg, 0.310 μmol, 11.78 μmol of glucose, 1 eq. of glucose) was dissolved in 6 mL of MilliQ water and previously prepared DO3AC$_{11}$-Gd^{3+} solution (6.5 mg, 12.2 μmol, 1.1 eq., 122 μL of Gd^{3+} solution) was added. After 44 hours of incubation at 25ºC, 8.43 mg of AI101 were obtained.

TEM: double distribution 1.5 ± 0.3 nm (75%) and 4.3 ± 0.6 nm (25%).

UV: λ= 521 nm, surface plasmon band.

IR (KBr): 3443 (broad band), 2920, 2848, 1616, 1088 cm^{-1}

^{1}H NMR (D_2O, 500 MHz) δ broad signal due to Gd ion. Unable to be assigned.

ICP: Gd 4.68 % and S 6.15 %.

$Au_{140}(C_{11}H_{21}O_6S)_{70}(C_{25}H_{47}N_4O_6S)_{17}Gd_{17}$ (Au 46.70 %, Gd 4.53% and S 4.72 %).

r_1= 7.38 (smM)$^{-1}$

r_2= 11.87 (smM)$^{-1}$

GlcC$_5$S-Au-SC$_5$DO3A-Gd glyconanoparticles (AI119): The GlcC$_5$S-Au glyconanoparticle (3.87 mg, 0.185 μmol, 3.51 μmol of glucose, 1 eq. of glucose) was dissolved in 4mL of MilliQ water and previously prepared DO3AC$_5$-Gd^{3+} solution (3.0 mg, 3.79 μmol, 1.1 eq., 38.0 μL of Gd^{3+} solution) was added. After 44 hours of incubation at 25ºC, 3.3 mg of AI119 were obtained.

TEM: double distribution 2.0 ± 0.3 nm (75%) and 4.8 ± 0.5 nm (25%).

UV: λ= 514 nm, surface plasmon band.

IR (KBr): 3440 (broad band), 2917, 2848, 1616, 1081 cm^{-1}

^{1}H NMR (D_2O, 500 MHz) δ broad signal due to Gd ion. Unable to be assigned.

ICP: Gd 3.14 % and S 4.38 %.

$Au_{140}(C_{11}H_{21}O_6S)_{76}(C_{19}H_{35}N_4O_6S)_{11}Gd_{11}$ (Au 49.51 %, Gd 3.11% and S 5.01 %).

r_1= 16.9 $(smM)^{-1}$

r_2= 27.9 $(smM)^{-1}$

$GlcC_7S$-Au-$SC_{11}DO3A$-Gd glyconanoparticles (AI104): The $GlcC_7S$-Au glyconanoparticle (5.66 mg, 0.049 μmol, 8.5 μmol of glucose, 1 eq. of glucose) was dissolved in 5 mL of MilliQ water and previously prepared $DO3AC_{11}$-Gd^{3+} solution (4.9 mg, 9.2 μmol, 1.1 eq., 92.0 μL of Gd^{3+} solution) was added. After 44 hours of incubation at 25ºC, 7.40 mg of AI104 were obtained.

TEM: 1.8 ± 0.3 nm.

UV: λ= 520 nm, surface plasmon band.

IR (KBr): 3421 (broad band), 2920, 2848, 1600, 1078 cm^{-1}

^{1}H NMR (D_2O, 500 MHz) δ broad signal due to Gd ion. Unable to be assigned.

ICP: Gd 4.14 % and S 6.65 %.

$Au_{314}(C_{13}H_{25}O_6S)_{140}(C_{25}H_{47}N_4O_6S)_{34}Gd_{34}$ (Au 48.04 %, Gd 4.15% and S 4.33 %)

r_1= 7.05 $(smM)^{-1}$

r_2= 11.80 $(smM)^{-1}$

$GlcC_9S$-Au-$SC_{11}DO3A$-Gd glyconanoparticles (AI105): The $GlcC_9S$-Au glyconanoparticle (5.68 mg, 0.050 μmol, 7.6 μmol of glucose, 1 eq. of glucose) was dissolved in 5 mL of MilliQ water and previously prepared $DO3AC_{11}$-Gd^{3+} solution (4.3 mg, 8.1 μmol, 1.1 eq., 81.0 μL of Gd^{3+} solution) was added. After 44 hours of incubation at 25ºC, 7.49 mg of AI105 were obtained.

TEM: 1.8 ± 0.2 nm.

UV: λ= 519 nm, surface plasmon band.

IR (KBr): 3433 (broad band), 2917, 2848, 1625, 1078 cm^{-1}

^{1}H NMR (D_2O, 500 MHz) δ broad signal due to Gd ion. Unable to be assigned.

ICP: Gd 3.21% and S 5.81%.

$Au_{314}(C_{15}H_{29}O_6S)_{125}(C_{25}H_{47}N_4O_6S)_{25}Gd_{25}$ (Au 50.95 %, Gd 3.24% and S 3.96 %).

r_1= 7.48 $(smM)^{-1}$

r_2= 13.00 $(smM)^{-1}$

$ManC_5S$-Au-$SC_{11}DO3A$-Gd glyconanoparticles (AI116): The $ManC_5S$-Au glyconanoparticle (4.72 mg, 0.046 μmol, 6.74 μmol of mannose, 1 eq. of mannose) was dissolved in 4.2 mL of MilliQ water and previously prepared $DO3AC_{11}$-Gd^{3+} solution (4 mg, 7.5 μmol, 1.1 eq., 75.1 μL of Gd^{3+} solution) was added. After 44 hours of incubation at 25ºC, 5.44 mg of AI116 were obtained.

TEM: 2.4 ± 0.4 nm.

UV: λ= 520 nm, surface plasmon band.

IR (KBr): 3417 (braod band), 2920, 2848, 1594, 1401, 1087 cm^{-1}

^{1}H NMR (D_2O, 500 MHz) δ broad signal due to Gd ion. Unable to be assigned.

ICP: Gd 3.0 % and S 5.46 %.

$Au_{314}(C_{11}H_{21}O_6S)_{127}(C_{25}H_{47}N_4O_6S)_{21}Gd_{21}$ (Au 55.13 % , Gd 2.94% and S 4.23 %).

r_1= 9.7 $(smM)^{-1}$

r_2= 16.5 $(smM)^{-1}$

$ManC_5S$-Au-SC_5DO3A-Gd glyconanoparticles (AI120): The $ManC_5S$-Au glyconanoparticle (2.07 mg, 0.0199 μmol, 2.96 μmol of mannose, 1 eq. of mannose) was dissolved in 3.0 mL of MilliQ water and previously prepared $DO3AC_5$-Gd^{3+} solution (2.5 mg, 3.2 μmol, 1.1 eq., 31.6 μL of Gd^{3+} solution) was added. After 44 hours of incubation at 25ºC, 3.60 mg of AI120 were obtained.

TEM: 1.8 ± 0.2 nm.

UV: λ= 520 nm, surface plasmon band.

IR (KBr): 3421 (broad band), 2927, 2851, 1594, 1401, 1087 cm^{-1}

^{1}H NMR (D_2O, 500 MHz) δ broad signal due to Gd ion. Unable to be assigned.

ICP: Gd 4.06 % and S 5.23 %.

$Au_{314}(C_{11}H_{21}O_6S)_{119}(C_{19}H_{35}N_4O_6S)_{29}Gd_{29}$ (Au 54.72 %, Gd 4.04% and S 4.20 %).

r_1= 15.5 $(smM)^{-1}$

r_2= 25.9 $(smM)^{-1}$

$CellobioseC_5S$-Au-$SC_{11}DO3A$-Gd glyconanoparticles (AI117): The $CellobioseC_5S$-Au glyconanoparticle (5.53 mg, 0.131 μmol, 4.32 μmol of cellobiose, 1 eq. of cellobiose) was dissolved in 4.5 mL of MilliQ water and previously prepared $DO3AC_{11}$-Gd^{3+} solution (2.3 mg, 7.5 μmol, 1.1 eq., 43.17 μL of Gd^{3+} solution) was added. After 44 hours of incubation at 25ºC, 5.84 mg of AI117 were obtained.

TEM: 1.8 ± 0.2 nm.

UV: λ= 520 nm, surface plasmon band.

IR (KBr): 3421 (broad band), 2924, 2848, 1622, 1074 cm^{-1}

^{1}H NMR (D_2O, 500 MHz) δ broad signal due to Gd ion. Unable to be assigned.

ICP: Gd 2.12 % and S 4.60 %.

$Au_{314}(C_{17}H_{31}O_6S)_{61}(C_{25}H_{47}N_4O_6S)_{12}Gd_{12}$ (Au 67.97%, Gd 2.04% and S 2.53%).

$\mathbf{r_1}$= 11.2 $(smM)^{-1}$

$\mathbf{r_2}$= 21.3 $(smM)^{-1}$

CellobioseC$_5$S-Au-SC$_5$DO3A-Gd glyconanoparticles (AI125): The CellobioseC$_5$S-Au glyconanoparticle (1.03 mg, 0.024 μmol, 0.781 μmol of cellobiose, 1 eq. of cellobiose) was dissolved in 2 mL of MilliQ water and previously prepared DO3AC$_5$-Gd^{3+} solution (1 mg, 1.27 μmol, 1.1 eq., 12.65 μL of Gd^{3+} solution) was added. After 44 hours of incubation at 25ºC, 3.60 mg of AI125 were obtained.

TEM: 2.0 ± 0.1 nm.

UV: λ= 520 nm, surface plasmon band.

IR (KBr): 3436 (braod band), 2917, 2848, 1622, 1078 cm^{-1}

^{1}H NMR (D$_2$O, 500 MHz) δ broad signal due to Gd ion. Unable to be assigned.

ICP: Gd 2.10 % and S 3.73 %.

$Au_{314}(C_{17}H_{31}O_6S)_{61}(C_{19}H_{35}N_4O_6S)_{12}Gd_{12}$ (Au 67.70%, Gd 2.07% and S 2.56%).

$\mathbf{r_1}$= 16.6 $(smM)^{-1}$

$\mathbf{r_2}$= 30.7 $(smM)^{-1}$

GalC$_5$S-Au-SC$_{11}$DO3A-Gd glyconanoparticles (AI118): The GalC$_5$S-Au glyconanoparticle (4.86 mg, 0.046 μmol, 7.05 μmol of galactose, 1 eq. of galactose) was dissolved in 4.2 mL of MilliQ water and previously prepared DO3AC$_{11}$-Gd^{3+} solution (4.1 mg , 7.7 μmol, 1.1 eq., 77.0 μL of Gd^{3+} solution) was added. After 44 hours of incubation at 25ºC, 4.15 mg of AI118 were obtained.

TEM: 1.7 ± 0.1 nm.

UV: No surface plasmon band.

IR (KBr): 3436 (broad band), 2924, 2851, 1594, 1401, 1084 cm^{-1}

^{1}H NMR (D$_2$O, 500 MHz) δ broad signal due to Gd ion. Unable to be assigned.

ICP: Gd 4.18 % and S 5.95 %.

$Au_{201}(C_{11}H_{21}O_6S)_{77}(C_{25}H_{47}N_4O_6S)_{20}Gd_{20}$ (Au 52.76 %, Gd 4.19 % and S 4.15 %).

$\mathbf{r_1}$= 8.0 $(smM)^{-1}$

$\mathbf{r_2}$= 12.9 $(smM)^{-1}$

GalC$_5$S-Au-SC$_5$DO3A-Gd glyconanoparticles (AI121): The GalC$_5$S-Au glyconanoparticle (3.26 mg, 0.031 μmol, 4.3 μmol of galactose, 1 eq. of galactose) was dissolved in 3 mL of MilliQ water and previously prepared DO3AC$_5$-Gd^{3+} solution (3.5 mg, 0.44 μmol, 1.1 eq., 44.3 μL of Gd^{3+} solution) was added. After 44 hours of incubation at 25ºC, 3.14 mg of AI121 were obtained.

TEM: 1.7 ± 0.2 nm.

UV: No surface plasmon band.

IR (KBr): 3430 (broad band), 2917, 2851, 1625, 1410, 1081 cm^{-1}

^{1}H NMR (D_2O, 500 MHz) δ broad signal due to Gd ion. Unable to be assigned.

ICP: Gd 3.62 % and S 5.33 %.

$Au_{201}(C_{11}H2_1O_6S)_{80}(C_{19}H_{35}N_4O_6S)_{17}Gd_{17}$ (Au 54.70 %, Gd 3.69 % and S 4.30 %).

r_1= 18.0 $(smM)^{-1}$

r_2= 30.6 $(smM)^{-1}$

LacC_5S-Au-SC_{11}DO3A-Gd glyconanoparticles (AI123): The LacC_5S-Au glyconanoparticle (4.41 mg, 0.032 μmol, 4.94 μmol of lactose, 1 eq. of lactose) was dissolved in 4.0 mL of MilliQ water and previously prepared DO3AC_{11}-Gd^{3+} solution (2.8 mg, 5.3 μmol, 1.1 eq., 52.6 μL of Gd^{3+} solution) was added. After 44 hours of incubation at 25ºC, 4.97 mg of AI123 were obtained.

TEM: 1.7 ± 0.3 nm.

UV: No surface plasmon band.

IR (KBr): 3424 (broad band), 2924, 2851, 1606, 1397, 1081 cm^{-1}

^{1}H NMR (D_2O, 500 MHz) δ broad signal due to Gd ion. Unable to be assigned.

ICP: Gd 2.69 % and S 5.68 %.

$Au_{314}(C_{17}H_{31}O_{11}S)_{116}(C_{25}H_{47}N_4O_6S)_{22}Gd_{22}$ (Au 48.11 %, Gd 2.69 % and S 3.44 %).

r_1= 9.6 $(smM)^{-1}$

r_2= 16.0 $(smM)^{-1}$

LacC_5S-Au-SC_5DO3A-Gd glyconanoparticles (AI126): The LacC_5S-Au glyconanoparticle (2.8 mg, 0.023 μmol, 3.14 μmol of lactose, 1 eq. of lactose) was dissolved in 3.0 mL of MilliQ water and previously prepared DO3AC_{11}-Gd^{3+} solution (3 mg, 3.8 μmol, 1.1 eq., 38.0 μL of Gd^{3+} solution) was added. After 44 hours of incubation at 25ºC, 2.2 mg of AI126 were obtained.

TEM: 1.6 ± 0.2 nm.

UV: No surface plasmon band.

IR (KBr): 3417 (broad band), 2924, 2848, 1606, 1397, 1078 cm^{-1}

^{1}H NMR (D_2O, 500 MHz) δ broad signal due to Gd ion. Unable to be assigned.

ICP: Gd 3.69 % and S 5.87 %.

$Au_{314}(C_{17}H_{31}O_{11}S)_{108}(C_{19}H_{35}N_4O_6S)_{30}Gd_{30}$ (Au 48.31 %, Gd 3.68 % and S 3.46 %).

r_1= 17.0 $(smM)^{-1}$

r_2= 29.5 $(smM)^{-1}$

MaltoseC_5S-Au-SC_{11}DO3A-Gd glyconanoparticles (AI124): The MaltoseC_5S-Au glyconanoparticle (3.22 mg, 0.024 μmol, 3.86 μmol of maltose, 1 eq. of maltose) was dissolved in 4.0 mL of MilliQ water and previously prepared DO3AC_{11}-Gd^{3+} solution (2.2 mg, 4.1 μmol, 1.1 eq., 41.3 μL of Gd^{3+} solution) was added. After 44 hours of incubation at 25ºC, 3.94 mg of AI124 were obtained.

TEM: 1.8 ± 0.2 nm.

UV: λ= 520 nm, surface plasmon band.

IR (KBr): 3430 (broad band), 2920, 2848, 1638, 1078 cm^{-1}

^{1}H NMR (D_2O, 500 MHz) δ broad signal due to Gd ion. Unable to be assigned.

ICP: Gd 3.05 % and S 4.23 %.

$Au_{314}(C_{17}H_{31}O_{11}S)_{131}(C_{25}H_{47}N_4O_6S)_{28}Gd_{28}$ (Au 44.38 %, Gd 3.16 % and S 3.66 %).

r_1= 12.8 $(smM)^{-1}$

r_2= 21.4 $(smM)^{-1}$

MaltoseC_5S-Au-SC_5DO3A-Gd glyconanoparticles (AI127): The MaltoseC_5S-Au glyconanoparticle (1.0 mg, 0.0128 μmol, 2.04 μmol of maltose, 1 eq. of mannose) was dissolved in 3.0 mL of MilliQ water and previously prepared DO3AC_5-Gd^{3+} solution (2.0 mg, 2.5 μmol, 1.1 eq., 25.3 μL of Gd^{3+} solution) was added. After 44 hours of incubation at 25 ºC, 1.77 mg of AI127 were obtained.

TEM: 1.8 ± 0.2 nm.

UV: λ= 520 nm, surface plasmon band.

IR (KBr): 3430 (broad band), 2917, 2848, 1638, 1074 cm^{-1}

^{1}H NMR (D_2O, 500 MHz) δ broad signal due to Gd ion. Unable to be assigned.

ICP: Gd 3.59 % and S 4.22 %.

$Au_{314}(C_{17}H_{31}O_{11}S)_{127}(C_{19}H_{35}N_4O_6S)_{32}Gd_{32}$ (Au 44.92 %, Gd 3.65 % and S 3.70 %).

r_1= 14.7 $(smM)^{-1}$

r_2= 25.7 $(smM)^{-1}$

T_1 measurements. Longitudinal relaxation time (T_1) of the paramagnetic GNPs was measured at different concentrations. The corresponding relaxivity values r_1 were calculated from the slopes of the curves $1/T_1$ vs the concentration of Gd (III) expressed in mM.

Water proton NMR relaxation time T_1 (longitudinal) of nanoparticle solutions (10, 5, 2.5, 1.25, 0.625 mg/mL) in MilliQ water, were measured at 37 ºC and 1.41 Tesla in a Bruker Minispec (MQ60) TD-NMR spectrometer. The values of T_1 were determined using the inversion-recovery method. 300 μL of the solutions were used for each determination and the fitting of the T_1 curve was done using an exponential decay. Three different measurements of T_1 were performed in every sample for statistical correction. Relaxivity r_1 was obtained from the slopes of the curves $1/T_1$ vs the concentration of Gd (III) expressed in mM. The commercial MRI contrast agent Dotarem® was used as a reference.

MRI phantoms. T_1 measurements, at different concentrations of Gd(III) (0, 5, 50, 100 and 200 μM), were performed in a Bruker Biospec at 11.7 teslas using a 72mm volumetric quadrature coil at room temperature. Saturation recovery pulse sequence with static TE (11ms) and variable TR (300, 650, 730, 1100, 1500, 2100, 2800, 3800, 5500, 12500 ms) values. Imaging parameters were as follows: field of view (FOV) = 34 x 34 mm2, matrix size (MTX) = 320 x 320, slice thickness (ST) = 0.5 mm, and averages (NEX) = 1. T_1 analysis was carried out using the image sequence analysis tool in Paravision 5 software (Bruker BioSpin, Ettlingen, Germany) with monoexponential curve-fitting of image intensities of selected regions of interest (ROIs). Spin lattice relaxation times (T_1) were measured using a Gradient Echo Sequence with 400 ms repetition time and 4.7 ms echo time.

^{17}O NMR experiments. The number of water molecules directly coordinated to the Gd(III) ion (q) was determined by measurement of Gd(III)-induced shifts of the water ^{17}O NMR resonance similarly to the procedure reported by Djanashvili and Peters.[29]

^{17}O NMR spectra were recorded at natural abundance in D_2O as the solvent on a Bruker Avance-500 spectrometer at 67.80 MHz. All samples were placed in 3 mm tubes with a total volume of 180 μL. Experiments were performed at 60ºC using 0.06 s acquisition time, 0.2 s acquisition delay and 512 scan averages in a Bruker broadband inverse probe. ^{17}O chemical shift was obtained from peak position.

^{1}H NMRD spectroscopy. The measurements were performed using a Stelar SmarTRACER relaxometer (0.01-80 MHz; $5x10^{-4}$-1.9 T) and a Bruker 2 T electromagnet. Pre-Polarize sequence and Fast Field Cycling (FFC) were used for low fields (0.01-3 MHz), No-Polarized sequence and FFC for half fields (3-10 MHz) and Saturation Recovery sequence and fixed magnetic field for

[29] K. Djanashvili and J. A. Peters, *Contrast Med. Mol. Imaging*, 2007, **2**, 67.

high fields (20-80 MHz). Longitudinal ^{1}H relaxation rates were measured for $GlcC_5S$-Au-SC_{11}DO3A-Gd and Dotarem® (DOTA-Gd) at 0.7 mM and 37 ºC.

Zeta Potential Measurements. The zeta potential (ζ) of $GlcC_5S$-Au-SC_{11}DO3A-Gd GNP was directly determined using a Malvern Zetasizer Nano ZS from Malvern Instruments. Three different solutions in HEPES (0.01 M) of 150 μg/mL of GNP at pH 4.4, 7.4 or 8.4 were placed in a folded capillary cell. Five replicates were measured for each sample, and the average value was reported as the ζ value.

CHAPTER 2

APPLICATION OF PARAMAGNETIC Gd-BASED GOLD GLYCONANOPARTICLES FOR THE SELECTIVE LABELLING OF CELL SURFACE RECEPTORS BY MAGNETIC RESONANCE IMAGING (MRI)

APPLICATION OF PARAMAGNETIC Gd-BASED GOLD GLYCONANOPARTICLES FOR THE SELECTIVE LABELLING OF CELL SURFACE RECEPTORS BY MAGNETIC RESONANCE IMAGING (MRI)

Molecular imaging of cells is giving an outstanding contribution to the non-invasive evaluation of bio- or pathological processes in living organisms by tracking the survival, migration, and differentiation of cells *in vivo*. The visualization of specific targets by cellular imaging requires markers capable to select different types of cells of interest at particular locations. The detection of these markers by positron emission tomography (PET) and magnetic resonance imaging (MRI) needs contrast agents that contain either detectable radioactive elements or magnetic metals. [1] High spatial resolution (>10 times higher than PET), excellent soft tissue contrast and non-invasiveness make MRI an attractive tool for cellular imaging. Cellular-level resolution in the absence of contrast agents often involves very high field MRI scanners, specialized coils, small field of view (FOV), and long acquisition times which are impractical technical requirements for cell tracking. The labelling of living cells with contrast agents has to ensure sufficient MR contrast agent uptake and the absence of intracellular aggregation and precipitation, adverse effects on cell proliferation, differentiation and migration, and cell toxicity. [2], [3] [4]

Iron oxide nanoparticles are the most extensively applied contrast agent in cell imaging and tracking studies due to their strong negative contrast effect, biocompatibility and variety in core size and coating surface. [4] It has been demonstrated that micrometer-sized particles of iron oxide (MPIOs) can be detected in agarose samples, in cultured cells, and even in mouse embryos by MRI and the resolution can be pushed up to single microparticles. Experiments studying the effect of particle size from 0.76 to 1.63 μm on MRI resolution, indicated that T_2* effects could be detected for single MPIOs at 50-μm resolution. [5]

Recent developments in engineered nanoparticles allow further possibilities for cell tracking. MR imaging is not specific to particular cells and the incorporation of functional groups to cross-linked iron oxide nanoparticles (CLIO) enables the coupling of a wide variety of specific

[1] M. M. J. Modo and J. W. M. Bulte, "Molecular and Cellular MR Imaging", ed. M. M. J. Modo and J. W. M. Bulte, CRC Press, Taylor & Francis Group, New York, **2007**.
[2] A.S. Arbab, L.A. Bashaw, B.R. Miller, E.K. Jordan, B.K. Lewis, H. Kalish and J.A. Frank, *Radiology*, **2003**, 229, 838–846 (Characterization of Biophysical and Metabolic Properties of Cells Labeled with Superparamagnetic Iron Oxide Nanoparticles and Transfection Agent for Cellular MR Imaging).
[3] L. Kostura, D.L. Kraitchman, A.M. Mackay, M.F. Pittenger and J.W. Bulte, *NMR Biomed*. **2004,** 17, 513–517 (Feridex labeling of mesenchymal stem cells inhibits chondrogenesis but not adipogenesis or osteogenesis).
[4] N. Muja and J.W.M. Bulte*, Progress in Nuclear Magnetic Resonance Spectroscopy*, **2009**, 55, 61–77 (Magnetic resonance imaging of cells in experimental disease models).
[5] E.M. Shapiro, S. Skrtic, K. Sharer, J.M. Hill, C.E. Dunbar and A.P. Koretsky, *PNAS*, **2004**, 101, 10901-10906 (MRI detection of single particles for cellular imaging).

molecules that increase the functionality and specificity of the nanoparticles. Tat peptide-functionalized superparamagnetic iron oxide nanoparticles with a PEG-modified phospholipid micelle coating were efficiently delivered into living cells. [6] Iron oxide conjugated to Tat peptide was previously used by Weissleder and co-workers for intracellular magnetic labelling. [7] Johansson *et al.* designed arginine–glycine–aspartate (RGD) labelled ultrasmall superparamagnetic iron oxide nanoparticles (USPIO) to visualize thrombus *in vitro* and *in vivo*. [8]

The common strategy for *in vivo* labelling and tracking of cells by MRI consists on *ex vivo* incubation of living cells with the contrast agents and transplantation of the labelled cell into the live animal. [9], [10] Because of the intrinsic difficulty of visualizing specifically labelled cells *in vivo*, examples of direct intravenous (i. v.) injection with iron oxide nanoparticles for imaging cell types are limited to cells that can phagocytose or endocytose the contrast agent. [11], [12] *In vivo* labelling and tracking of neural progenitor cells have been performed by directly stereotactic injection of iron oxide particles into lateral ventricles. [13], [14], [15], [16], [17]

---

[6] N. Nitin, L.E. LaConte, O. Zurkiya, X. Hu, G. Bao, *J. Biol. Inorg. Chem*., **2004**, 9, 706–712 (Functionalization and peptide-based delivery of magnetic nanoparticles as an intracellular MRI contrast agent).

[7] L. Josephson, C. H. Tung, A. Moore, and R. Weissleder, *Bioconjug Chem*, **1999**, 10, 186–191, (High-efficiency intracellular magnetic labeling with novel superparamagnetic-Tat peptide conjugates).

[8] L.O Johansson, A. Blomerud, H.K. Ahlstrom, D.L. Ladd and D.K. Fujii, *J. Magn. Reson. Imaging*, **2001**, 134, 615 (A targeted contrast agent for magnetic resonance imaging of thrombus, implications of spatial resolution).

[9] S. G. Crich, L.Biancone, V. Cantaluppi, D. Duò, G. Esposito, S. Russo, G. Camussi, and S. Aime, *Magnetic Resonance in Medicine*, **2004**, 51, 938–944 (Improved Route for the Visualization of Stem Cells Labeled With a Gd-/Eu-Chelate as Dual (MRI and Fluorescence) Agent).

[10] L.Biancone, S. G. Crich, V. Cantaluppi, G. M. Romanazzi, S. Russo, E. Scalabrino, G. Esposito, F. Figliolini, S. Beltramo, P. C. Perin, G. P. Segoloni, S. Aime and G. Camussi, *NMR Biomed*. **2007**, 20, 40–48 (Magnetic resonance imaging of gadolinium-labeled pancreatic islets for experimental transplantation).

[11] Y. Zahng, S. J. Dodd, K. S. Hendrich, M. Williams and C. Ho, *Kidney Ind.*, **2000**, 58, 1300-1310 (Magnetic resonance imaging detection of rat renal transplant rejaction by monitoring macrophages infiltration).

[12] Y. L. Wu, Q. Ye, L. M. Foley, T. K. Hitches, K. Sato, J. B. Williams and C. Ho, *Proc. Nat. Acad, Sci. USA,* **2006**, 113, 1852-1857 (*In situ* labeling of immune cells with iron oxide particles: an approach to detect organ rejection by cellular MRI).

[13] R. A. Panizzo, P. G. Kyrtatos , A. N. Price, *et al.*, *Neuroimage*, **2009**, 44, 1239-1246 (*In vivo* magnetic resonance imaging of endogenous neuroblasts labelled with ferumoxide-polycation complex).

[14] E. M. Shapiro, O. Gonzalez-Perez, J. M. Garcia-Verdugo, *et al.*, *Neuroimage*, **2006**, 32, 1150-1157 (Magnetic resonante Imaging of the migration of neuronal precursors generated in the adult rodent brain).

[15] J. P. Summer, E. M. Shapiro, D. Maric, *et al., Neuroimage,* **2009**, 44, 671-678 (*In vivo* labelling of adult neural progenitors for MRI with micron size particles of iron oxide: quantification of labelled cell phenotype).

[16] R. Vreys, G. Vande Velde, O. Krylychkina, *et al., Neuroimage,* **2010**, 49, 2094-2103 (MRI visualiztion of endogenous neural progenitor cell migration along the RMS in the adult mouse brain: validation of various MPIO labelling strategies).

[17] B. J. Nieman, J. Y. Shyu, J. J. Rodriguez, *et al., Neuroimage,* **2010**, 50, 456-464 (*In vivo* MRI of neural cell migration dynamics in the Mouse brain).

Gd(III)-based contrast agents are also promising in cell tracking and fate-mapping experiments. [18] However, the relatively low T_1 contrast effects and the reduced relaxivity at high magnetic fields are the main reasons why only few examples of Gd-based MR probes for cell labelling have been reported in spite of the advantages of T_1-weigthed images (positive contrast, short acquisition times, and wide use in the clinic). [4] Other major shortcomings for labelling cells with Gd-based contrast agents are their low intracellular labelling efficiency and their reduced contrast signal once internalized by cells. Targeted Gd-based contrast agents have also been reported in order to obtain high local concentrations of the imaging probe at particular site which will enhance the sensitivity. However, the delivery of targeted contrast agents *in vivo* presents also critical problems. [19]

Due to these difficulties, some cell tracking studies with these typically T_1-contrast agents had to rely on T^*_2 (negative contrast). [20] In this sense, the most recently described advance is the development of Gadofluorine M, an amphiphilic gadolinium-based contrast agent that can be readily incorporated into mesenchymal stem cells [21], glioma cells [22], and macrophages [23] without the use of transfection agents.

Gold nanoparticles are appealing scaffolds due to the opportunity of easy (bio)conjugation of Gd-chelates on metal surface in combination with other molecules. The synthesis of gold nanoparticles capped with a Gd-based contrast agent has been developed aiming at increasing the relaxivity values. By attaching thiol-derivatized Gd(III) chelates on gold nanoclusters, relaxivities ranging from 3 to 60 $mM^{-1}s^{-1}$ per Gd(III) have been obtained. [24], [25], [26], [27], [28], [29], [30], [31]

---

[18] S. Aime, C. Cabella, S. Colombatto, S. Geninatti Crich, E. Gianolio and F. Maggioni, *J. Magn. Res. Imag.* **2002**, 16, 394–406 (Insights into the Use of Paramagnetic Gd(III) Complexes in MR-Molecular Imaging Investigations)

[19] D. Artemov *J. Cell. Biochem.* **2003**, 90, 518-524 (Molecular Magnetic Resonance Imaging with Targeted Contrast Agents)

[20] M. Modo, D. Cash, K. Mellodew, S.C. Williams, S.E. Fraser, T.J. Meade, J. Price, H. Hodges, *Neuroimage* **2002**, 17, 803–811 (Tracking of transplanted stem cells by magnetic resonance microscopy in rats with global ischaemic brain damage).

[21] F.L. Giesel, M. Stroick, M. Griebe, H. Troster, C.W. von der Lieth, M. Requardt, M. Rius, M. Essig, H.U. Kauczor, M.G. Hennerici, M. Fatar, *Invest. Radiol*. **2006**, 41, 868–873 (Gadofluorine m uptake in stem cells as a new magnetic resonance imaging tracking method: an in vitro and in vivo study).

[22] I.S. Nolte, S. Gungor, R. Erber, E. Plaxina, J. Scharf, B. Misselwitz, L. Gerigk, H. Przybilla, C. Groden, M.A. Brockmann, *Magn. Reson. Med*. **2008**, 59, 1014–1020 (In vitro labeling of glioma cells with gadofluorine M enhances T_1 visibility without affecting glioma cell growth or motility).

[23] T.D. Henning, O. Saborowski, D. Golovko, S. Boddington, J.S. Bauer, Y. Fu, R. Meier, H. Pietsch, B. Sennino, D.M. McDonald, H.E. Daldrup-Link, *Eur. Radiol*. **2007**, 17, 1226–1234 (Cell labeling with the positive MR contrast agent Gadofluorine M).

[24] J.-L. Bridot, A.-C. Faure, S. Laurent, C. Rivière, C. Billotey, B. Hiba, M. Janier, V. Josserand, J.-L. Coll, L. V. Elst, R. Muller, S. Roux, P. Perriat and O. Tillement, *J. Am. Chem. Soc.* **2007**, 129, 5076-5084 (Hybrid gadolinium oxide nanoparticles: Multimodal contrast agents for in vivo imaging).

Targeted Gd-based gold nanoparticles have also been prepared for *in vivo* and /or cellular MRI. Highly specific targeted recognition and binding is provided by monoclonal antibodies. Chung and co-workers to selectively target breast cancer cells combining MRI and phototherapy used gold nanoparticles functionalized with anti-HER2 antibodies chemically conjugated to DTPA-Gd. [32] Gd(III)-labeled gold nanoparticles with covalently attached oligonucleotides [30] or biotin [31] have recently been reported as targeted MRI contrast agents. Mirkin and Meade prepared Gd-containing oligonucleotide-gold nanoparticles (13 nm 16.9 mM^{-1} s^{-1} at 1.41 T, down to 5.1 mM^{-1} s^{-1} at 14.1 T) that could penetrate cells and accumulate to allow successful cellular MR imaging at high fields with low micromolar Gd(III) concentration. [30] These nanoparticles were able to increase ~50-fold the cell uptake compared to the clinical contrast agent Dotarem® (DOTA–Gd).

Peptides, proteins, and antibodies are the most frequently molecules used to get targeted contrast agents. [19] On the contrary, carbohydrates have been scarcely applied to obtain targeted probes in spite of the great information they encode (so-called glyco-code). [33] Glycans conjugated to small paramagnetic molecules have been already used as new targeted imaging probes, [34] including responsive agents to glycosidase enzyme. [35] Also Gd-loaded macromolecules and iron oxide nanoparticles have been conjugated to sugars to confer them targeting properties. Dendrimeric-type conjugates of gadolinium complexes displaying multiple copies of galactosyl

---

[25] P.-J. Debouttière, S. Roux, F. Vocanson, C. Billotey, O. Beuf, A. Favre-Réguillon, Y. Lin, S. Pellet-Rostaing, R. Lamartine, P. Perriat and O. Tillement, *Adv. Funct. Mater.* **2006**, 16, 2330-2339 (Design of gold nanoparticles for magnetic resonance imaging)

[26] L. Frullano and T. J. Meade, *J. Biol. Inorg. Chem.* **2007**, 12, 939-949 (Multimodal MRI contrast agents)

[27] C.-P. Tsai, Y. Hung, Y.-H. Chou, D.-M. Huang, J.-K. Hsiao, C. Chang, Y.-C. Chen and C.-Y. Mou, *Small,* **2008**, 4, 186-191 (High-contrast paramagnetic fluorescent mesoporous silica nanorods as a multifunctional cell-imaging probe)

[28] J.-A. Park, H.-K. Kim, J.-H. Kim, S.-W. Jeong, J.-C. Jung, G.-H. Lee, J. Lee, Y. Chang, T.-J. Kim, *Bioorg. Med. Chem. Lett.* **2010**, 20, 2287–2291 (Gold nanoparticles functionalized by gadolinium–DTPA conjugate of cysteine as a multimodal bioimaging agent)

[29] L. Moriggi, C. Cannizzo, E. Dumas, C. R. Mayer, A. Ulianov and L. Helm, *J. Am. Chem. Soc.* **2009**, 131, 10828-10829(Gold Nanoparticles Functionalized with Gadolinium Chelates as High-Relaxivity MRI Contrast Agents).

[30] Y. Song, X. Xu, K.W. MacRenaris, X.Q. Zhang, C.A. Mirkin and T.J. Meade, *Angew. Chem. Int. Ed.* **2009**, 48, 9143-9147 (Multimodal Gadolinium-Enriched DNA–Gold Nanoparticle Conjugates for Cellular Imaging)

[31] M. F. Warsi, R. W. Adams, S. B. Duckett and V. Chechik, **2010**, 46, 451-453 (Gd-functionalised Au nanoparticles as targeted contrast agents in MRI: relaxivity enhancement by polyelectrolyte coating)

[32] Y. T. Lim, M. Y. Cho, B. S. Choi, J. M. Lee and B. H. Chung, *Chem. Commun*. **2008**, 4930–4932 (Paramagnetic gold nanostructures for dual modal bioimaging and phototherapy of cancer cells)

[33] H.-J. Gabius, H.-C. Siebert, S. Andry, J. Jiménez-Barbero, and H. Rüdiger, *ChemBioChem* **2004,** 5, 740-764 (Chemical Biology of the Sugar Code)

[34] L. Cipolla, M. Gregori and P.-W. So, *Curr. Med. Chem.* **2011**, 18, 1002-1018 (Glycans in Magnetic Resonance Imaging: Determinants of Relaxivity to Smart Agents, and Potential Applications in Biomedicine).

[35] A.Y. Louie, M.M. Hüber,, E.T. Ahrens, U. Rothbächer, R. Moats, R.E. Jacobs, S.E. Fraser and T. J. Meade, *Nat. Biotech.* **2000**, 18, 321-25 *(In vivo* visualization of gene expression using magnetic resonance imaging).

residues for selectively targeting endogenous lectins such as the asialoglycoprotein receptor [36], [37] have been proposed. [38], [39], [40], [41] The targeting properties of simple sugars have been also used by Huang *et al*. to prepare superparamagnetic iron oxide glyconanoparticles (T_2 agents) as MRI probes to detect and differentiate cancer cells based on the different expression of carbohydrate receptors at cell surface. [42] [43]

In this Thesis, we have profited from the great information contained in carbohydrates to prepare Gd-based gold nanoclusters as contrast agents for targeting and labelling cells. Even the simplest saccharide (glucose, mannose, galactose, glucosamine or fucose) contains a wealth of information for target cellular receptors (lectins). Furthermore, carbohydrates are highly hydrophilic and usually non-immunogenic assuring both biocompatibility and water solubility to the imaging probe which may avoid subsequent clearance *in vivo* by macrophages and increase proton density around the paramagnetic metal ion, respectively. Monomeric carbohydrates bind specifically to their receptors (lectins) [44] with low affinity (millimolar range), but the avidity for the receptors highly increases when carbohydrates are clustered. [45] The multivalent presentation of the sugars onto the gold surface is a way to achieve a strong interaction with the receptor.

The combination of multivalent glycoconjugates and paramagnetic complexes on a very same gold nanocluster is the strategy we have chosen to target cellular lectins with high avidity and to reach high sensitivity in MRI. The paramagnetic Gd-based gold glyconanoparticles presented in Chapter 1, which can work as T_1-agents, are the first gold clusters that incorporate in well defined

[36] J. Lunney and G. Ashwell, *Proc. Natl. Acad. Sci. U. S. A*. **1976**, 73, 341-343 (A hepatic receptor of avian origin capable of binding specifically modified glycoproteins).
[37] R. J. Stockert, and A. G. Morell, *Hepatology* **1983**, 3, 750-757 (Hepatic Binding Protein: The Galactose-Specific Receptor of Mammalian Hepatocytes).
[38] D.R. Vera, M.H. Buonocore, E.R. Wisner, R.W. Katzberg and R.C Stadalnik, *Acad. Radiol.* **1995**, 2, 497-506 (A molecular receptor-binding contrast agent for magnetic resonance imaging of the liver).
[39] J.P. André, C.F.G.C. Geraldes, J.A. Martins, A.E. Merbach, M.I.M. Prata, A.C. Santos, J.J.P. Lima and É. Tóth, *Chem. Eur. J.* **2004**, 10, 5804-16 (Lanthanide(III) complexes of DOTA–glycoconjugates: a potential new class of lectin-mediated medical imaging agents.)
[40] D.A. Fulton,; E.M. Elemento, S. Aime, L. Chaabane, M. Botta and D. Parker, *Chem. Commun.* **2006**, 10,1064-66. (Glycoconjugates of gadolinium complexes for MRI applications).
[41] M.I.M. Prata, A.C. Santos, S. Torres, J.P. André, J.A. Martins, M. Neves, M.L. Garcìa-Martìn, T.B. Rodrigues, P. Lòpez-Larrubia, S. Cerdàn and C.F.G.C. Geraldes, *Contrast Med. Mol. Imaging* **2006**, 1, 246-258 (Targeting of lanthanide(III) chelates of DOTA-type glycoconjugates to the hepatic asyaloglycoprotein receptor: cell internalization and animal imaging studies).
[42] K. El-Boubbou and X. Huang, *Curr. Med. Chem.* **2011**, 18, 2060-2078 (Glyco-Nanomaterials: Translating Insights from the "Sugar-Code" to Biomedical Applications).
[43] K. El-Boubbou, D. C. Zhu, C. Vasileiou, B. Borhan, D. Prosperi, W. Li and X. Huang, *J. Am. Chem. Soc.* **2010**, 132, 4490-4499 (Magnetic Glyco-Nanoparticles: A Tool To Detect, Differentiate and Unlock the Glyco-Codes of Cancer via Magnetic Resonance Imaging).
[44] H. Lis, and N. Sharon, *Chem. Rev*. **1998**, 98, 637-674 (Lectins - Carbohydrate-Specific Proteins That Mediate Cellular Recognition).
[45] J. J. Lundquist and E. J. Toone, *Chem. Rev.* **2002**, 102, 555-578 (The Cluster Glycoside Effect).

ratio both sugars and Gd-complexes in a multivalent fashion. In order to check whether these GNPs could work as T_1 reporters of cellular receptors, three of the prepared GNPs bearing the monosaccharides mannose, galactose or glucose (Figure 2.1) were tested for labelling selectively different cell lines that express specific lectins at their surface.

The cell lines selected are Burkitt lymphoma cells (Raji and Raji-DC-SIGN), hepatocytes (HepG2), and murine glioma cells (GL261). Raji DC-SIGN cells were selected because they overexpress the receptor DC-SIGN (Dendritic Cell-Specific Intercellular adhesion molecule-3-Grabbing Non-integrin), a calcium-dependent and tetrameric lectin which specifically recognizes oligomannosides and Lewis blood group antigens through multivalent protein–carbohydrate interactions. [46] Raji cells that do not express DC-SIGN were used as controls. Monosaccharides with equatorial 4-hydroxyl groups (*e.g.* mannose and glucose) preferentially bind to receptor DC-SIGN respect to galactose which has axial 4-hydroxyl groups. [47]

A

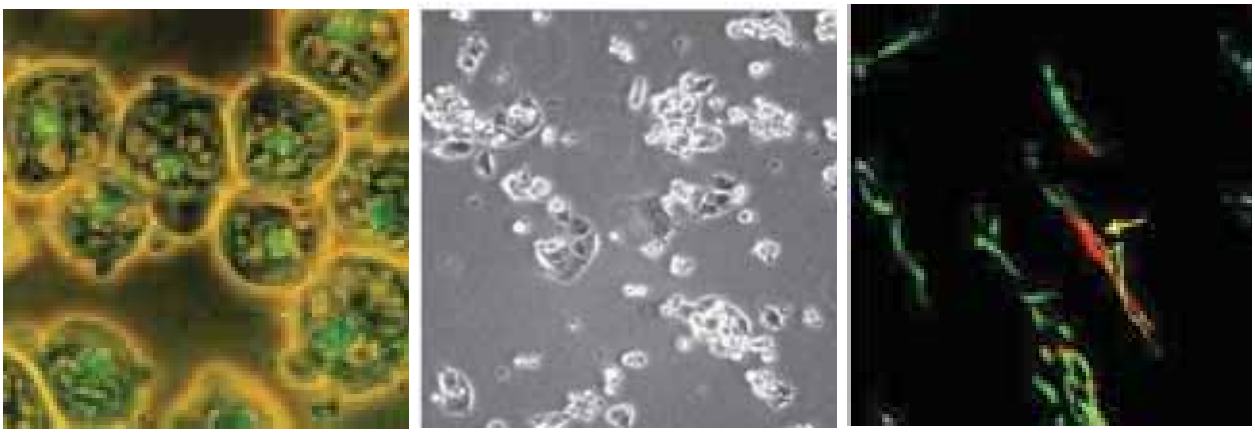

Raji cells HepG2 cells GL261 cells

B

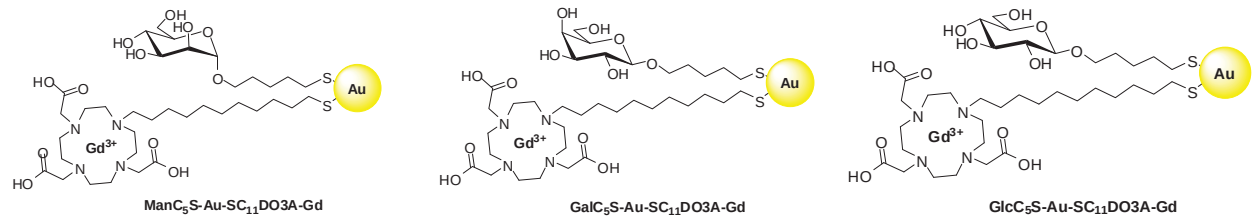

$ManC_5S$-Au-SC_{11}DO3A-Gd $GalC_5S$-Au-SC_{11}DO3A-Gd $GlcC_5S$-Au-SC_{11}DO3A-Gd

Figure 2.1: *A) Images of the cells used in these experiments: Burkitt lymphoma cells (Raji, Raji-DC-SIGN), hepatocytes (HepG2) and murine glioma cells (GL261). These cells lines are known to express glycan-binding receptors. B) Paramagnetic Gd-based gold GNPs ($ManC_5S$-Au-SC_{11}DO3A-Gd, $GalC_5S$-Au-SC_{11}DO3A-Gd, $GlcC_5S$-Au-SC_{11}DO3A-Gd) used in cellular labelling.*

[46] Y. Guo, H. Feinberg, E. Conroy, D. A. Mitchell, R. Alvarez, O. Blixt, M. E. Taylor, W. I. Weis, K. Drickamer, *Nat. Struct. Mol. Biol.* **2004**, 11, 591–598 (Structural basis for distinct ligand-binding and targeting properties of the receptors DC-SIGN and DC-SIGNR).

[47] S. V. Su, P. Hong, S. Baik, O. A. Negrete, K. B. Gurney, and B. Lee, *J. Biol. Chem.* **2004**, 279, 19122–19132 (DC-SIGN Binds to HIV-1 Glycoprotein 120 in a Distinct but Overlapping Fashion Compared with ICAM-2 and ICAM-3).

HepG2 cells were the second type of selected cell line. They are known to express the β-galactose/*N*-acetylgalactosamine binding lectin named asialoglycoprotein receptor. [**¡Error! Marcador no definido.**] This hetero-oligomeric receptor is expressed almost exclusively in hepatic parenchymal cells and binds specifically to galactosyl-terminal glycoproteins. [**¡Error! Marcador no definido.**] The role of multivalence in the binding of synthetic oligosaccharides to this lectin has been demonstrated by the pioneer work of Lee and colleagues. [48] The multimerization of β-galactoside moieties on gold nanoparticles should thus ensure a good interaction with HepG2 cells. The murine glioma cells (GL261) were also selected because they will be used to generate the glioma in mice for the *in vivo* evaluation of the Gd-based glyconanoparticles (see Chapter 3). Raji and GL261 cell lines are supposed to overexpress glucose receptors such as GLUT transporters [49] and show a highly increase of the glucose uptake typical of tumour cells. [50] The Gd-based GNPs incorporating mannose ($ManC_5S$-Au-$SC_{11}DO3A$-Gd) and galactose ($GalC_5S$-Au-$SC_{11}DO3A$-Gd) are expected to target respectively Raji DC-SIGN and HepG2 with significant selectivity, while the glucose ($GlcC_5S$-Au-$SC_{11}DO3A$-Gd) will preferentially label GL261 glioma cells.

1. Results and discussion

The first step before adding the GNPs to the cells was the evaluation of their cytotoxicity. None of the GNPs were cytotoxic at concentration 100 μg/mL after 24 hours of incubation with cells.

1.1 Checking the cytotoxicity of the Gd-GNPs

To check whether $ManC_5S$-Au-$SC_{11}DO3A$-Gd, $GalC_5S$-Au-$SC_{11}DO3A$-Gd and $GlcC_5S$-Au-$SC_{11}DO3A$ GNPs were cytotoxic, the 3-(4.5-dimethylthiazol-2-yl)-5-(3-carboxymethoxyphenyl)-2-(4-sulfophenyl)-2H-tetrazolium (MTS) [51] viability assay for Raji cells and the 3-(4,5-dimethylthiazol-2-yl)-2,5-diphenyltetrazolium bromide (MTT) [52] viability assays for HepG2 and GL261 cells were performed. The different GNPs were dissolved in water (concentrations:

[48] Y. C. Lee, R. R. Townsend, M. R. Hardy, J. Lonngren, J. Arnarp, M. Haraldsson and H. Lonn, *Biol. Chem*. **1983**, 258, 199-202 (Binding of Synthetic Oligosaccharides to the Hepatic Gal-GalNAc Lectin)
[49] M. Mueckler, *Eur. J. Biochem.* **1994**, 219, 713-725 (Facilitative glucose transporters)
[50] M. Hatanaka, *Biochim. Biophys. Acta* **1974**, 355, 77–104. (Transport of sugars in tumor cell membranes).
[51] A. H. Cory, T. C. Owen, J. A. Barltrop and J. G. Cory, *Cancer Commun*. **1991**, 3, 207-212 (Use of an aqueous soluble tetrazolium/formazan assay for cell growth assays in culture).
[52] T. Mosmann, *J. Immunol. Methods* **1983**, 65, 55-63 (Rapid colorimetric assay for cellular growth and survival: application to proliferation and cytotoxicity assays).

from 0 to 100 µg/mL) and incubated with Raji, HepG2 or GL261cells for 24 hours. Figure 2.6 demonstrates that cell viability is not affected after incubation of 24 h at various concentrations of GNPs. In particular, the cellular viability was more than 80% up to 100 µg/mL concentration. The standard deviations (±SD) were obtained on a triplicate analysis (n = 3).

The rest of the GNPs synthesized in this Thesis (Chapter 1) were also tested for cytotoxicity in GL261 cells. No cytotoxicity was observed up to 100 µg/mL concentration of GNPs (Figure 2.6).

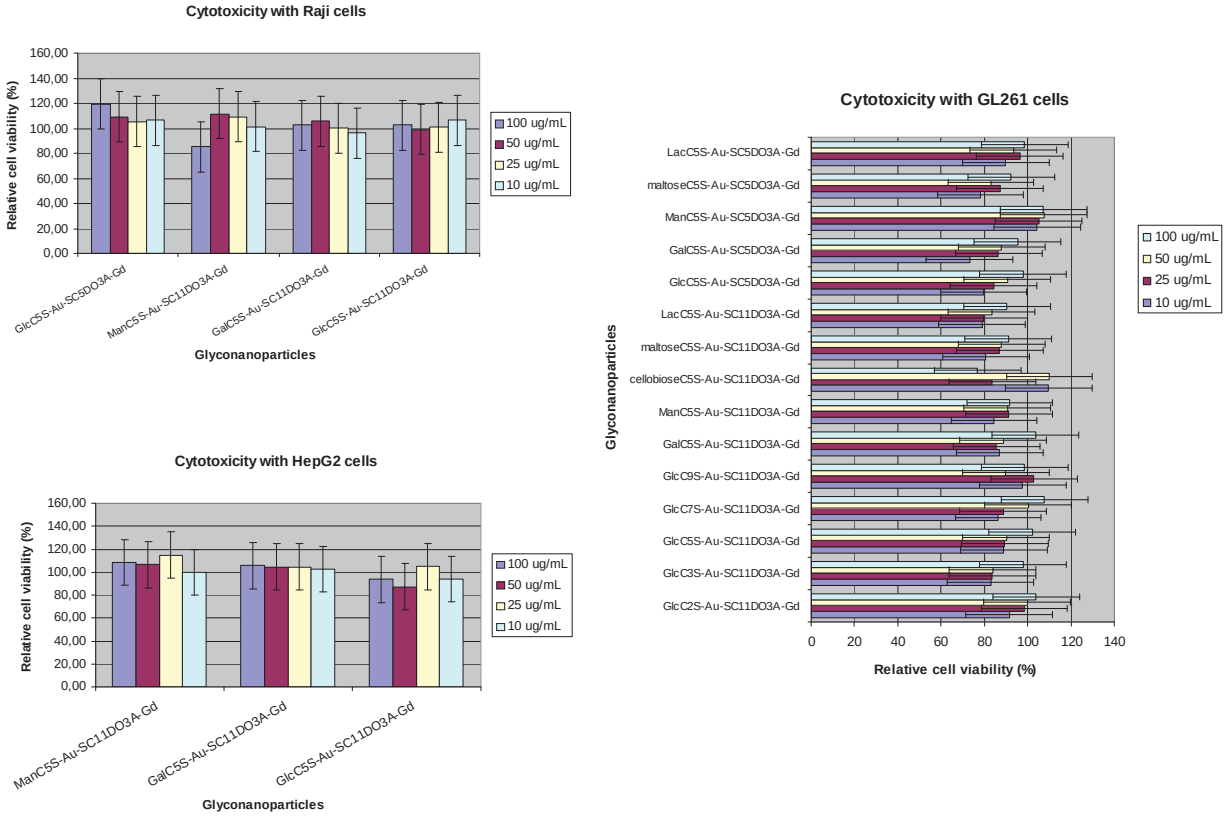

Figure 2.6: *Cytotoxicity results after incubation (24 hours) of Raji, HepG2 or GL261 cells with Gd-GNPs. The results show that cellular viability was more than 80% up to 100 µg/mL concentration.*

1.2 Labelling and imaging of fixed cells with Gd-based GNPs

To target surface receptors, cells were fixed and incubated with the Gd-GNPs. The fixation of cells is a process by which a dead cell is preserved as close to its natural state as possible. When a cell is fixed, any ongoing biochemical reactions stop, but an increase on their mechanical strength or stability is achieved. This increase on the strength and rigidity can help to preserve the morphology (shape and structure) of the cell and, thus, any study related to the surface of the cell (studies of the receptors, for example) can be carried out.

A

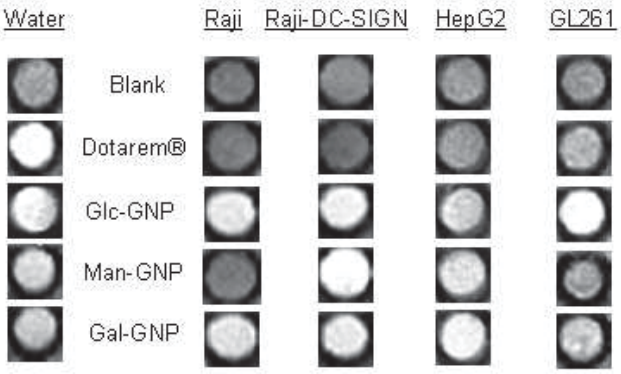

B

	SAMPLE	T_1 (ms) at 11.7 T	
Water	Water	3390±50	3050±89
Phantoms	Dotarem®	1229±33	1250±35
	$GlcC_5S$-Au-SC_{11}DO3A-Gd	1263±17	1276±21
	$ManC_5S$-Au-SC_{11}DO3A-Gd	1351±50	1339±51
	$GalC_5S$-Au-SC_{11}DO3A-Gd	1560±45	1545±42
Medium	Medium	2900 ± 62	3012± 70
Raji	Raji cells	2998±49	2914±64
	$GlcC_5S$-Au-SC_{11}DO3A-Gd	982±14	993±16
	$ManC_5S$-Au-SC_{11}DO3A-Gd	2323±64	2342±58
	$GalC_5S$-Au-SC_{11}DO3A-Gd	1280±32	1278±37
	Dotarem®	2683±57	2854±65
Raji-DC-SIGN	Raji DC-SIGN cells	3102±54	3052±83
	$GlcC_5S$-Au-SC_{11}DO3A-Gd	854±15	874±13
	$ManC_5S$-Au-SC_{11}DO3A-Gd	950±16	948±19
	$GalC_5S$-Au-SC_{11}DO3A-Gd	1086±22	1082±24
	Dotarem®	2961±49	2845±52
HepG2	HepG2 cells	2990±51	2999±95
	$GlcC_5S$-Au-SC_{11}DO3A-Gd	1244±20	1240±19
	$ManC_5S$-Au-SC_{11}DO3A-Gd	1307±37	1340±41
	$GalC_5S$-Au-SC_{11}DO3A-Gd	739±9	751±11
	Dotarem®	2754±51	2798±48
GL261	GL261 cells	3044±55	3001±81
	$GlcC_5S$-Au-SC_{11}DO3A-Gd	857±20	894±25
	$ManC_5S$-Au-SC_{11}DO3A-Gd	1420±39	1418±32
	$GalC_5S$-Au-SC_{11}DO3A-Gd	1140±19	1160±17
	Dotarem®	2662±36	2856±43

Figure 2.2: *A) T_1-weighted MR image at 11.7 T and 25 ºC of water, and of 130 μM (Gd concentration) water solutions of Dotarem®, $GlcC_5S$-Au-SC_{11}DO3A-Gd (Glc-GNPs), $ManC_5S$-Au-SC_{11}DO3A-Gd (Man-GNPs) and $GalC_5S$-Au-SC_{11}DO3A-Gd (Gal-GNPs) (**left**) and phantom images of Raji, Raji DC-SIGN, HepG2 and GL261 cells after incubation with the GNP solutions for 1 hour at 37 ºC (**right**). B) Table of*

the calculated T_1 values of the phantoms. Two independent experiments were performed in order to check the reproducibility.

The three selected Gd-based gold GNPs were incubated with 130 μM concentration of Gd for 1 hour at 37 ºC with Raji, Raji-DC-SIGN, HepG2 or GL261 fixed cells and MRI of the corresponding phantoms were performed at 11.7 T and 25 ºC in order to check the selectivity to label the cells of the different GNPs. The T_1-weighted images of the phantoms and the values of the corresponding relaxation times are given in Figure 2.2.

In order to obtain T_1 values (Figure 2.2B) from the images, a region of interest (ROI) was drawn on each of the phantoms in the image at a given slice. The mean signal intensity of the ROI was computed at all the repetition times (TR). These data were then fitted to a saturation recovery exponential function (see Experimental Part).

The selected paramagnetic GNPs could afford good contrast T_1-weighted MR images after incubation with fixed cells depending on their carbohydrate coating. When the cells were fixed and incubated with 130 μM Dotarem®, T_1-weighted MR images reveal no contrast enhancement in cell pellets (Figure 2.2), probably due to the hydrophilicity of Dotarem® that hamper internalization by cells.

Incubation of fixed Raji-DC-SIGN cells with **ManC_5S-Au-SC_{11}DO3A-Gd** afforded T_1-weighted images with bright contrast (hiperintensive, decrease of T_1 values) (Figure 2.2A) with a value calculated from the cell phantom images of T_1= 950 ms (Figure 2.2B). This is in agreement with the fact that Raji-DC-SIGN cells over-express a mannose receptor (DC-SIGN) on their surface. Similar value (T_1= 854 ms) was obtained for **GlcC_5S-Au-SC_{11}DO3A-Gd** which showed enhanced contrast respect to the cells alone or incubated with Dotarem, confirming that glucose has good affinity for these cells. **GalC_5S-Au-SC_{11}DO3A-Gd** showed less affinity (T_1= 1086 ms) for Raji-DC-SIGN than the mannose-GNPs. In contrast, Raji cell images (T_1= 2320 ms) clearly indicate much less expression of mannose receptors. **GlcC_5S-Au-SC_{11}DO3A-Gd** afforded very similar brightness after incubation both with Raji (T_1=982 ms) and Raji DC-SIGN (T_1=854 ms) cells, indicating that the binding of these GNPs to both cell lines is practically the same. **GalC_5S-Au-SC_{11}DO3A-Gd** also showed binding with both cells lines showing bright images at 11.7 T with T_1 values of 1280 ms for Raji cells and 1086 ms for Raji DC-SIGN cells. These results indicate that Raji cells express both glucose- and galactose-binding proteins on their surface, but mannose receptors are expressed in much less extent.

T_1-weighted MR images for HepG2 after incubation with **GalC_5S-Au-SC_{11}DO3A-Gd** showed high contrast enhancement (T_1=739 ms) (Figure 2.2A). **GlcC_5S-Au-SC_{11}DO3A-Gd** and **ManC_5S-Au-SC_{11}DO3A-Gd** images also showed an increase in brightness respect to the controls

(T_1= 1244 ms and 1307 ms, respectively), indicating a binding to the cells, although in less extent than the galactose-GNPs, as expected.

The incubation of fixed GL261 cells with **$GlcC_5S$-Au-SC_{11}DO3A-Gd** afforded the brightest T_1-weighted MR images (T_1= 857 ms) followed by **$GalC_5S$-Au-SC_{11}DO3A-Gd** (T_1= 1140 ms) and **$ManC_5S$-Au-SC_{11}DO3A-Gd** (T_1= 1420 ms) (Figure 2.2). This result indicates that **$GlcC_5S$-Au-SC_{11}DO3A-Gd** is the one with the strongest binding (lowest T_1) to GL261 receptors. However, the T_1 lowering with **$ManC_5S$-Au-SC_{11}DO3A-Gd** and **$GalC_5S$-Au-SC_{11}DO3A-Gd** indicate that these cells also express mannose and galactose receptors, although to a less extent than glucose as the corresponding T_1-weighted images clearly show.

Comparing the T_1-weighted MR images of control cell pellets with cells incubated with GNPs, a T_1 reduction of 68% was achieve after incubation of Raji-DC-SIGN cells with **$ManC_5S$-Au-SC_{11}DO3A-Gd** respect to untreated cells (Table 2.1). Similar results were obtained after incubation of **$GalC_5S$-Au-SC_{11}DO3A-Gd** with HepG2 cells (T_1 reduction of 74%) and **$GlcC_5S$-Au-SC_{11}DO3A-Gd** with GL261 cells (T_1 reduction of 70%). Summarizing, GNPs incorporating glucose bound similarly to all cell lines (~60-70 % reduction). The Man-GNPs bound preferably to Raji- DC-SIGN, while the decrease of T_1 value in Raji cells represents only a 20 %. In HepG2 and GL261 cell lines the T_1 reduction by incubating Man-GNPs is around 55 %, while Gal-GNPs are preferably bound to HepG2 (~ 80%) as expected (Table 2.1).

Table 2.1: *Qualitative evaluation of binding selectivity of GNPs to cellular lines based on T_1 reduction (%).*

GNP	Raji	Raji- DC-SIGN	HepG2	GL261
$GlcC_5S$-Au-SC_{11}DO3A-Gd	++ (70%)	++ (75%)	+ (60%)	++ (70%)
$ManC_5S$-Au-SC_{11}DO3A-Gd	+ (25%)	++ (70%)	+ (55%)	+ (55%)
$GalC_5S$-Au-SC_{11}DO3A-Gd	+ (60%)	+ (60%)	++ (80%)	+ (60%)

Although the specificity of GNPs to label the cells is not 100%, the GNPs are able to differentiate one type of cells from others which can be used as MRI T_1-probes to target and unveil cell receptors. In general, it is evident that Gd-based paramagnetic gold GNPs can work as selective T_1-reporters of cellular receptors depending on their sugar coating. In addition, the high local

concentration of sugars on GNP (multivalence) increases the affinity of carbohydrates for the protein and facilitates the visualization of T_1-weighted images of cells.

A

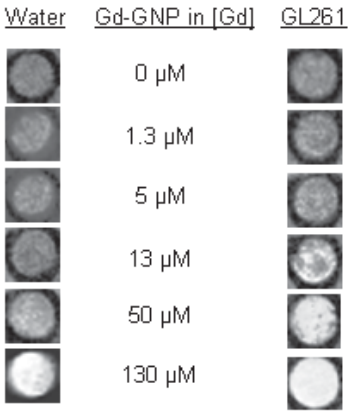

B

SAMPLE	[Gd] µM	T_1 (ms) at 11.7 T		r_1 ($s^{-1}mM^{-1}$)at 11.7 T
Water	0	3397±48	2982±77	
Medium	0	2900 ± 62	3012± 70	
GL261	0	3044±55	2943±80	
$GlcC_5S$-Au-SC_{11}DO3A-Gd	1.3	3177±132	2948±131	2.7
	5	3167±110	3067±110	
	13	3118±29	2969±73	
	50	2894±42	2656±57	
	130	1263±17	1270±20	
GL261+$GlcC_5S$-Au-SC_{11}DO3A-Gd	1.3	3237±75	2781±84	5.9
	5	2903±67	2791±121	
	13	2352±29	2479±98	
	50	1425±28	1546±89	
	130	897±30	950±36	

Figure 2.3: *A) T_1-weighted MR image of water and water solutions of $GlcC_5S$-Au-SC_{11}DO3A-Gd, at 1.3, 5, 13, 50, 130 µM (Gd concentration) at 11.7 T* ***(left)*** *and of GL261 cells after incubation for 1 hour with 1.3, 5, 13, 50, 130 µM (Gd concentration) (25 ºC)* ***(right)****. B) Table of the calculated T_1 values at 11.7 T of $GlcC_5S$-Au-SC_{11}DO3A-Gd GNPs and the incubation of GL261 with GNP for 1 hour. Two independent experiments were performed in order to check the reproducibility.*

Once we demonstrated that different carbohydrates can select cell receptors working as T_1-targeted contrast agents, we verified the minimum concentration of paramagnetic GNPs which is required to produce a significant brightening effect. To this aim, experiments with GL261 cells

and **GlcC$_5$S-Au-SC$_{11}$DO3A-Gd** GNP were performed at lower concentrations of Gd (1.3, 5, 13, 50 μM). T_1-weighted MR images showed contrast enhancement when cells were incubated with 13 and 50 μM (in Gd concentration) of GNP **GlcC$_5$S-Au-SC$_{11}$DO3A-Gd** (Figure 2.3). Respect to untreated cells, T_1 analysis revealed a 23% and 53% T_1 reduction with 13 and 50 μM (Gd concentration), respectively. These results demonstrate that GNPs at 50 μM (Gd concentration) were sufficient to produce significant T_1-weighted contrast enhancement of small cell populations which present a specific-sugar binding receptor on their surface.

To quantify Gd(III) concentration taken up by cells, T_1 values of the recovering media was measured. The Gd(III) concentration (μM) was calculated by interpolation of $1/T_1$ to the curve obtained by plotting the concentration of the corresponding GNP (phantoms at 11.7 T) in terms of Gd(III) millimolarity *vs* the corresponding $1/T_1$ (T_1 in seconds) (see Chapter 1). The concentration of Gd taken up by the cells after incubation with 130 μM of Gd was around 30 μM.

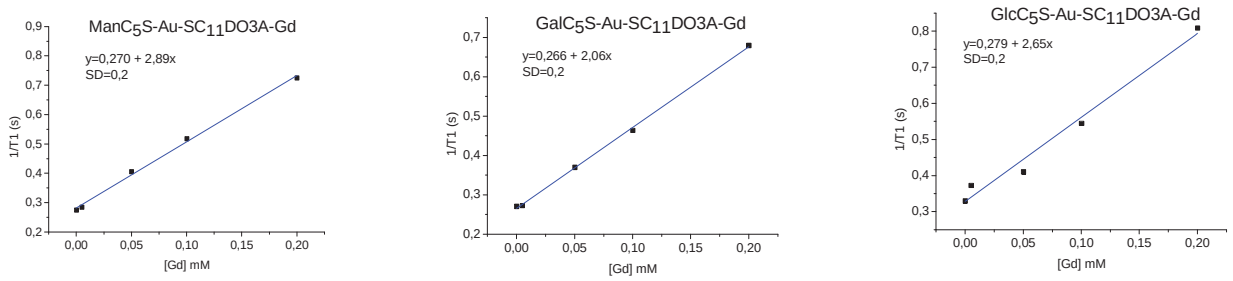

$$1/T_1 \text{ (recov. media)} = 1/T_1 \text{ (buffer)} + r_1 \text{ [Gd]}$$

Recovering media	T_1 *(ms)*; $1/T_1$ (s)	[Gd] (μM) in media	[Gd] (μM) in the cell
Raji DC-SIGN + Man-GNP	1906; 0.525	83	47
HepG2 + Gal-GNP	2000; 0.5	98	32
GL261 + Glc-GNP	1742; 0.574	108	22

The specificity of GNPs GlcC$_5$S-Au-SC$_{11}$DO3A-Gd for glucose-binding receptors was tested by competition experiments. Pre-incubation of fixed GL261 cells with free glucose up to 1 M following by treatment with Gd-GNP showed MR images with T_1 values similar to cells incubated

only with $GlcC_5S$-Au-SC_{11}DO3A-Gd, pointing out that the high concentration of glucose is unable to block the receptor. In contrast, MR images of cells pre-treated with gold nanoparticles coated 100 % with glucose in 3 mM concentration ($GlcC_5S$-Au) showed the same T_1 values as the control cells, indicating that **$GlcC_5S$-Au-SC_{11}DO3A-Gd** was unable to interact with the receptors when saturated by $GlcC_5S$-Au GNPs. These results clearly indicate that 3 mM concentration of glucose onto glyconanoparticles is enough to inhibit the binding of **$GlcC_5S$-Au-SC_{11}DO3A-Gd** to the corresponding receptor, while up to 1 M concentration of free sugar was not able to block the receptor. This result can be attributed to the increase of local concentration of carbohydrates on the GNPs, associated to a multivalent effect, which enhance the avidity of glucose for the receptor.

In an attempt to improve the sensitivity of T_1-weighted images of the labelling cells, the Gd-GNP $GlcC_5S$-Au-SC_5DO3A-Gd having higher relaxivity value (r_1=16.9 $s^{-1}mM^{-1}$) at 1.4 T than $GlcC_5S$-Au-SC_{11}DO3A-Gd (7.1 $s^{-1}mM^{-1}$) have been tested. The different chain's lengths of the gadolinium complexes ($DO3AC_XS$-Gd) have been shown to influence the relaxivity values of GNPs at 1.41 T (Chapter 1, Tables 1.6 and 1.7). If the length of the glycoconjugate and of the DO3A-derivative are the same (5 carbon atoms), the relaxivity values in water are higher than those of the GNPs bearing different length. Although, the relaxivity of all the GNPs suffer a dramatic decrease and become similar (r_1= 2.5 $s^{-1}mM^{-1}$ for $GlcC_5S$-Au-SC_{11}DO3A-Gd and r_1= 4.0 $s^{-1}mM^{-1}$ for $GlcC_5S$-Au-SC_5DO3A-Gd) when GNPs are measured at 11.7 T (see Chapter 1, Figure 1.8B), we decided to perform labelling experiments with $GlcC_5S$-Au-SC_5DO3A-Gd GNP. The nanoparticle (130 μM in Gd(III) concentration) was incubated with fixed GL261 cells for 1 hour and the T_1-weighted MR images of the cell pellets were taken at 11.7 T.

A

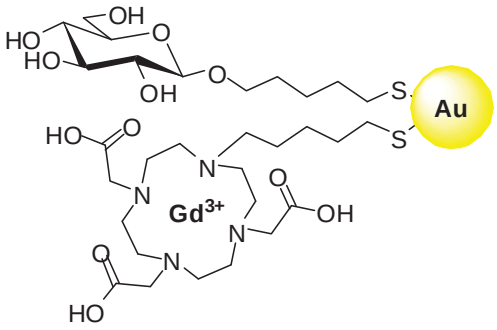

B

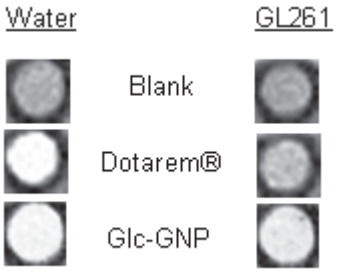

C

	SAMPLE	T_1 (ms) at 11.7 T	T_1 reduction (%)
Water	Water	3309±65	
Medium	Medium	3012±62	
Phantoms in water	Dotarem®	1585±38	52
	$GlcC_5S$-Au-SC_{11}DO3A-Gd	1263±17	62
	$GlcC_5S$-Au-SC_5DO3A-Gd	1162±30	65
GL261	Dotarem®	2662±36	12
	GL261 cells	3243±46	0
	$GlcC_5S$-Au-SC_{11}DO3A-Gd	857±20	72
	$GlcC_5S$-Au-SC_5DO3A-Gd	1230±33	60

Figure 2.4: *A) Schematic representation of $GlcC_5S$-Au-SC_5DO3A-Gd glyconanoparticle. B) T_1-weighted MR image at 11.7 T and 25 ºC of water, Dotarem® and $GlcC_5S$-Au-SC_5DO3A-Gd at 130 µM (Gd concentration) in water **(left)** and phantom images of GL261 cells after incubation with the GNPs for 1 hour at 37 ºC **(right)**. C) Table of the calculated T_1 values of the phantoms.*

As it was expected, GL261 cells were labelled with $GlcC_5S$-Au-SC_5DO3A-Gd GNP (Figure 2.4); however no much difference was observed neither in the image brightness nor in the decrease of T_1 values (60% versus 70%) comparing to the incubation of GL261 with $GlcC_5S$-Au-SC_{11}DO3A-Gd. The results obtained in this experiment show the strong influence of the magnetic field going from 1.4 to 11.7 T, but also that the higher relaxivity values obtained at 11.7 T in solution for $GlcC_5S$-Au-SC_5DO3A-Gd GNPs (r_1=4.0 $s^{-1}mM^{-1}$) in comparison to the ones obtained (T_1 = 857 ms) with $GlcC_5S$-Au-SC_{11}DO3A-Gd GNPs (r_1=2.5 $s^{-1}mM^{-1}$) do not correspond to the moderate response obtained (T_1 = 1230 ms) in the *in vitro* cell experiments. As a consequence, it is expected an unpredictable behaviour for the Gd-GNPs when tested *in vivo*. However, the results obtained in

the cellular assays described in this chapter have helped to select the Gd-GNPs for the *in vivo* glioma MR imaging (see Chapter 3) and can further help in the design of smart contrast agents with improved properties for *in vivo* applications.

1.3 Labelling of live cells with Gd-based GNPs

The labelling of living cells with Gd-based contrast agents is still a challenge and only few reports have been published. [32], [**¡Error! Marcador no definido.**], [**¡Error! Marcador no definido.**], [35], [53] Strategies are being developing for the intracellular delivery of nanoparticles. [54] As internalization mechanisms are blocked in the case of fixed cells, the binding of GNPs is only due to carbohydrate receptors (lectins) present at cell surface. On the contrary, living cells can internalize the GNP by receptor mediated endocytosis, but also by many other non-specific uptake mechanisms (pinocytosis pathways not mediated by receptors). [54], [55] In the experiments with the fixed cells, Gd-GNPs have shown to selectivity label the different cell lines depending on the receptors express on the cell surface (DC-SIGN, asialoprotein or glucose receptors). Because of glucose, mannose and galactose-GNPs target specific receptors, it is expected that they will be uptake and internalized by receptor-mediated endocytosis by the live cells.

Then a series of experiments aiming at labelling the selected cells alive with Gd-GNPs have been carried out. The attempts performed with GL261 were unsuccessful. However, some results have been obtained when Raji and Raji-DC-SIGN cells when they were incubated with 130 μM (Gd(III) concentration) of **ManC$_5$S-Au-SC$_{11}$DO3A-Gd** GNP. Brighter T_1-images as well as a decrease in T_1 value with respect to the controls were observed for both type of cell (Figure 2.5). In the case of Raji a T_1 value of 1746 ms was obtained (50 % decrease), while the incubation with Raji-DC-SIGN afforded T_1=1558 ms (55 % decrease). These results showed that both Raji and Raji-DC-SIGN living cells uptake the mannose-GNP, although the uptake of Raji-DC-SIGN is slightly higher probably due to the mannose-binding receptors on their surface. The bright image obtained when living Raji cells are incubated with the **ManC$_5$S-Au-SC$_{11}$DO3A-Gd** (Figure 2.5) can be due to other mechanisms of internalization that are active in live cells but absence in fixed Raji cells.

---

[53] T. Yamane, K. Hanaoka, Y. Muramatsu, K. Tamura, Y. Adachi, Y. Miyashita, Y. Hirata and T. Nagano, *Bioconjugate Chem.* **2011**, 22, 2227-2236 (Method for enhancing cell penetration of Gd^{3+}-based MFI contrast agents by conjugation with hydrophobic fluorescent dyes).

[54] L.Y.T. Chou, K. Ming and W.C.W. Chang, *Chem. Soc. Rev*. **2011**, 40, 233-245 (Strategies for the intracellular delivery of nanoparticles).

[55] S. D. Conner and S. L. Schmid, *Nature* **2003**, 422, 37-44 (Regulated portals on entry into the cell)

A

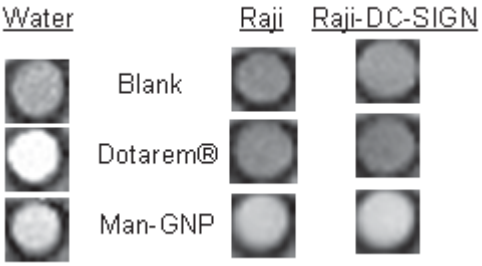

B

	SAMPLE	T_1 (ms) at 11.7 T
Water	Water	3014±144
Medium	Medium	2900±62
Phantoms	Dotarem®	1229±33
	$ManC_5S$-Au-SC_{11}DO3A-Gd	1351±50
Raji	Raji living cells	3075±110
	$ManC_5S$-Au-SC_{11}DO3A-Gd	1746±83
	Dotarem®	3148±128
Raji-DC-SIGN	Raji DC-SIGN living cells	3460±168
	$ManC_5S$-Au-SC_{11}DO3A-Gd	1558±38
	Dotarem®	3460±168

Figure 2.5: *A) T_1-weighted MR image at 11.7 T of phantoms of water, medium, Dotarem® and $ManC_5S$-Au-SC_{11}DO3A-Gd at 130 μM (Gd concentration)* ***(left)*** *and phantoms of live Raji and Raji DC-SIGN cells incubated for 4 hour with 130 μM (Gd concentration) of $ManC_5S$-Au-SC_{11}DO3A-Gd (Man-GNP) and Dotarem® at 11.7 T and 37 ºC* ***(right)****. B) Table of the corresponding T_1 values of the phantom at 11.7 T.*

In the case of Raji-DC-SIGN cells, the MR images are brighter in fixed cells (T_1= 950 ms) than in living cells (T_1= 1588 ms) as reported in Figures 2.2B and 2.5B. This decrease in the brightness could be due to mechanisms that take place in living cells after internalization, such as GNP exocytic release or "quenching" effect on relaxivity of endosome entrapped Gd-GNPs [56]. Thus it is presumable that the uptake of **$ManC_5S$-Au-SC_{11}DO3A-Gd** by live Raji-DC-SIGN cells influences the relaxation properties of these GNPs.

[56] E. Gianolio, F. Arena,G. J. Strijkers, K. Nicolay, A. Högset and S. Aime, *Magn. Reson. Med.* **2011**, 65, 212-219 (Photochemical Activation of Endosomal Escape of MRI-Gd-Agents in Tumor Cells).

It has been also recently reported that the confinement into endosomal vesicles of Gd-based MRI probes may negatively affect the proton relaxation enhancement in the corresponding MR images depending on the Gd-concentration inside the cell. [57], [58], [59] In fact, it has been shown that a ‘‘quenching’’ effect on the observed relaxivity of Gd-HPDO3A takes place when the concentration of Gd(III) in the endosomal compartments is increased to $1x10^9$ contrast agent per cell due probably to self-aggregation which impede the water exchange. [56] In our experiments, the amount of **$ManC_5S$-Au-SC_{11}DO3A-Gd** GNP incubated with cells is low (130 μM in Gd) in comparison with the one which is necessary for having a “quenching” in the case of small molecules (in the order of millimolar). So, it is not presumably that this kind of “quenching” effect takes place. However, in order to understand which phenomena govern the behaviour of Gd-GNPs in living cells and to achieve high labelling efficiencies with Gd-based paramagnetic gold GNPs more experiments are needed.

2. Conclusions

In this chapter, we demonstrated that paramagnetic Gd-based gold GNPs are non-cytotoxic for a variety of cells and can be applied for the selective labelling of cells receptors. By following the enhancement of the brightness of T_1-weighted images of cells and the decrease of the corresponding T_1 values, the sugar-receptors on the cell surface can be evaluated. The sugar-driven selectivity due to specific carbohydrate-protein binding allows the identification of carbohydrate receptors at cell surface and the targeting of specific cells where these receptors are preferentially expressed. The multimerization of carbohydrates on the gold nanoparticles allows the enhancement of the contrast in T_1-weighted images of cells by increasing the concentration and avidity of the sugars for their corresponding receptors.

The most important question that has still to be answer is the labelling of live cell by Gd-GNPs. This issue demands to address the study of their uptake and the monitoring of their fate into the cells. To achieve this goal, fluorescently labelled Gd-GNPs would be desirable.

[57] E. Terreno, S. Geninatti Crich, S Belfiore, L. Biancone, C. Cabella, G. Esposito, A. D. Manazza, S Aime, *Magn. Reson. Med.* **2006**, 55, 491–497 (Effect of the intracellular localization of a Gd-based imaging probe on the relaxation enhancement of water protons).

[58] G. J. Strijkers, S. Hak, M. B. Kok, C. S. Springer and K. Nicolay, *Magn. Reson. Med.* **2009**, 61, 1049–1058 (Three-compartment T1 relaxation model for intracellular paramagnetic contrast agents).

[59] M. B. Kok, S. Hak, W. J. M. Mulder, D. W. J. van der Schaft, G. J. Strijkers and K. Nicolay, *Magn. Reson. Med.* **2006**, 61, 1022–1032 (Cellular compartmentalization of internalized paramagnetic liposomes strongly influences both T_1 and T_2 relaxivity)

3. Experimental part

Cytotoxicity assay. The viability of GL261 and HepG2 cells was determined by using the MTT method. Briefly, 10^4 cells/well were seeded into 96-well plates in 100 µL complete medium and incubated at 37 ºC in 5% CO_2 atmosphere. After 24 hours, the medium was replaced with a fresh one containing nanoparticles at different concentrations (0-100 μgmL^{-1}). After 20 hours incubation period, 20 µL of MTT (5 mg mL^{-1} in phosphate buffer pH 7.4) was added to each well. After 4 hours of incubation at 37 ºC and 5% CO_2 for exponentially growing cells and 15 min for steady-state confluent cells, the medium was removed, formazan crystals were dissolved with 200 µL of DMSO, and the solution was vigorously mixed to dissolve the reacted dye. The absorbance of each well was read on a multiplate reader (GENios Pro instrument from TECAN) at 550 nm.
The toxicity of the GNPs towards Raji cells was studied at 0-100 μgmL^{-1} concentration range using a MTS standard protocol. $1 \cdot 10^4$ cells/well were seeded into 96-well plates in 80 µL complete medium and then, GNPs solution (20 µL) at desired concentration was added and incubated at 37 ºC, 5% CO_2 atmosphere. After 20 h, 20 µL of MTS solution (5 mg mL^{-1}) were added to each well and cells were still incubated for 4 h at 37 ºC, 5% CO_2 atmosphere. Finally, the absorbance of the samples was measured at 490 nm on the multiplate reader.

Cells and culture conditions. All media and reagents were obtained from commercial suppliers (Sigma-Aldrich or Lonza) and used without further purification unless otherwise indicated. The Raji line of lymphoblast-like cells, established from a Burkitt's lymphoma, and Raji-DC-SIGN transfectants (transfectants generation) were grown in Roswell Park Memorial Institute (RPMI)-1640 medium supplemented with 10% fetal bovine serum (FBS), 2 mM L-glutamine and streptomycin/penicillin (100 UmL^{-1} penicillin and 100 μgmL^{-1} streptomycin). Cells were subcultured following American Type Culture Collection (ATCC) recommendations at 37 ºC in an atmosphere of 5% CO_2 and 95 % air. The murine glioma cells, GL261 line, were grown as monolayer cultures on culture flasks in RPMI-1640 medium supplemented with 10% fetal bovin serum (FBS) and 4 mM L-glutamine at 37 ºC in an atmosphere of 5 % CO_2 and 95% air. The HepG2 line, established from hepatocellular carcinoma, was cultured in Minimum Essential Medium Eagle (M-5650), supplemented with 10% FBS and 2 mM L-glutamine at 37 ºC in an atmosphere of 5% CO_2 and 95% air.

Incubation of fixed cells with Gd-GNPs. GL261 and HepG2 (~$5 \cdot 10^5$ cells per well) were seeded in 6 wells plates and grown 24 hours at 37 ºC in an atmosphere of 5% CO_2 and 95% air. Cells were washed three times with warm (37 ºC) 10 mM phosphate buffered saline (PBS), fixed with 2.5% formaldehyde (10 min at r.t.) and again washed three times with 10 mM PBS to remove any residual formaldehyde. Cells were detached with trypsin-ethylenediamine tetraacetic acid (EDTA) solution, washed twice with cold 10 mM PBS by centrifugation (440 *g*, 5 min, 4 ºC) and put them in a round bottom 96 well plate (~10^6 cells per well).

Raji or Raji-DC-SIGN (~$3 \cdot 10^6$ cells per well) were put in a round bottom 96 well plate. Cells were washed twice with 10 mM PBS by centrifugation (500 *g*, 5 min, 4 ºC), fixed with 2.5% formaldehyde (10 min at r.t) and again washed three times with 10 mM PBS by centrifugation (500 *g*, 5 min, 4 ºC) to remove any residual formaldehyde.

GL261, HepG2, Raji and Raji-DC-SIGN pellets were resuspended in a 130 μM (Gd (III) concentration) culture media solution of GNPs or Dotarem® and incubated for 1 hour at 37 ºC in an atmosphere of 5% CO_2 and 95% air. After incubation, plate was centrifuged (500 *g*, 5 min, 4 ºC) and supernatant was collected. Pellets were washed twice with cold PBS (10 mM) by centrifugation (500 *g*, 5 min, 4 ºC) to remove the unbound GNPs or Dotarem®. Finally, pellets were re-suspended in ~30 μL cold PBS (10 mM) and put it into sealed jet Pasteur pipette. The pipettes were kept at 4 ºC, overnight to allow pellet formation. The pipettes were cut and put into a plastic cup with Plasticine on the bottom and subjected to MRI experiments (imaged at 11.7 T).

GL261 cells were also incubated with $GlcC_5S$-Au-SC_{11}DO3A-Gd at 1.3, 5, 13 or 50 μM (Gd (III) concentration).

Gd-GNPs uptake by living cells. Raji or Raji-DC-SIGN (~$3 \cdot 10^6$ cells per well) were put in a round bottom 96 well plate and centrifugated (500 *g*, 10 min, 4 ºC). Raji and Raji-DC-SIGN pellets were resuspended in a 130 μM (Gd (III) concentration) culture media solution of $ManC_5S$-Au-SC_{11}DO3A-Gd or Dotarem® and incubated for 4 hours at 37 ºC in an atmosphere of 5% CO_2 and 95% air. After incubation, plate was centrifuged (500 *g*, 5 min, 4 ºC) and supernatant was collected. Pellets were washed twice with cold 10 mM PBS by centrifugation (500 *g*, 5 min, 4 ºC) to remove the unbound GNPs or Dotarem®. Finally, pellets were re-suspended in ~30 μL cold 10 mM PBS and put it into sealed jet Pasteur pipette. The pipettes were kept at 4 ºC, overnight to allow pellet formation. The pipettes were cut and put into a plastic cup with Plasticine on the bottom and subjected to MRI experiments (imaged at 11.7 T).

MRI and T_1 values. T_1 measurements at 1.41 T (60 MHz) were performed at 37 ºC in a Bruker Minispec MQ60 (Bruker Biospin, Ettlingen, Germany) by the inversion recovery method.

T_1 measurements were performed in a Bruker Biospec at 11.7 teslas using a 72 mm volumetric quadrature coil at room temperature. Saturation recovery pulse sequence with static echo time TE (11 ms) and variable TR (300, 650, 730, 1100, 1500, 2100, 2800, 3800, 5500, 12500 ms) value was used. Imaging parameters were as follows: field of view (FOV) = 34 x 34 mm^2, matrix size (MTX) = 320 x 320, slice thickness (ST) = 0.5 mm, and averages (NEX) = 1. T_1 analysis was carried out using the image sequence analysis tool in Paravision 5 software (Bruker BioSpin, Ettlingen, Germany) with monoexponential curve-fitting of image intensities of selected regions of interest (ROIs). T_1 values were obtained from images drawing a ROI on each of the phantoms in the image at a given slice. The mean signal intensity of the ROI was computed at all the repetition times (TR). These data were then fitted to a saturation recovery exponential function T_1-weighted images were measured using a Gradient Echo Sequence with 400 ms repetition time and 4.7 ms echo time.

CHAPTER 3

APPLICATION OF PARAMAGNETIC Gd-BASED GOLD GLYCONANOPARTICLES FOR *IN VIVO* MAGNETIC RESONANCE IMAGING OF GLIOMA IN MICE

APPLICATION OF PARAMAGNETIC Gd-BASED GOLD GLYCONANOPARTICLES FOR *IN VIVO* MAGNETIC RESONANCE IMAGING OF GLIOMA IN MICE

In the framework of our research program aiming at the application of the paramagnetic glyconanoparticles to the diagnosis of brain tumors in the initial stage, we present in this chapter the study of the synthesized paramagnetic Gd-based gold glyconanoparticles (Gd-GNPs) as contrast agents *in vivo* in MRI pre-clinical assays. [1] Their biodistribution and toxicological profile have also been determined because of its relevance towards potential clinical application. [2] MRI (at 7 T) was used to visualize the T_1-positive contrast enhancement induced by the paramagnetic nanoparticles in an orthotopic GL261 generated glioma in C57/BL6 mice [3] and compare with contrast produced by gadoteric acid (Dotarem®). The *in vivo* biodistribution of these nanoparticles in the main mice organs at different times was also monitored in mice with and without tumors. Precisely, the amount of gold and gadolinium in the examined organs was determined by Inductively Coupled Plasma Mass Spectrometry (ICP-MS) analysis at different time points post-contrast administration. Furthermore, analyses of biochemical parameters of the injected animals as well as *post-mortem* microscopic examinations of animal tissues (histopathology) were also performed.

In the introduction of this Thesis, we have widely discussed the importance of using nanotechnology-based tools in MRI, and more generally in multimodal imaging. The first results on the design and preparation of Gd-based gold glyconanoparticles (Gd-GNP) as T_1-probes were published in 2009. [4] The idea was to use carbohydrate coatings to confer high biocompatibility and stability to the nanoclusters and, at the same time, profit from the presence of carbohydrate receptors (lectins) on the surfaces of eukaryotic cells to direct the Gd-functionalized glyconanoparticles towards specific tissues or organs. In particular, one of the seminal ideas behind this project was based on the use of glucose to target the GLUT-1 transporters, which are expressed in brain endothelium, in order to cross the blood brain barrier (BBB) in healthy animals and to take advantage of the glucose-coating to achieve accumulation of nanoparticles in glioma,

[1] The *in vivo* MRI experiments were carried out by the Grup d'Aplicacions Biomèdiques de la RMN (GABRMN) in Universitat Autónoma de Barcelona directed by Prof. Carles Arús.
[2] Biodistribution and toxicological profile experiments were done by the group of Simó Schwartz in CIBBIM-Nanomedicine, Hospital Universitari Vall d'Hebron.
[3] R.V. Simões, M.L. García-Martín, S. Cerdán, C. Arús, *NMR Biomed.* **2008**, 21, 251-264 (Perturbation of mouse glioma MRS pattern by induced acute hyperglycemia).
[4] M. Marradi, D. Alcântara, J. Martínez de la Fuente, M. L. García-Martín, S. Cerdán and S. Penadés, *Chem. Commun.* **2009**, 26, 3922–3924 (Paramagnetic Gd-based gold glyconanoparticles as probes for MRI: tuning relaxivities with sugars).

because tumor cells show an increased uptake of glucose in comparison to normal brain cell. [5], [6] Furthermore, attaching the Gd-complex to the gold glycoclusters longer circulation time in blood, reduction of the toxicity and immunogenicity, and a better biodistribution should be expected.

The use of nanoparticles *in vivo* demands for toxicity studies both at cellular and organ levels. We have demonstrated in the previous chapters that our Gd-GNPs are not toxic to different cell lines, including the GL261 cell line (murine glioma cells) used in *in vivo* models, at concentrations as high as 100 μg/mL. However, recent investigations about toxicology of nanoparticles have raised some concerns on the *in vivo* use of these new materials in relation to a specific type of toxicity which has to do with their dimensions (nanotoxicology) [7] and which includes also immunotoxicity [8]. Many studies have applied gold nanoparticles [9], gold nanorods [10] and gold nanoshells [11] for small animal *in vivo* imaging and cancer detection, but it is of extreme importance to address (nano)toxicology issues before the use of these materials can advance towards clinical applications.

Preliminary studies of the *in vivo* application of Gd-GNP incorporating glucose and lactose indicated that glucose-GNPs produce positive contrast in glioma in mice, while lactose-GNPs were not able to reach the tumour. [4], [12] In this chapter, we present the MRI studies carried out on the ability of $GlcC_5S$-Au-SC_{11}DO3A-Gd GNPs to enhance the contrast of T_1-weighted images of glioma in mice after intravenous injection. $GlcC_5S$-Au-SC_{11}DO3A-Gd GNPs were chosen because they proved to be the best T_1-probe at 7 T in the preliminary *in vivo* imaging of GL261glioma in mice. [4] In addition, in the cellular study presented in Chapter 2, these Gd-GNPs produced the higher contrast enhancement *in vitro* with GL261 glioma cells among all GNPs tested. We studied first the $GlcC_5S$-Au-SC_{11}DO3A-Gd prepared by "direct" synthesis. In a

[5] O. Warburg, *Science* **1956**, 123, 309-314 (On the origin of cancer cells).
[6] M. Hatanaka *Biochim. Biophys. Acta* **1974**, 355, 77-104 (Transport of sugars in tumor cell membranes).
[7] G. Oberdoerster, *J. Intern. Med*. **2010**, 267, 89–105(Safety assessment for nanotechnology and nanomedicine: concepts of nanotoxicology)
[8] M.. Dobrovolskaia,D R.. Germolec and J. L. Weaver, *Nat. Nanotechnol.* **2009**, 4, 411-414 (Evaluation of nanoparticle immunotoxicity).
[9] X. Qian, X.-H. Peng, D. O. Ansari, Q. Yin-Goen, G. Z. Chen, D. M. Shin, L. Yang, A. N. Young, M. D. Wang and S. Nie, *Nat. Biotech*. **2008**, 26, 83–90 (In vivo tumor targeting and spectroscopic detection with surface-enhanced Raman nanoparticle tags.)
[10] T. Niidome, M. Yamagata, Y. Okamoto, Y. Akiyama, H. Takahashi, T. Kawano, Y. Katayama and Y. Niidome *J. Control. Rel*. **2006**, 114, 343-347 (PEG-modified Au-nanorods with a stealth character for in vivo applications)
[11] P. Diagaradjane, A. Shetty, J. C. Wang, A. M. Elliott, J. Schwartz, S. Shentu, H. C. Park, A. Deorukhkar, R. J. Stafford, S. H. Cho, J. W. Tunnell, J. D. Hazle and Sunil Krishnan, *Nano Lett*. **2008**, 8, 1492-1500 (Modulation of in vivo tumor radiation response via gold nanoshell-mediated vascular-focused hyperthermia: characterizing an integrated antihypoxic and localized vascular disrupting targeting strategy)
[12] D. Álcantara Parra, PhD Thesis, Sevilla, **2008**. (Diseño y síntesis de gliconanopartículas magnéticas. Aplicaciones como agentes de contraste en resonancia magnética de imagen)

second series of experiments, we also tested the Gd-GNPs prepared by the "stepwise" ligand place exchange reaction because this method has shown to assure the reproducibility of the content of Gd in the GNPs. We have also monitored the biodistribution and toxicity of both $GlcC_5S$-Au-SC_{11}DO3A-Gd GNPs in real-time (dynamic) and *post-mortem* MRI experiments.

1. Results

1.1 *In vivo* imaging of glioma and whole-body biodistribution after injection of $GlcC_5S$-Au-SC_{11}DO3A-Gd GNP prepared by "direct" synthesis

As reported in detail in Chapter 1, the $GlcC_5S$-Au-SC_{11}DO3A-Gd GNPs prepared by "direct" synthesis contains 6.1% of Gd(III) and shows longitudinal relaxivity values of r_1= 6.2 $s^{-1}mM^{-1}$ at 1.4 T (60 MHz). The values of the GNPs previously prepared by direct synthesis were 2.5% of Gd(III) and r_1= 3.1 $s^{-1}mM^{-1}$. [4], [12] The GNPs prepared in this Thesis by the direct method (r_1= 6.2 $s^{-1}mM^{-1}$) have been tested to image *in vivo* a generated glioma in mice in collaboration with the "Grup d'Aplicacions Biomèdiques de la RMN (GABRMN)" and their biodistribution and toxicity in imaged mice have been evaluated in collaboration with the group CIBBIM-Nanomedicine at the Vall d'Hebron Hospital both groups at the Universitat Autònoma de Barcelona.

MR Imaging of glioma in mice. GL261 murine glioma cells were used to generate the tumour by stereotactically injection into the brain of six female C5BL/6 mice of 18-20 weeks and 20-25 g weight following an established protocol. [3], [13] The monitoring of tumour growth by T_2-MR images demonstrated the expected increase in tumour size and gross morphology over 10 days post-inoculation of GL261 cells (Figure 3.1, left).

Once the tumors reached the desire volume, three animals were injected with Dotarem® and other three animals with $GlcC_5S$-Au-SC_{11}DO3A-Gd. One mouse that was not inoculated with GL261 cells was used as negative control in this study. The paramagnetic probes were injected into mice in tail vein as a bolus (72-84 μL, 0.04 mmol Gd/Kg, 10-15 sec duration) for Dynamic Contrast Enhanced (DCE)-T_1 MRI studies.

[13] S. Cha, G. Johnson, Y. Z.Wadghiri, O. Jin, J. Babb, D. Zagzag and D. H. Turnbull, *Mag Reson Med.* **2003**, 49:848-855 (Dynamic, contrast-enhanced perfusion MRI in mouse gliomas: correlation with histopathology).

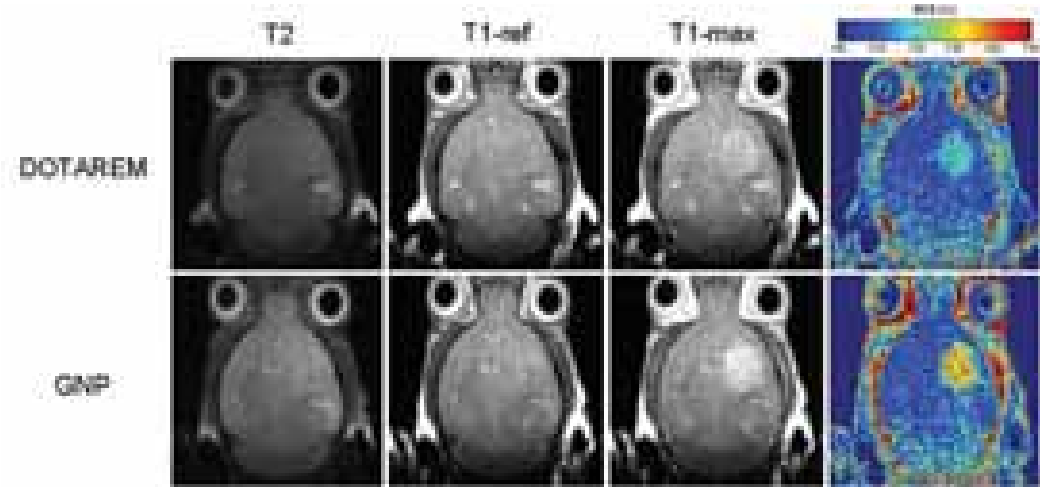

Figure 3.1: *From left to right, representative axial T_2-weighted images (Rapid Acquisition by Relaxation Enhancement (RARE) sequence was used) at 7 T (69x69 µm/pixel); DCE-T_1 images (T_1-ref vs T_1-max, 138x138 µm/pixel) and RCE maps of two mouse brains bearing a GL261 glioma, one studied with DOTAREM® (top row) and the other with $GlcC_5S$-Au-SC_{11}DO3A-Gd "direct" method) (bottom row). T_1-ref images were acquired before injecting the contrast agent bolus, while T_1-max images correspond to the point of maximum contrast enhancement (3 minutes after injection) after DOTAREM® or GNP administration. All processing and post-processing of DCE-T_1 images was carried out with IDL (RSI, France) home written scripts, as described [14]. Maps that translated the maximum contrast enhancement at each pixel of the FOV at the time of maximum enhancement were also generated.*

Both Dotarem® and $GlcC_5S$-Au-SC_{11}DO3A-Gd injected mice showed positive contrast enhancement on T_1-weighted images at 7 T (T_1-ref *vs* T_1-max; Figure 3.1, middle). T_1-max was obtained 3 min after injection. The Gd-GNPs showed a significantly ($p<0.0001$) higher enhancement in GL261 tumours (123.8±3.8 %) as compared to Dotarem® (113.1±2.5 %) at the same Gd (III) concentration, as it is shown in the Relative Contrast Enhancement (RCE) maps (Figure 3.1, right). Figure 3.2 shows the time-course data obtained with the quantification of RCE in T_1-weighted images. Both signals decrease constantly during the time the images were taken (35 min). On the contrary, surrounding contralateral non-tumoral areas of the mice brain remain practically constant for 35 min after GNP or Dotarem® injection.

[14] E. Rodriguez, R. V. Simões, A. Roig, E. Molins, N. Nedelko, A. Slawska-Waniewska, S. Aime, C. Arús, M. E. Cabanas, C. Sanfeliu, S. Cerdán and M. L. García-Martín,. *Magn. Res. Mater. Phys.* **2007**, 20, 27-37 (An iron-based T_1 contrast agent made of iron-phosphate complexes: in vitro and in vivo studies).

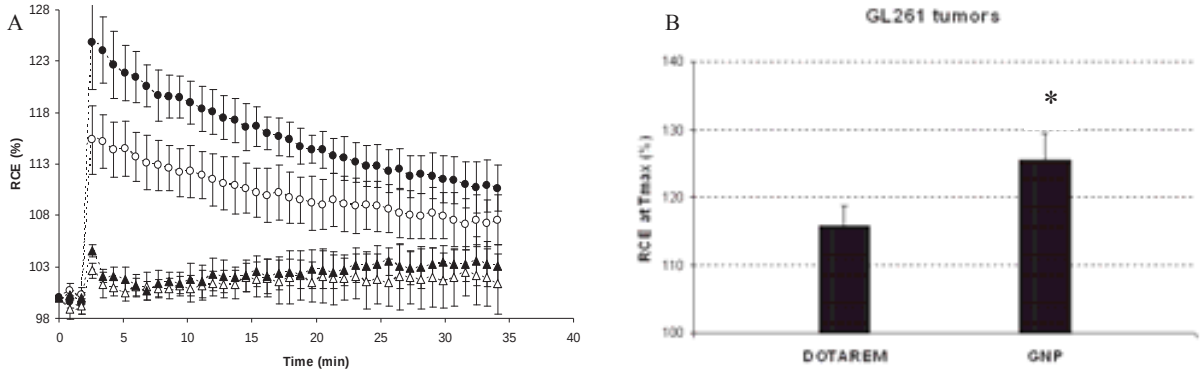

Figure 3.2: *A) Relative contrast enhancement (RCE) time-course curves obtained from the quantification of dynamic contrast enhanced (DCE)-T_1 images. Each curve displays the average contrast enhancement obtained for each group (Dotarem®, open symbols; Gd-GNP, filled symbols) in both tumour (circles) and surrounding contralateral non-tumoral areas (triangles). Values correspond to the results obtained from 3 animals/group and 3 slices/animal, i.e. n=9 independent measurements/group. B) Relative contrast enhancement (RCE) at the time of maximum enhancement (3 min after injection) between the two groups of animals studied (Dotarem®, 113.1±2.5 %, or Gd-GNP injection, 123.8±3.8 %). The contrast enhancement obtained with the Gd-GNP is significantly higher than that obtained with Dotarem® (* p < 0.001).*

Table 3.1: *Values obtained with DCE-T1 MRI studies carried out with GL261 mice. RCE at maximum and standard deviation. Number of observations in each case n=3 with 3 slices/animal, i.e. n=9 independent measurements/group. * = p<0.001 in comparison with DOTAREM values.*

Injected compound	Mean RCE at T_1-max (%)	SD
DOTAREM	113.14	2.47
$GlcC_5S$-Au-SC_{11}DO3A-Gd	123.77*	3.82

Biodistribution and toxicity of $GlcC_5S$-Au-SC_{11}DO3A-Gd in tumour injected mice. For the biodistribution and toxicity studies, 4 mice (3 orthotopically injected and 1 wild type) were administered with 0.04 mmol Gd/Kg of GNP (Group 1, animals 1.1 to 1.4). Two mice did not receive any orthotopical injection nor contrast agent (Group 2, animals 2.1 to 2.2). Twenty-four hours after GNP injection and imaging, urine samples were collected. Then, mice were anaesthetized and blood was extracted by cardiac puncture and collected in tubes without anti-coagulants. Main organs (liver, spleen, kidney, lung, brain, and tumour) were collected, pictured, weighted and fixed in formalin (non-buffered) and frozen. All formalin fixed samples were paraffin embedded. Paraffin blocks containing spleen, liver and kidneys were cut (4 μm) and Haemotoxylin-Eosin (HE)-stained, for histological evaluation.

Blood samples were centrifuged (10 min, 2000 rpm) and serum was frozen until biochemical evaluation. In total 10 parameters were evaluated (BUN, CREA, CA, PT, ALB, ALT, AST, ALP, BIL and GLU) using a dual wavelength reflectometer with end-point and kinetic assays (Spotchem EZ) at the Vall d'Hebron's Animal Facility. Gold content was determined in some of the frozen samples (blood, liver, spleen, kidney, brain, tumor and lungs) by inductively coupled plasma mass spectrometry (ICP-MS), at the Unitat de Analisis Metalics of the Universitat de Barcelona.

Macroscopical examination of the organs did not show any significant lesion or tissue-specific gold accumulation in any of the animals (Figure 3.3)

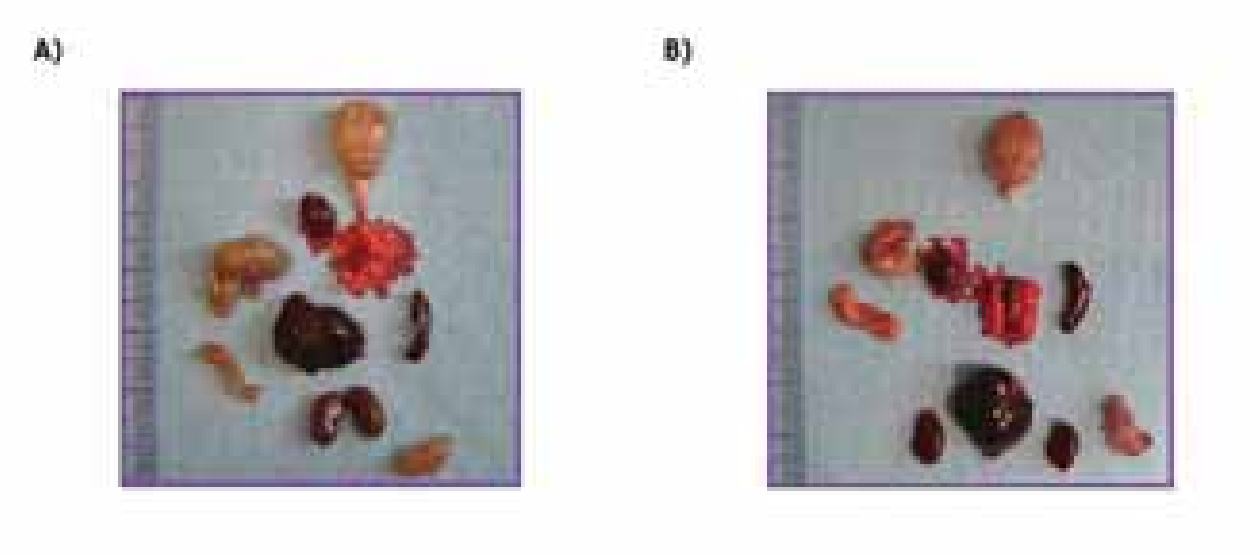

Figure 3.3. ***Macroscopical evaluation of organs corresponding to GNP-administered mice.*** *Pictures showing the macroscopical appearance of collected tissues in a mouse bearing a GL261 tumour –see localization of the tumour in the right hemisphere (**A**) and a control mouse (**B**), both injected with 0.04 mmol of Gd/Kg of GNP. Liver of both animals show a darker colour than usual, but no difference was observed by visu when comparing to non-injected animals.*

Histology examination showed some unspecific alterations in the liver of most of the animals of both groups, such as moderate lipid degeneration and the presence of golden pigment inside the cells of the mononuclear phagocytic system of the liver. The same pigment was also found in the spleen. No difference was found between GNP-administered and control animals. The rest of the organs observed did not present any significant lesion (Figure 3.4).

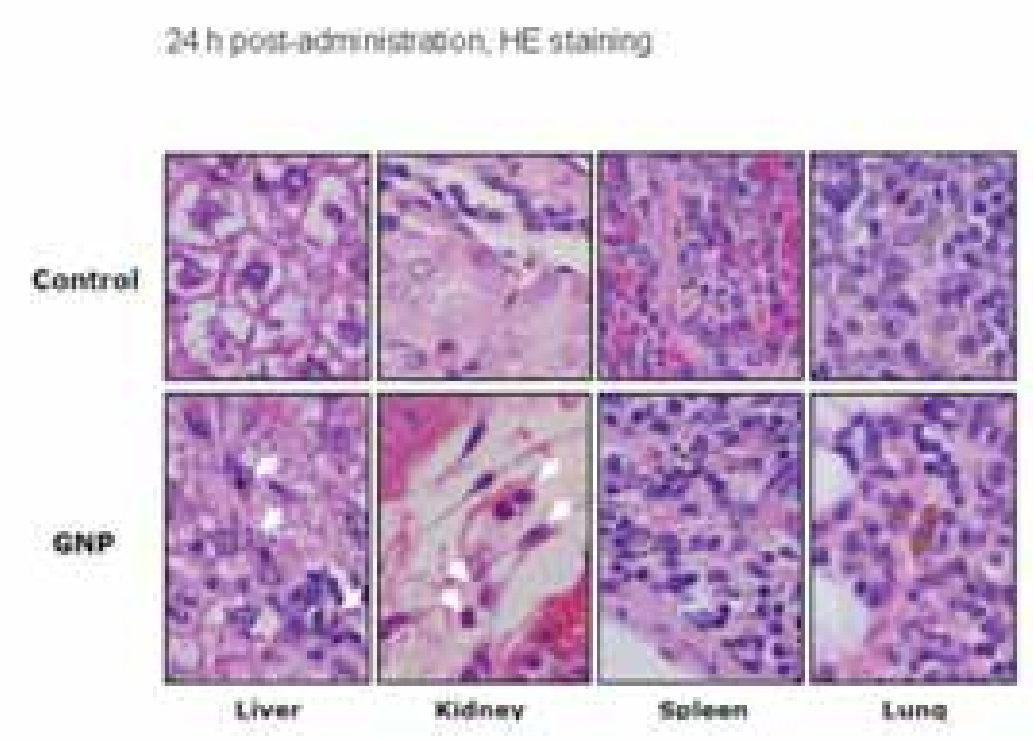

Figure 3.4. *Haematoxilyn-Eosin (HE) staining of liver, kidney, spleen and lung 24 hours post-adimistration of GNP to tumoural mice. No difference is observed between GNP-administered and control animals.*

The toxicological profile of the Gd-GNP was also performed. Renal function was assessed measuring blood urea nitrogen (BUN) (i. e. a measurement of the nitrogen in the blood in the form of urea) and creatinine (CREA). Hepatic function was evaluated using aspartate transaminase (AST), alanine transaminase (ALT), alkaline phosphatase (ALP), total bilirubin (BIL), albumin (ALB) and total proteins (TP) values. Serum glucose (GLU) and calcium (Ca) were also determined (Table 3.2). All these results need to be interpreted with caution because the machine used for serum determinations (Spotchem EZ) was still being optimized at the moment of the analysis. Among all studied parameters ALB and ALT showed considerably low values, in both GNP-treated and control animals. These results are probably due to the lack of sensitivity of the machine (Spotchem EZ), and were not related with the experimental procedure. Samples of animals G1.1 and G2.1 were not evaluated because not enough serum was obtained from blood extractions or because the high hemolyzation of the sample advised against its analysis. Among all studied parameters ALB and ALT showed considerably low values, in both GNP-treated and control animals. These results are probably due to the lack of sensitivity of the machine (Spotchem EZ), and were not related with the experimental procedure.

Table 3.2*: Results of the analysis of 10 different biochemical parameters in serum of mice injected with Gd-GNPs*

Animal			Biochemical parameters									
	Tumour	Gd-GNP	BUN (mg/dL)	CREA (mg/dL)	AST (UI/L)	ALT (UI/L)	ALP (UI/L)	BIL (mg/dL)	TP (g/dL)	ALB (g/dL)	GLU (g/dL)	Ca (g/dL)
G1.2	+	+	25	1.1*	106	17	71	0.4	4.3	2.3	141	8.3
G1.3	+	+	22	0.6	415	36	58	0.7	4	<1*+	246*	7.6
G1.4	-	+	18	0.6	<10*+	<10+	67	<0.2+	3.8	<1*+	260*	6.7
G2.4	-	-	21	0.8	109	<10+	143	<0.2+	4.2	<1*+	190	<3*+

Reference values from reference 15.
(*) Data outside reference standards.
(+) Values denoted with a "minor than" sign (<) indicate that the obtained values are below the detection limit of the machine used for determinations.
BUN: blood serum urea, CREA: creatinine, AST: aspartate transaminase, ALT: alanine transaminase, ALP: alkaline phosphatase, BIL: bilirubin, TP: total proteins, ALB: albumin GLU: glucose, and Ca: calcium.

Two out of four animals showed hyperglycemia. This is a very unspecific result and cannot be related to the administration of the GNP. Also, food intake of the animals was not controlled before their sacrifice and this could have contributed to the high variability on the GLU values among different animals. The rest of the values fell within the reference values.

Analysis of the gold content by ICP-MS in different tissues was used as a way to track Gd-GNPs biodistribution. By this technique gold content in blood of non-administered mice (Group 2) resulted bellow its detection limits (0.05 ppm) indicating that all gold content in GNP-administered mice (Group 1) was due to nanoparticles accumulation. The amount of Au in blood, liver, spleen, kidney, lung, brain, and tumour was determined in the tumoral mice. Tissue biodistribution of Au twenty four hours post-administration indicates that Au is mainly accumulated in the spleen and liver (Figure 3.5). This may probably indicates the retention of gold nanoparticles in the reticule-endothelial system (RES). Nanoparticle quantities in blood remained low (3.46 ± 1.04 ppm) as well as the nanoparticle content in brain and tumour (0.71 ± 0.54 ppm and 6.80 ± 2.51 ppm, respectively) (Figure 3.5). Contrast agent accumulation in tumours was found to be twice higher than in blood and almost 10 times higher than in the normal contralateral hemisphere. The latter result indicates that the GNP tends to accumulate in the tumours due to enhanced permeability and retention (EPR) and/or to carbohydrate-mediated targeting.

[15] C. Mazzaccara, G. Labruna, G. Cito, M. Scarfò, M. De Felice, L. Pastore and L. Sacchetti1, *PLoS ONE* **2008**, 3, e3772 (Age-Related Reference Intervals of the Main Biochemical and Hematological Parameters in C57BL/6J, 129SV/EV and C3H/HeJ Mouse Strains).

A B

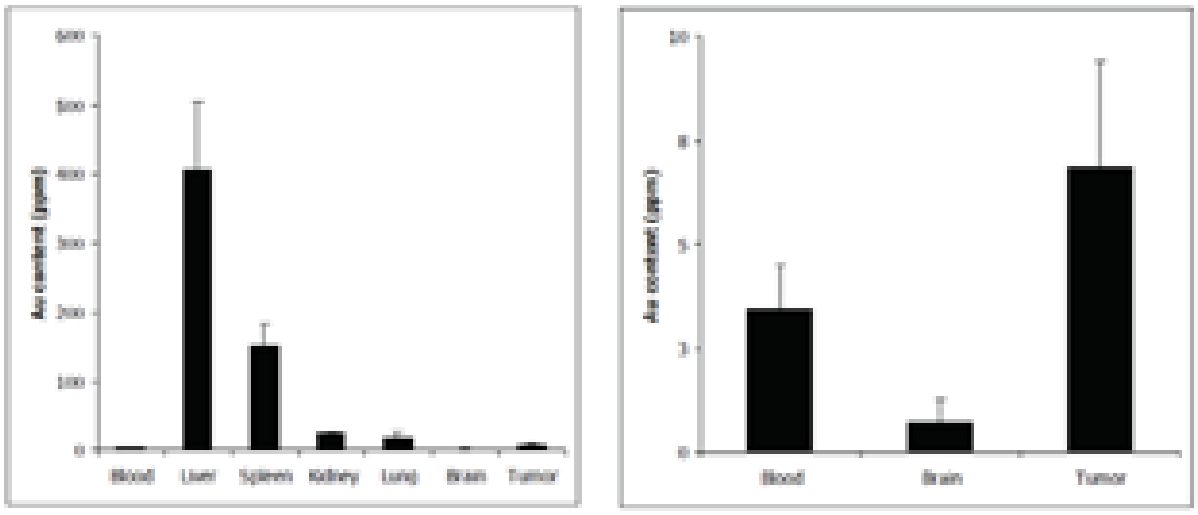

Figure 3.5. *Gold biodistribution as measured by ICP-MS 24 hours post-administration. A) Among all organs analyzed liver and spleen showed the higher gold accumulation (~400 ppm and 150 ppm, respectively). Gold was accumulated in brain and brain-tumours less (< 7 ppm) than in other organs.* ***B)*** *Expansion of selected organs indicates that gold content in tumors was almost 10 times than in the contralateral brain. Values correspond to the results obtained from n=3 animals.*

Excretion, biodistribution, and toxicity assay of $GlcC_5S$-Au-SC_{11}DO3A-Gd injected in healthy mice. To clarify further the biodistribution of Gd-GNPs and how they are eliminated from the body, imaging of the whole body, longitudinal biodistribution and toxicity assays of the $GlcC_5S$-Au-SC_{11}DO3A-Gd were carried out in C57BI/6J healthy mice. The idea was to check: (i) whether the accumulation of Gd (III) corresponds to that observed in the images; and (ii) whether the accumulation of both metals (Au and Gd) follows the same biodistribution pattern.

Seventeen mice were divided in three different groups (G1, n=5; G2, n=6; and G3, n=6) and biodistribution and toxicological profile experiments were performed. In each group, half of the mice were administered with 0.04 mmol Gd/Kg of GNP in PBS, and the other half with the vehicle (PBS) in the tail vain (i.v.). Animals in G1 (2 GNP-treated and 3 PBS-treated) and G2 (3 GNP-treated and 3 PBS-treated) were administered and sacrificed after 1h and 48 h post-administration, respectively. Animals in G2 were maintained in metabolic cages during 48 h post-administration in order to collect urine and faeces. Animals in G3 (3 GNP-treated and 3 PBS-treated) were administered and imaged by whole-body MRI i) immediately post-administration, ii) 48 h, and iii) 14 days post-administration (see Figure 3.7). Afterwards, the animals were sacrificed and tissue sampling on this group was also performed. In all cases, urine in bladder was

collected and blood was extracted by cardiac puncture. Main organs (liver, spleen, kidney, brain, lungs, heart, pancreas, stomach, intestines and calf muscle) were collected, pictured and weighted. *Macroscopical evaluation* of necropsies mice revealed darker livers in GNP-injected animals of G2 (sacrificed at 48 hours) comparing to control animals. We did not observe any other lesion or significant differences between treated and control animals.

In the *biochemical parameters* of blood plasma samples no significant differences were observed between animals treated with GNP and those that received vehicle, indicating that GNP administration of 0,04 mmol Gd/Kg of GNP did not induce a significant impairment of the renal or hepatic function (data not shown).

Haematoxilyn-Eosin (HE), Silver Enhacement and Prussian Blue staining were used to performed *histopathology studies*. Haematoxilyn-Eosin (HE) is the commonly used staining for histopathology studies. Silver enhancement staining is used for detection of gold and reveals GNP deposits as black to dark brown deposits due to their content in this metal. Prussian blue staining, which is used for detection of iron containing deposits, labels the hemosiderin (containing mainly iron) with a brilliant blue staining. These stains allow the differentiation between gold deposits and hemosiderin both seen as light or dark brown granulated areas in HE stained samples.

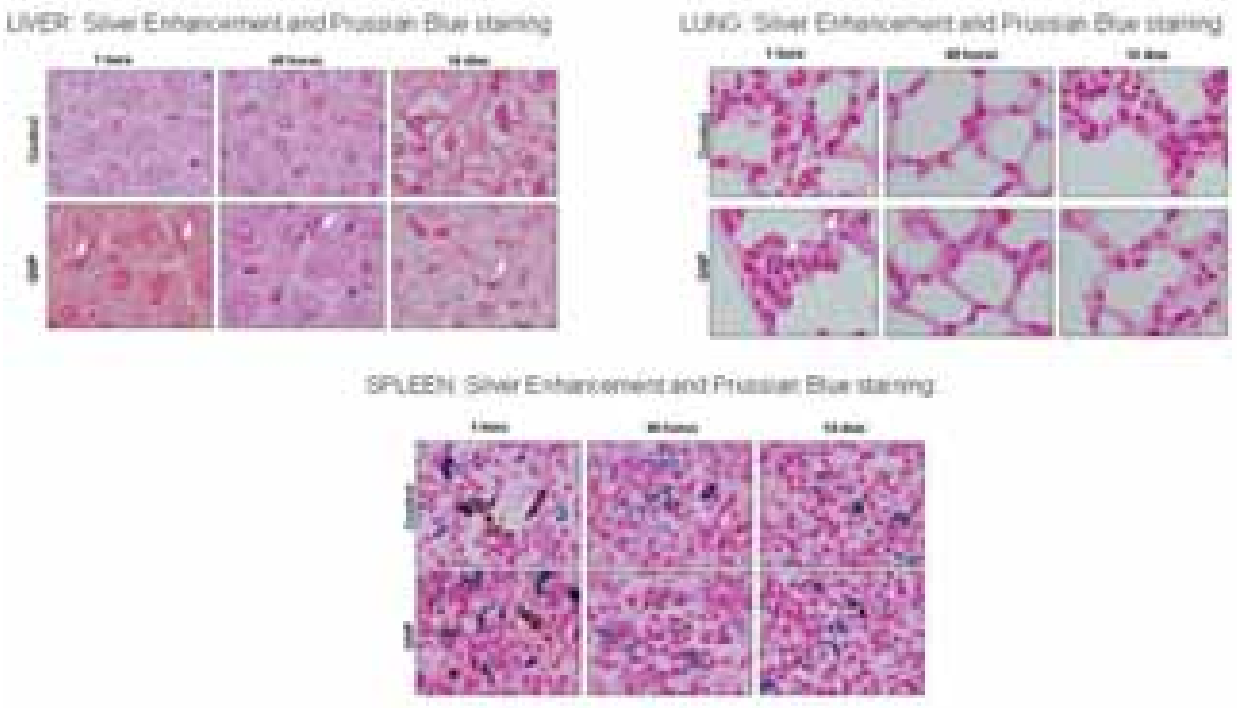

Figure 3.6. *Silver Enhancement and Prussian Blue staining of liver, spleen and lung 1 hour, 48 hours and 14 days post-administration of GNP.*

The histological evaluation reveals no major lesions in liver, kidney, spleen and lung. However, silver staining combined with Prussian Blue staining confirms that liver and spleen contain gold deposits, mainly located inside Kuppfer and inflammatory cells (Figure 3.6). Analyzing organ by organ, the general structure of liver in control animals is normal as well as in the animals injected with the GNP. In the latter, round to oval granules of dark-brown pigment primarily located inside Kupper cells cytoplasm were observed (white arrows). The structure of spleen of control and GNP injected animals is normal. Granules and large aggregates of yellowish-brown pigment were found in both groups. In the case of lung, the general structure of the organ is normal.

Whole-body MR images of one mouse (G3) were taken at different time points (1 h, 48 h and 14 days) after Gd-GNP injection in order to check the Gd (III) accumulation in organs. High contrast enhancement is especially detected in the bladder after 1 h indicating clearly that Gd is being excreted through the urine (Figure 3.7). However, no contrast enhancement was observed in the liver, concluding that no high levels of the paramagnetic ion are found in this organ, at least not enough to see contrast in MRI. At 48 h, most contrast is lost also in the bladder indicating that the animals are able to excrete the Gd-GNPs.

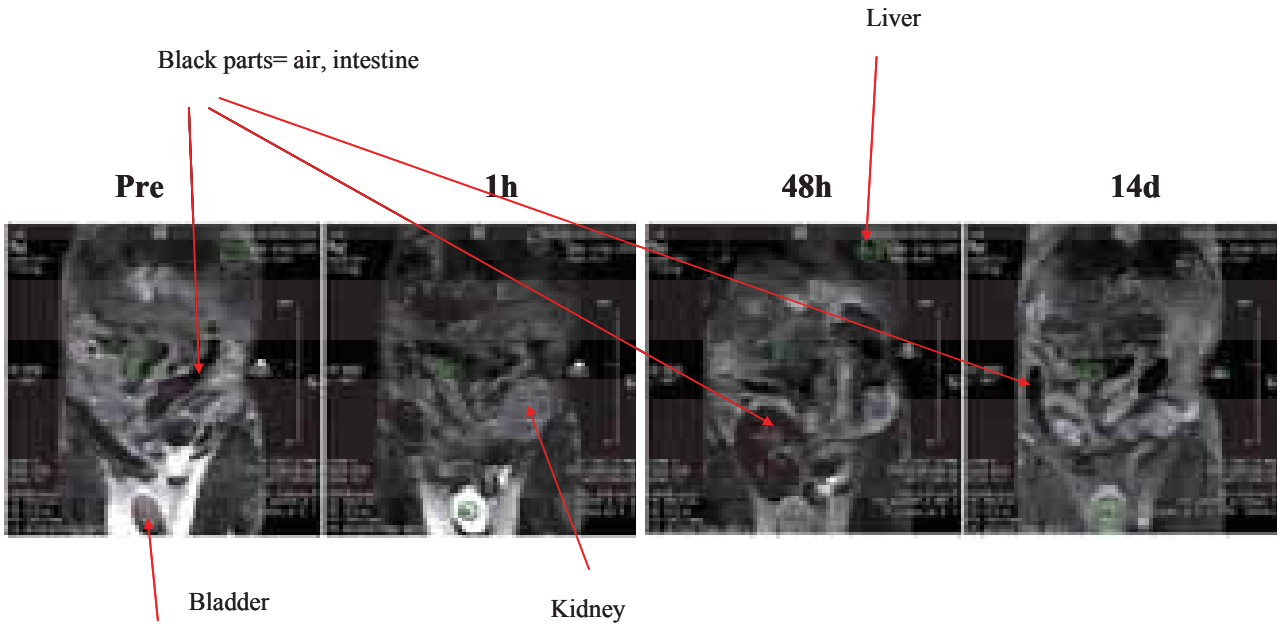

Figure 3.7. *Whole-body axial T_1-weighted MR images (Multi-slice multi-echo (MSME) sequence) at 7 T (234 x 234 µm/pixel) of one mouse before the injection of Gd-GNP (***Pre***) and 1 hour, 48 hours and 14 days post-administration of GNP.*

As images give only a qualitative indication of the contrast distribution, we have also determined *the accumulation of the Au and Gd in the same organ by ICP-MS/ICP-OES*. Gold content in blood of GNP non-administered mice resulted below its detection limits (0.05 ppm) indicating that all gold content in GNP-administered mice was due to nanoparticle accumulation. Two other experiments with Group 1 (sacrificed 1 h after injection) and with Group 3 (sacrified 48 h after injection) were performed to quantify the amount of Au and Gd(III) accumulated in blood, liver, kidney and urine. Figure 3.8 shows that plasmatic gold concentration was around 13 % of the injected dose (ID) 1 h post-administration. Gold content in plasma samples collected 48 h and 14 days post-administration was extremely low, indicating that gold nanoparticles were rapidly cleared from the blood. Among all the samples analyzed, liver was, by far, the organ with the highest gold content. One hour after administration gold found in liver represented 30% of ID. The content of gold slightly increased 48 h post-administration and was maintained two weeks after administration. These results are in agreement with the dark granules found in liver Kupffer cells of GNP treated mice.

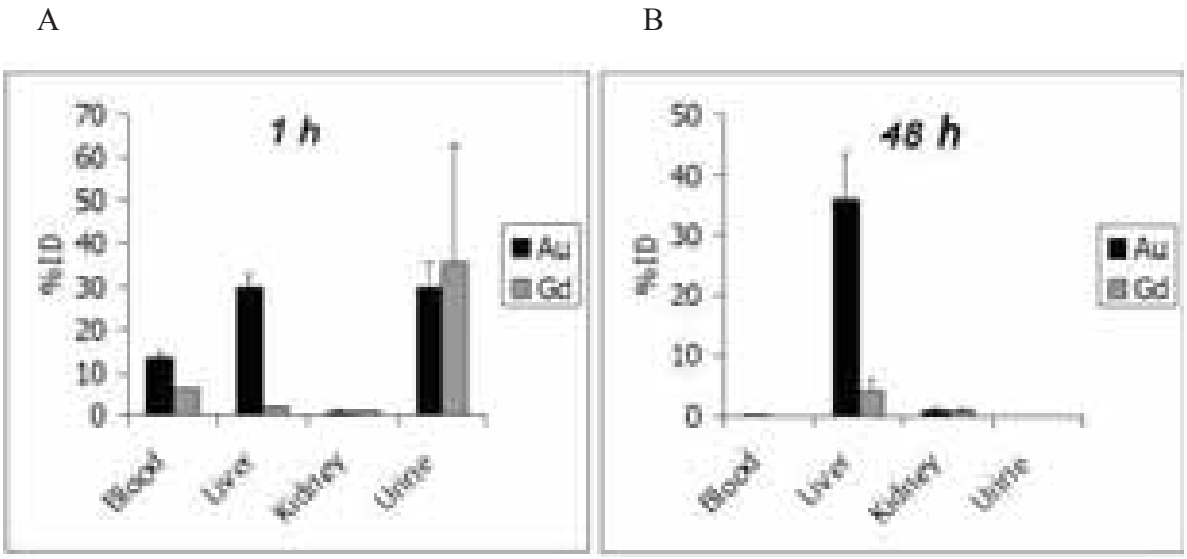

Figure 3.8. *Au and Gd (III) biodistribution as percentage of the GNPs injected dose (ID) per tissue. The results showed less accumulation of Gd (III) in the liver related to gold (A and B). The accumulation of Au in this organ remains high even after 48 hours post-administration (B).*

With respect to other organs analyzed, only spleen contained gold doses above 1% ID. As for the liver, gold content in spleen did not reduce significantly with the time. On the other hand, 1h post-administration lungs contained 0.93 % ID (data not shown), probably due to the presence of GNP aggregates in circulation that are entrapped in lung capillaries. However, this percentage tent to reduce with the time. Other organs such us pancreas, hearth, intestine or muscle did not show

significant gold accumulation (data not shown). In the animals maintained in metabolic cages, up to 60% ID of gold is found in the urine after 48 h of administration, indicating that the nanoparticles are mainly excreted by the kidneys. Less than 5% ID of gold was found in the faeces. Although biliary excretion of the nanoparticles cannot be excluded, it might happen that gold concentrations found in faeces were due to cross-contamination with urine collected from metabolic cages.

Furthermore, Figure 3.8 also shows that gold is accumulated in the liver but no Gd(III). If both atoms are kept together on the same nanoparticles, the Au/Gd ratio in the liver should be around 1. However, the Au/Gd ratio obtained in this experiments are 14 and 8 at 1 h and 48 h post-administration, respectively, indicating that Gd (III) is not attached to the GNP at these time points. This contradiction may be due to the formation of weak Gd-complexes with the hydroxyl groups of the glucose and release of the Gd after *in vivo* injection.

1.2 Imaging of glioma in mice and biodistribution after injection of $GlcC_5S$-Au-SC_{11}DO3A-Gd GNPs prepared by Ligand Place Exchange (LPE)

The results obtained in the i*n vivo* and biodistribution experiments with $GlcC_5S$-Au-SC_{11}DO3A-Gd GNP synthesized by "direct" method indicate that at a time point Au and Gd tend to dissociate (Au/Gd ratio $\neq$ 1). In order to avoid this problem, we developed a more robust preparation protocol where the Gd (III) is previously chelated by the DO3A-derivative and then introduce on the gold surface by ligand place exchange reaction (LPE). $GlcC_5S$-Au-SC_{11}DO3A-Gd GNP prepared by this method (see Chapter 1) was tested *in vivo* for imaging and biodistribution similarly as described in section 1.1 for the Gd-GNPs prepared by the direct method.

Table 3.3 shows the r_1 values of Dotarem® and $GlcC_5S$-Au-SC_{11}DO3A-Gd GNP synthesized by LPE and direct method at 1.4 T and 7 T. The value obtained at 7 T for $GlcC_5S$-Au-SC_{11}DO3A-Gd is three times lower than that obtained at 1.4 T (r_1= 2.4 $s^{-1}mM^{-1}$ *vs* r_1= 7.4 $s^{-1}mM^{-1}$).

Table 3.3: *Relaxativity values at 1.4 T and 7 T*

Gd-GNP	% Gd	**1.4 T r_1 ($s^{-1}mM^{-1}$)**	**7.0 T r_1 $s^{-1}mM^{-1}$**
Dotarem®	NM	3.50	2.5
$GlcC_5S$-Au-SC_{11}DO3A-Gd (by LPE protocol)	7.0	7.4	2.4
$GlcC_5S$-Au-SC_{11}DO3A-Gd (by direct method)	6.1	6.2	NM

NM: Not measured.

Imaging of glioma in mice. GL261 murine glioma cells were used to generate the tumour as previously explained (section 1.1). The monitoring of tumour growth by T_2-MR images demonstrated the expected increase in tumour size and gross morphology over 10 days post-inoculation of GL261 cells (Figure 3.9, left).

Once the tumours reached the desire volume, three animals were injected with Dotarem® and another three with $GlcC_5S$-Au-SC_{11}DO3A-Gd as explained in section 1.1.

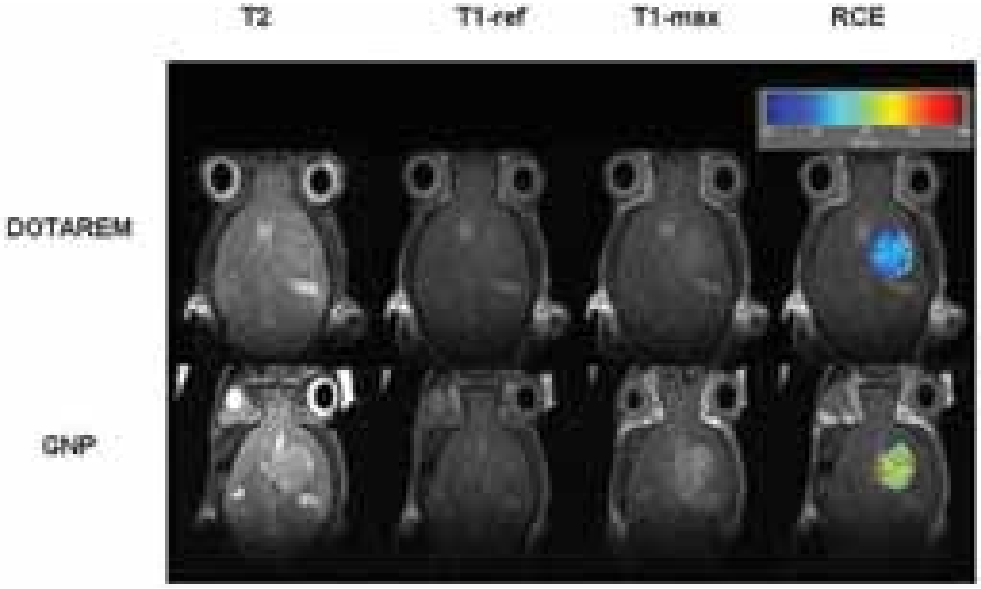

Figure 3.9: *From left to right, representative axial T_2-weighted images (Rapid Acquisition by Relaxation Enhancement (RARE) sequence was used) at 7 T (69x69 µm/pixel); DCE-T_1 images (T_1-ref vs T_1-max, 138x138 µm/pixel) and RCE maps of two mice (animal C171, top row and C532, bottom row) bearing a GL261 glioma, one studied with DOTAREM® (top row) and the other with $GlcC_5S$-Au-SC_{11}DO3A-Gd "LPE" method (bottom row). T_1-ref images were acquired before injecting the contrast agent bolus, while T_1-max images correspond to the point of maximum contrast enhancement (3 minutes after injection for DOTAREM and 6 minutes for Gd-GNP) after contrast agent administration. DCE-T1 data were processed on a platform for pharmacokinetic analysis provided by Dr. Andrés Santos, using IDL (ITT Visual Information Solutions, Boulder, CO, USA). RCE maps were calculated for each pixel as the ratio between the maximum signal enhancement and the average intensity before bolus injection. The same RCE scale was used for both cases and only pixels from the tumoural area are shown in the colour-coded right column images.*

T_1-max was obtained 3 min after injection. The Gd-GNPs obtained by LPE showed a higher enhancement in GL261 tumours (121.6±7.2 %) as compared to Dotarem® (113.1±2.5 %) at the same Gd (III) concentration, as it is shown in the Relative Contrast Enhancement (RCE) maps (Figure 3.9, right).

Figure 3.10 shows the time-course obtained with the quantification of T_1-weighted images. This difference was statistically significant at the time of maximum enhancement ($p < 0.001$) as shown in the bar chart of Figure 3.10B. Three minutes after injection (maximum enhancement) the RCE of the animals injected with GNP was 121.6 % while the animals injected with Dotarem® showed a RCE of 113.1 %. Both signals decrease constantly during the time the images were taken (35 min). On the contrary, surrounding contralateral non-tumoral areas of mice remain practically constant for 35 min after GNP or Dotarem® injection.

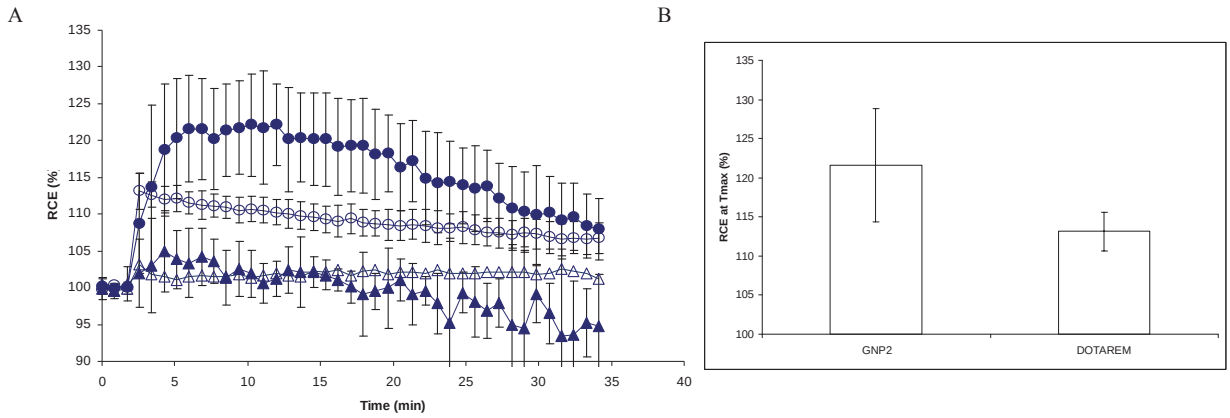

Figure 3.10: *A) RCE time-course curves obtained from the quantification of DCE-T_1 images. Each curve displays the average contrast enhancement obtained for each group (DOTAREM®, open symbols; Gd-GNP, filled symbols) in both tumour (circles) and surrounding contralateral non-tumoral areas (triangles). Values correspond to the results obtained from 3 animals/group and 3 slices/animal, i.e. n=9 independent measurements/group. B) RCE at the time of maximum enhancement (3 min after contrast agent injection for DOTAREM and ca 6 min for Gd-GNP) between the two groups of animals studied. See table 3.4 for numbers and signification.*

Table 3.4: *Values obtained with DCE-T_1 MRI studies carried out with GL261 mice. RCE at maximum and standard deviation. Number of observations in each case n=3 with 3 slices/animal, i.e. n=9 independent measurements/group. * = p=0.004 in comparison with DOTAREM values. No statistically significant differences were obtained in the comparison Gd-GNP obtained by "direct" method (table 3.1) and Gd-GNP obtained by LPE (p=0.44).*

	Mean RCE at Tmax (%)	SD
DOTAREM	113.14	2.47
$GlcC_5S$-Au-SC_{11}DO3A-Gd	121.62*	7.21

Biodistribution and toxicity of GlcC5S-Au-SC$_{11}$DO3A-Gd in tumour injected mice. After *in vivo* MRI assays, mice were sacrificed 24 h post GNP administration. Liver, spleen, kidneys, lung, tumour and brain were the organs analysed by ICP-MS.

Tissue biodistribution of Au 24 h post-administration indicates that Au is mainly accumulated in the spleen and liver, as in the experiments done with the GNP prepared by the "direct" method (Figure 3.11). When the %ID is compared, 24 h post-administration liver retains 28 % ID of Au and 16. % of Gd in the case of the GNP prepared by (LPE), whereas with the GNP synthesized by the "direct" method, just 1 h post-administration those numbers are 28 (± 3) % and 2. (± 0.1) %, respectively. This means, that with a similar liver retention of Au, more Gd is kept in the liver with the GNP prepared by LPE, than with the GNP synthesized by the "direct" method. Indeed, the Au/Gd ratio of the % ID in the liver is 1,75, indicating that Gd and Au coexist on the nanoparticle (Figure 3.11). ICP determinations also confirm that 24 h post-administration gold (Au) accumulates in tumour. Precisely, 15 times more Au is found in tumour than in the contralateral hemisphere, an indication of the preference of the tumour for the glucose bearing GNP.

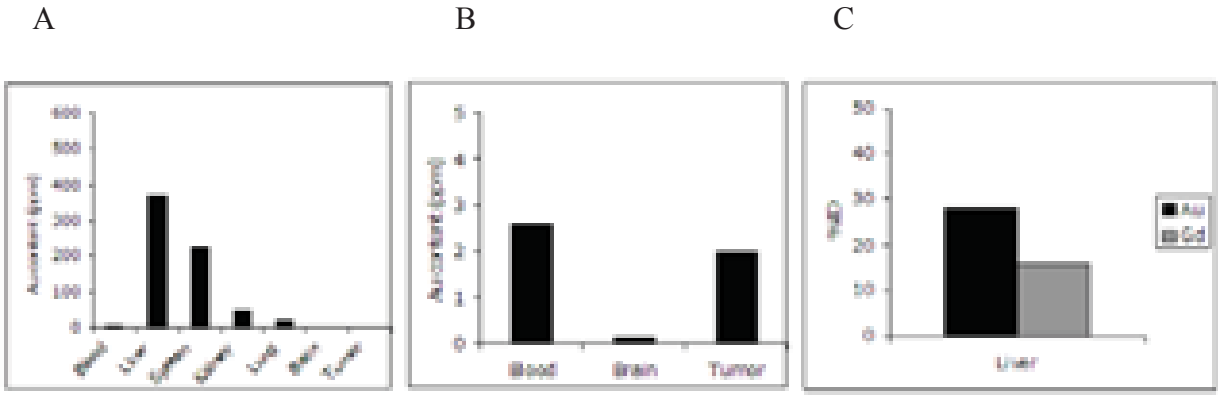

Figure 3.11: *Gd-based paramagnetic gold GNP biodistribution as measured by ICP-MS 24 hours post-administration. Among all organs analyzed liver and spleen showed the higher gold accumulation. The accumulation of gold in brain and brain-tumors is less than in other organs, but interestingly nanoparticle content in tumors was found to be almost 15 times than in contralateral hemisphere (**A** and **B** images).**C:** Au and Gd(III) GNP biodistribution as percentage of the injected dose (ID) per tissue. The results showed accumulation of Au and Gd(III) in the liver in a similar amount, indicating that they both are together in the GNP.*

Toxicological profile. As in the previous experiments, different biochemical parameters were cheeked in order to determine the toxicity of the GNP (Table 3.5). One out of four animals showed hyperglycemia. This is a very unspecific result and can not be related to the administration of the Au-GNP. Also, food intake of the animals was not controlled before their sacrifice and this could have contributed to the high variability on the GLU values among different animals.

In general, all biochemical parameters are in line with the reference values indicating correct renal function of the mice evaluated. No toxicity is observed in blood or urine parameters after 24 h administration of the GNP.

Table 3.5: *Results of the analysis of 8 different biochemical parameters in mice serum.*

Animal			Biochemical parameters									
	Time	Glc-GNP	BUN (mg/dL)	CREA (mg/dL)	AST (UI/L)	ALT (UI/L)	ALP (UI/L)	BIL (mg/dL)	TP (g/dL)	ALB (g/dL)	GLU (g/dL)	Ca (g/dL)
1	24 h	+	33.5*	0.32	106	20	NM	0*	3.22	2.5	243.9	NM
2		-	39	0.32	131	27	NM	0.1	3.97	2.6	282.1*	NM
3		-	46.2	0.35	326	36	NM	0*	3.47	2.6	210.9	NM
5		+	43	0.32	128	23	NM	0*	3.36	2.6	198.8	NM

Reference values from [15]
(*) Data outside reference standards
NM: Not measured.
BUN: serum urea, CREA: creatinine, AST: aspartate transaminase, ALT: alanine transaminase, ALP: alkaline phosphatase, BIL: bilirrubin, TP: total proteins, ALB: albumin GLU: glucose and Ca: calcium.

As in the GNP synthesized by "direct" synthesis, in the case of $GlcC_5S$-Au-$SC_{11}DO3A$-Gd GNP synthesized by LPE method, no major organ lesions are observed in the *histopathology experiments*. Silver Enhancement and Prussian Blue staining confirms that in liver and spleen of mice were gold deposits (Figure 3.12).

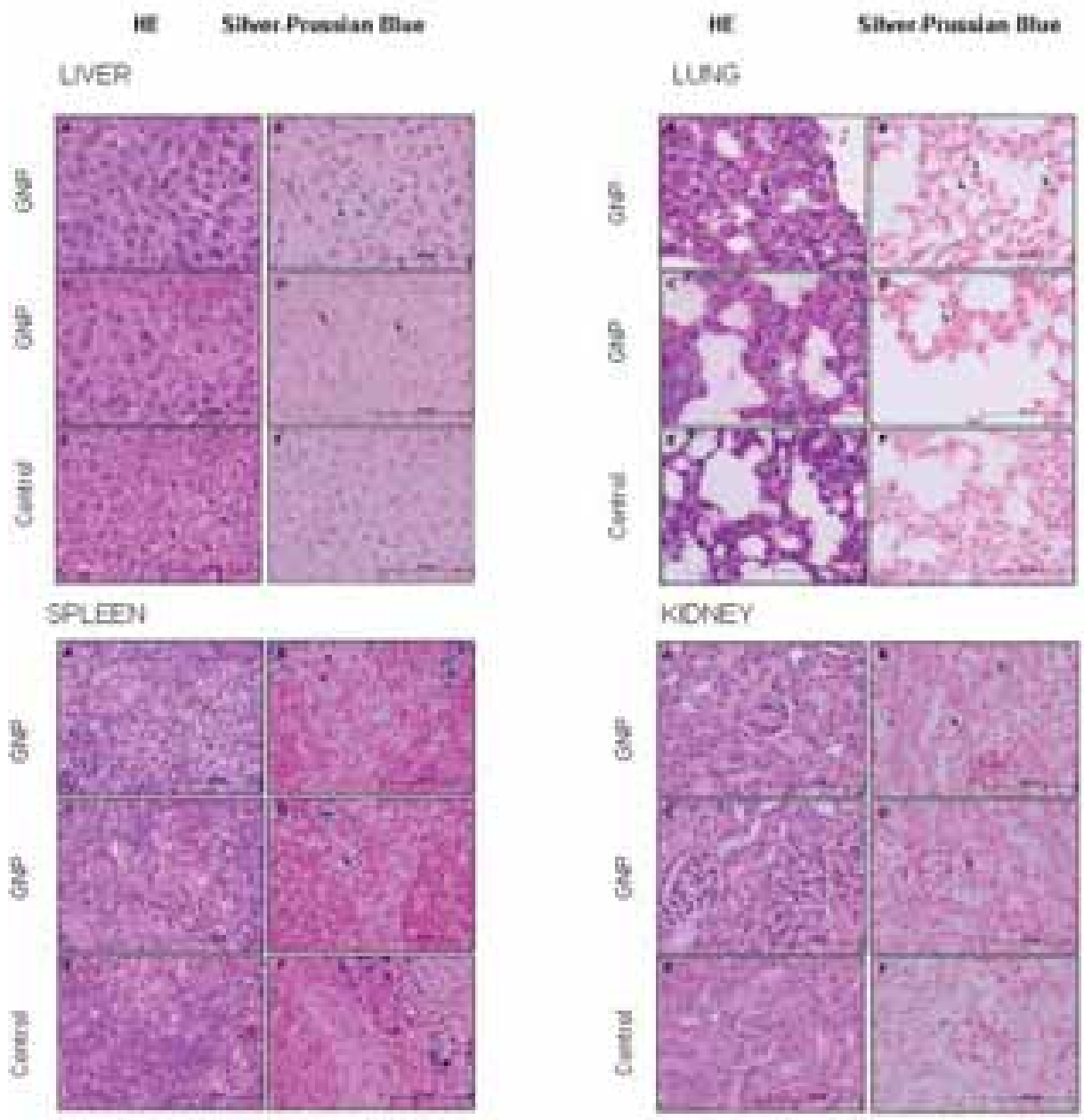

Figure 3.12: *Haematoxilyn-Eosin (HE), Silver Enhancement and Prussian Blue staining of liver, spleen, kidney and lung 24 hours post-administration of GNP. A and B are animals with higher degree of GNP deposition pattern, C and D are animals from a mild-low GNP deposition pattern and E and F are contol animals. LIVER: In A and B GNP is located intracytoplasmatic inside Kupffer cells or free in the sinusoids. C and D show middle deposition pattern (arrows). In E and F, control animals, no gold deposits are observed. SPLEEN: The Silver enhancement/Prussian Blue staining permits the differentiation between GNP (dark-brown briefringent pigmentation) and the hemosiderin (blue staining). In A and B GNP is mostly located in red, but also in white pulp, either inside the cytoplasm of macrophages (arrowhead) or free in the parenchyma (arrows). C and D show mild-low GNP deposition pattern (arrows). E and F are control animals, with no GNP deposits. LUNG: A and B are animals with mild GNP deposition pattern. C and D are animals with a very-low GNP (arrows) deposition pattern. E and F are, control animals, with no GNP deposits. KIDNEY: No dark-brown birrefrigent pigment deposition was detected in kidney sections stained with HE in any of the animals. However, few small golden deposits were identified by Silver enhancement/Prussian Blue staining. A and B are animals with low GNP deposition pattern. C and D are animals with a low GNP (arrows) deposition pattern. E and F are, control animals, with no GNP deposits. (See Appendix for further details).*

2. Discussion

Imaging of glioma in mice. Both *in vivo* experiments done with either $GlcC_5S$-Au-SC_{11}DO3A-Gd prepared by the "direct" method or by ligand place exchange (LPE) method showed good tumour contrast comparing to Dotarem®. Contralateral non-tumoral areas of mice brain did not show any contrast when GNPs or Dotarem® were injected, indicating that the accumulation of the contrast agent takes place in the tumour, probably due to the compromised BBB in grade IV GL261 tumors, which causes a much higher permeability of the tumor as compared to contralateral part of brain, and higher glucose uptake by tumour cells.

The Gd-GNP prepared by LPE did not show better contrast than those obtained by the "direct" method. No statistically significant differences were obtained when both Gd-GNPs were compared (tables 3.1 and 3.4).

Biodistribution. The most remarkable result obtained with the GNP prepared by the **"direct"** method is that GNP biodistribution assays demonstrated that tumors accumulated ten times more contrast agent than non-tumoral contralateral hemisphere, and twice the amount in circulating blood. Twenty-four hours after contrast administration, almost 50% of the administered gold content is concentrated in liver and spleen and, in less extend, in lung and kidneys, confirming the data published in the literature regarding small gold nanoparticles for humans. [16] The elimination of the GNP by kidney is indirectly shown in the results obtained 1 hour post-administration; the amount of gold and gadolinium in urine is ~30% and ~40% of the injected dose, respectively (Figure 3.8). This result is further confirmed by the whole body MR image 48 hours post-administration of Gd-GNPs, where no contrast is seen in the bladder indicating excretion of the GNP (Figure 3.7).

The results obtained when the Gd-GNP was injected in a healthy mouse confirm that in the brain of a sane mouse the accumulation of GNP is one order of magnitude lower than in the tumoral brain (see Appendix III). It is also worth to comment the different accumulation of gold and gadolinium in liver 1 h and 48 h after injection in the healthy mice (Figure 3.8). The high ratio of Au/Gd in the liver after 1 h and 48 h of GNP injection was 14 and 8, respectively, suggesting that Gd was release from gold core and metabolized differently (Table 3.6). As it was explained in Chapter 1, when "direct" method is used to synthesize Gd-based paramagnetic GNPs having carbohydrates and DO3A derivatives, the whole nanoparticles are incubated with $GdCl_3$ to form

[16] A, S. Thakor, J. Jokerst, C. Zavaleta, T. F. Massoud and S. S. Gambhir, *Nano Lett*. **2011**, 11, 4029-4036 (Gold Nanoparticles: A Revival in Precious Metal Administration to Patients).

the Gd-complexes. The risk of this incubation is that Gd(III) could be also chelated by hydroxyl groups of the sugars. This chelating is much weaker than the one obtained with DO3A compound, so that Gd(III) could be lost through the body after injection of the GNPs in mice.

Table 3.6: *Percentages of Au and Gd in GNPs determined by ICP-MS, calculated Au/Gd ratio. and Au/Gd ratio found in the liver for $GlcC_5S$-Au-SC_{11}DO3A-Gd prepared by "direct" method and ligand place exchange (LPE) method*

.

Synthetic Methodology	% Au	% Gd	Au/Gd ratio	Au/Gd ratio in the liver[a]		
				1 h	24 h	48 h
"Direct"	34.0	6.1	5.6	14.5	NT	8.3
LPE	31.0	4.9	6.3	NT	1.75	NT

(*) *The normalized Au/Gd ratio for % of ID is 1.*
([a]) Percentages of Au/Gd (29/2 and 37/4 for "direct" and 28/16 for LPE) of the ID obtained in liver by ICP-MS.
NT: Not calculated.

In the **Ligand Place Exchange (LPE)** method, a GNP functionalized with carbohydrates (glucose in this case) is incubated with a previously formed Gd-DO3AC_{11}SH complex (see Chapter 1). By this method all the Gd (III) present in the GNP is chelated by the DO3A derivative which avoids the risk of having Gd (III) ion chelated by the hydroxy groups of the sugars. The Au/Gd ratio obtained in the liver 24 h after injection of the GNP is 1.75. This result confirms that the LPE method is better than the direct method for the preparation of robust Gd-based paramagnetic gold glyconanoparticles.

Biodistribution assays also show that the highest amount of GNP was accumulated in spleen and liver 24 h post-injection as it happened in the previous experiments with the "direct" method GNPs (Figure 3.11 and Figure 3.5). The tumoral hemisphere accumulated less gold than other organs, but the content in tumours was almost 15 times that in contralateral hemisphere, reproducing the results obtain with the GNP prepared by "direct" synthesis.

The *toxicological studies* done with GNPs prepared by the "direct" method and the one prepared by the LPE method showed no signs of acute toxicity. Adverse effects of Gd-based MRI contrast agents on cardiovascular and renal systems have been reported. [17], [18] An explanation of these

[17] H. Ersoy and F. J. Rybicki, *J. Magn. Reson. Imag.* **2007**, 26, 1190–1197 (Biochemical safety profiles of gadolinium-based extracellular contrast agents and nephrogenic systemic fibrosis).

effects can rise from the kinetic instability of the complexes when Gd (III) is chelated by open chain ligands, like DTPA. In the experiments done in this Thesis, the Gd-complex is form with a derivative of DO3A which is a cyclic chelant and its thermodynamic and kinetic stability is higher than in the open chain ligands, however, more experiments are needed to confirm that there is not free Gd(III) in the body. For this reason, we also prepared DOTA-N-(2-aminoethyl)ethanamide Gd(III)-complex derivatives, as explained in Chapter 1, in the search of even more stable Gd-complex than DO3A-complex. MRI studies with this new derivative have not still carried out.

[18] S.-P. Lin and J. J. Brown, *J. Magn. Reson. Imag.* **2007**, 25, 884–899 (MR contrast agents: physical and pharmacologic basics).

3. Experimental part

Animals and cells. Seven C57BL/6 female mice (Charles-River Labs., France) of 20-25 g weight were used in this study. Animals were obtained from Charles River Labs (France) and housed at the Animal Facility of the *Universitat Autònoma of Barcelona* (UAB, *Servei d'Estabulari*). The studies were carried out according to protocols approved by the local/institutional ethics committee, according to the regional and state legislation (protocols DARP GC 2147 and GC 3255).

The GL261 mouse glioma cell line was obtained from the Tumour Bank Repository at the National Cancer Institute, Frederick, MD, USA. Cells were grown in RPMI-1640 culture medium supplemented with 2.0 g/L sodium bicarbonate, 0.285 g/L L-glutamine, 10% foetal bovine serum and 1% penicillin-streptomycin solution. Culture medium and chemicals were purchased from Sigma-Aldrich (St. Louis, MO, USA) unless otherwise indicated. Culture plastic was obtained from Nunc.

Brain tumors. Tumours were induced in six mice by intracranial stereotactic injection of GL261 cells into the caudate nucleus, essentially as described in [13]. Briefly, analgesia was administered to each animal 15 min before the surgical procedure (Meloxicam 1.0 mg/Kg, subcutaneous). Mice were anesthetized with ketamine–xylasine (80–10 mg/Kg, intraperitoneal) and then immobilized on a stereotactic holder (Kopf Instruments, Tujunga, CA, USA). After the scull was exposed, a 1.0 mm hole was made 2.3 mm lateral (right) to the midline, as measured from the *Bregma*, using a high speed micro-driller (Fine Science Tools, Heidelberg, Germany). A 26G Hamilton syringe (Reno/NV,USA), positioned on a digital push-pull microinjector (KD Scientific, Holliston/MA, USA) was then advanced 2.3 mm from the cortical surface into the striatum, and 4 µL RPMI-1640 medium containing 10^5 GL261 cells were injected at a rate of 2 µL/min. Three to five minutes after the injection had finished, the syringe was slowly removed, the scission site closed with suture silk (5.0) and the animal left to recover in a warm environment (about 25 ºC). Analgesia was administered immediately after animal recovery (Buprenorphine 0.1 mg/Kg, subcutaneous) and 24 and 48 hours post-surgery (Meloxicam, 1.0 mg/Kg, subcutaneous).

Toxicity Studies. 24 hours after the MRI explorations, animals injected with the glyconanoparticle were sacrificed by cervical dislocation. Each animal was dissected and its liver, kidney, spleen, brain (and tumour), lungs, heart, pancreas, stomach and muscle were extracted; urine and blood

samples were also collected. All samples wereanalyzed by Induced Coupled Plasma-Mass Spectrometry (ICP-OES) at the *Unidad de Análisis Elemental* of the *Servicios Científico-Técnicos* (*Universidad de Barcelona*).

Contrast agent. The contrast agent used in the first experiments was $GlcC_5S$-Au-SC_{11}DO3A-Gd GNP synthesized by "direct" synthesis. It presented two diameters: 4.34 nm (24%) and 2.49 nm (76%). 104.36 mg of $GlcC_5S$-Au-SC_{11}DO3A were dissolved in 4.17 mL of a saline solution (NaCl 0.9%). Taking into account the ICP estimation of gadolinium (Gd) content for the GNP, the final concentration was 9.7 mM in this metallic ion and the amount administrated to each animal was 0.04 mmol Gd/Kg.

The contrast agent used in the second set of experiments was $GlcC_5S$-Au-SC_{11}DO3A-Gd glyconanoparticles synthesized by Ligand Place Exchange method. It also presented two diameters (1.5 ± 0.3 nm (75%) and 4.3 ± 0.6 nm (25%). 20 mg of $GlcC_5S$-Au-SC_{11}DO3A was dissolved in 0.8 mL of a saline solution (NaCl 0.9%). Taking into account the ICP estimation of gadolinium (Gd) content for the GNP, the final concentration was 11.12 mM in this metallic ion and the amount administrated to each animal was 0.04 mmol Gd/kg.

A commercial injectable solution of Gd (DOTAREM®, Guerbet, Roissy, France, 0,5 mmol of Gd(III)/mL) was used as a standard to compare the enhancement obtained by MRI with the glyconanoparticle. The commercial solution was administrated at the same gadolinium dose described for both GNPs.

In vivo set-up. MRI studies were carried out at the NMR facility of the Universitat Autònoma de Barcelona (Cerdanyola del Vallès, Spain), using a 7 T horizontal magnet (*BioSpec 70/30*; Bruker BioSpin, Ettlingen, Germany) equipped with actively shielded gradients (B-GA12 gradient coil inserted into a B-GA20S gradient system) and a quadrature receive surface coil, actively decoupled from a volume resonator with 72 mm inner diameter. Anesthesia was performed with isoflurane at 0.5-1.5% in O_2, maintaining the respiratory frequency between 40-60 breaths/min. Body temperature was maintained between 36.5-37.5 ºC with a recirculating water system incorporated in the animal bed, and measured with a rectal probe. Breathing rate and temperature were constantly monitored (SA Instruments, Inc., New York, USA). Before immobilization in the animal holder each of the mice was canulated in the tail vein using a home-built multi-delivery polyethylene tubing system. In this case, a 30G 2-way catheter was connected, through polyethylene tubing, to 2 independent 1 mL syringes (Becton-Dickinson S.A., Madrid, Spain)

loaded with heparinized-saline (40 U/ml) and one contrast agent, namely Glc-GNP from the "direct" method")at 9.7 mM in Gd and Glc-GNP from the LPE, 11.12 mM in Gd.

MRI acquisition. All animals inoculated with GL261 glioma cells were initially scanned for brain tumour detection (10 days after stereotactic injection) with a rapid T_2-weighted sequence, RARE (Rapid Acquisition by Relaxation Enhancement); Turbo Factor, 8; field of view (FOV), 19.2x19.2 mm; matrix (MTX), 128x128 (150x150 μm/pixel); number of slices (NS), 5; slice thickness (ST), 1 mm; interslice-thickness (IST), 1.1 mm; TR/TE, 2000/36 ms; number of averages (NA), 1; total acquisition time (TAT), 24 sec. Horizontal, coronal and sagittal reference images were acquired with this method.

T_2-weighted images with higher resolution were acquired from three horizontal sections of the brain in order to have a good morphological characterization of the tumours. The same sequence was used for this purpose (RARE) with slight modifications: FOV, 17.6x17.6 mm; MTX, 256x256 (69x69 μm/pixel); NS, 3; TR/TE, 3000/36 ms; NA, 4; TAT, 4 min 48 sec. A Dynamic Contrast Enhanced T_1 study (DCE-T_1) was then performed using the same three sections described before. For this, a MSME (Multi-Slice-Multi-Echo) sequence was used with: MTX, 128x128 matrix (138x138 μm/pixel); TR/TE, 200/8.5 ms; NA, 2; number of repetitions (NR), 41; TAT, ~35min. The contrast bolus was administered after the third repetition of the complete T_1-weighted sequence.

Processing and post-processing of MR data. DCE-T_1 data were processed on a platform for pharmacokinetic analysis recently developed within the intramural CIBER-BBN project PROGLIO by the group directed by Dr. Andrés Santos, Biomedical Image Technologies, ETSI Telecomunicación, Universidad Politécnica de Madrid, using IDL (ITT Visual Information Solutions, Boulder, CO, USA) and also with IDL (RSI, France) home written scripts, as described [19]. RCE maps were calculated for each pixel as the ratio between the maximum signal enhancement and the average intensity before bolus injection. In this way, time-course curves that quantified the average contrast enhancement inside the tumours and in surrounding non tumour-bearing areas of the brain parenchyma (defined from regions of interest, ROIs) were generated. Moreover, maps that translated the maximum contrast enhancement at each pixel of the FOV at the time of maximum enhancement were also generated (relative contrast enhancement, RCE).

[19] E. Rodriguez, R. V. Simões, A. Roig, E. Molins, N. Nedelko, A. Slawska-Waniewska, S. Aime, C. Arús, M. E. Cabanas, C. Sanfeliu, S. Cerdán and M. L. García-Martín,. *Magn Reson Mater Phy*. **2007**; 20, 27-37(An iron-based T1 contrast agent made of iron-phosphate complexes: in vitro and in vivo studies).

Statistical Analysis. A two-tailed Student's T-test for independent samples was used for statistical analysis, with $p < 0.05$ set as significance level. Measurements from the same animal but corresponding to different slices were considered as independent measurements/cases. The average contrast enhancement in the ROI inside the tumours was compared between animals injected with different contrast agents. Normality was first inspected in each group by the Kolmogorov-Smirnov test and variance homogeneity with the Levene test. For both tests, the significance level was $p > 0.05$.

MRI acquisition (biodistribution studies). All animals studied were initially scanned with a *T1*-weighted sequence, MSME (Multi slice – multi echo); field of view (FOV), 120x30 mm; matrix (MTX), 512x128 (234x234 μm/pixel); number of slices (NS), 10; slice thickness (ST), 1 mm; interslice-thickness (IST), 1.1 mm; TR/TE, 350/10 ms; number of averages (NA), 4; total acquisition time (TAT), 2m59sec. Axial whole body images were acquired with this method, before and after contrast bolus administration for the first time point (1h). The same sequence, parameters and orientation were used for each subsequent time point (24h, 48h and 14 days). A small capillary filled with Gd-GNP ("direct" method) solution at the same administered concentration was used as an internal calibration for the maximum contrast enhancement achievable in each case.

Experimental conditions for biodistribution and toxicological profile studies. At established time points after GNP injection, urine samples were collected after administering 1 ml of water by oral gavages. Then, mice were anaesthetized with isofluorane and blood was extracted by cardiac puncture and collected in tubes without anti-coagulants. Main organs (liver, spleen, kidney, brain, tumor, lungs, heart, pancreas, stomach, and calf muscle) were collected, pictured, weighted and fixed in formalin (non-buffered) and frozen. All formalin fixed samples were paraffin embedded. Paraffin blocks containing spleen, liver, lung and kidneys were cut (4 μm) and HE, Silver Enhancement and Prussian Blue staining were performed, for histological evaluation. Blood samples were centrifuged (10 min, 2000 rpm) and serum was frozen until biochemical evaluation. In total 10 parameters were evaluated (BUN, CREA, CA, PT, ALB, ALT, AST, ALP, BIL and GLU) were assessed using standard techniques. Gold content was determined in some of the frozen samples (blood, liver, spleen, kidney, brain, tumor and lungs) by inductively coupled plasma mass spectrometry (ICP-MS).

CONCLUDING REMARKS

CONCLUDING REMARKS

- A new protocol based on Ligand Place Exchange (LPE) method for the preparation of paramagnetic Gd-based gold glyconanoparticles has been used to obtain a small library of well-reproducible Gd-GNPs. Gd-GNPs incorporating monosaccharides (glucose, mannose, and galactose) or disaccharides (lactose, cellobiose, and maltose) have been prepared. The LPS method ensures the correct chelation of the paramagnetic ion in Gd-GNPs in comparison with the so-called "direct" method

- The Gd-GNPs have been completely characterized by TEM, UV-Vis, IR, ^{1}H-NMR and inductively coupled plasma atomic emission spectroscopy (ICP-AES). In addition, one of the GNPs ($GlcC_5S$-Au-$SC_{11}DO3A$-Gd) was characterized by Z-potential, ^{17}O-NMR and Proton Nuclear Magnetic Relaxation Dispersion (^{1}H-NMRD) spectroscopy.

- Longitudinal (T_1) and transversal (T_2) relaxation times of the Gd-GNPs have been measured in water solution at different concentrations in order to calculate the relaxivity values (r_1 and r_2) on the basis of the Gd(III) content of each paramagnetic GNP. Differences in relaxivity values up to two times were observed by changing the nature of the sugar and the relative position of the sugar with respect to the Gd(III).

- Gd-GNPs bearing glucose, mannose or galactose were applied for the selective labeling of cells sugar receptors (lectins) by MRI. Burkitt lymphoma cells (Raji and Raji-DC-SIGN), hepatocytes (HepG2), and murine glioma cells (GL261) were incubated with Gd-GNPs. Raji-DC-SIGN expresses the lectin DC-SIGN which specifically recognizes oligomannosides and Lewis blood group antigens. HepG2 cells express the β-galactose/*N*-acetylgalactosamine binding lectin named asialoglycoprotein receptor. GL261 have been used to generate the glioma in mice for the *in vivo* evaluation of the Gd-based glyconanoparticles. From the T_1-weighted images, it is evident that Gd-based paramagnetic gold GNPs can work as selective T_1-reporters of cellular receptors depending on their sugar coating.

- Multimerization of carbohydrates on the gold nanoparticles allows the enhancement of the contrast in T_1-weighted images of cells by increasing the local concentration of sugars and the affinity for the corresponding receptor

- *In vivo* experiments to image glioma in mice have been carried out using $GlcC_5S$-Au-SC_{11}DO3A-Gd GNP obtained either by "direct" synthesis or by LPE methodology. In both cases a great enhancement of the T_1 contrast in glioma was observed.

- The evaluation of the biodistribution and toxicological profile show that the glyconanoparticles are mainly excreted by kidneys, although some accumulation in liver occurs. However, no significant impairment of the renal or hepatic function is induced. ICP determinations Au/Gd (III) ratio in liver of animals injected with Gd-GNPs prepared by "direct" and LPE methods indicated that the LPE one ensures a better Gd (III) chelation than the "direct" synthesis.

- The preparation, characterization and application of a small library of paramagnetic Gd-based glyconanoparticles as biocompatible, biofunctional and water-soluble probes for Magnetic Resonance Imaging (MRI) has been achieved in this PhD Thesis.

To sum up, we have improved the preparation of Gd-based paramagnetic gold GNPs ensuring the correct chelation of the paramagnetic ion by the DO3A. We have demonstrated that these GNPs can be used to selectively label lectins in cells and that they are good contrast agents for brain tumors.

APPENDIX I

CHARACTERIZATION OF SPACERS, NEOGLYCOCONJUGATES and DO3A and DOTA-EdA DERIVATIVES

APPENDIX I

1. Selected NMR spectra

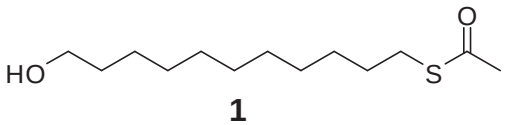

1

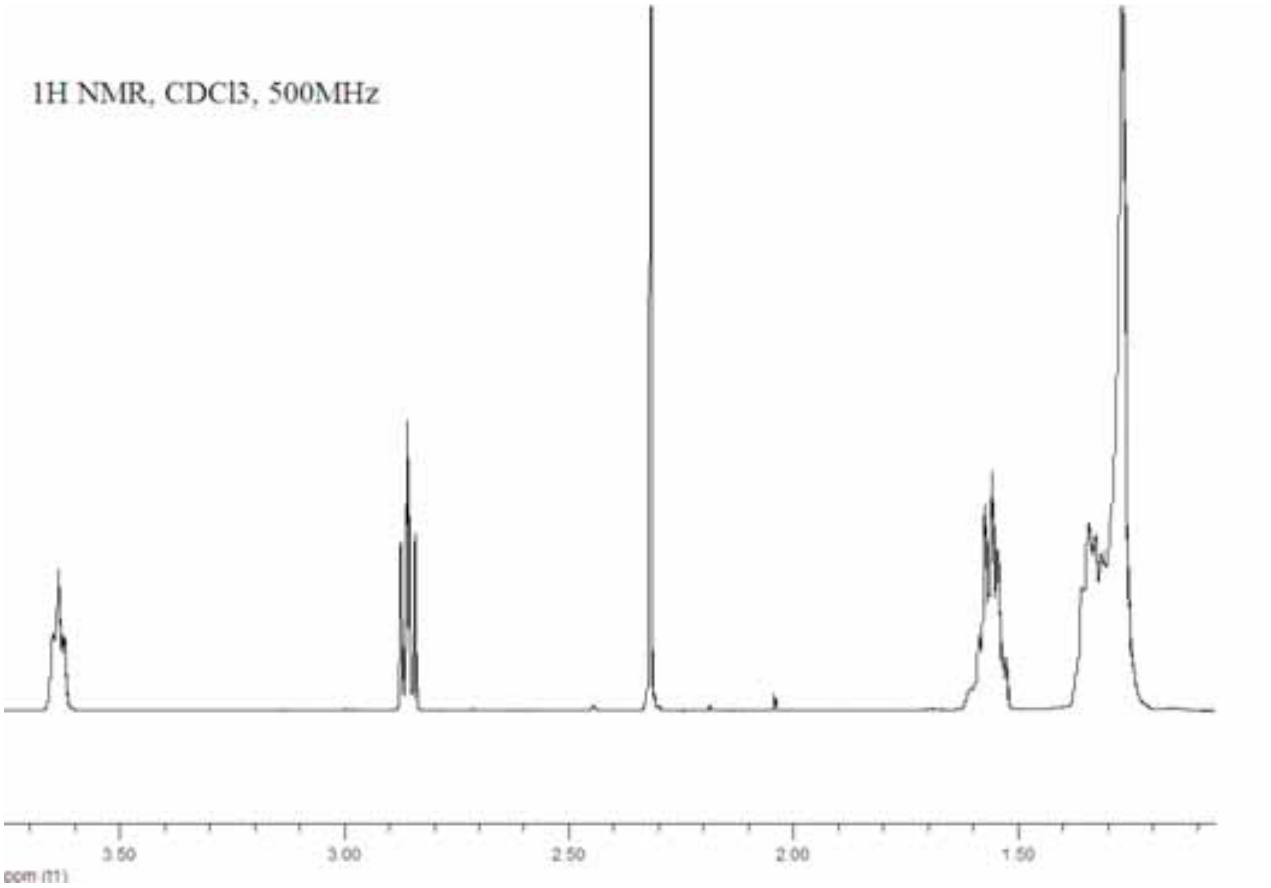

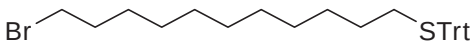

2

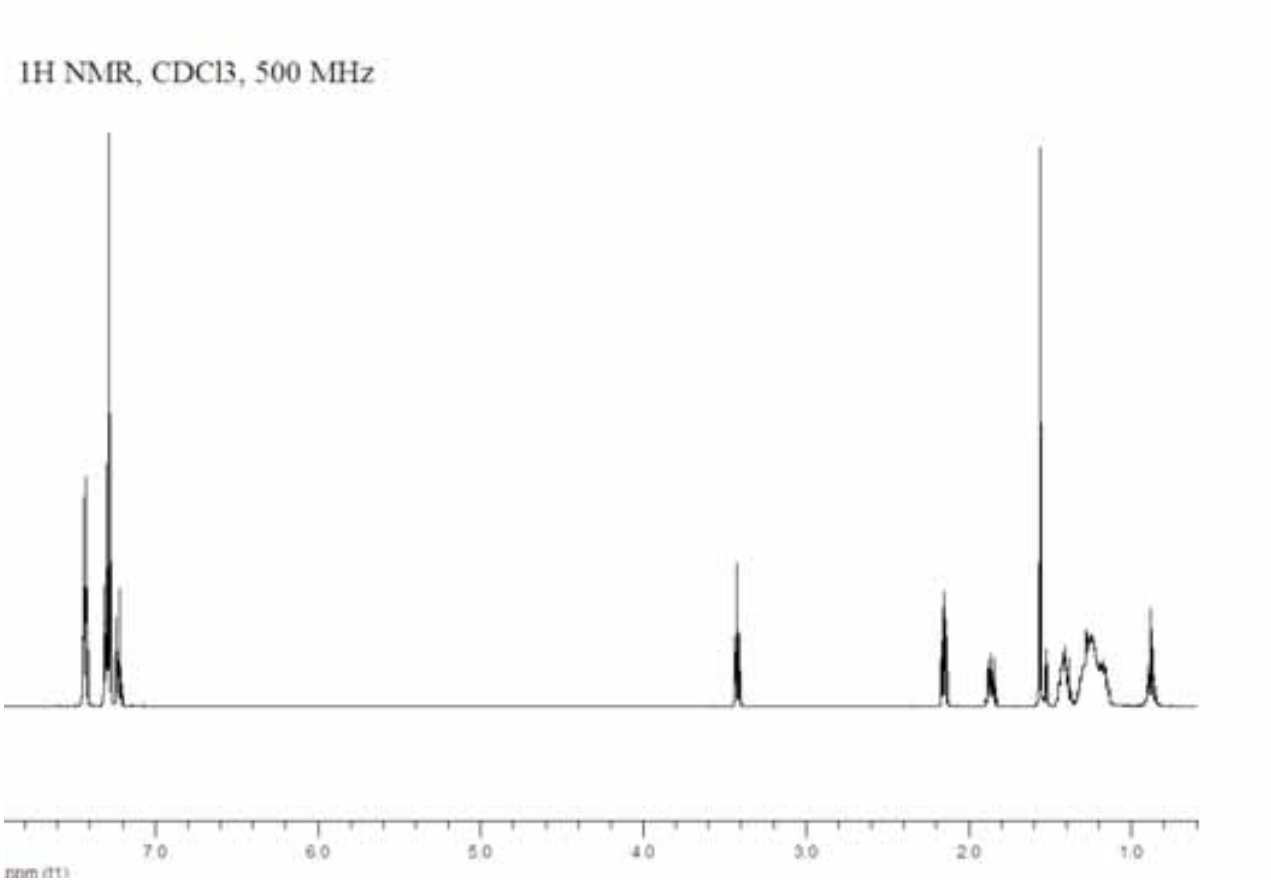

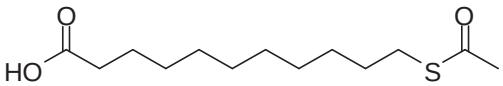

3

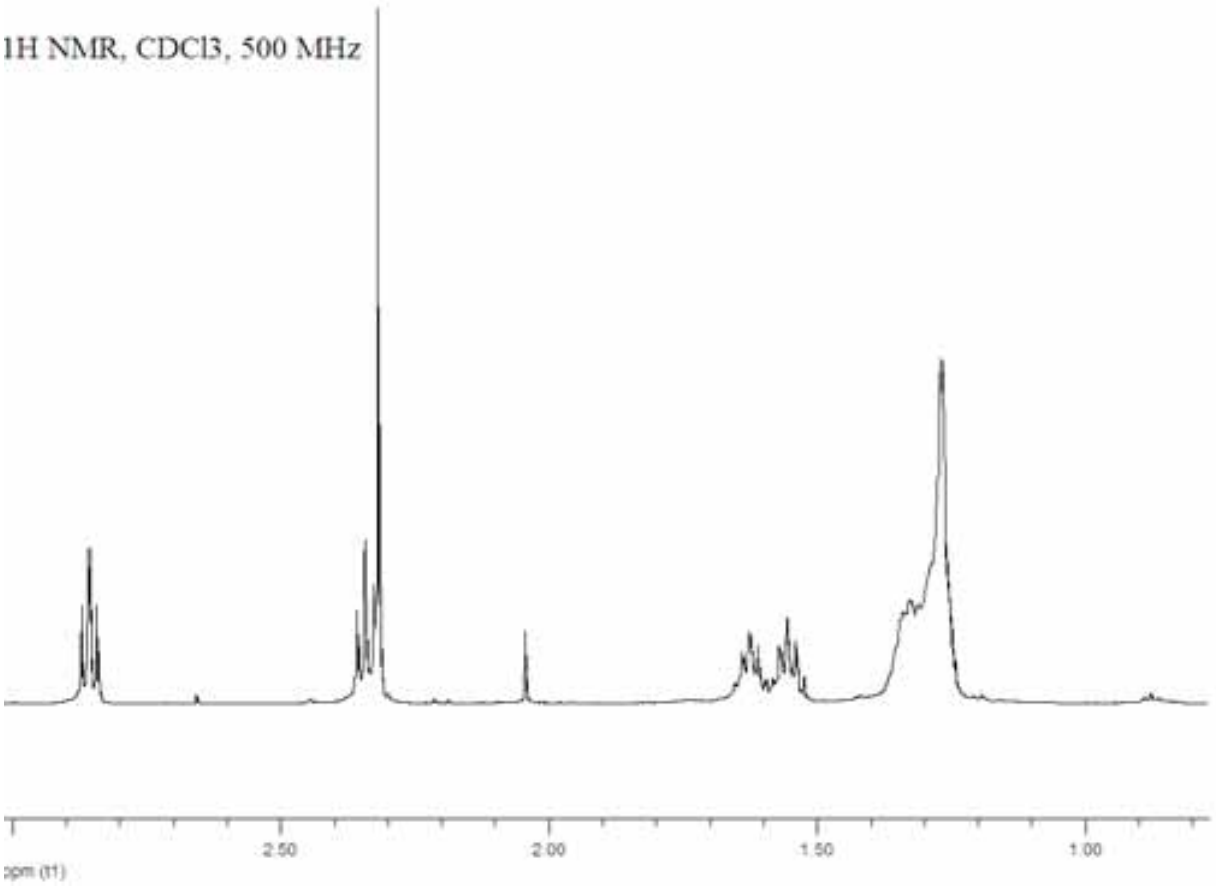

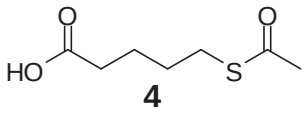
O
HO
S
O

4

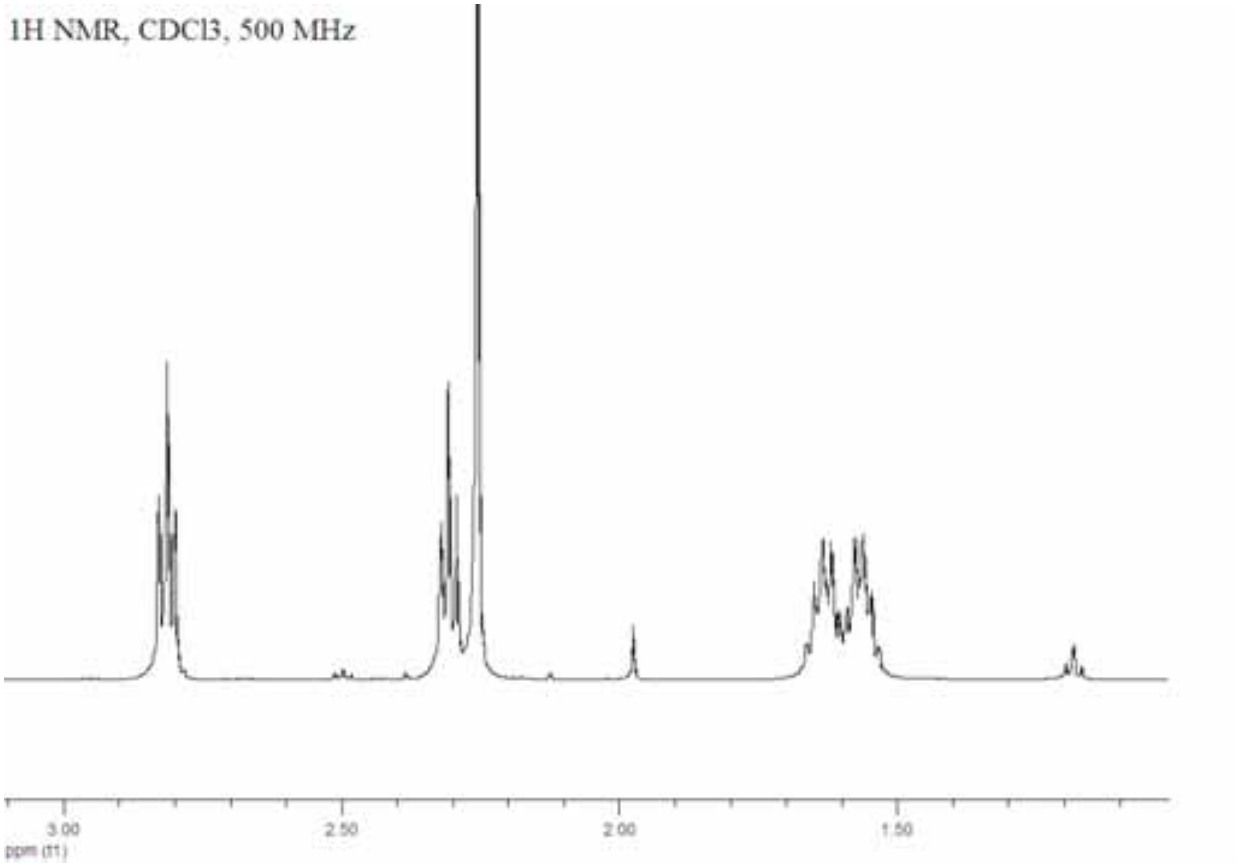
1H NMR, CDCl3, 500 MHz
3.00
2.50
2.00
1.50
ppm (f1)

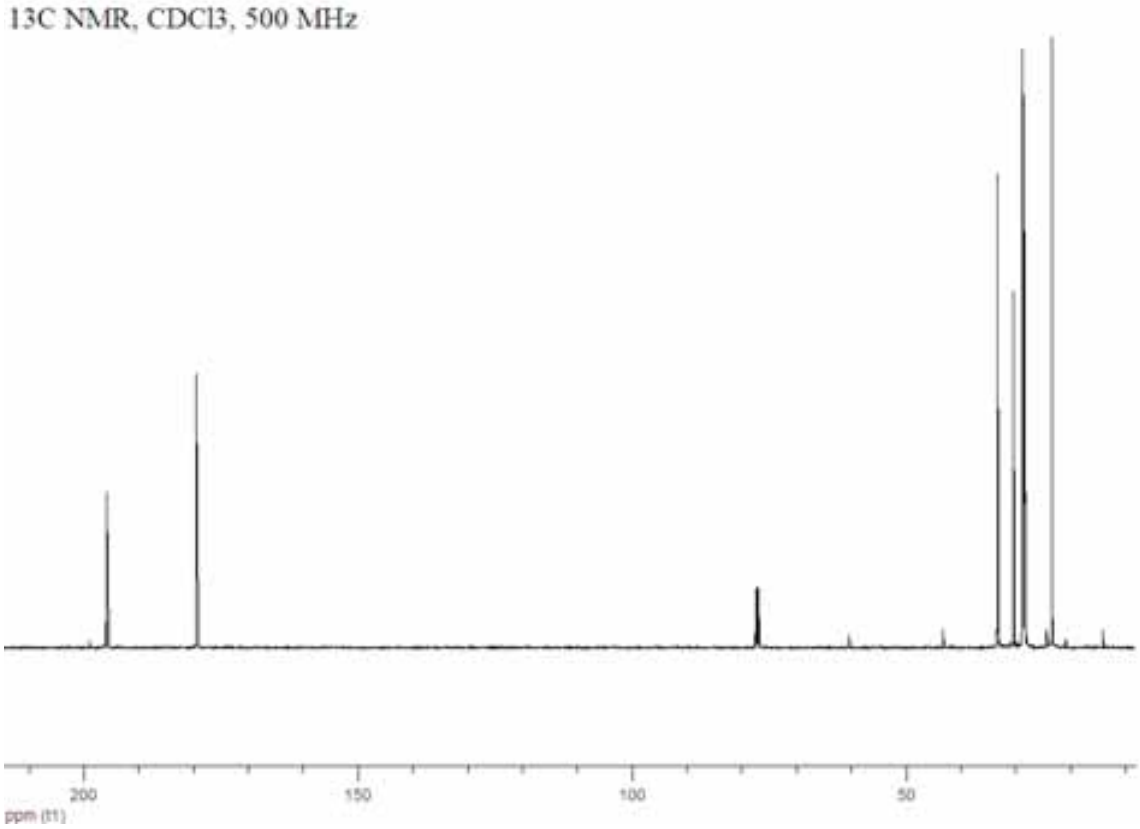
13C NMR, CDCl3, 500 MHz
200
150
100
50
ppm (f1)

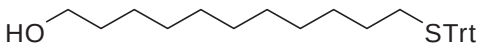

5

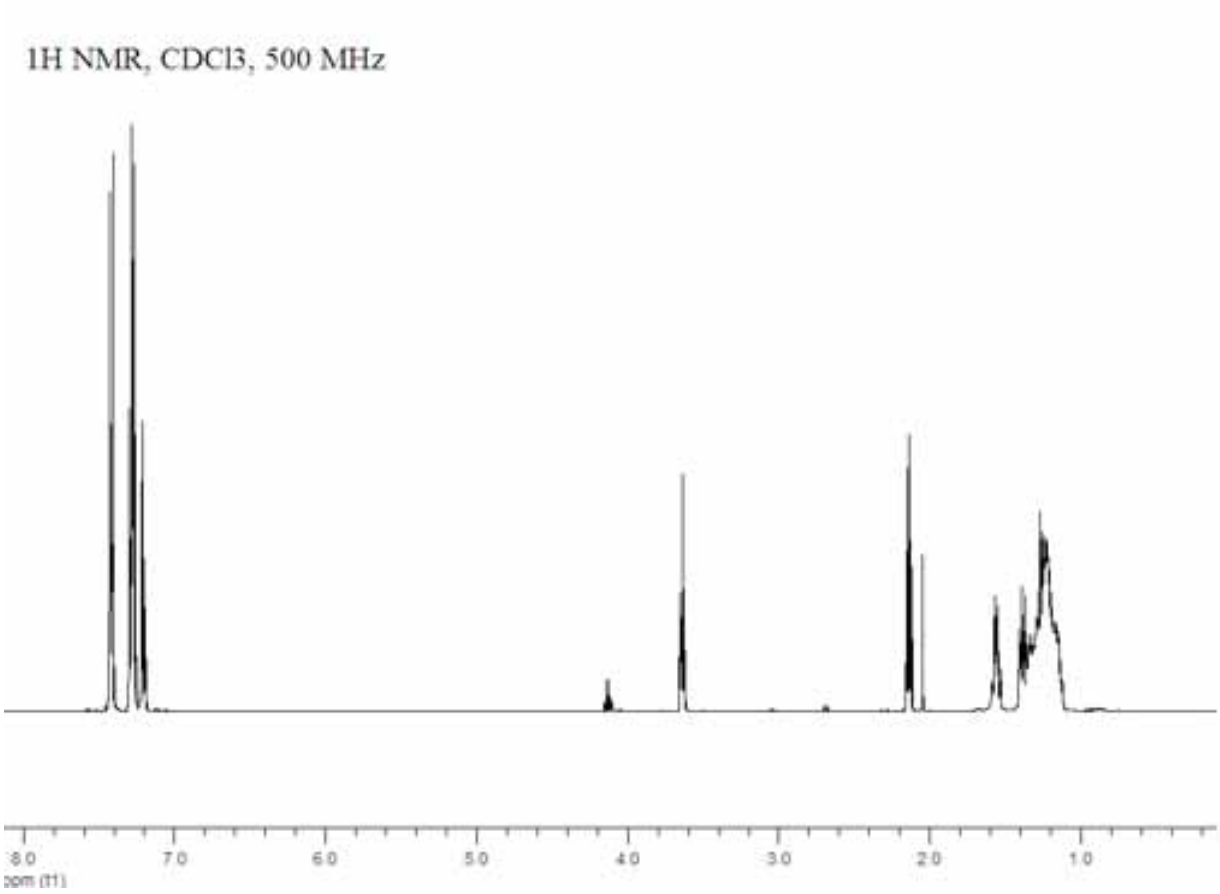

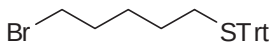
Br
STrt

6

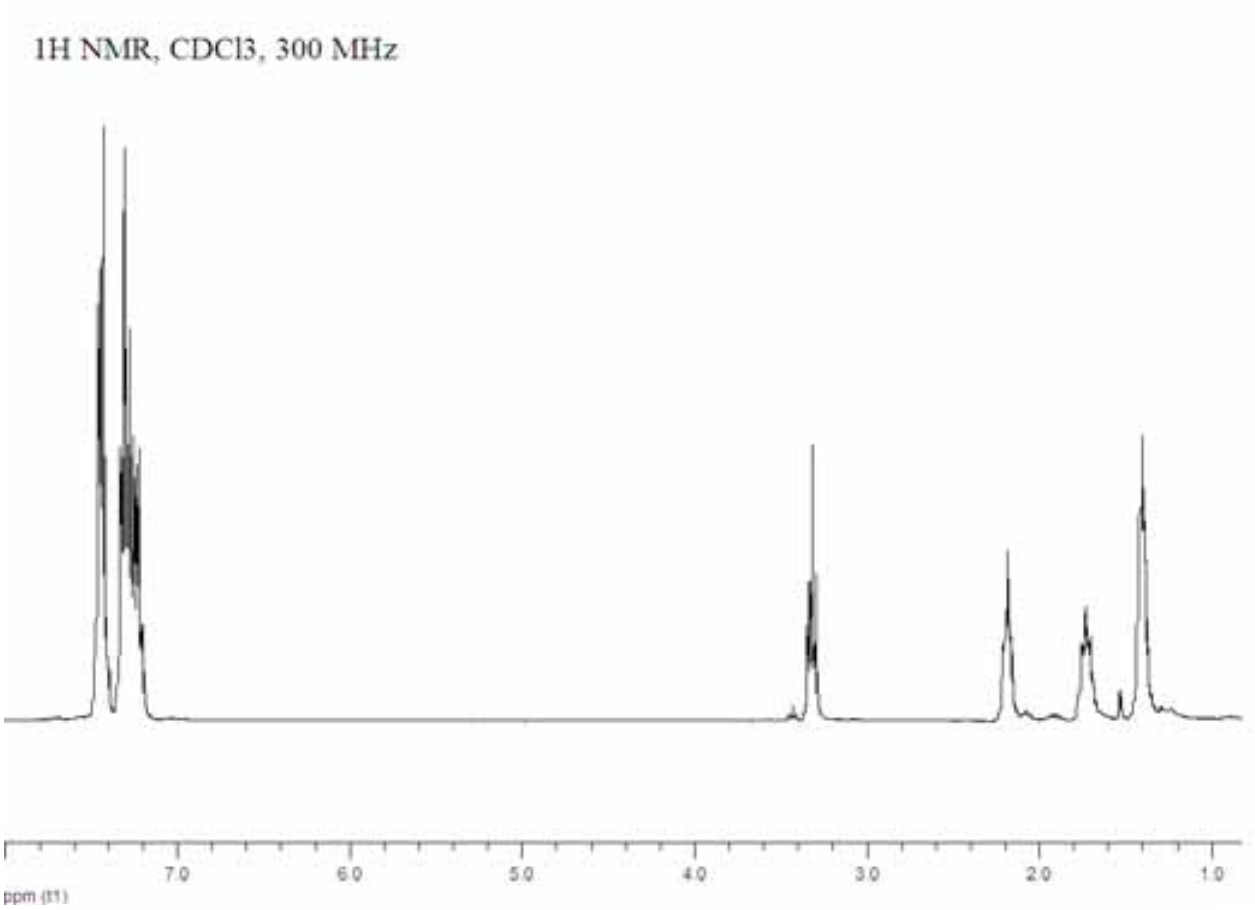
1H NMR, CDCl3, 300 MHz
7.0
6.0
5.0
4.0
3.0
2.0
1.0
ppm (t1)

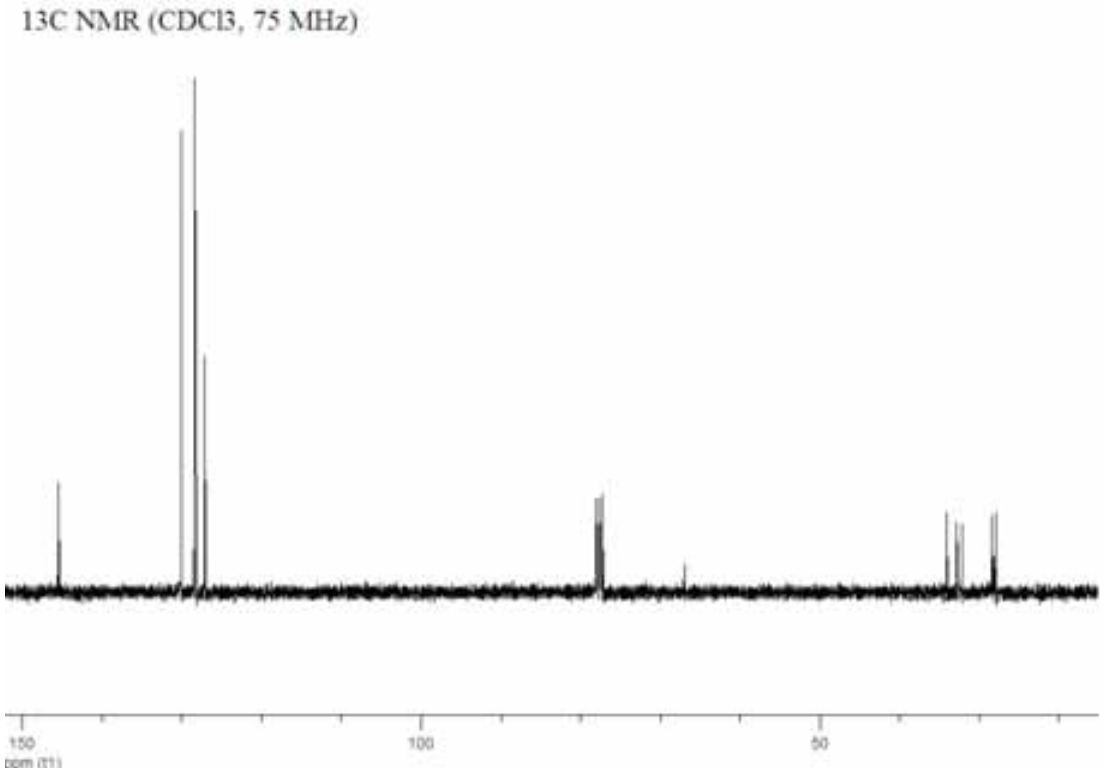
13C NMR (CDCl3, 75 MHz)
150
100
50
ppm (t1)

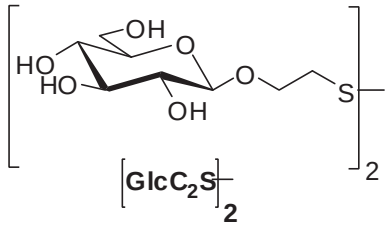
OH
O
HO
HO
OH
O
S
2
GlcC2S
2

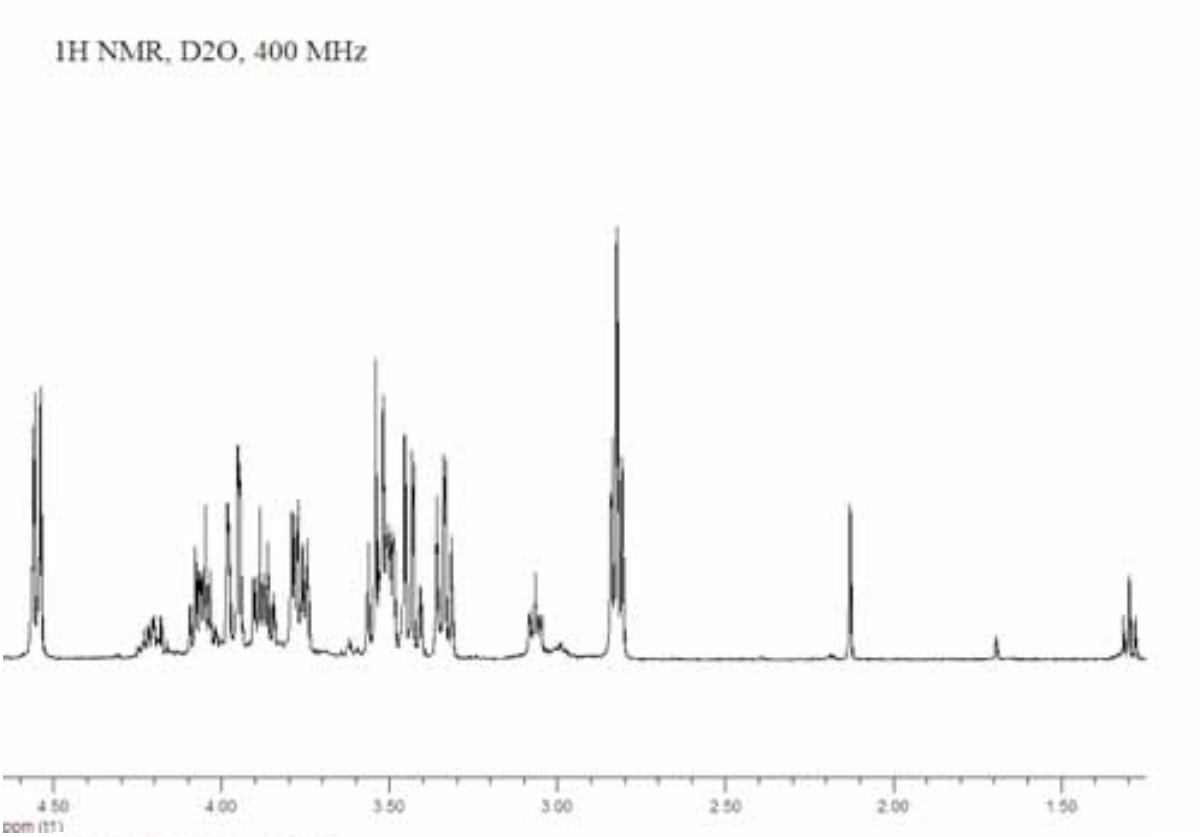
1H NMR, D2O, 400 MHz
4.50
4.00
3.50
3.00
2.50
2.00
1.50

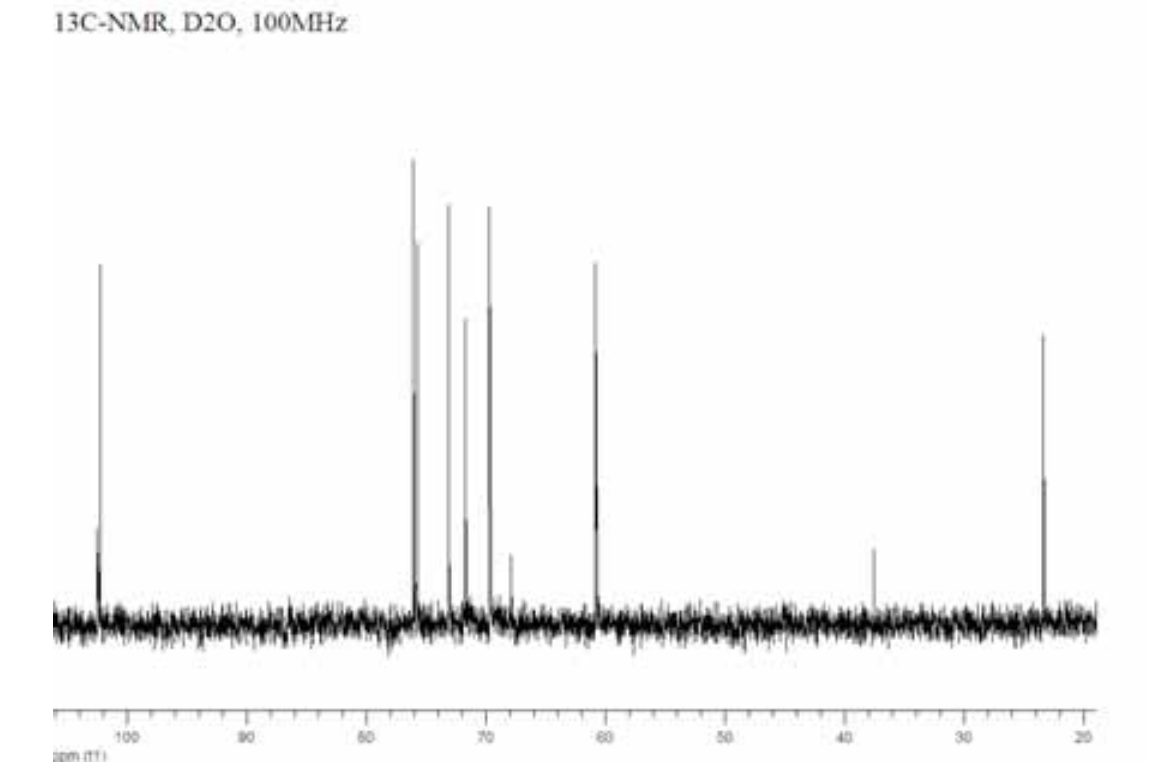
13C-NMR, D2O, 100MHz
100
90
80
70
60
50
40
30
20

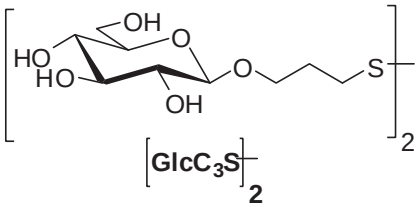
OH
O
HO
HO
O
S
OH
2

GlcC$_3$S]$_2$

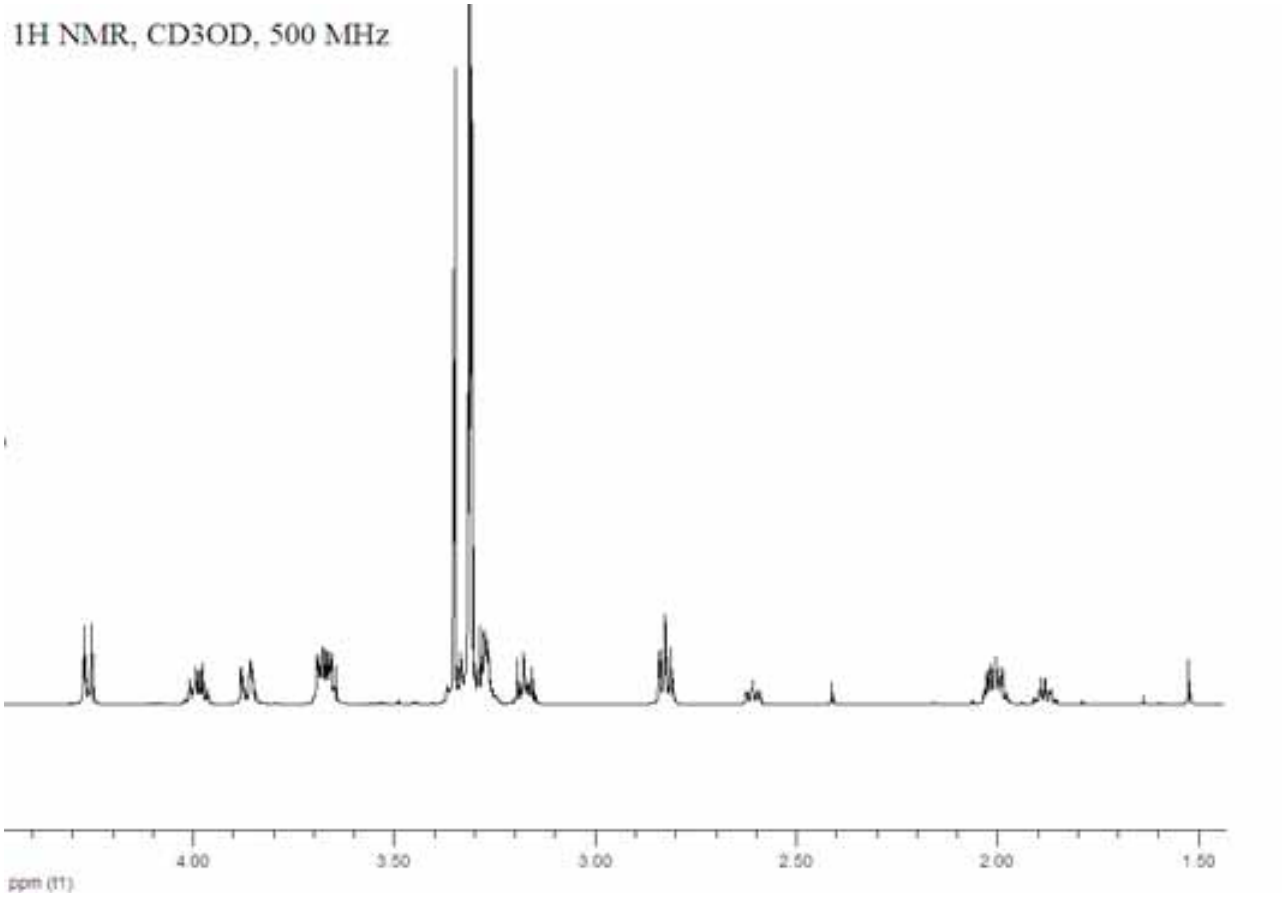
1H NMR, CD3OD, 500 MHz
4.00
3.50
3.00
2.50
2.00
1.50
ppm (f1)

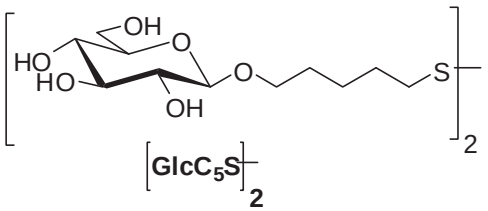
OH
O
HO
HO
O
S
OH
2

GlcC$_5$S]$_2$

2

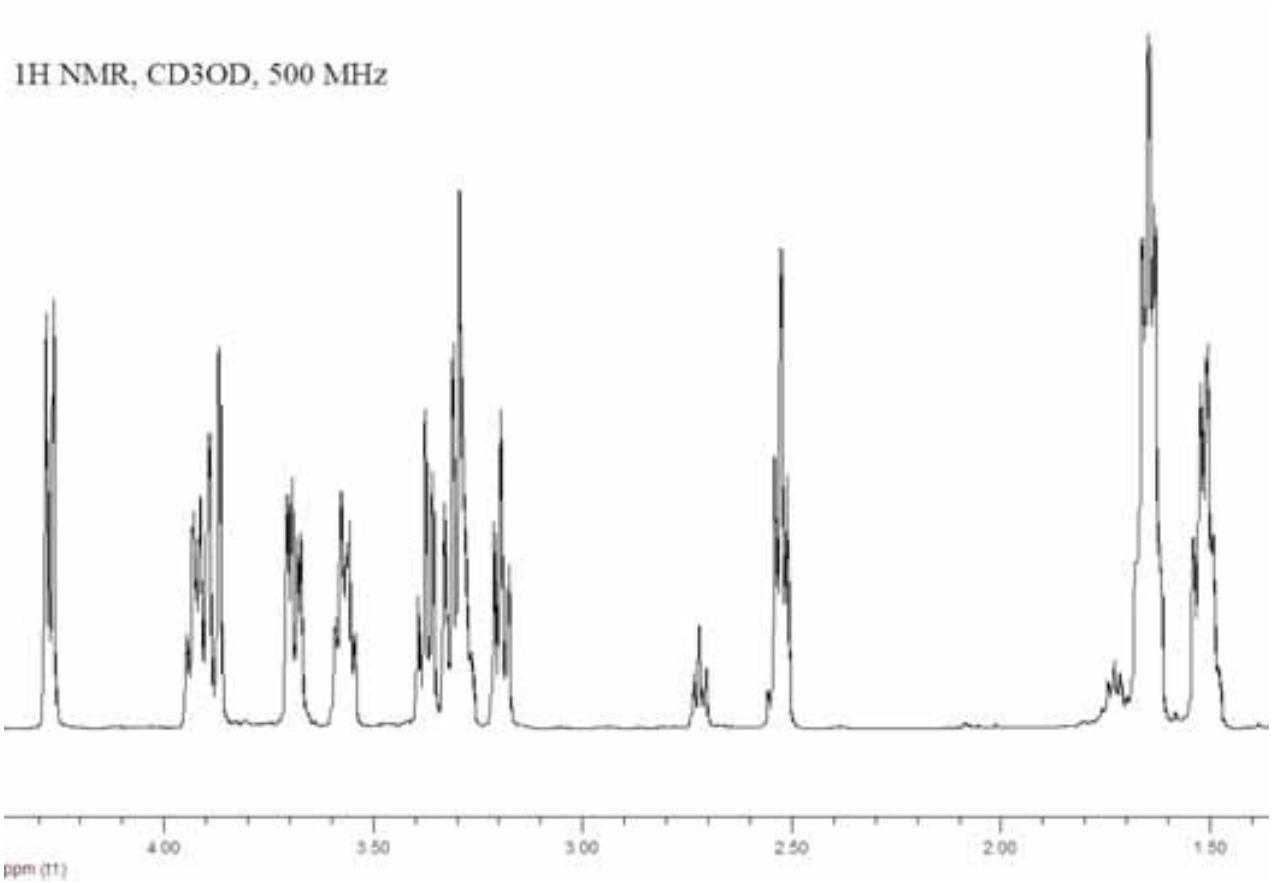
1H NMR, CD3OD, 500 MHz
4.00
3.50
3.00
2.50
2.00
1.50
ppm (t1)

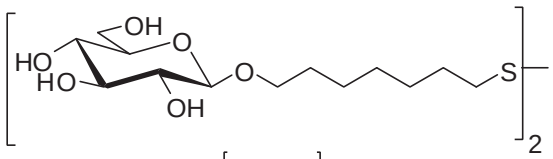
OH
HO
HO
O
OH
O
S
2

GlcC$_7$S]$_2$

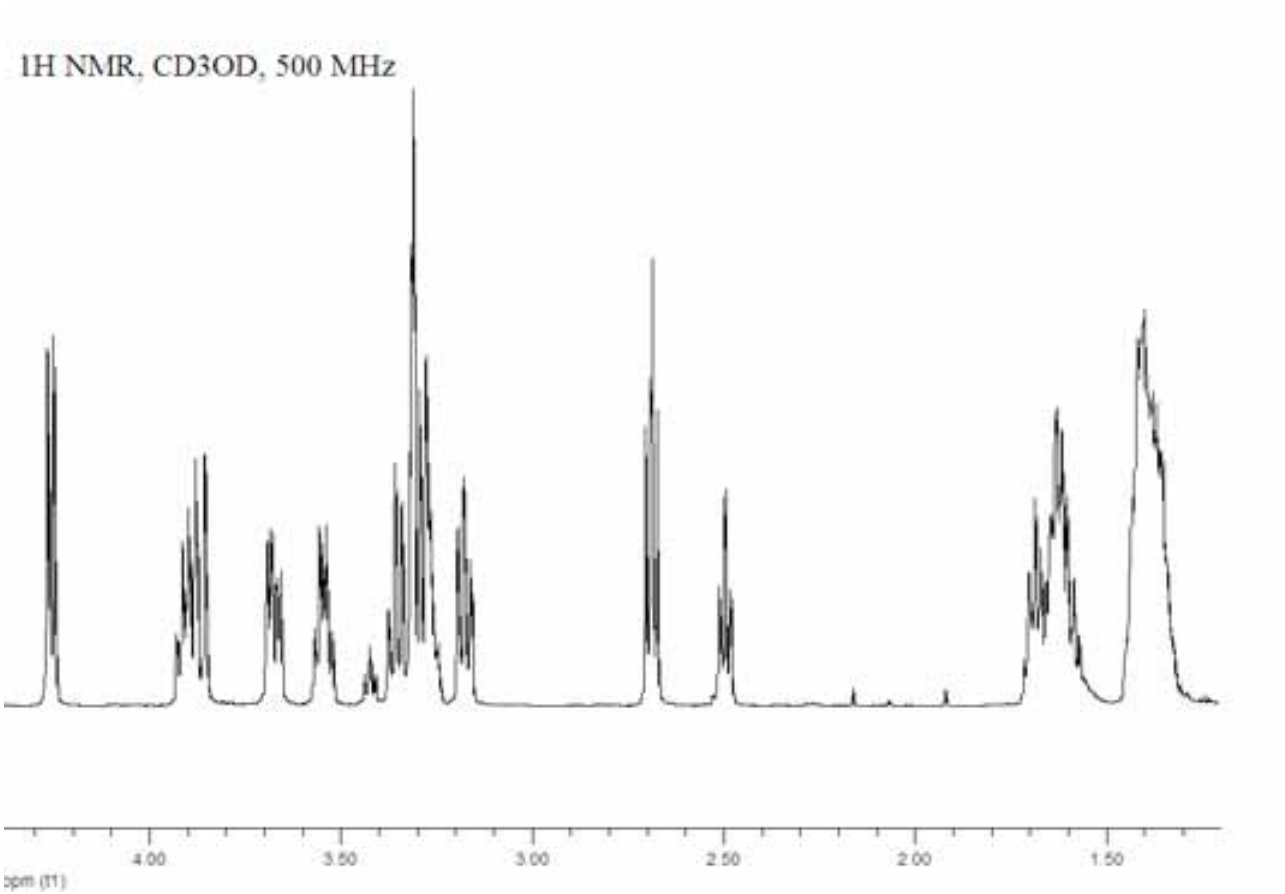
1H NMR, CD3OD, 500 MHz
4.00
3.50
3.00
2.50
2.00
1.50
ppm (t1)

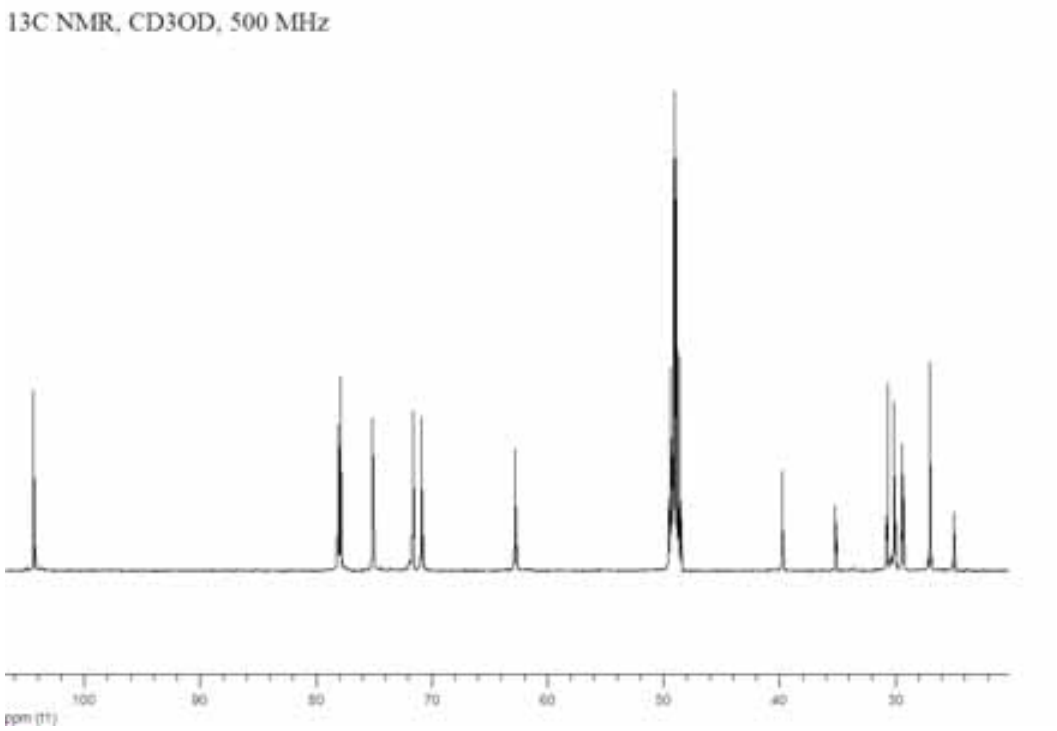
13C NMR, CD3OD, 500 MHz
100
90
80
70
60
50
40
30
ppm (t1)

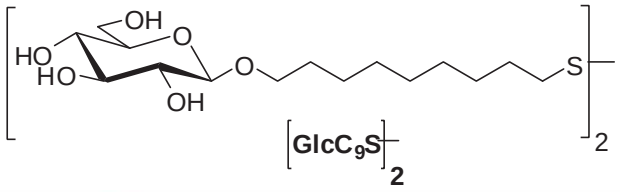
OH
HO
HO
O
O
OH
S
2

GlcC$_9$S]$_2$

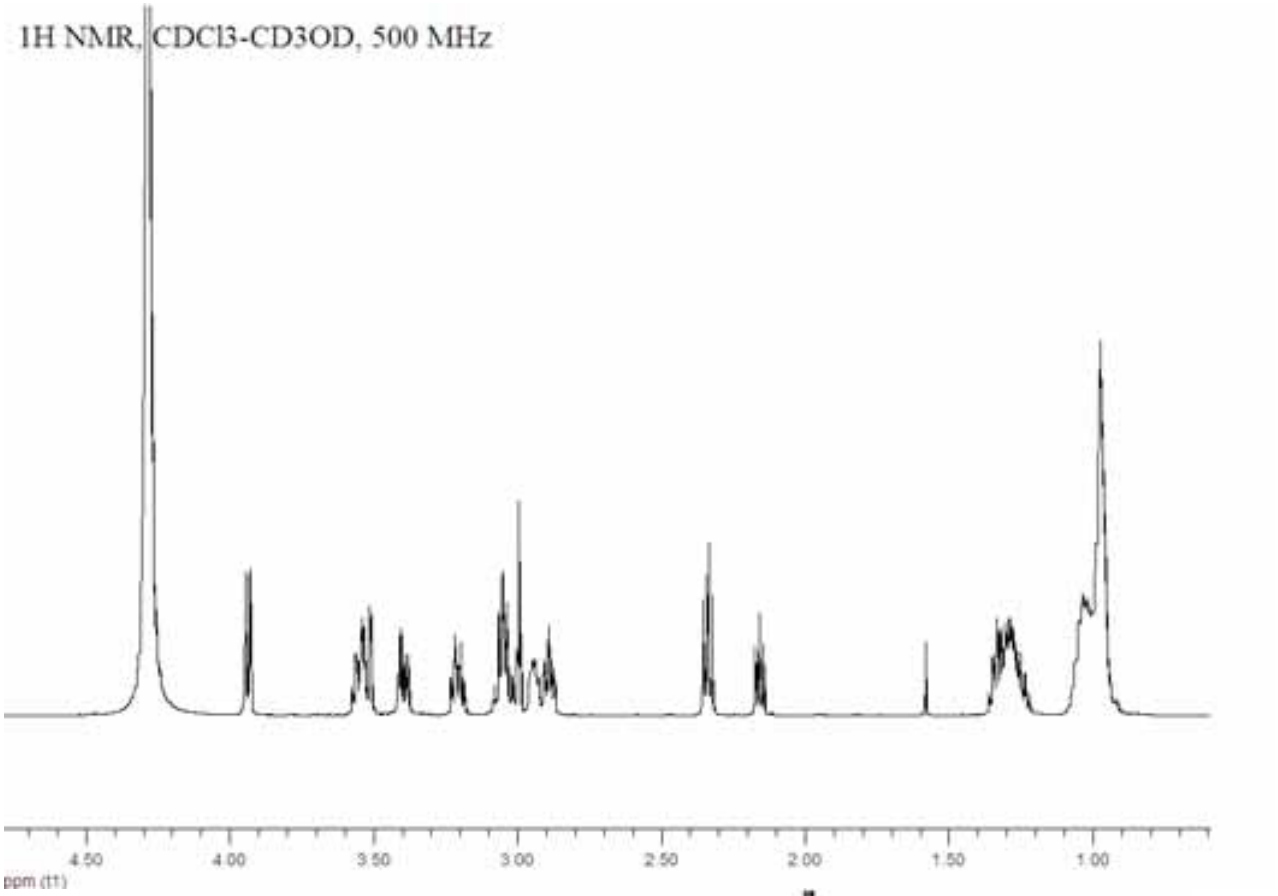
1H NMR, CDCl3-CD3OD, 500 MHz
4.50
4.00
3.50
3.00
2.50
2.00
1.50
1.00
ppm (t1)

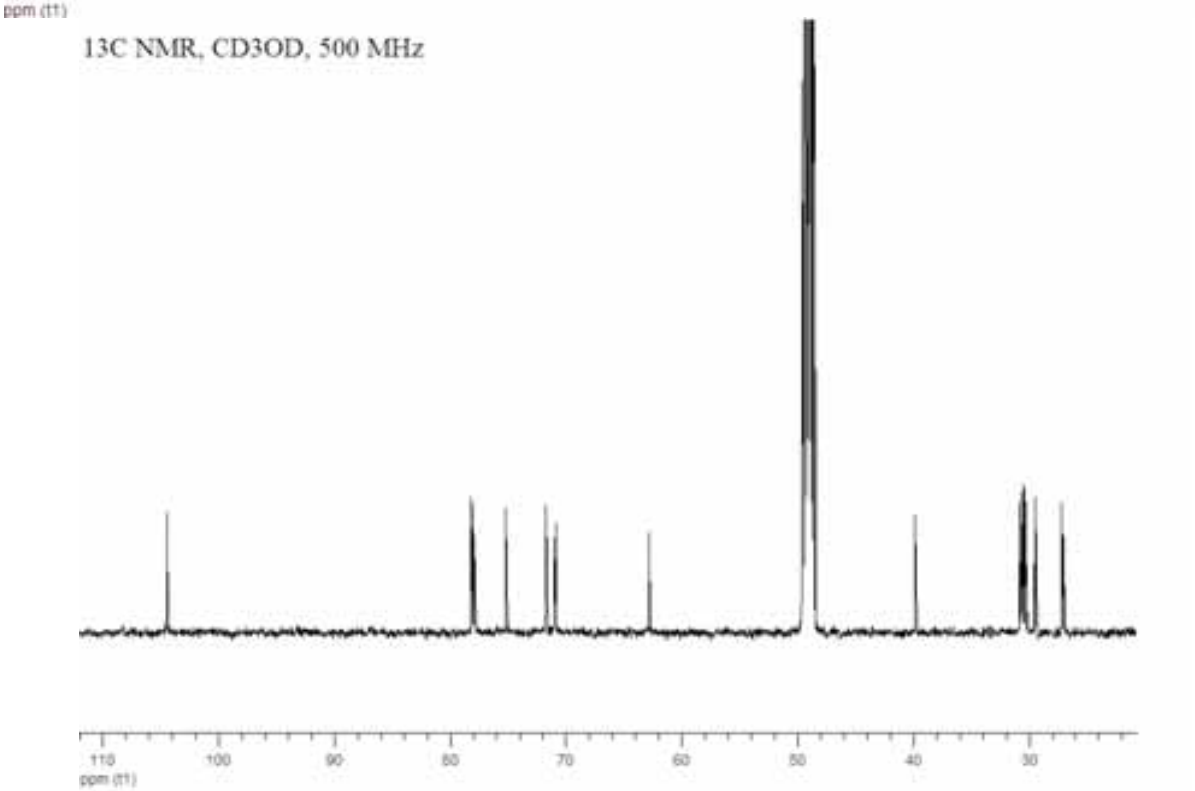
13C NMR, CD3OD, 500 MHz
110
100
90
80
70
60
50
40
30
ppm (t1)

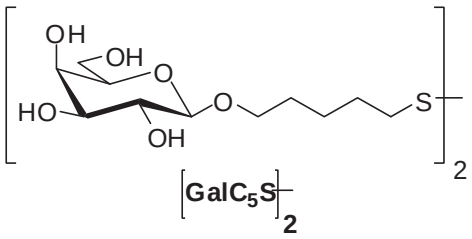
OH
OH
O
HO
O
S
OH
2

$GalC_5S]_2$

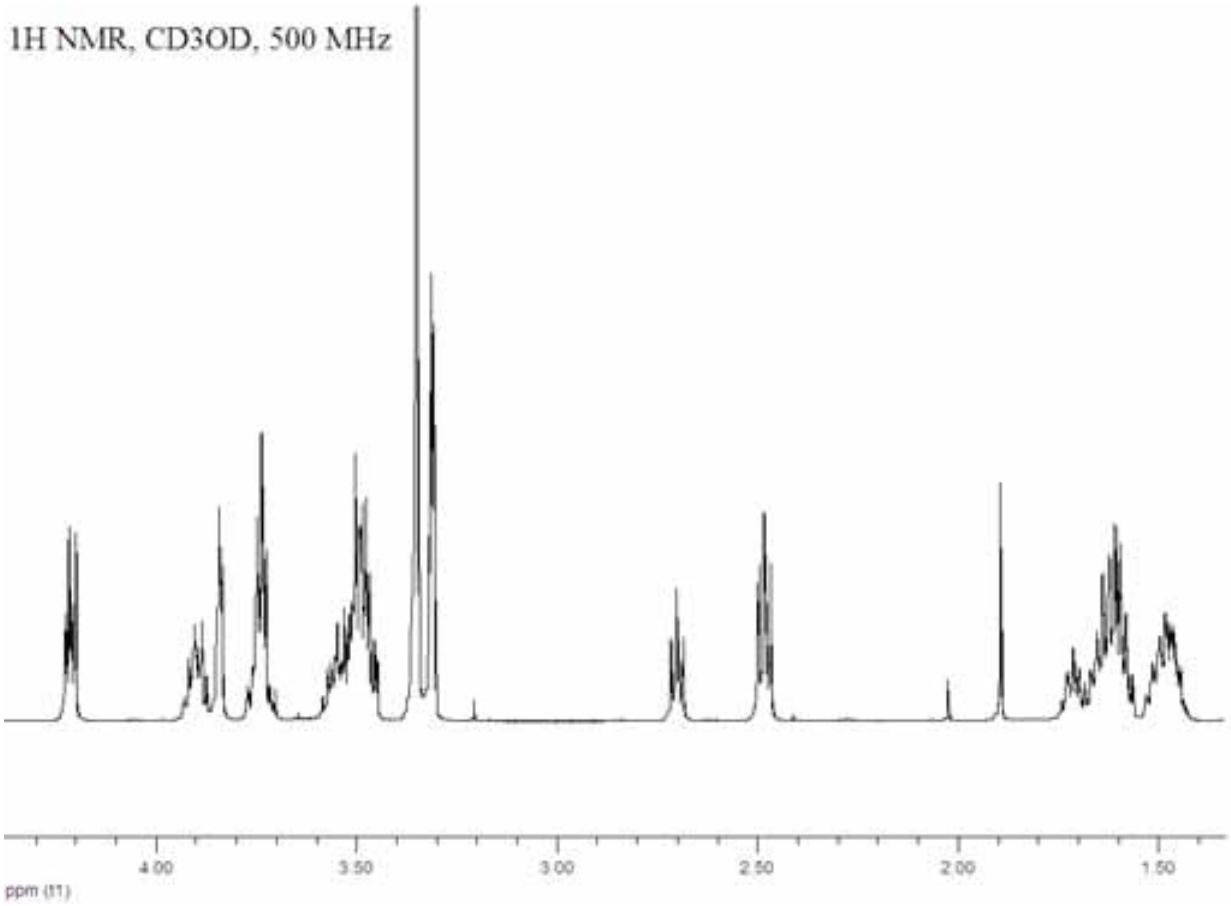
1H NMR, CD3OD, 500 MHz
4.00
3.50
3.00
2.50
2.00
1.50
ppm (t1)

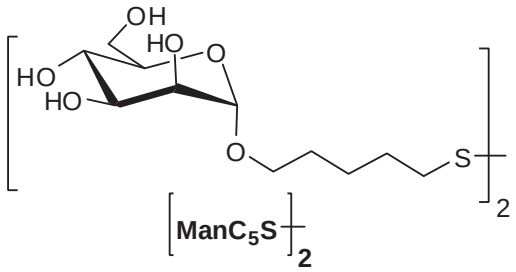
OH
HO
HO
HO
O
O
S
2
ManC5S
2

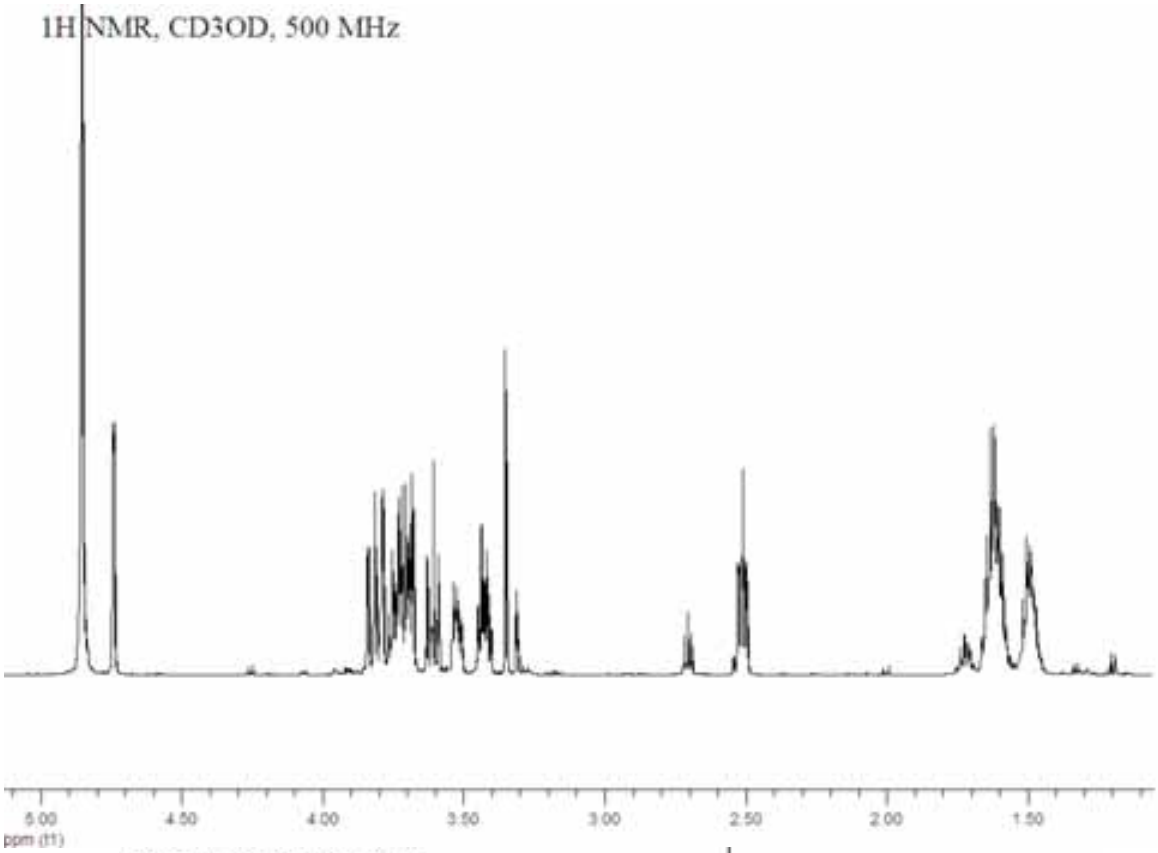
1H NMR, CD3OD, 500 MHz
5.00
4.50
4.00
3.50
3.00
2.50
2.00
1.50
ppm (f1)

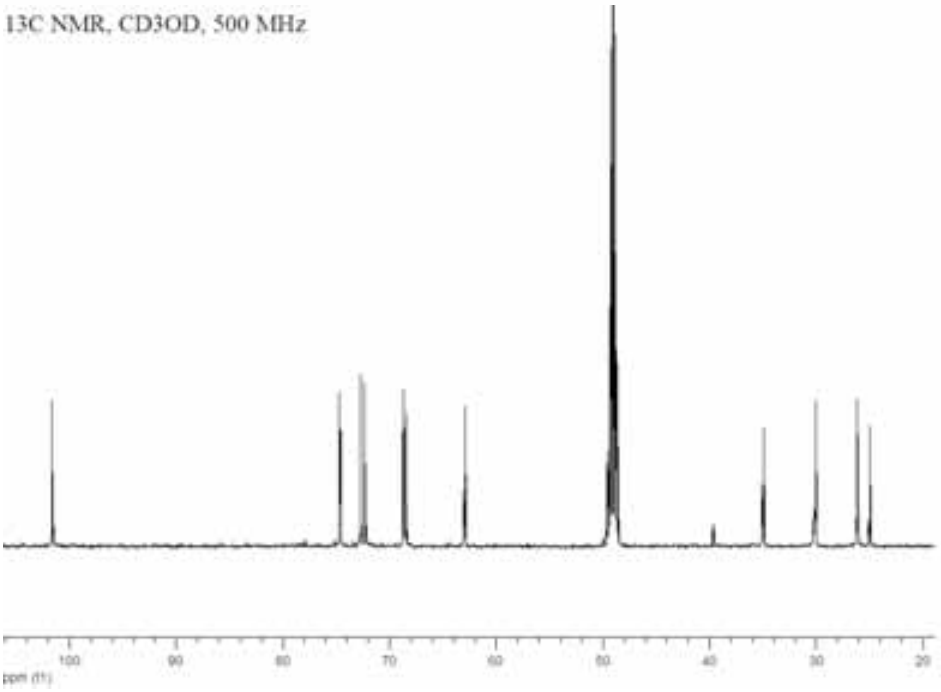
13C NMR, CD3OD, 500 MHz
100
90
80
70
60
50
40
30
20
ppm (f1)

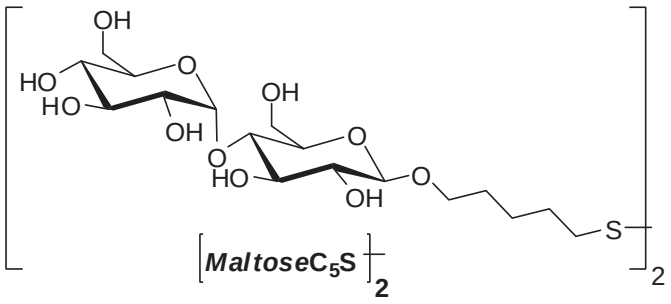
OH
HO
HO
O
OH
O
HO
OH
O
O
OH
S
2
MaltoseC_5S
2

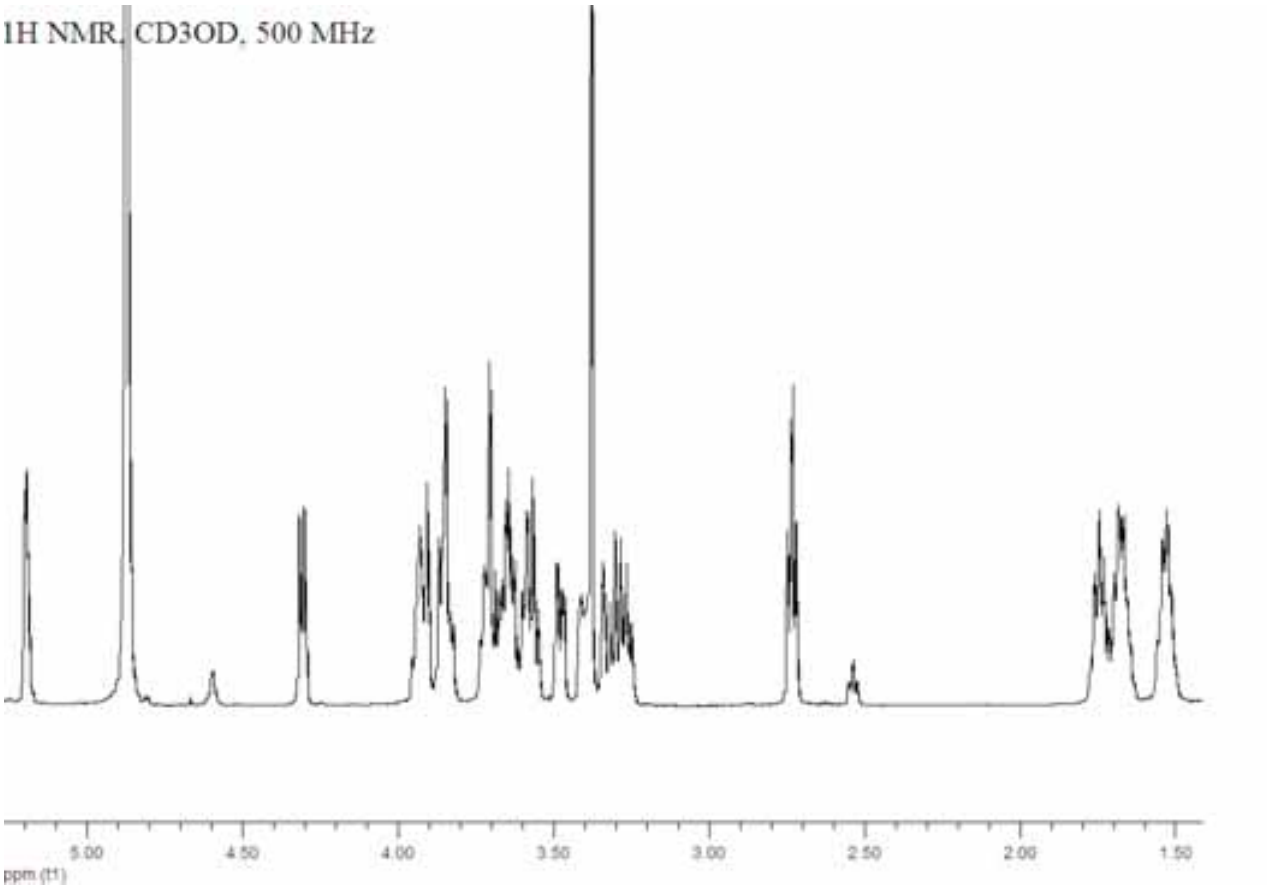
1H NMR, CD3OD, 500 MHz
5.00
4.50
4.00
3.50
3.00
2.50
2.00
1.50
ppm (f1)

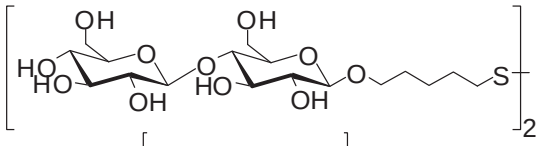

***Cellobiose*C_5S**$_2$

2

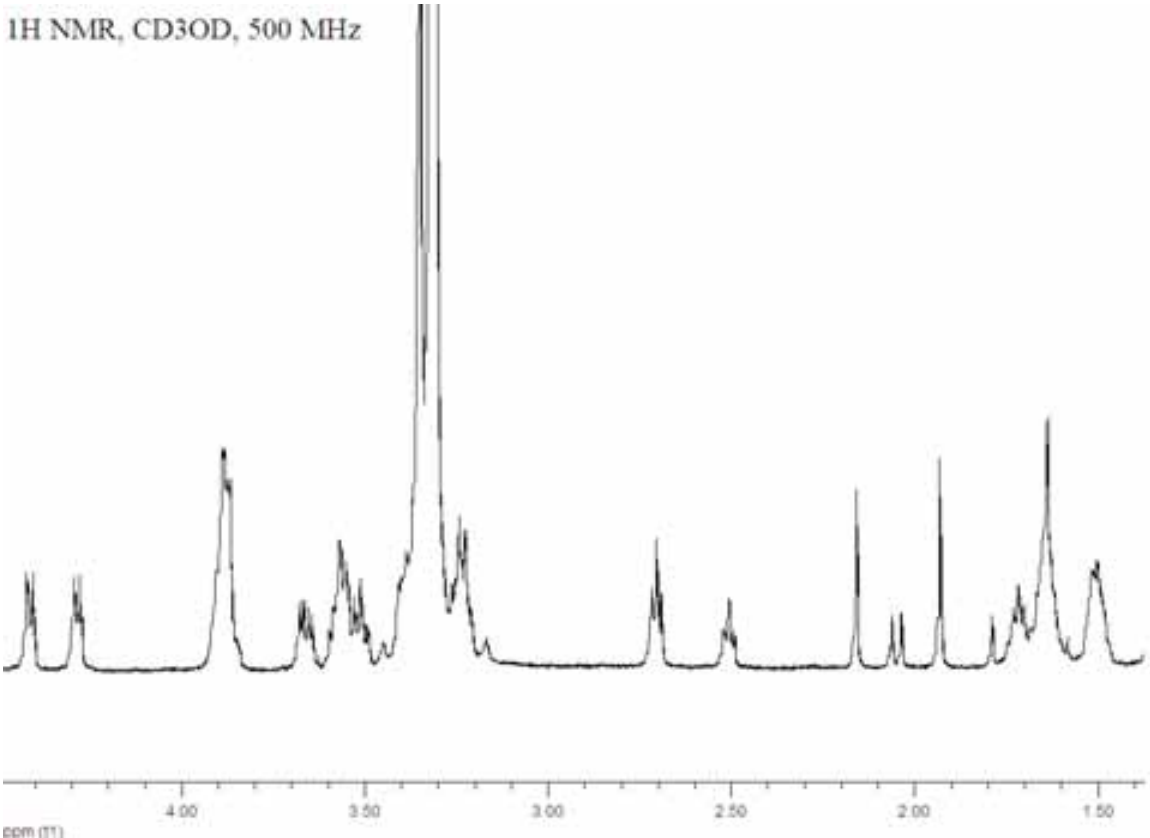

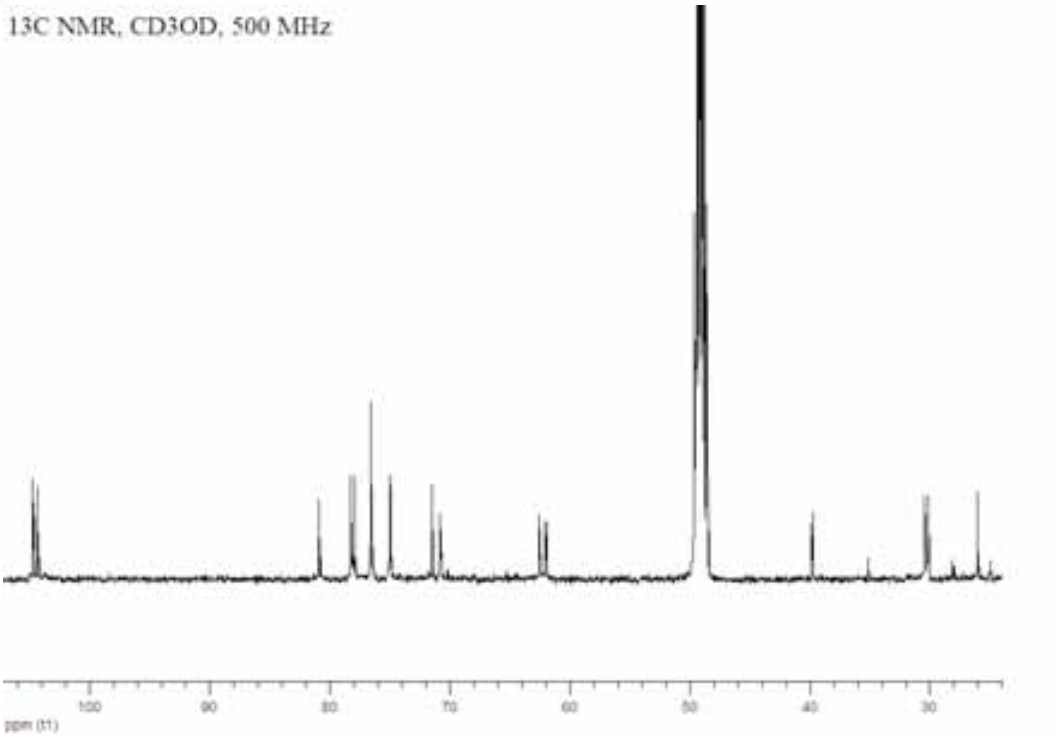

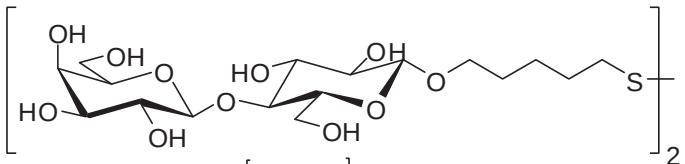
OH
OH
O
HO
OH
O
HO
OH
OH
O
O
S
2

$[LacC_5S]_2$

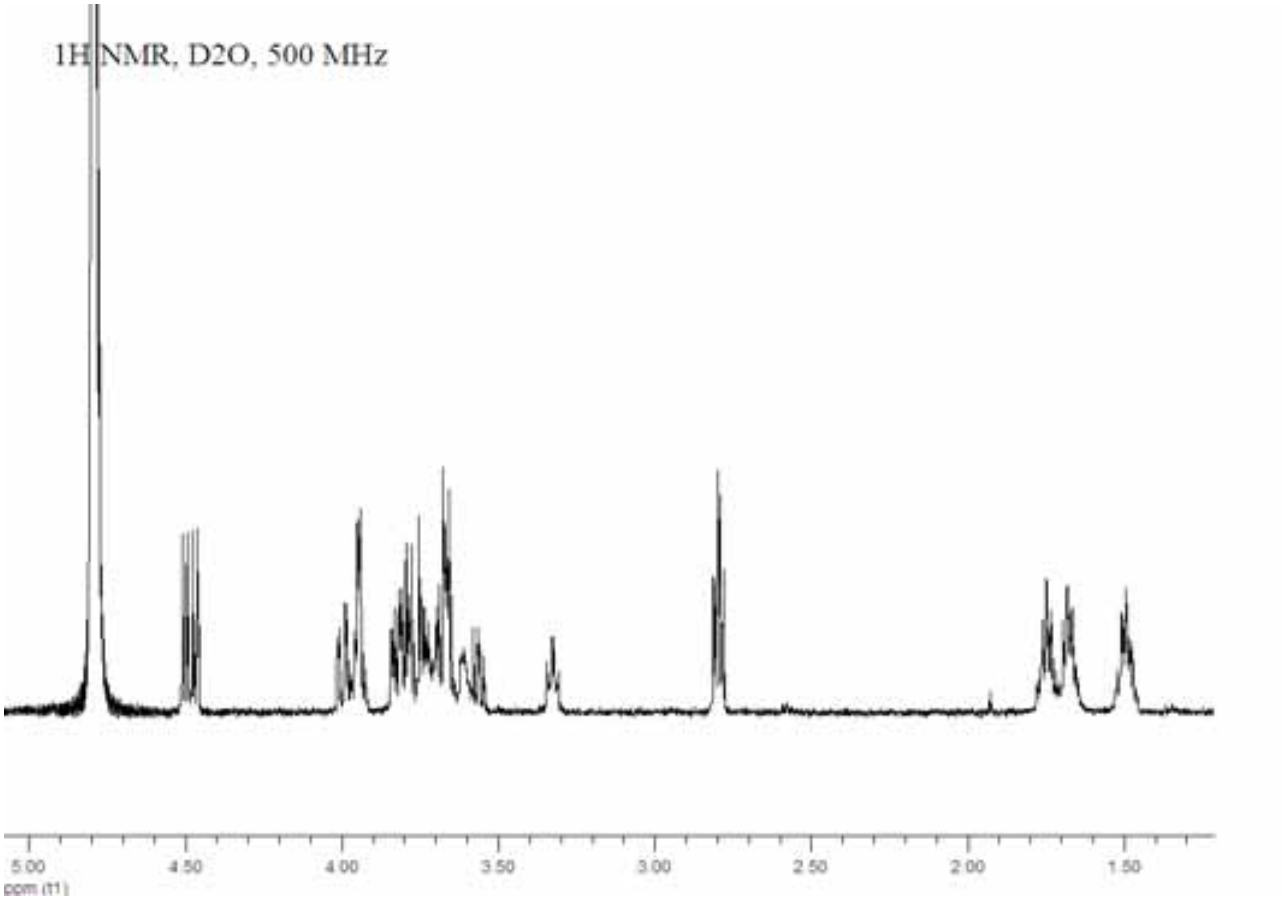
1H NMR, D2O, 500 MHz
5.00
4.50
4.00
3.50
3.00
2.50
2.00
1.50
ppm (f1)

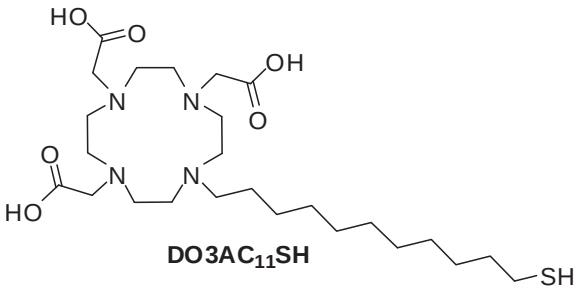
HO
O
OH
O
N
N
O
HO
N
N
SH

DO3AC$_{11}$SH

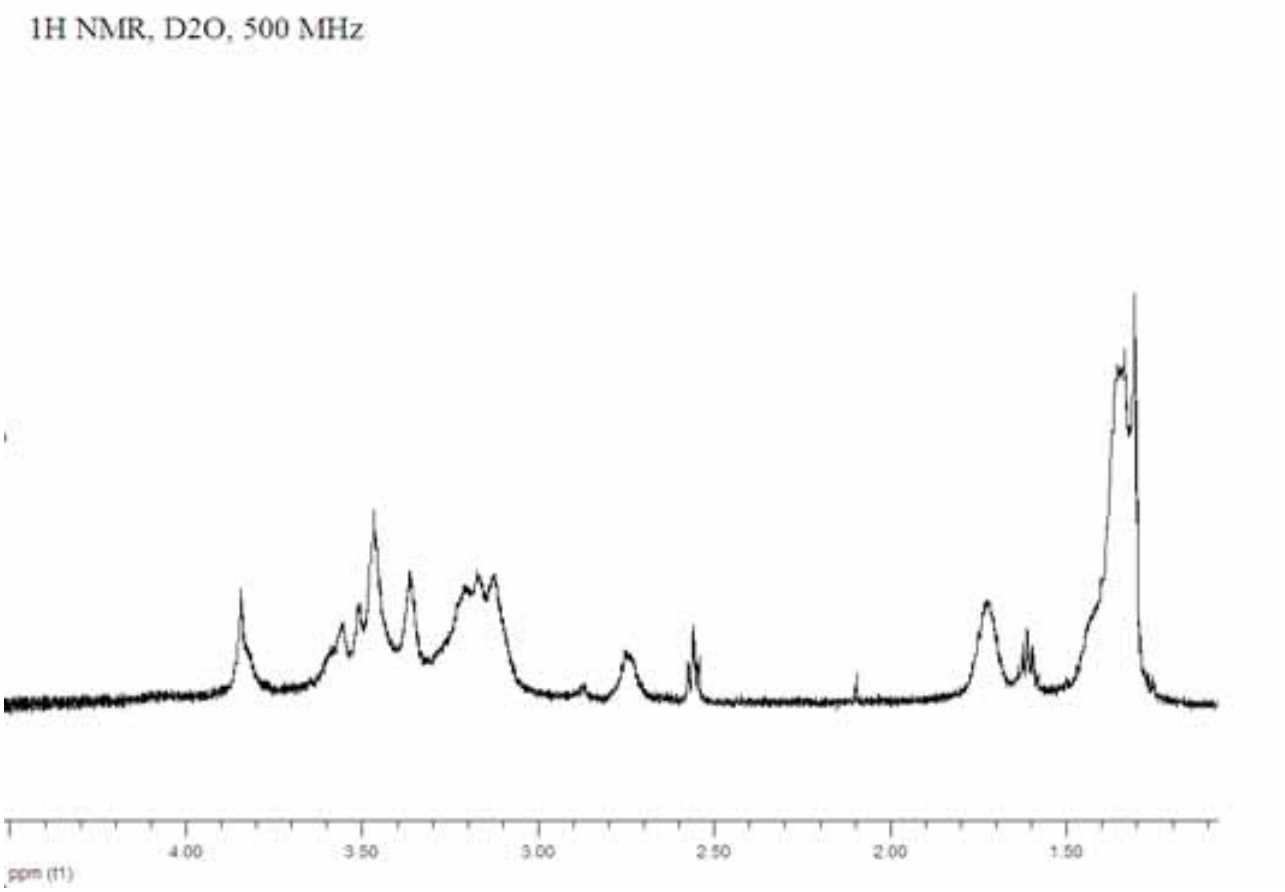
1H NMR, D2O, 500 MHz
4.00
3.50
3.00
2.50
2.00
1.50
ppm (f1)

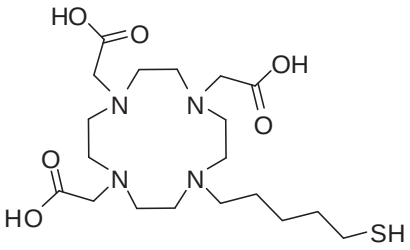

DO3AC$_5$SH

1H NMR, D2O, 500 MHz

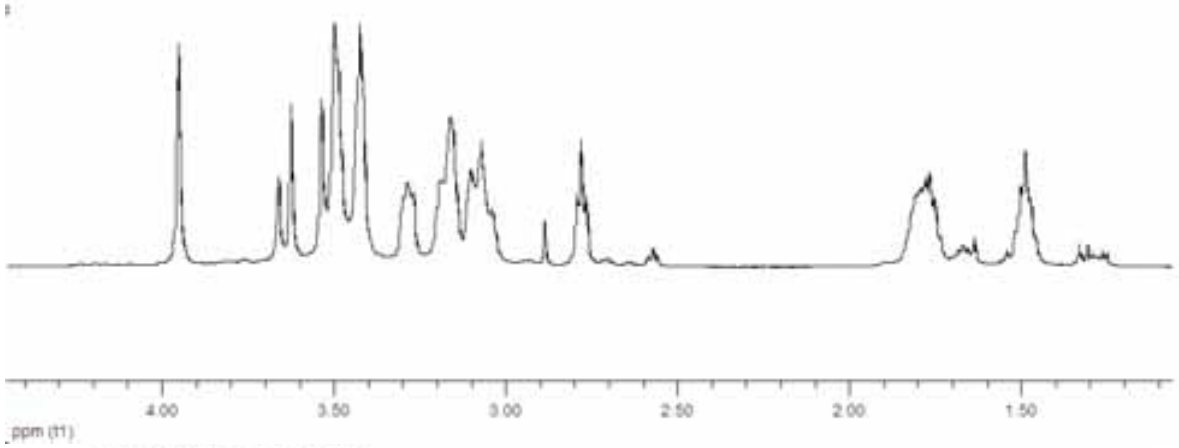

13C NMR, D2O, 500 MHz

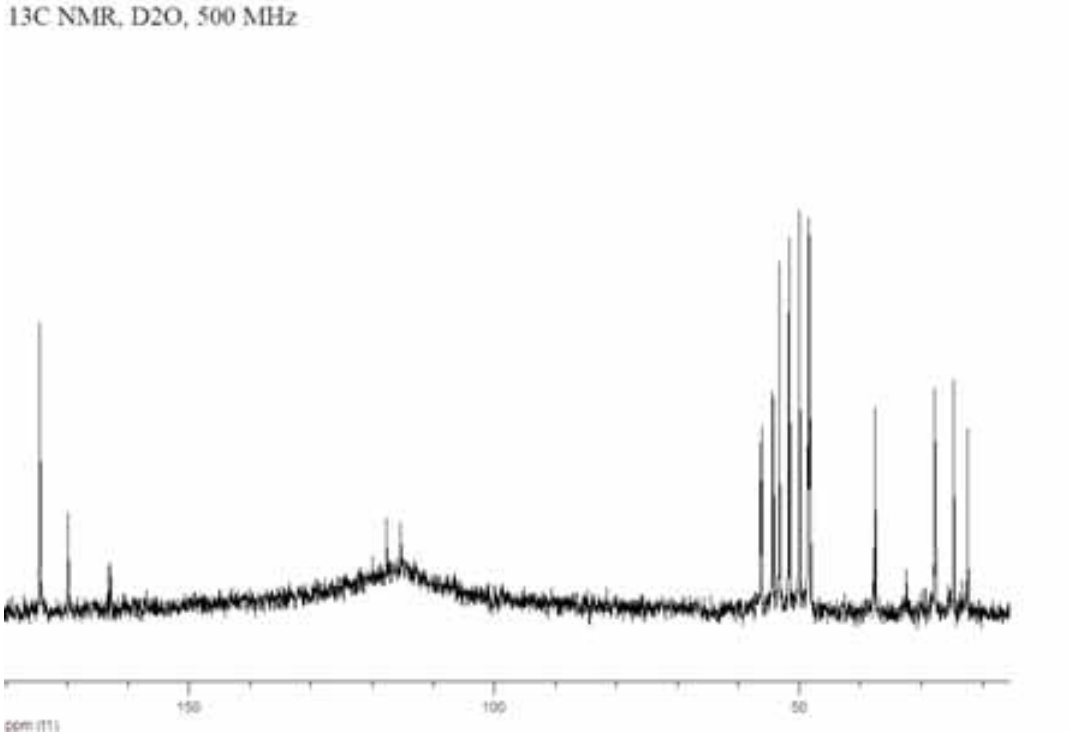

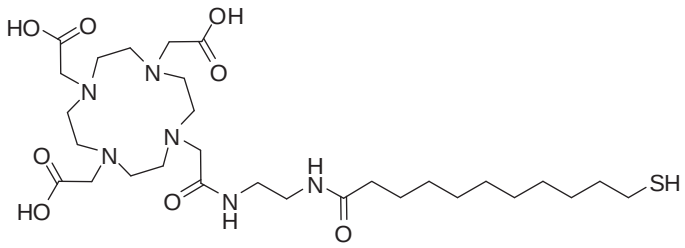

DOTA-EdAC$_{11}$SH

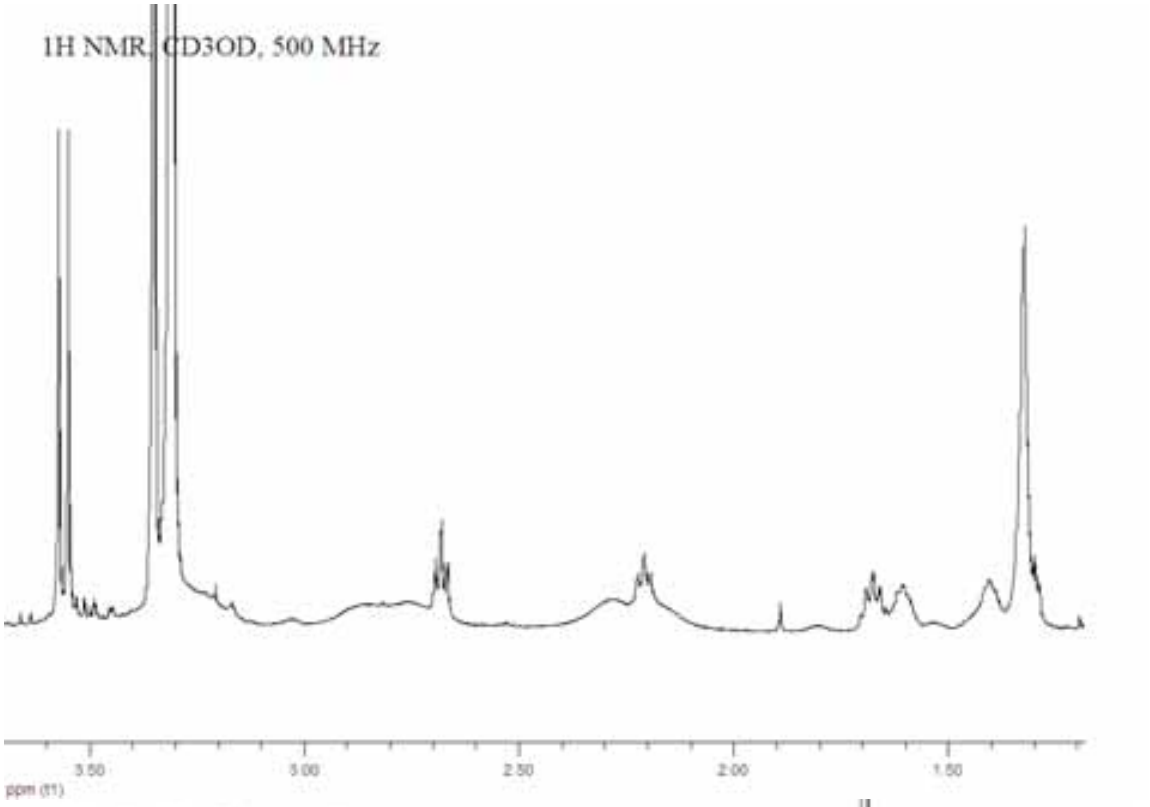

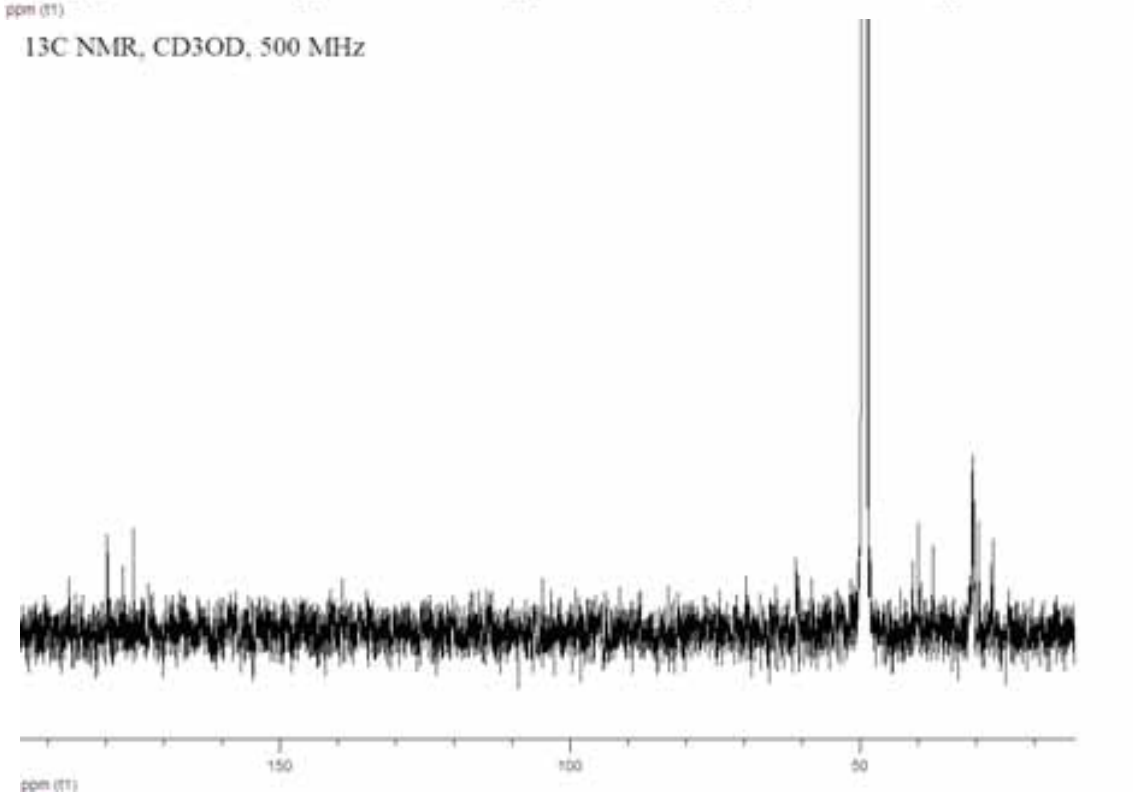

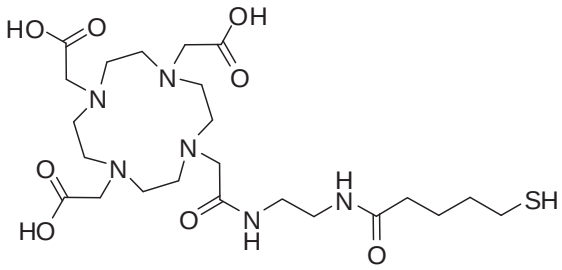

DOTA-EdAC$_5$SH

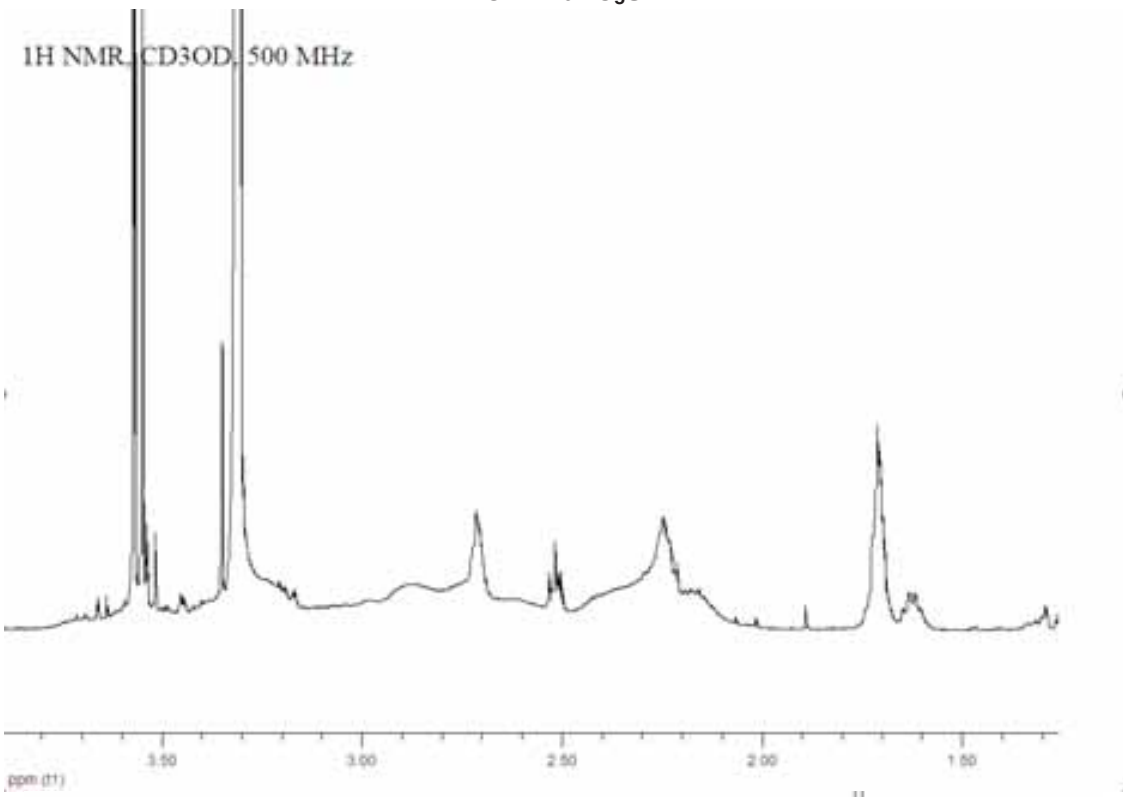

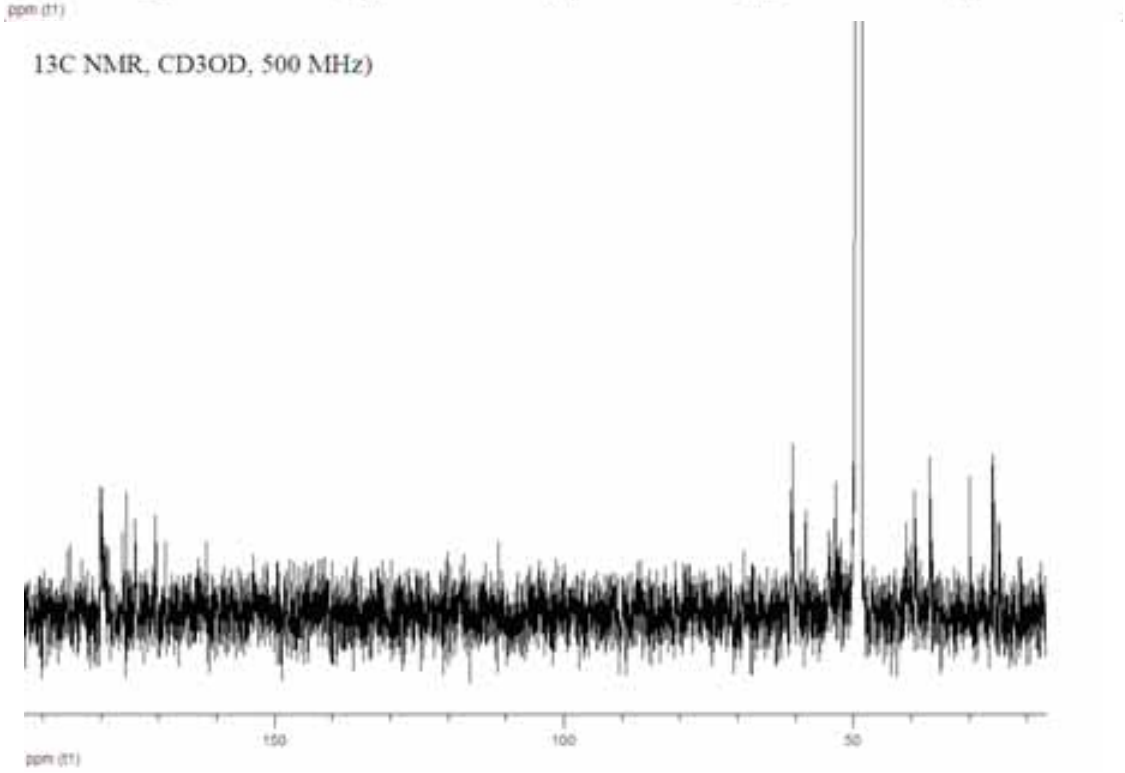

APPENDIX II

CHARACTERIZATION OF SELECTED GLYCONANOPARTICLES

1. Selected 100% GNPs

GlcC$_5$S-Au

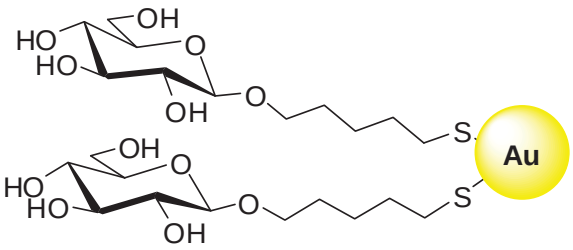

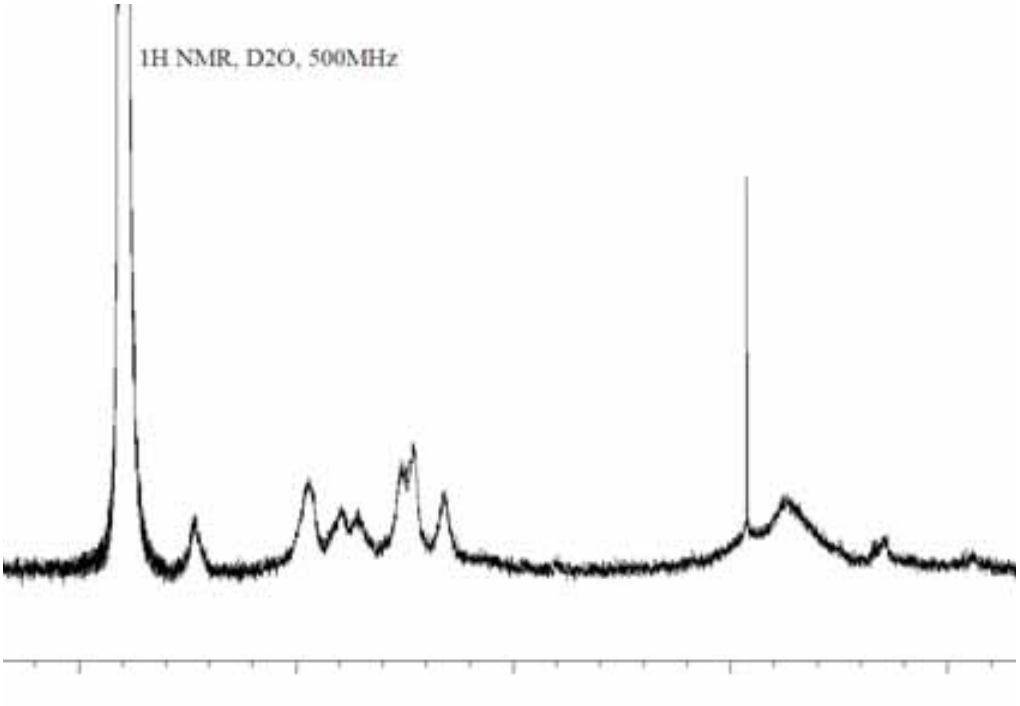

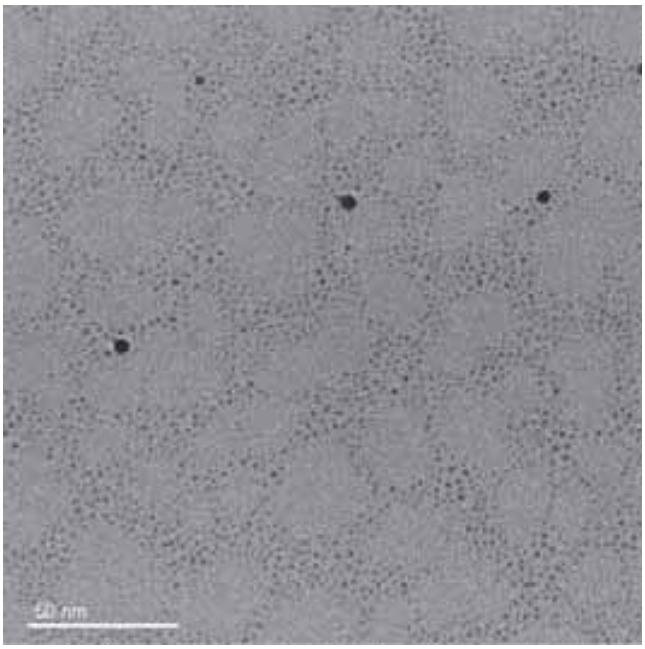

ManC_5S-Au

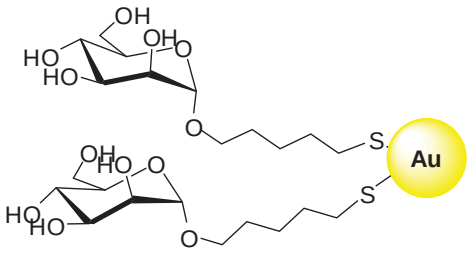

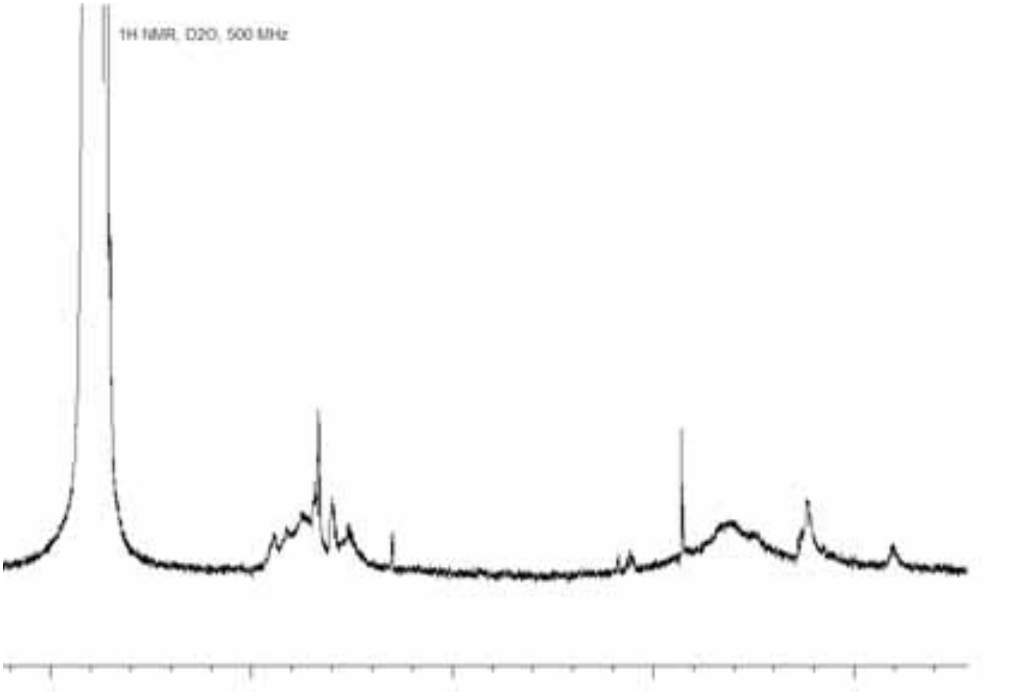

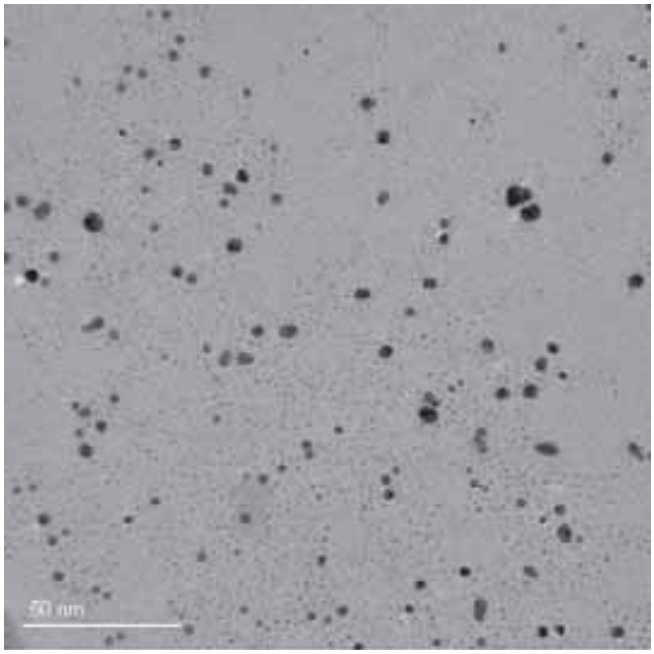

LacC_5S-Au

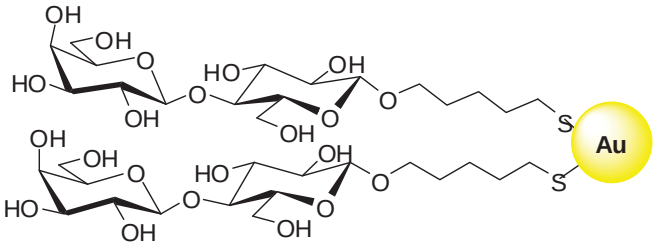
OH
OH
O
HO
OH
O
HO
OH
O
OH
O
S
Au
OH
OH
O
HO
OH
O
HO
OH
O
OH
O
S

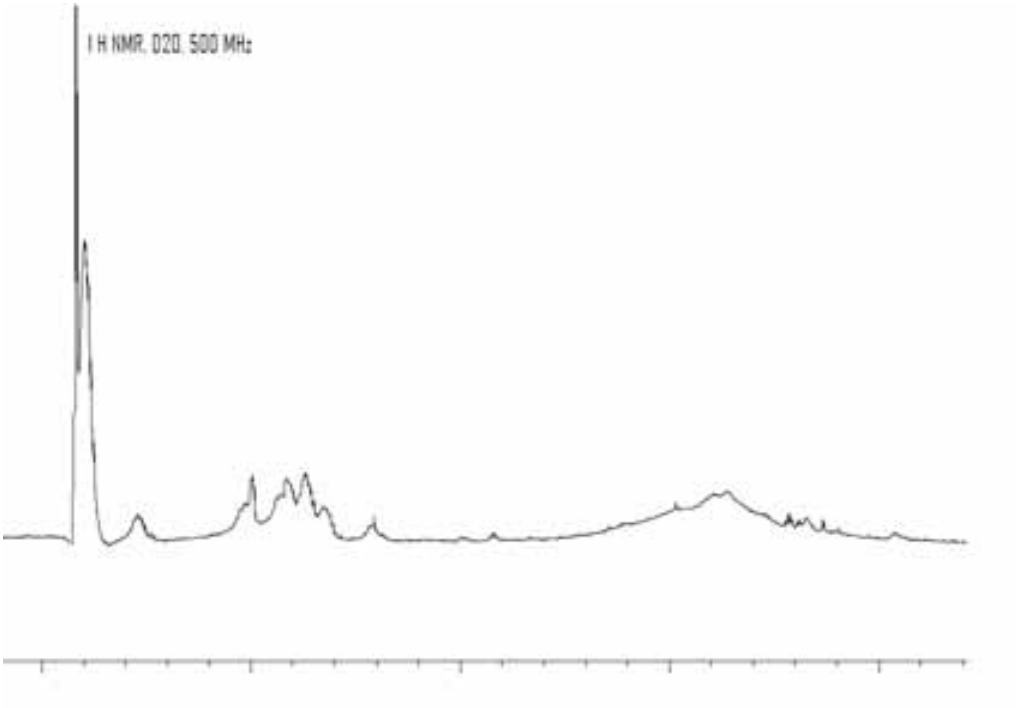
1 H NMR, D2O, 500 MHz

2. Selected Gd-GNPs

GlcC$_2$S-Au-SC$_{11}$DO3A-Gd

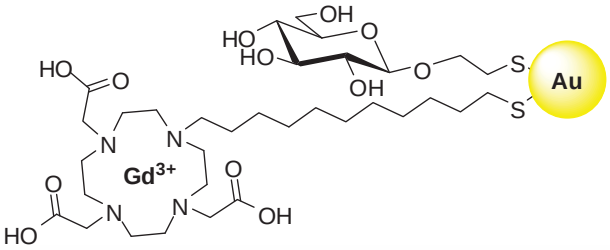

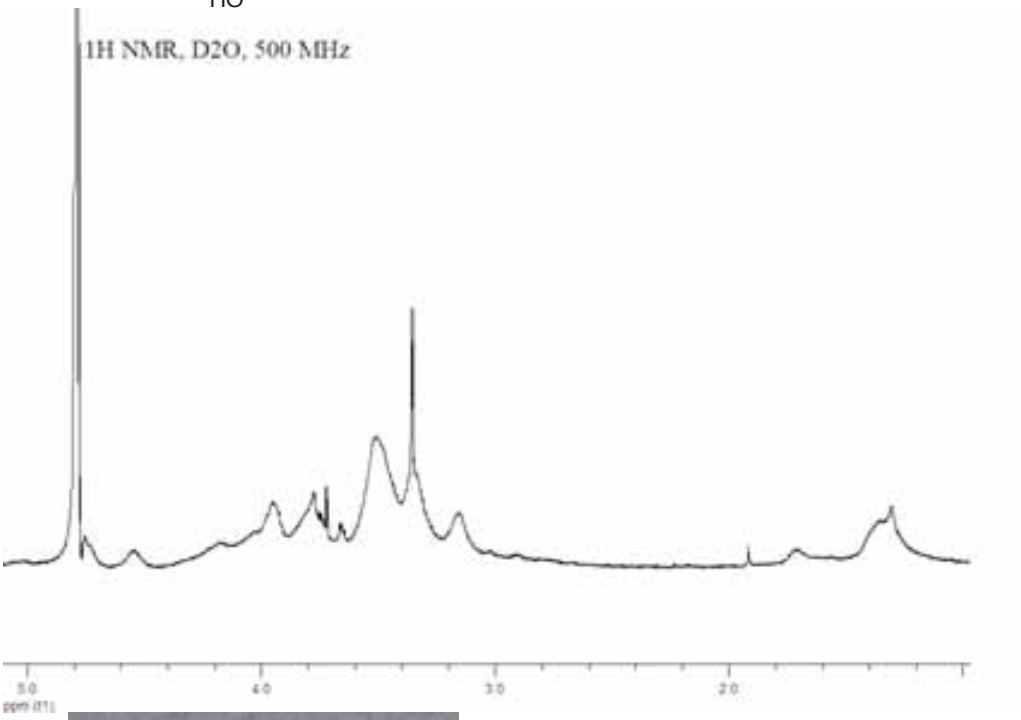

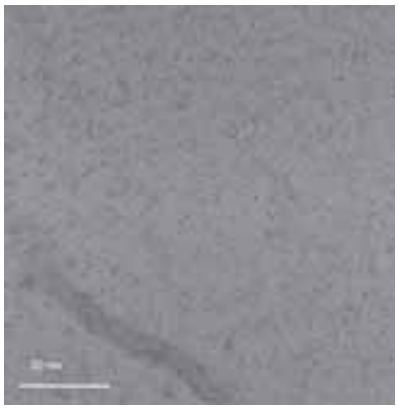

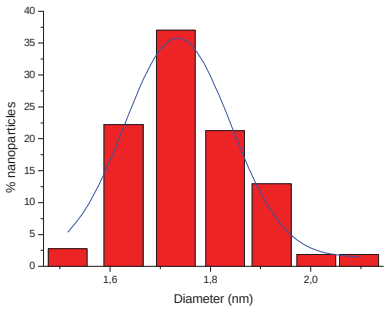

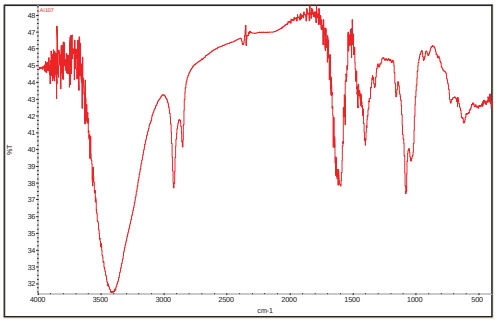

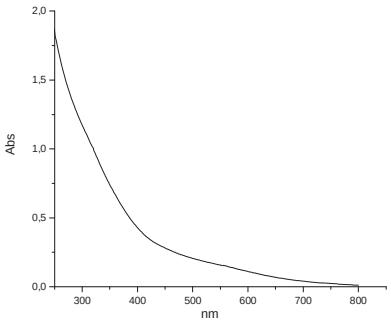

$GlcC_3S$-Au-$SC_{11}DO3A$-Gd

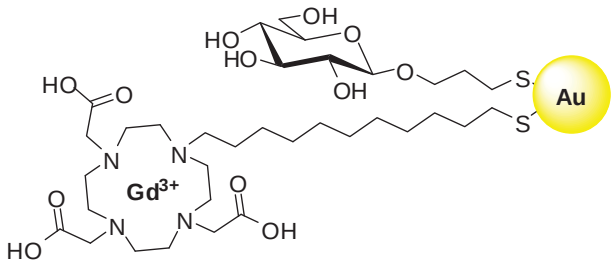

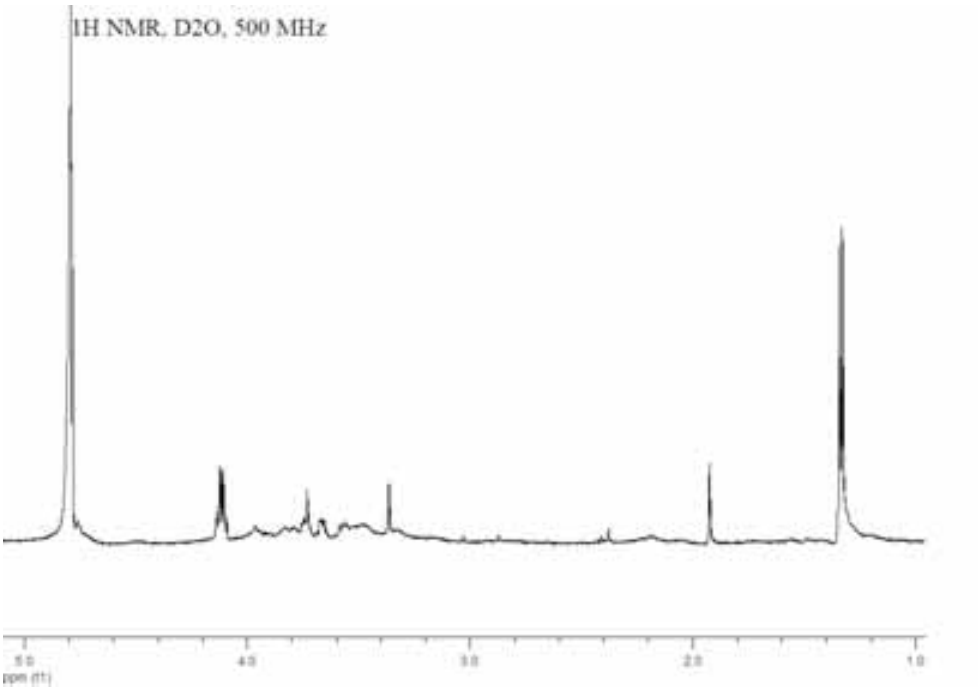

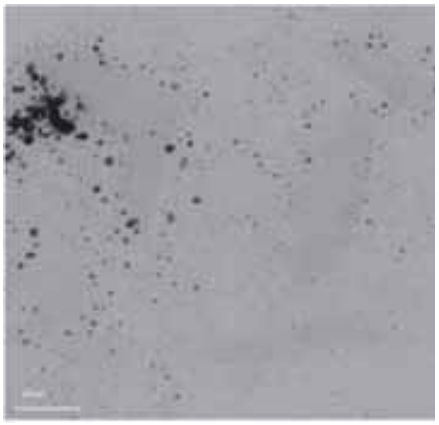

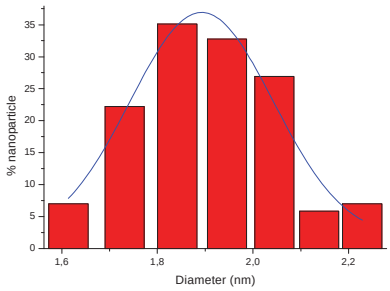

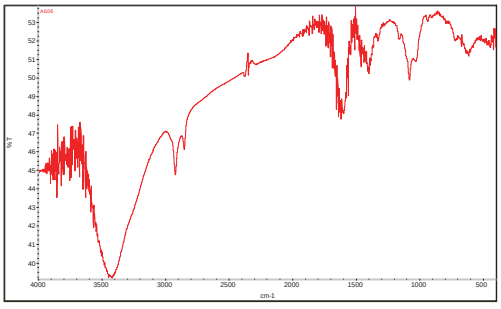

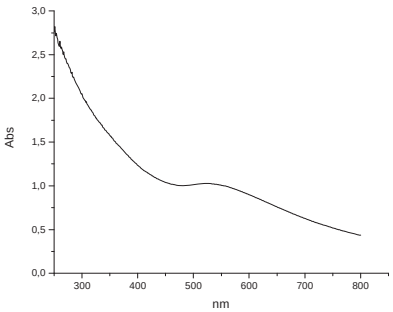

$GlcC_5S$-Au-$SC_{11}DO3A$-Gd

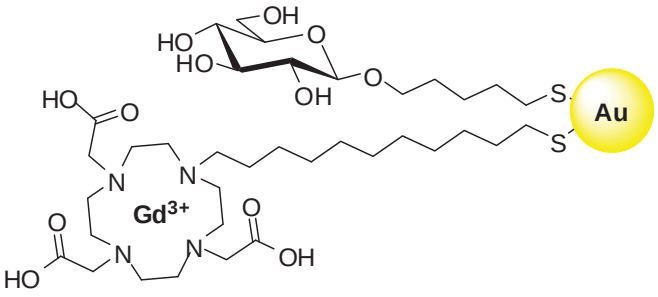

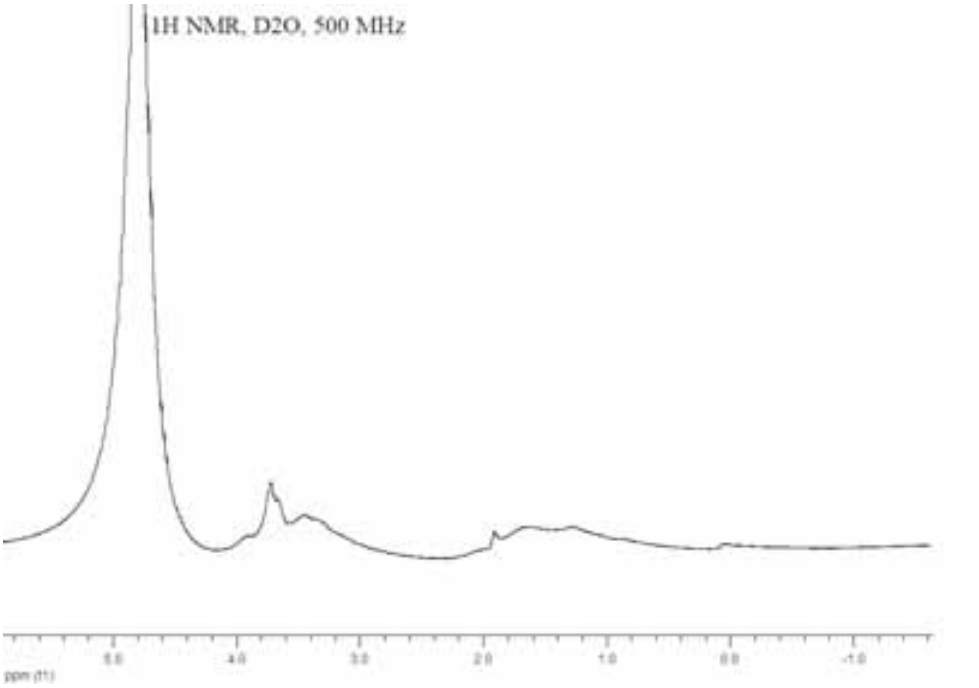

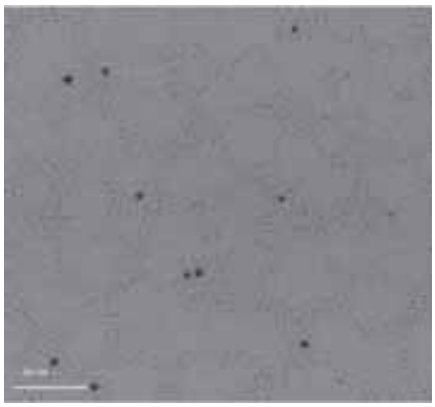

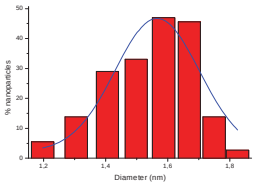

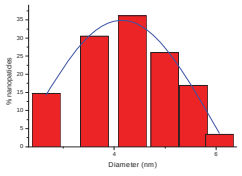

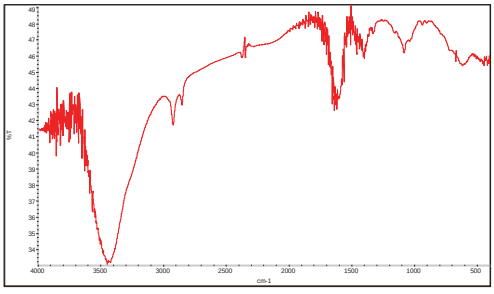

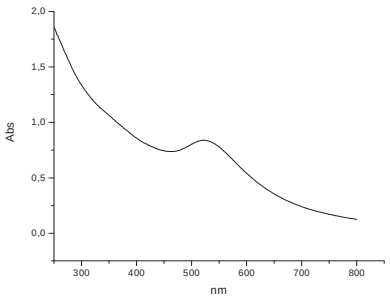

GlcC$_5$S-Au-SC$_5$DO3A-Gd

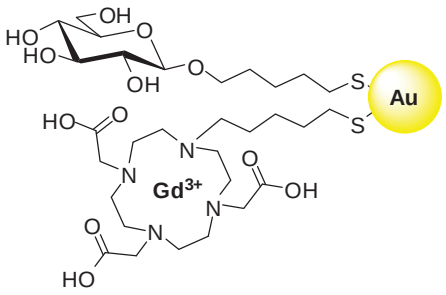

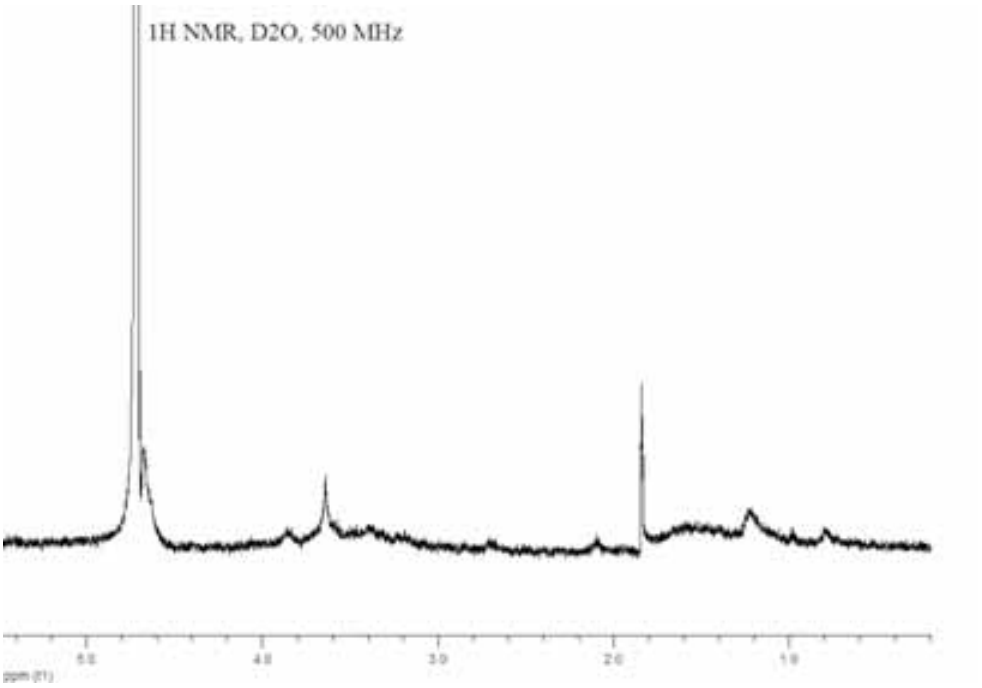

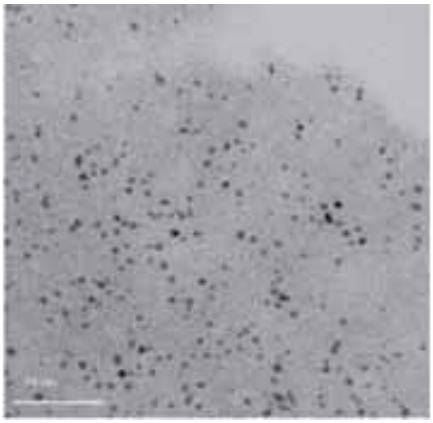

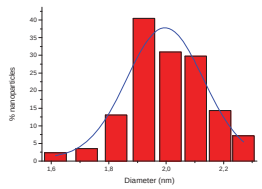

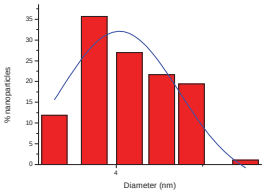

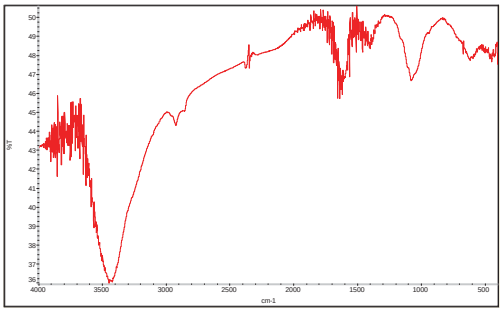

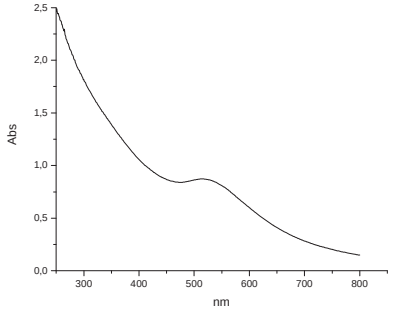

$GlcC_7S$-Au-$SC_{11}DO3A$-Gd

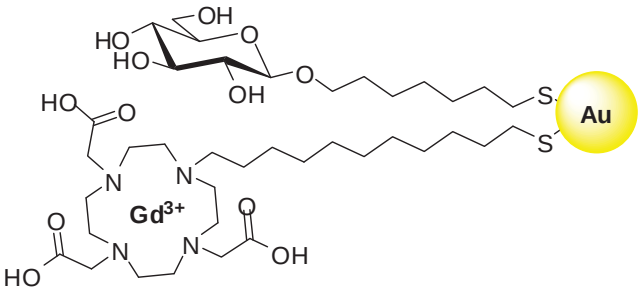

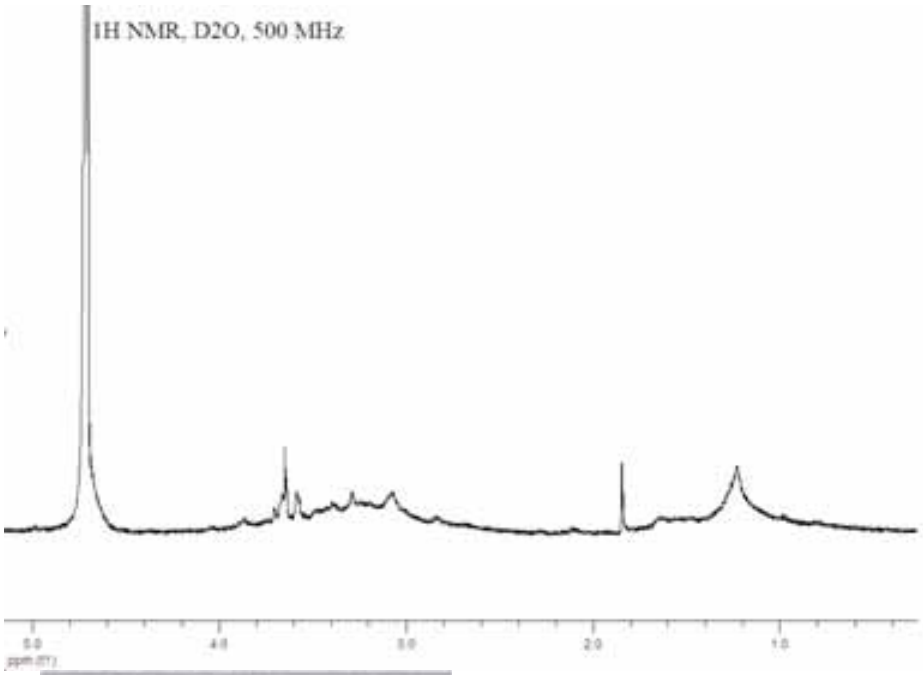

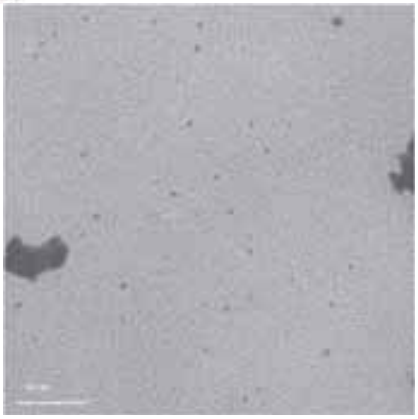

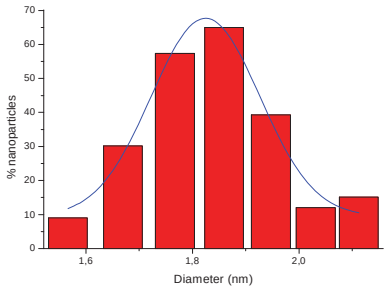

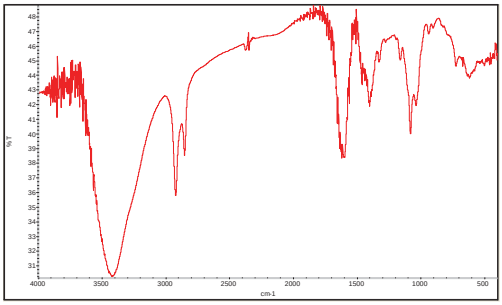

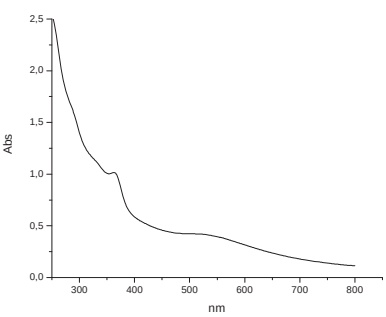

$GlcC_9S$-Au-$SC_{11}DO3A$-Gd

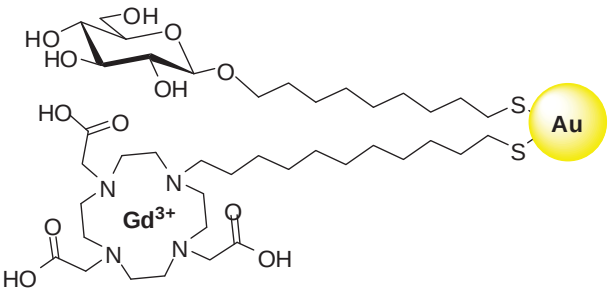

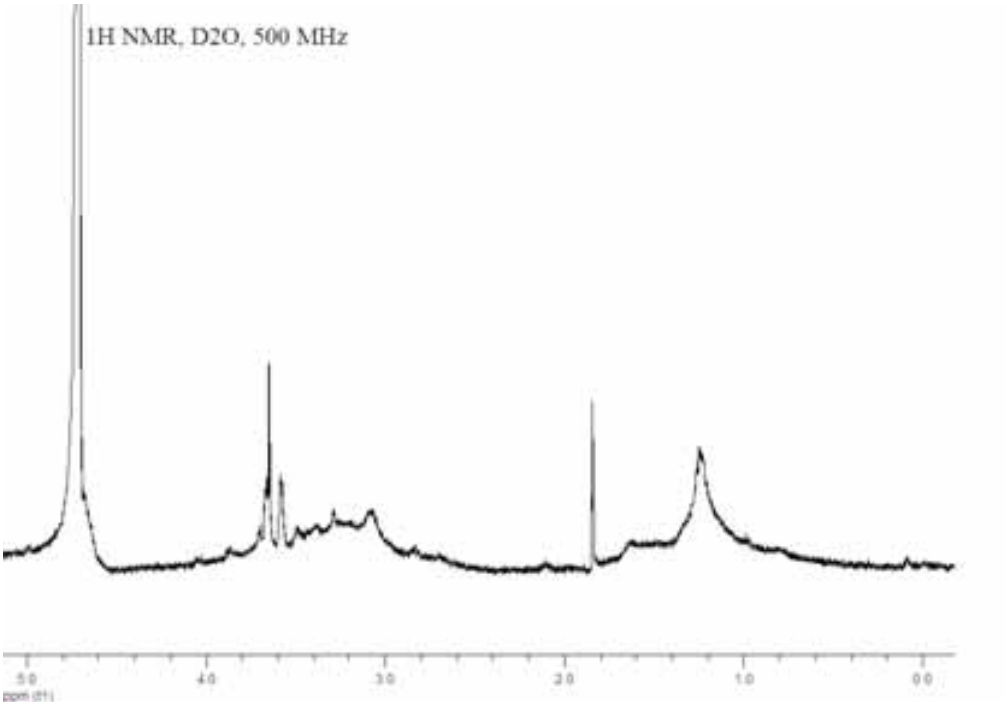

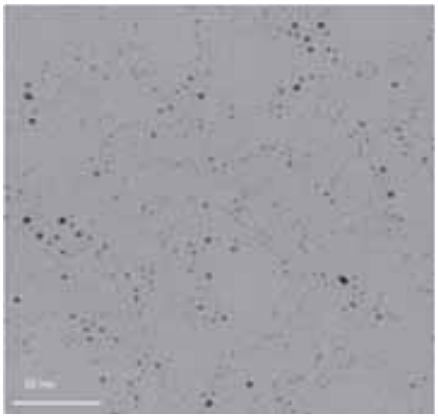

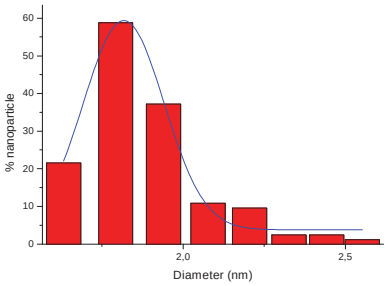

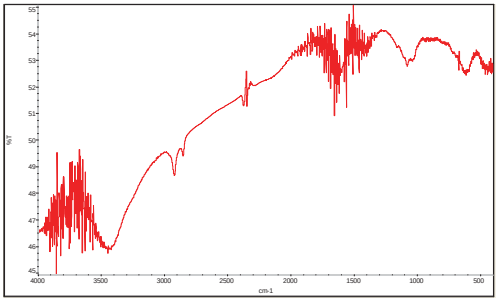

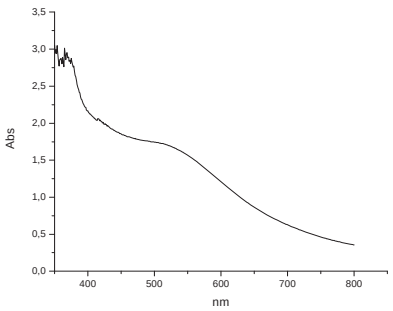

$GalC_5S$-Au-$SC_{11}DO3A$-Gd

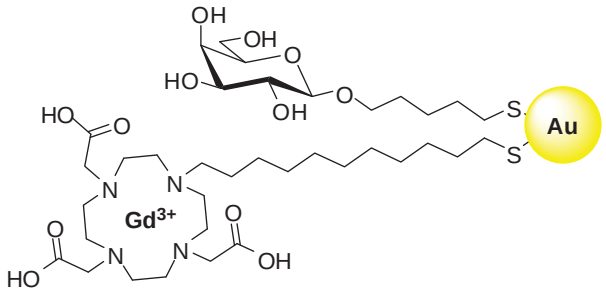

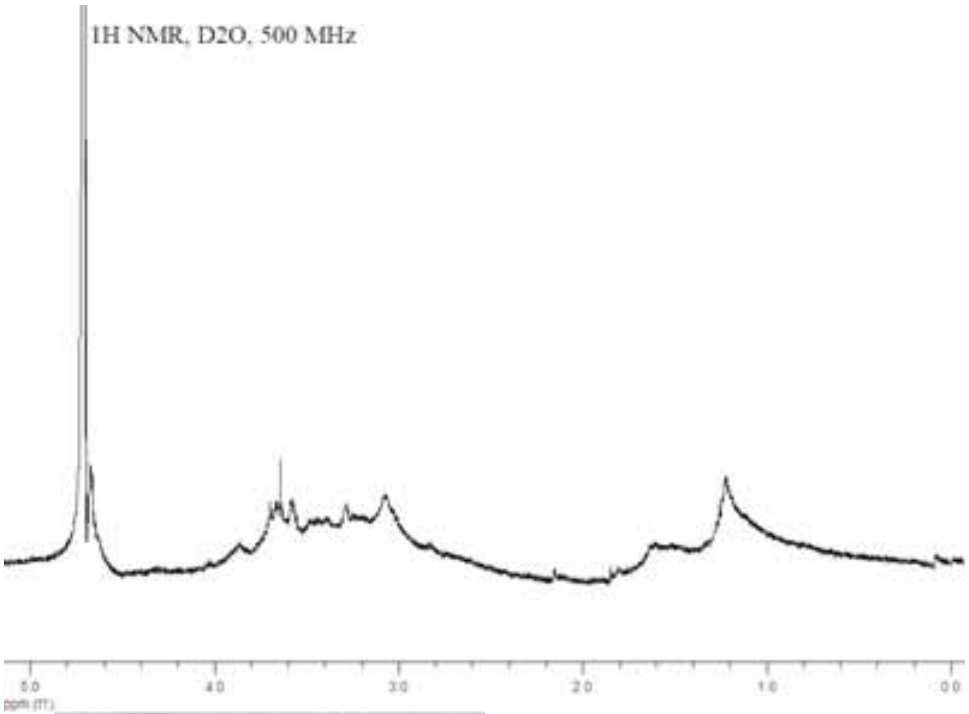

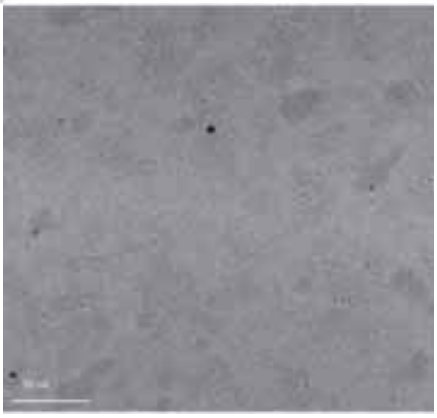

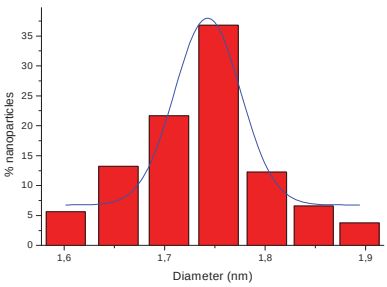

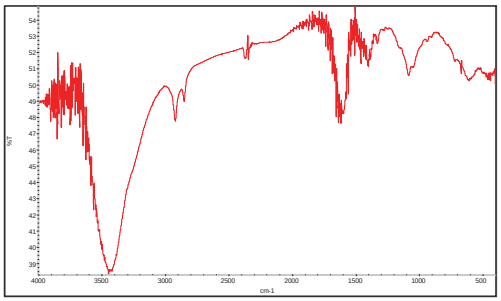

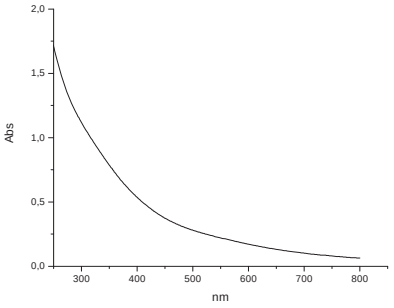

$GalC_5S$-Au-SC_5DO3A-Gd

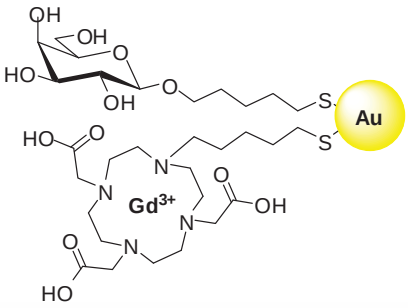

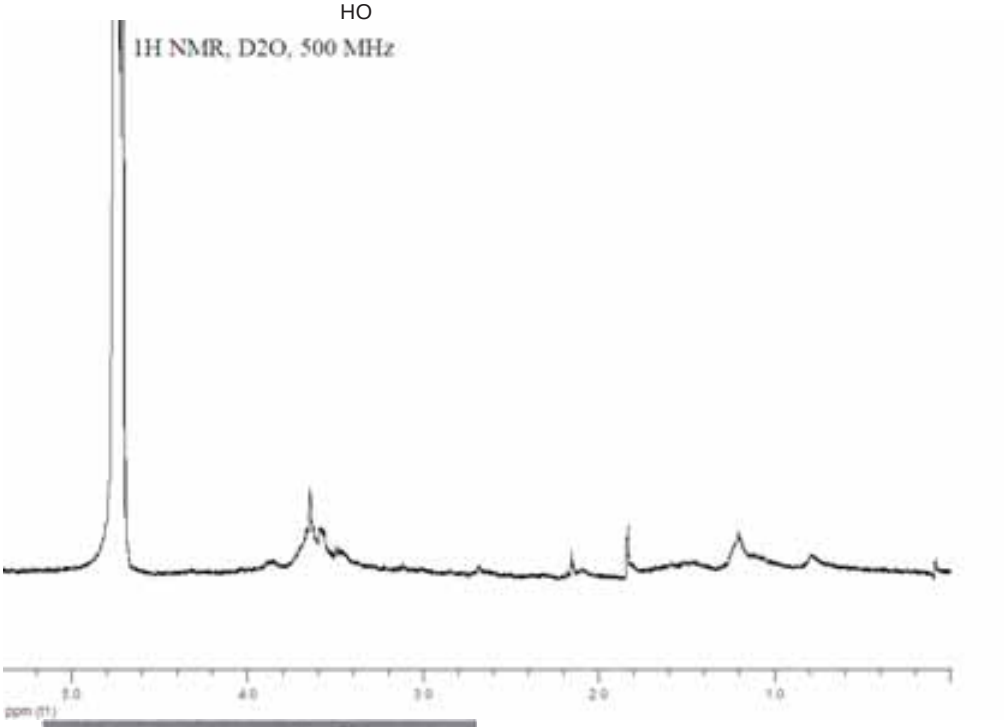

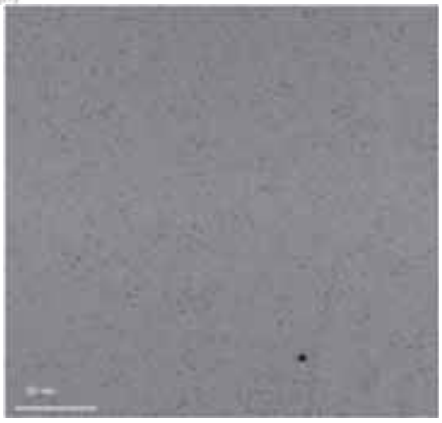

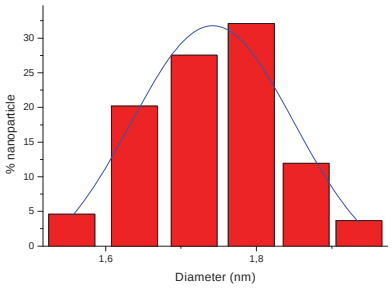

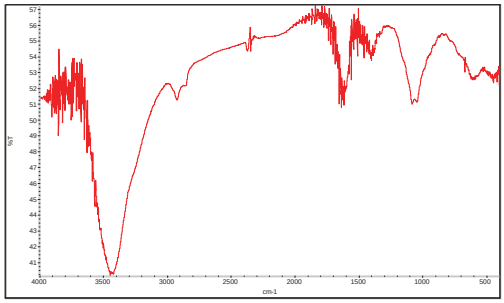

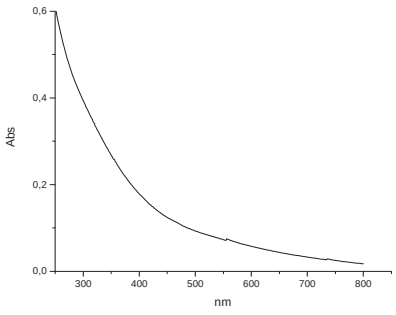

$ManC_5S$-Au-$SC_{11}DO3A$-Gd

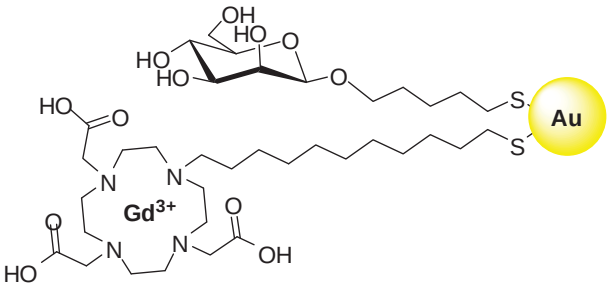
OH
HO
HO
HO
O
O
S
Au
S
HO
O
N
N
Gd3+
O
O
N
N
OH
HO

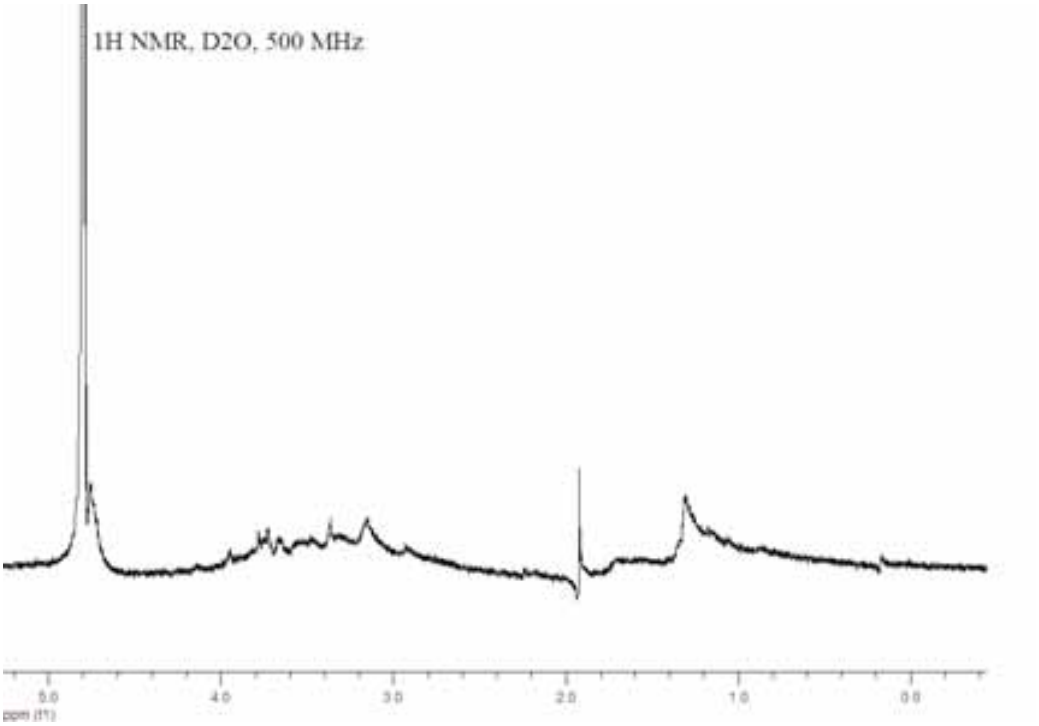
1H NMR, D2O, 500 MHz
5.0
4.0
3.0
2.0
1.0
0.0

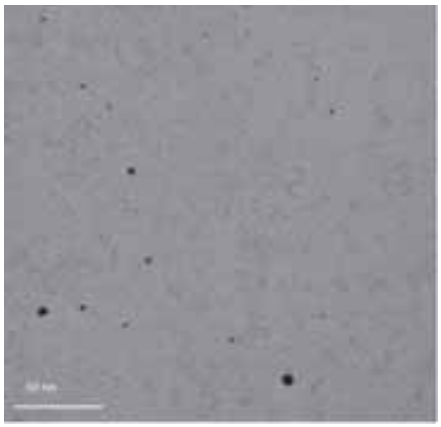

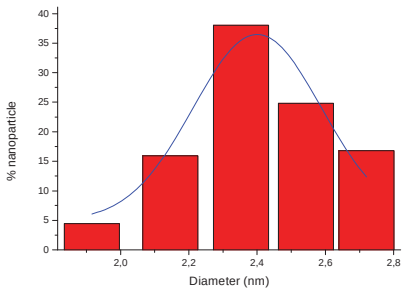
% nanoparticle
Diameter (nm)
2,0
2,2
2,4
2,6
2,8

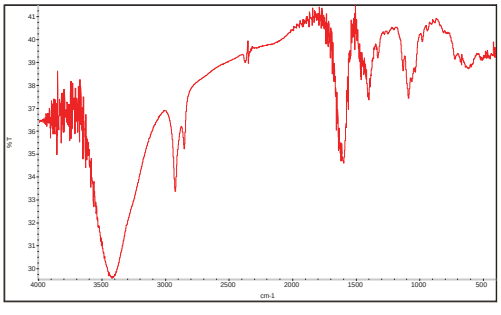
%T
cm-1

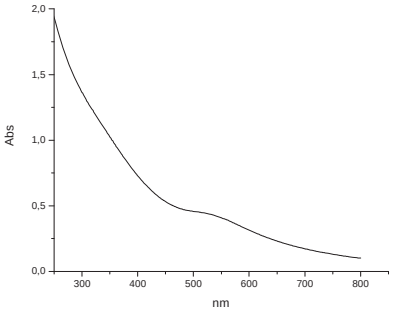
Abs
nm
300
400
500
600
700
800

ManC$_5$S-Au-SC$_5$DO3A-Gd

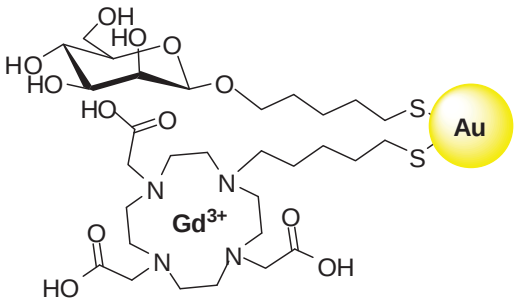

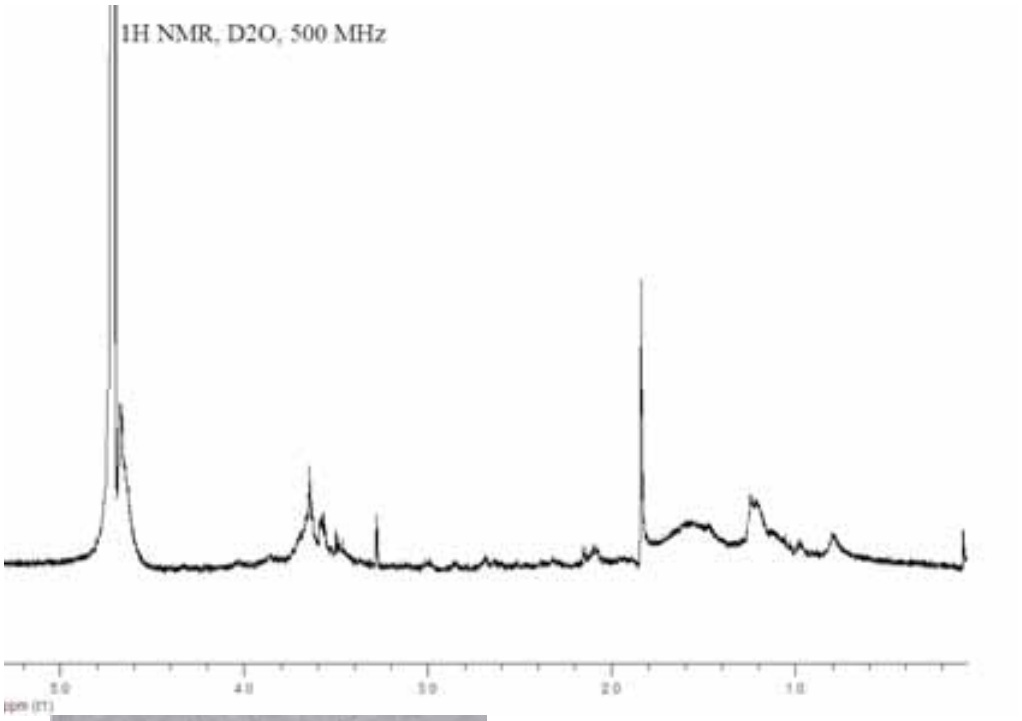

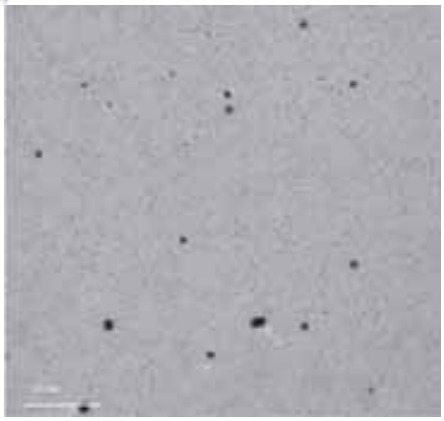

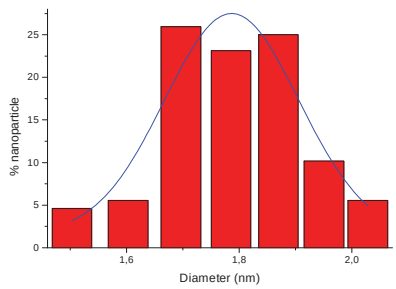

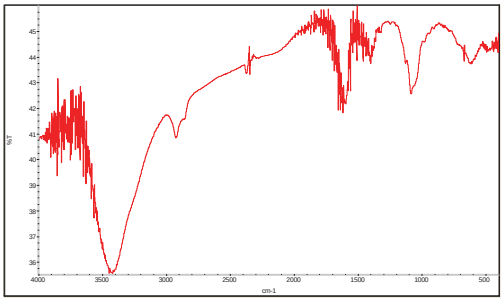

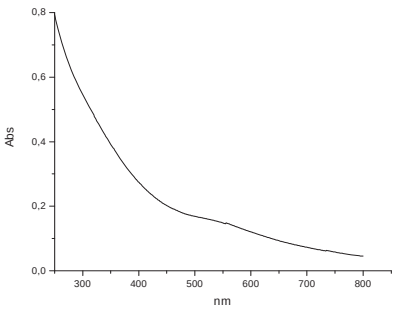

***Cellobiose*C$_5$S-Au-SC$_{11}$DO3A-Gd**

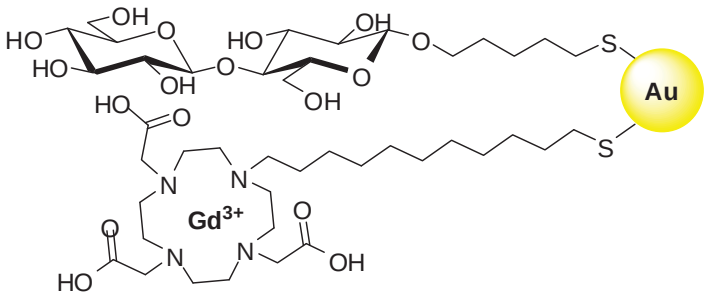

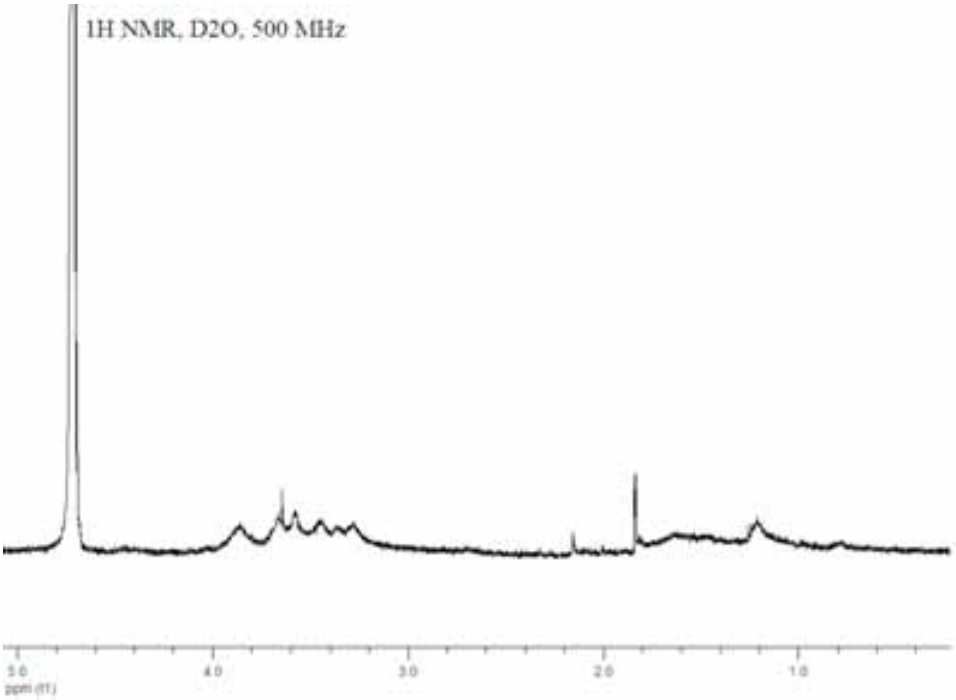

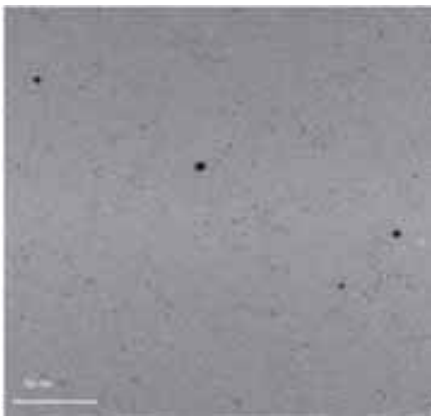

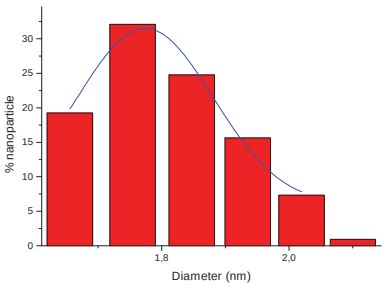

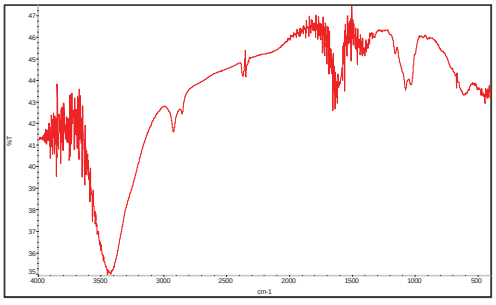

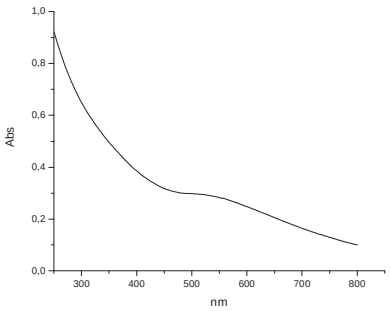

CellobioseC_5S-Au-SC_5DO3A-Gd

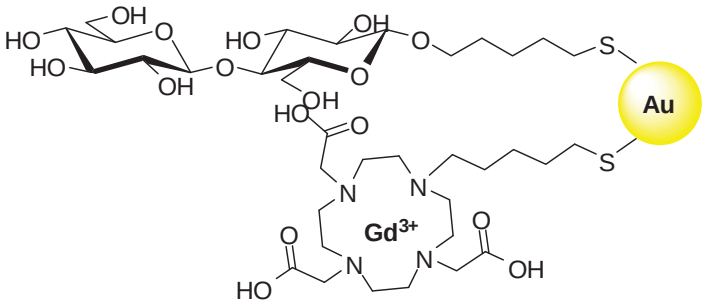

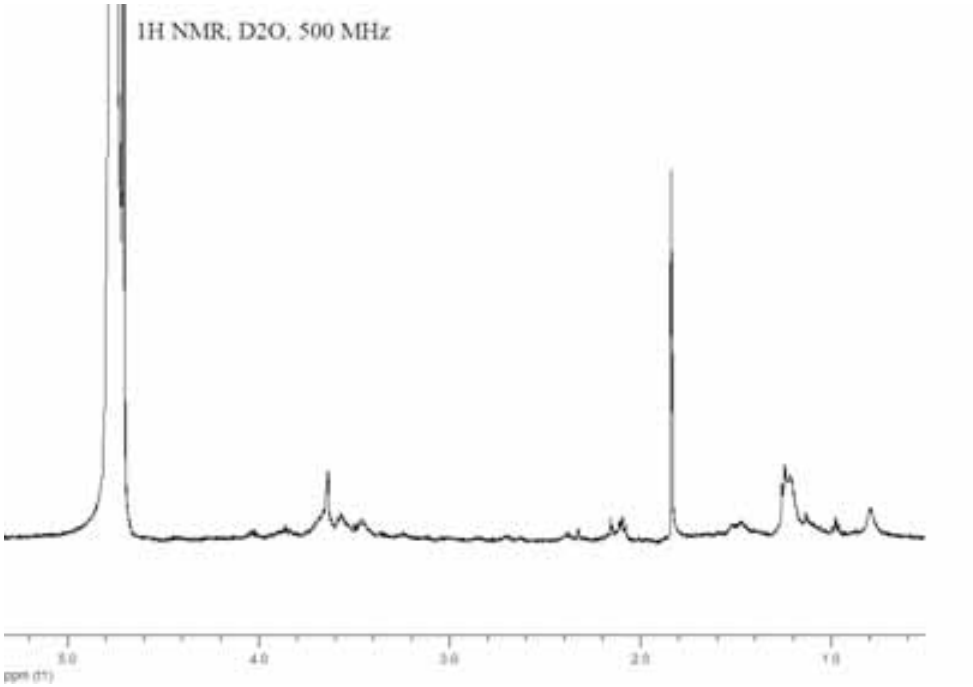

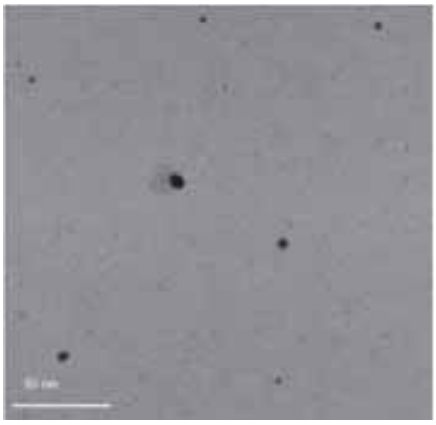

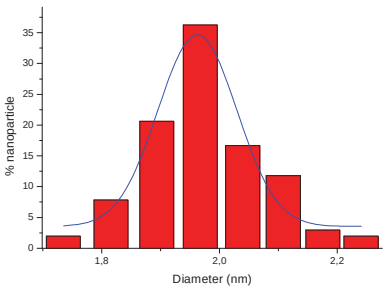

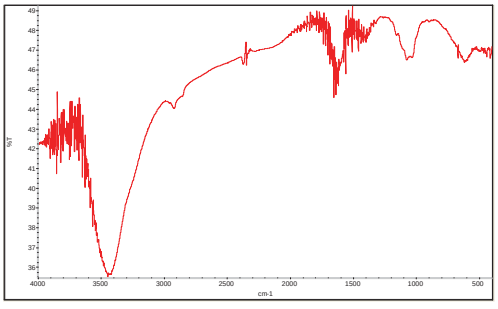

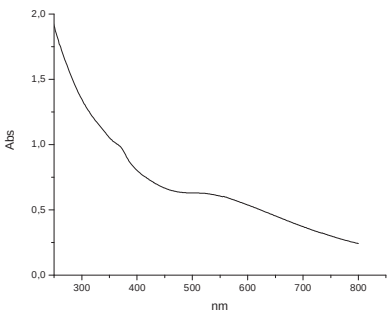

MaltoseC_5S-Au-SC_{11}DO3A-Gd

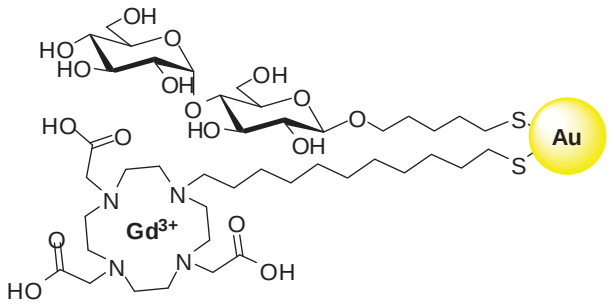

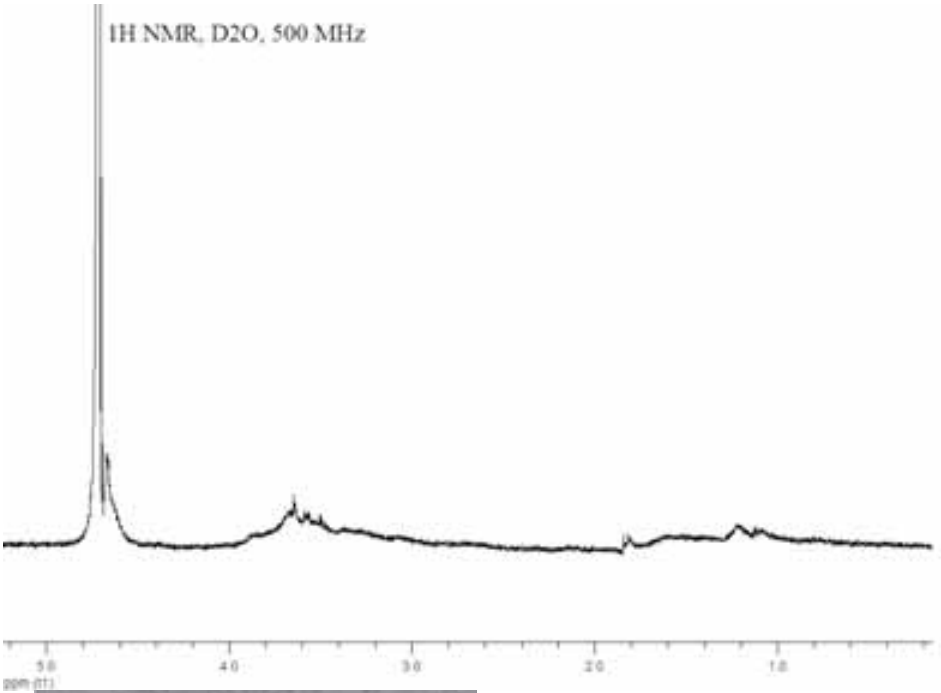

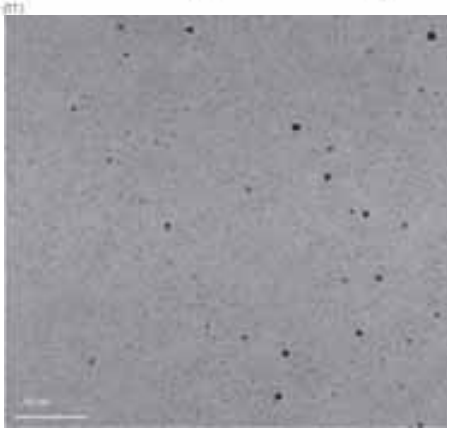

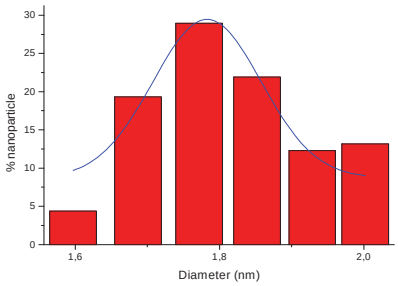

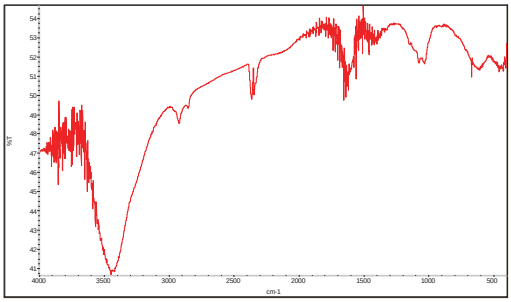

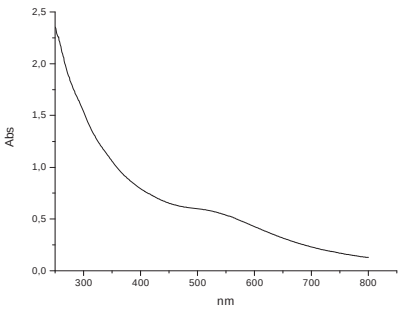

MaltoseC_5S-Au-SC_5DO3A-Gd

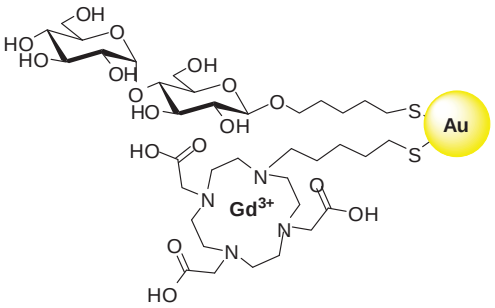

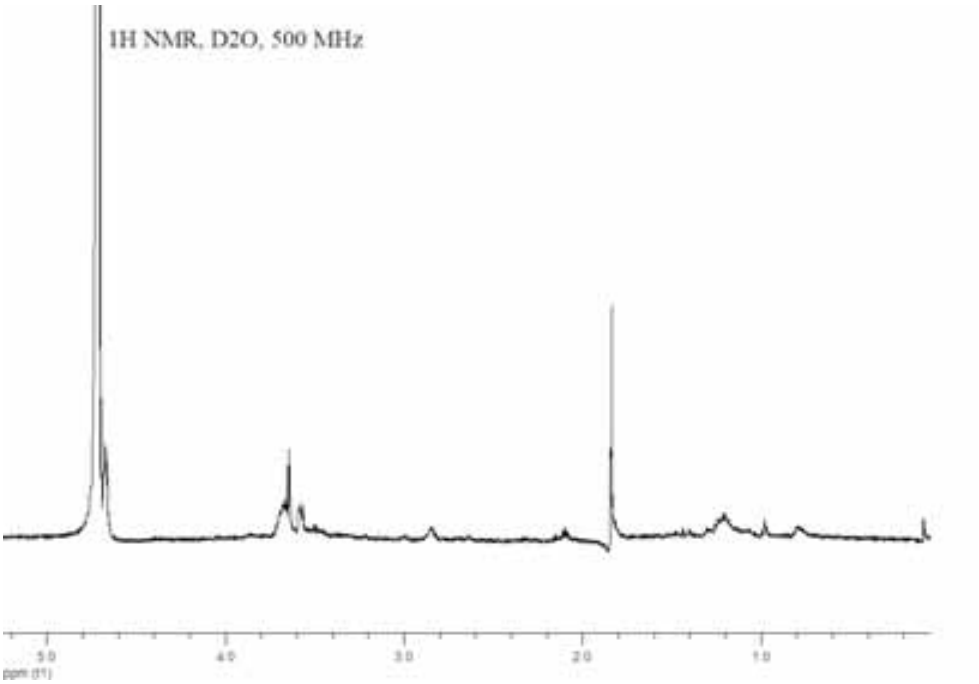

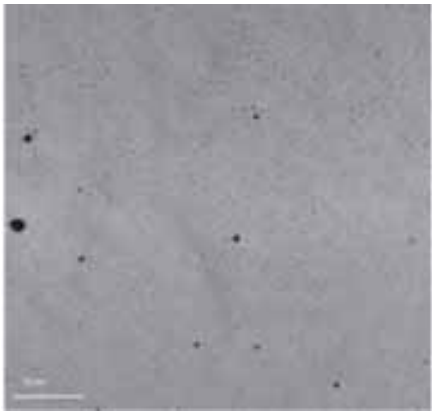

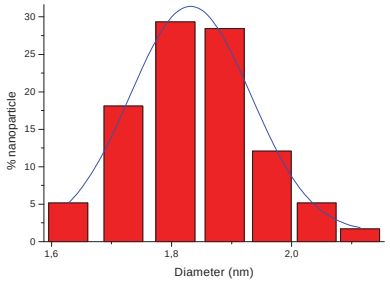

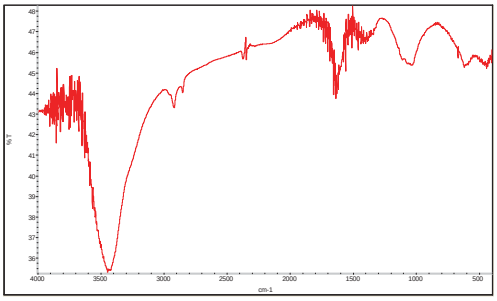

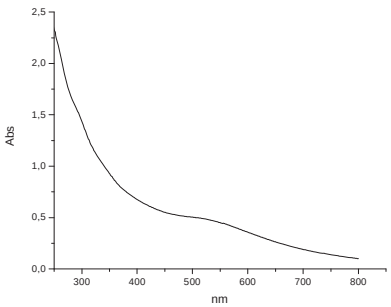

$LacC_5S$-Au-SC_5DO3A-Gd

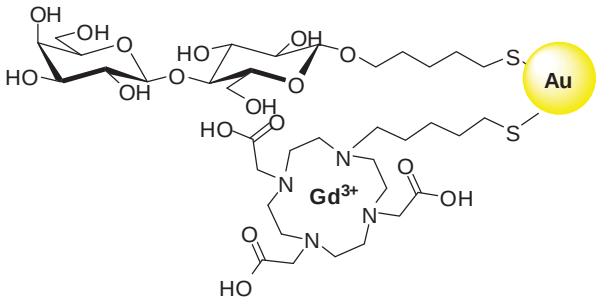

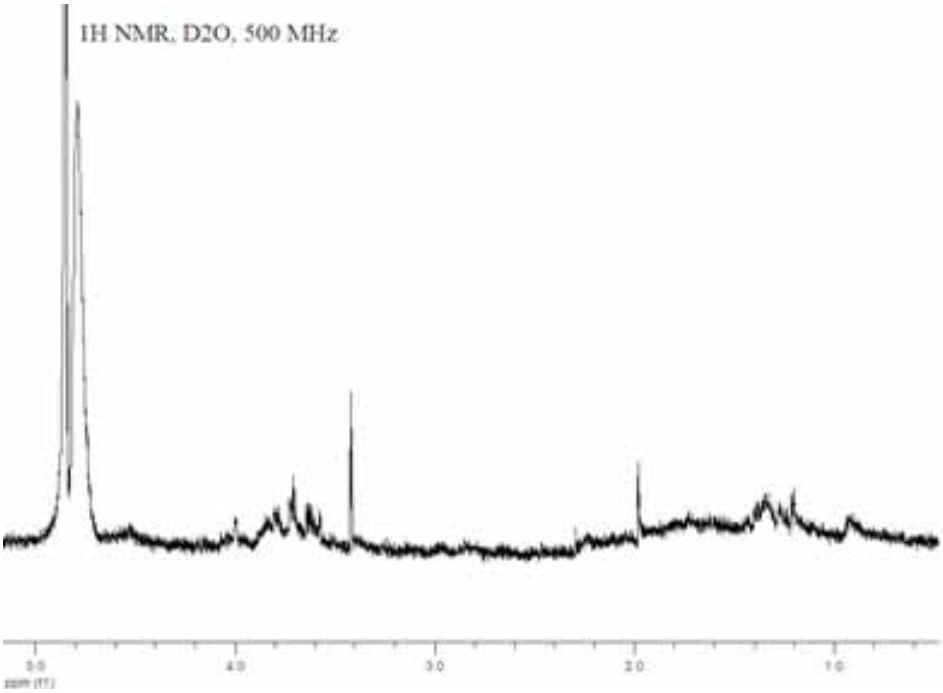

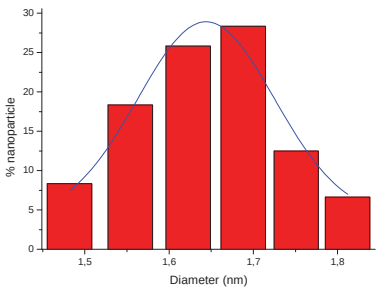

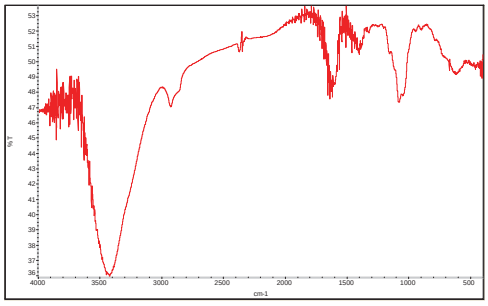

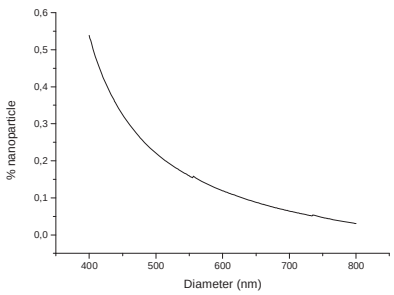

APPENDIX III

BIODISTRIBUTION STUDIES

1. Longitudinal biodistribution and toxicity assay of gold nanoparticles (GNP; $GlcC_5S$-Au-$SC_{11}D03A$-Gd)

Biological material/animals: Mice: **C57BL6 female** (12-16 weeks old), n=6

Samples recovered: **heart, lung, liver, spleen, kidneys**

Cells: **GL261** (murine glioma cells) injected sterotactically into mice brain. Note: Glioma tumors were all collected for ICP analysis and their histological evaluation is not included here Au-GNPs: **$GlcC_5$5-Au-SC_{11}D03A**, synthesized by the group of Dr. S. Penades.

Histological processing: Formalin fixation and paraffin embedding, as usual.

Sections were stained with:

-Haematoxylin-Eosin (HE).

-A combination of **Silver enhancement staining** (for detection of gold nanoparticles) and **Prussian Blue** (for detection of iron containing deposits, combined with Nuclear Fast Red as counterstainig). This stain allows the differentiation between golden deposits and hemosiderin both seen as light or dark brown granulated areas in HE stained samples. Silver enhancement staining reveals GNP deposits as black to dark brown deposits due to their content in gold, whereas the Prussian Blue labels the hemosiderin (containing mainly iron) with a brilliant blue staining.

Samples analyzed **Liver, spleen, kidneys and lung** of mice in two groups.

Group #1 (G1): Sacrificed 24 hours post GNP administration (i.v.). n=4

Group #2 (G2): With no GNP administration, as controls. n=2.

Hearts of animals in both groups were also analyzed and was found to be apparently normal (figures not shown). See **Table 1** and Figures 1 to 4, for more details.

Conclusions

All animals administered with GNP show gold deposits (positively identified by Silver enhancement/Prussian Blue staining) in cells of the reticuloendothelial system (RES).

The greater gold accumulation is seen in livers of GNP administered mice, followed by spleen, lung and kidneys, in this order. The presence of gold deposits in lungs might indicate the detention of nanoparticle

aggregates in the pulmonary alveoli after i.v. administration. Considerable differences are observed among the GNP treated mice, regarding the quantity of gold deposits. Animals #1 and #7 show a higher degree of gold deposition in all organs analyzed, compared to animals #2 and #3, that received the same or even higher GNP dose (see Table 1). All these observations are in accordance with results obtained from the ICP analysis.

Table 1. Summary of the animals analyzed, including the administered dose and date of sacrifice.

Group	Treatment	Animal #	Admin. date	Sacrifice date	Weight (g)	Injected Vol. (µl)	Conc. (mg/ml.)		Injected Dose (ID, mg)	
							Gd	Au	Gd	Au
G1	GNP	1	06/4/2011	7/4/2011	20	70	1.75	5.47	0.122	0.383
G1	GNP	3	12/5/2011	13/5/2011	20	70	1.75	5.47	0.122	0.383
G1	GNP	4	17/5/2011	18/5/2011	19	150	0.87	2.74	0.131	0.410
G1	GNP	7	12/5/2011	13/5/2011	20	?	1.75	5.47	?	?
G2	-	5	-	13/5/2011	20	-				
G2	-	6	-	13/5/2011	22	-				

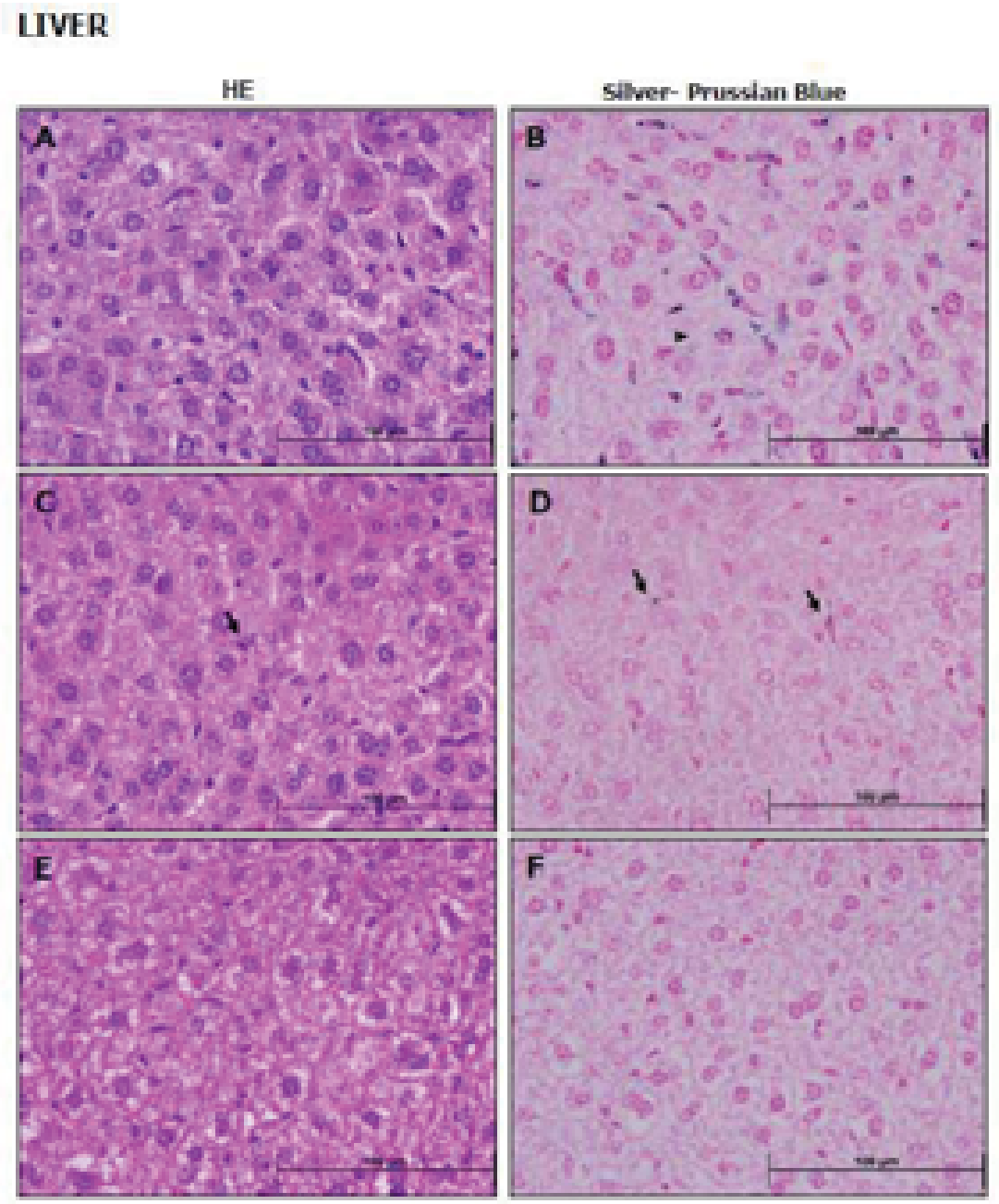

Figure 1. *Liver (40x). (A, B) Animals from G1 with higher degree of GNP deposition pattern (animals #1 and #7). GNP is located intracytoplasmatic inside Kupffer cells or free in the sinusoids. (C, D) Animals from G1 with a mild-low GNP (arrows) deposition pattern (animals #3 and #4). (E, F) G2, control animals, where no gold deposits are observed.*

HE staining shows that the general architecture of the liver parenchyma is normal. Some hepatocytes showed mild glycogen storage and small foci of chronic periportal inflammation, composed by lymphocytes and some mononuclear cells, both are an unspecific change related to C57Bl/6 mice.

In G1 animals we observed round to oval granules of birefringent golden dark-brown pigment primarily located inside the Kupffer cells cytoplasm, although can also appear free in the sinusoids (arrowheads in the figure), but we can not detect granules inside the hepatocytes. Moreover we detect two patterns of deposition; a couple of animals (#1 and #7) showed a high degree of deposition meanwhile the other two animals (#3 and #4) showed only a mild deposition of GNP. No additional abnormalities were observed.

Silver stain clearly increases both the sensibility and the specificity when detecting GNP's comparing to HE. The golden identity of the dark precipitates seen in HE staining is confirmed by the silver staining (detecting specifically gold) and the absence of signal with Prussian blue staining (confirming that deposits do not correspond to hemosiderin).

As it is said before, we observe differences in the administered GNP's animals, two animals have a high intracitoplasmatic deposit in Kupffer cells and free in the hepatic sinusoids, and the other two animals have only a mild-low grade deposition.

Control animals (G2) do not have any kind of gold deposition and the hemosiderin pattern was, as expected, similar to the GNP treated animals.

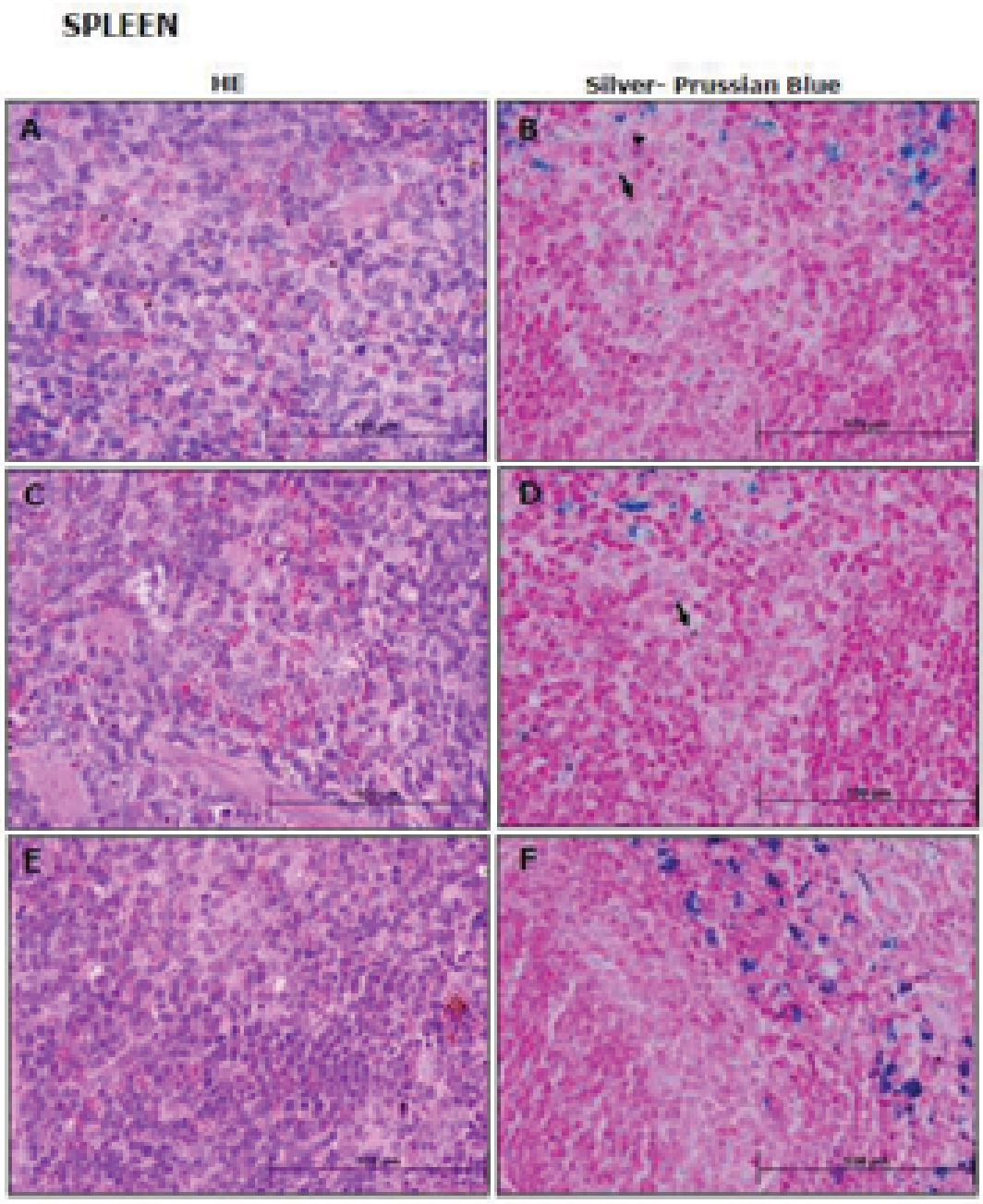

Figure 2. **Spleen (40x).** *(**A**, **B**) Animals from G1 with higher degree of GNP deposition pattern (animals #1 and #7). GNP mostly located in red, but also in white pulp, either inside the cytoplasm of macrophages (arrowhead) or free in the parenchyma (arrows). (**C**, **D**) Animals from G1 with a mild-low GNP (arrows) deposition pattern (animals #3 and #4). The Silver enhancement/Prussian Blue staining permits the differentiation between GNP (dark-brown briefringent pigmentation) and the hemosiderin (blue staining). (**E**, **F**) G2, control animals, with no GNP deposits.*

HE shows that the spleen structure from either control or GNP animals was similar and compatible with normality. Granules and large aggregates of yellowish brown pigment were

found in both groups, mostly located in red, but also in white pulp, either inside the cytoplasm of macrophages or free in the parenchyma. The morphology of these granules was very irregular in shape and size in spleen and liver.

When using Silver enhancement/Prussian blue staining we detect blue stain mainly in the red pulp but also in the white pulp. Moreover hemosiderin presence is considered normal in spleen specifically inside macrophages cytoplasm from the red pulp. However in the white pulp we are able to distinguish granules of golden dark-brown pigment indicating GNP's deposition. As we described before from the GNP's administered group, two of the animals have a higher deposition pattern than the other two animals. In control group (G2) we only can distinguish blue staining in the red pulp corresponding to hemosiderin

deposits.

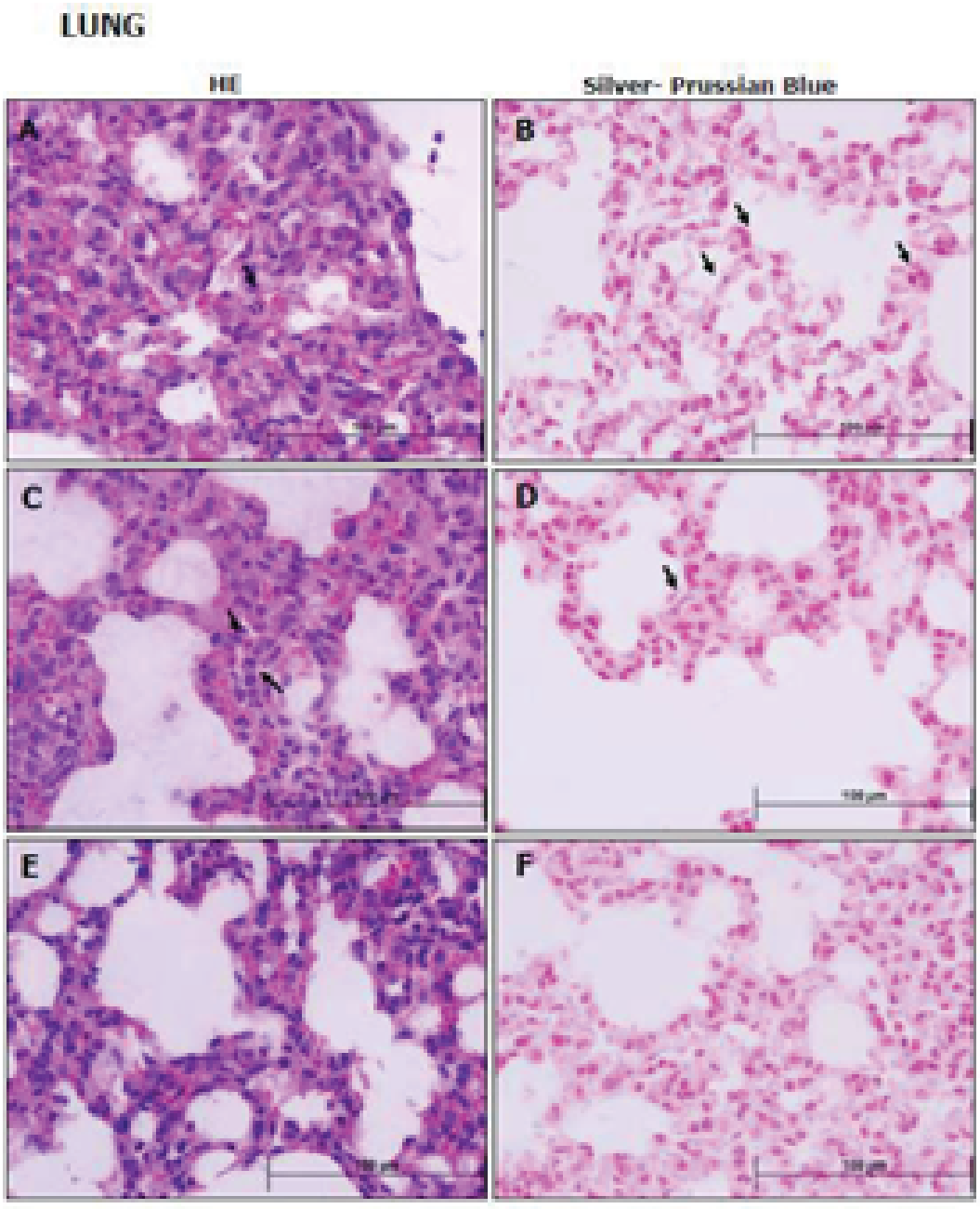

Figure 3. *Lung (40x). (**A**, **B**) Animals from G1 with mild GNP deposition pattern. (**C**, **D**) Animals from G1 with a very-low GNP (arrows) deposition pattern. (**E**, **F**) G2, control animals, with no GNP deposits.*

HE staining revealed that lung parenchyma from either control or GNP animals was compatible with normality. Granules of golden brown pigment were found in G1 with HE. There are two different kinds gold deposition in lungs, on the one hand we observed well defined round to oval dark granules inside the cytoplasm of macrophages (similar to those seen in liver) and on the other hand, gold deposition formed a fine black film that sometimes can be confused with an artifact of the stain.

In lungs, silver stain also helps to detect GNP deposits. These GNP deposits are only detected in G1, and they have a bigger size than those in the liver and spleen. The two animals with higher general deposition pattern in other organs have a mild deposition and a very low deposition was detected in the other two animals. Granules of golden brown pigment are located primarily inside the cytoplasm of interstitial macrophages but also extracellular. Their big size may be due to the formation of some aggregates that has been detained in the pulmonary alveoli. After learning that, we were also able to recognize gold deposits in HE sections (see arrows in Fig3 A and C). Control group does not show any specific staining.

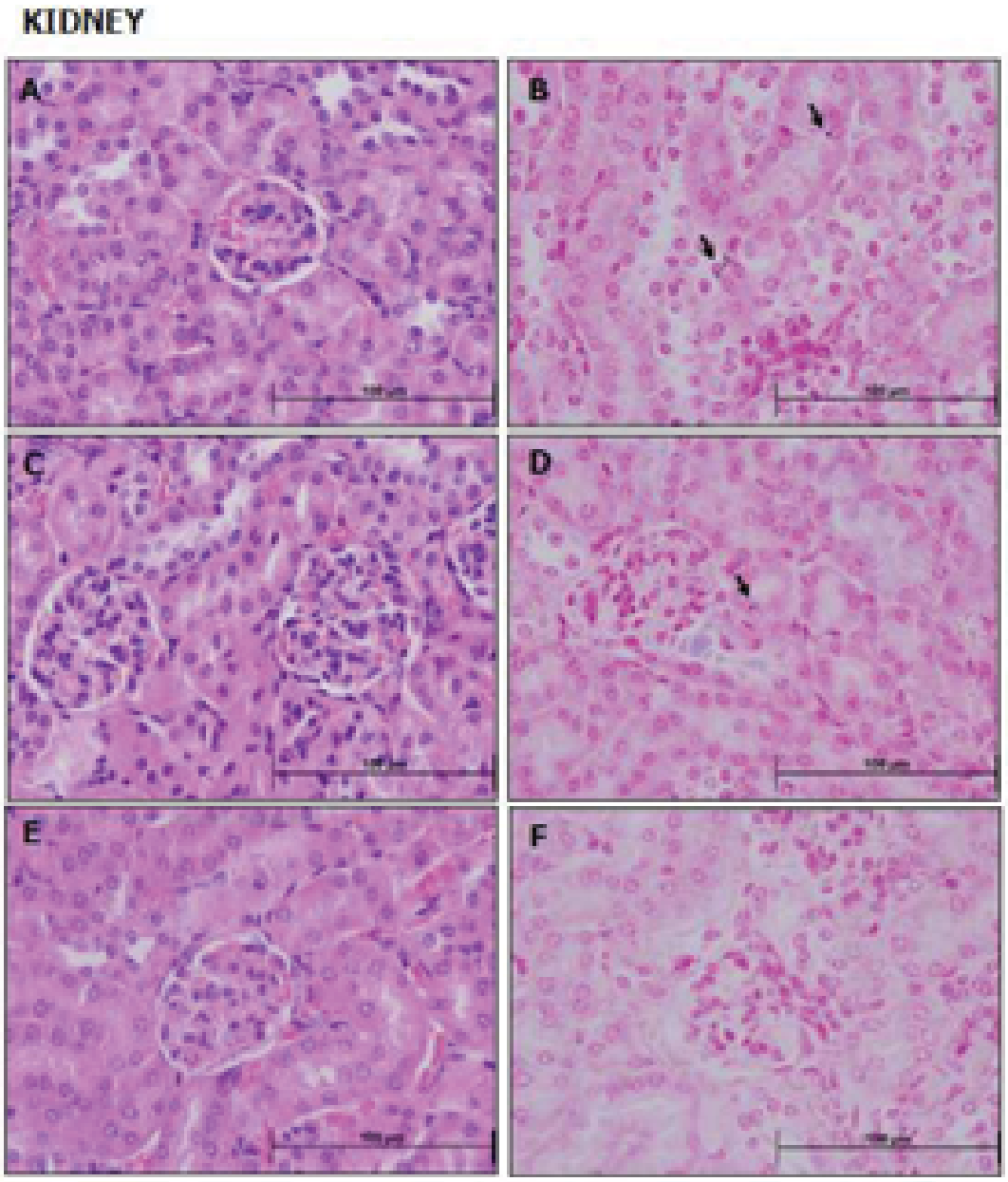

Figure 4. *Kidney (40x). No dark-brown birrefrigent pigment deposition was detected in kidney sections stained with HE in any of the animals. However, few small golden deposits were identified by Silver enhancement/Prussian Blue staining. (**A**, **B**) Animals from G1 with low GNP deposition pattern (animals #1 and #7). (**C**, **D**) Animals from G1 with a low GNP (arrows) deposition pattern (animals #3 and #4). (**E**, **F**) G2, control animals, with no GNP deposits.*

Silver enhancement staining allowed the detection of gold, although in all G1 animals the size and quantity of golden deposits is very low. Granules of golden brown pigment are located free in the interstitium or inside the cytoplasm of macrophages. Control group showed no deposition. We can

state that the amount of accumulation in the kidney is the lowest compared with the liver, spleen and lung.

2. ICP-MS results of in vivo experiments with $GlcC_5S$-Au-$SC_{11}DO3A$-Gd GNP prepared by "direct" synthesis

Animal	Tissue	Au (ppm)
1	Blood	3.61
	Liver	387 and 305 **(1)**
	Spleen	133
	Kidney	25.9
	Brain	0.76
	Tumor	4.00
	Lung	9.4
2	Blood	5.48, 5.36 (solution) and 3.51 (coagulum) **(2)**
	Liver	481
	Spleen	185
	Kidney	25.7
	Brain	0.72 and 0.31 **(1)**
	Tumor	8.19
	Lung	21.7
3	Blood	3.66 (solution) and 3.88 (coagulum) **(2)**
	Liver	4.99
	Spleen	167
	Kidney	27.1
	Brain	1.42
	Tumor	8.46
	Lung	27.8
4	Blood	3.04 (solution) and 0.98 (coagulum) **(2)**
	Liver	296
	Spleen	114
	Kidney	22.9
	Brain	0.14
	Lung	10.3

(1) Results of two different digestions. The difference in the sample concentration indicates the uncertainty of the analysis and, specially, the inhomogeneities of the tissue analysed.

(2) In the blood samples, two or three different digestions were done due to the high weight of the samples . In addition to this, the samples showed a clear inhomogeneity (solution and coagulum).